STRENGTH RELIABLITY OF SHORT AND SLENDER COMPOSITE STEEL-CONCRETE COLUMNS

BY

BRYAN WILLIAM SKRABEK

A Thesis
Submitted to the Faculty of Graduate Studies
in Partial Fulfillment of the Requirements
for the Degree of

MASTER OF SCIENCE

Department of Civil Engineering
University of Manitoba
Winnipeg, Manitoba

(c) December, 1989

STRENGTH RELIABILITY OF SHORT AND SLENDER COMPOSITE STEEL-CONCRETE COLUMNS

BY

BRYAN WILLIAM SKRABEK

A thesis submitted to the Faculty of Graduate Studies of the University of Manitoba in partial fulfillment of the requirements of the degree of

MASTER OF SCIENCE

© 1990

Permission has been granted to the LIBRARY OF THE UNIVERSITY OF MANITOBA to lend or sell copies of this thesis, to the NATIONAL LIBRARY OF CANADA to microfilm this thesis and to lend or sell copies of the film, and UNIVERSITY MICROFILMS to publish an abstract of this thesis.

The author reserves other publication rights, and neither the thesis nor extensive extracts from it may be printed or otherwise reproduced without the author's written permission.

ABSTRACT

Structural reliability analysis requires that the relationship between the probability distribution of member resistance and the probability distribution of load effects be known so that realistic member understrength and overload factors can be computed for design purposes.

In this study, the probability distribution of the ratio of theoretical to nominal (design code) strength for composite steel-concrete beam-columns was established and the major variables affecting the probability distribution identified. The beam-columns studied were comprised of a structural steel wide flange shape surrounded by a reinforcing bar cage and completely encased in concrete.

A computer program was used to calculate the theoretical and nominal strengths. The accuracy of the theoretical model was established by comparisons to test specimens documented in the literature.

Probability distributions of the geometric and mechanical properties of the variables which determine the resistance of the beam-column were established by reviewing existing literature.

The Monte Carlo technique was used to simulate the resistance of typical beam-columns in order to determine both the probability distribution of the member resistance and the variables having the most effect on the lower tail of the probability distribution.

For short composite beam-columns, the variables that affected the probability distributions of the strength were the specified concrete strength, ratio of structural steel area to gross area of cross-section, slenderness ratio and end eccentricity ratio.

The same variables were found to affect the strength probability distributions of slender composite beam-columns except that the effect of specified concrete strength became negligible for beam-columns with very large slenderness ratios and the effect of end eccentricity ratio became negligible for large eccentricity ratios.

ACKNOWLEDGMENTS

The author would like to acknowledge the assistance of the National Sciences and Engineering Council of Canada for providing funding through research grants to Dr. S.A. Mirza.

Sincere appreciation goes to Dr. S.A. Mirza for his guidance and extreme patience during this investigation.

Special thanks are due to Mr. C.E. Mickelson, P. Eng., for providing support and encouragement.

TABLE OF CONTENTS

LIST OF FIGURES

LIST OF TABLES

1 INTRODUCTION

The probability-based limit states designs are based on limiting the probability of failure to an acceptable level. The actual strength of a structural member differs from the nominal strength calculated by the designer due to variations in the material strength, variations in dimensions and geometry of the member, and variations in the accuracy of equations used to compute the nominal strength. Similarly, the load effects upon a member differ from assumed values due to the variation in loadings over the lifetime of the structure. To compute the probability of failure due to load effects being higher than anticipated and/or member strength being lower than anticipated, the statistical descriptions of variations of both the load effects and the member resistance must be known. The statistical combination of these two variations allows the probability of failure to be calculated. This procedure is referred to as reliability analysis.

This study reports the strength statistics required for use in the reliability analysis of composite beam-columns in which steel shapes are encased in concrete. The factors contributing to the variation of the ratio of actual (theoretical) strength to nominal (design code) strength of composite beam-columns are identified. The importance of each factor to the overall strength variation and the conditions

under which it applies are analyzed. This work will facilitate the reliability analysis of representative composite steel-concrete beam-columns currently underway at Lakehead University.

The composite beam-columns investigated consist of a rolled structural steel wide flange section surrounded by a cage of reinforcing bars and entirely encased in concrete. The column cross-section is rectangular and meets the reinforcement requirements of ACI (American Concrete Institute) 318-83 (1983) and CSA (Canadian Standards Association) CAN3-A23.3-M84 (1984) design codes. Assumptions regarding the theoretical behavior of the cross-section and the member (beam-column) are discussed in Chapter 2. Assumptions regarding the behavior of the cross-section and the column with respect to the design codes are discussed in Chapter 3.

1.1 OVERVIEW OF STUDY

The design procedure for composite beam-columns specified in ACI Standard 318-83 accounts for the probability of understrength by the use of capacity reduction factors of less than 1.0. Similarly, CSA Standard CAN3-A23.3-M84 considers the probability of understrength by assigning material understrength factors of less than 1.0. To account for the probability of load effects being greater than the nominal design values, specified loads are multiplied by a

factor greater than 1.0 in both cases. To satisfy the strength requirements of these standards Equation 1.1 must be satisfied.

$$\text{Factored Resistance} \geq \text{Effects of Factored Loads} \qquad (1.1)$$

Consider a large number of columns, each designed to have the same resistance to load effects and each assumed to be subjected to the same specified loading. Due to variations in geometry and constituents material strengths of the column, the actual resistance of each column will vary. The distribution of column resistance (R) is represented by the horizontal axis of Figure 1.1(a). The live and dead loads are also variable and, therefore, each column will be subjected to different maximum load effects during its lifetime. The distribution of maximum load effects (U) is represented by the vertical axis in Figure 1.1(a). The 45-degree line represents the condition where the load effect U equals the resistance R. Combinations of U and R that fall above the 45-degree line represent the failure condition where $R < U$ (Mirza 1985a).

A function, $Y = R/U$, is used to simplify the reliability analysis (Mirza 1985a). The distribution of the value of Y is represented in Figure 1.1(b). The function has a mean

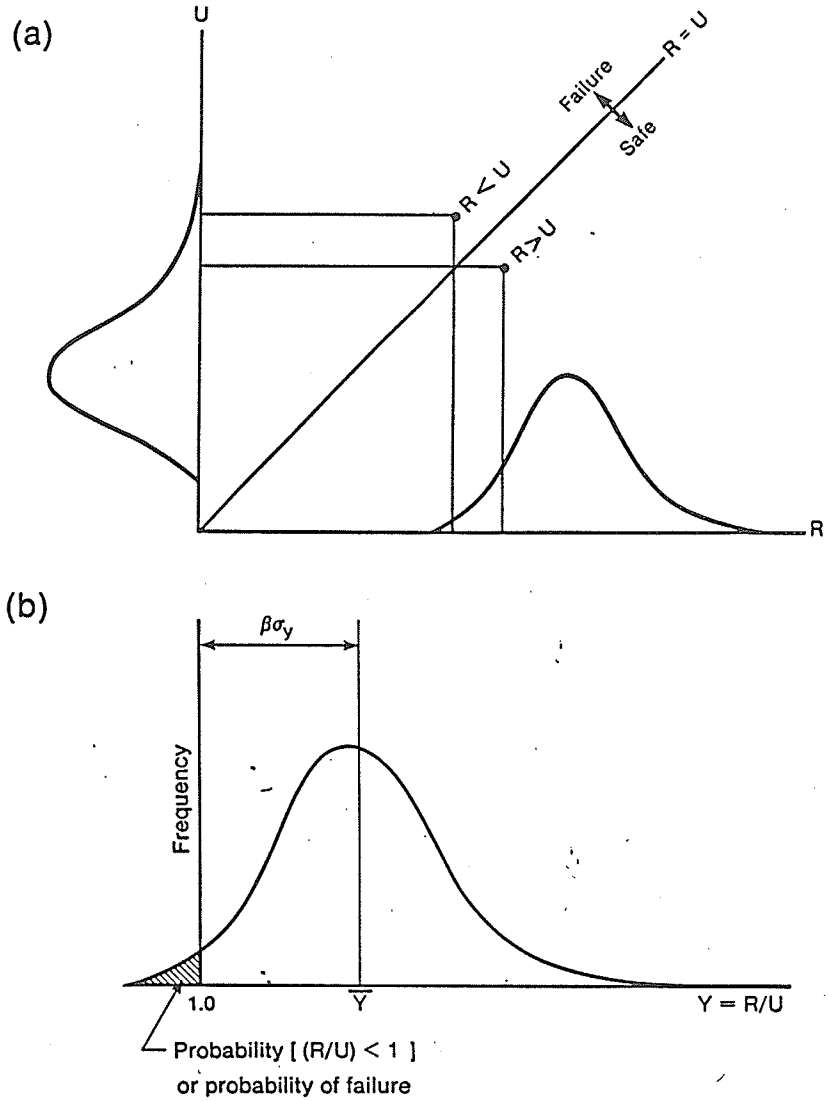

Figure 1.1 - Definition of failure, probability of failure, and safety index β (Mirza 1985a)

value $\overline{Y}$, and a standard deviation of σ_y. A particular column will fail if its value of Y is less than 1.0. Hence, the shaded area in Figure 1.1(b) represents the failure condition. The ratio of the shaded area to the entire area under the curve of Y is the probability of failure. The safety index, β, is a multiple of standard deviation of Y by which the mean value of Y exceeds the failure level. If the type of probability distribution of Y is known, the probability of failure can be calculated from β. An increase in β due to an increase in $\overline{Y}$, or a decrease in σ_y, or both, increases the margin of safety and vice versa. The value β is therefore a measure of structural reliability (Mirza 1985a).

To compute the value of the strength reduction (or material understrength) and load factors, the statistical properties of both the column strength and the load effects must be considered concurrently. This can be accomplished by use of a step-wise reliability analysis technique as presented by Mirza (1985a) and reproduced as follows:

(a) derivation of statistical models for material strengths and geometric properties;
(b) selection of equations to predict theoretical strengths;
(c) derivation of the probability distribution of the strength of representative structural members;
(d) description of load and load effect statistics;

(e) selection of a target safety index β based on code calibration studies;

(f) selection of design code format and load factors; and

(g) calculation of resistance (or material understrength) factors based on representative structural members and relative occurrences of different types of loading in buildings where these members occur.

In this study, items (a), (b) and (c) have been completed for composite steel-concrete beam-columns subject to the limitations discussed below. Items (d) through (g) describe the work that is currently in progress as part of another study at Lakehead University.

The composite beam-columns studied meet the following assumptions regarding loading and support conditions as shown in Figure 1.2:

(a) the columns are pin-ended and the effective length is equal to the actual length;

(b) bending is in single curvature about the major axis;

(c) end moments are equal and opposite producing a uniform primary moment distribution along the length of the beam-column;

(d) no lateral load is applied between the ends of the column; and

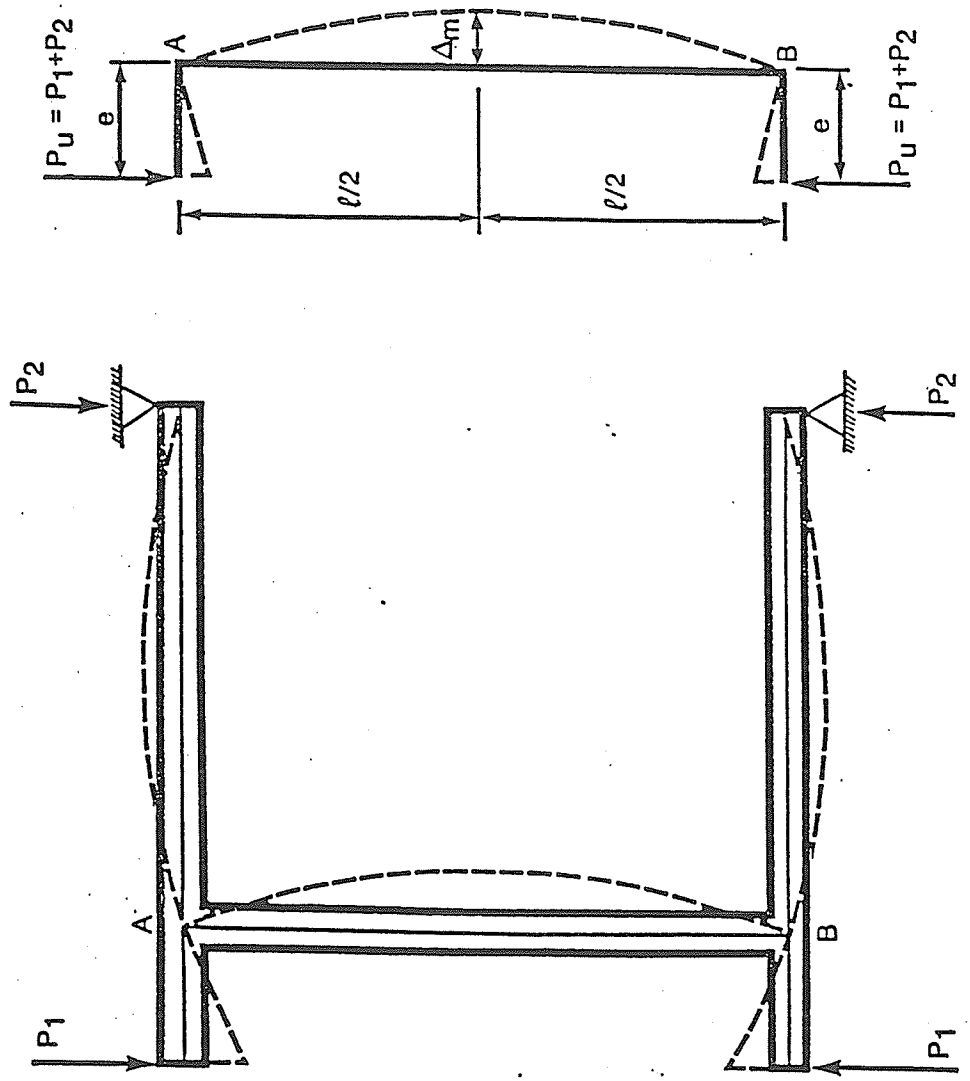

(a) Model of Column in Symmetrical Single Curvature (b) Forces on Column

Figure 1.2 - Loading and Support Conditions of Columns Studied (Mirza 1990)

(e) loading is progressive to failure and is of short duration such that creep and shrinkage effects of concrete are not considered.

The loading configuration described by (a) to (d) above provides for maximum secondary moments due to deflection at the mid-height of the beam-column and is an extreme case for beam-columns in non-sway frames designed in accordance with ACI 318-83 and CSA A23.3-M84. Shrinkage of concrete, corrosion of steel components and increase of concrete strength due to maturation are ignored. It was assumed that the beneficial effects due to increase in concrete strength with time would compensate for any decrease in strength due to creep and shrinkage of concrete and corrosion of structural and reinforcing steel.

1.2 OUTLINE OF RESEARCH PROGRAM

A computer program was used to calculate the theoretical resistance of composite steel-concrete beam-columns. The program is based on equations and assumptions considered to be of greater accuracy than design code equations. The accuracy (model error) of the theoretical strength program was established by comparisons with existing test data of the ultimate strength of composite beam-columns. The theoretical computer program is discussed in detail in Chapter 2.

A computer program designed to calculate the nominal capacity of composite steel-concrete beam-columns was used to compare the theoretical member strength to that allowed by the design codes. The nominal capacity is based on the specified mechanical and geometric properties of the column components and on the equations given by design codes. The nominal program subroutine is discussed in Chapter 3.

Probability distributions of the mechanical and geometric properties of column components were taken or derived from data available in the literature. The probability distributions are discussed in Chapter 4.

A Monte Carlo technique (Chapter 5) was used to establish the statistical properties of the member strength. This method consists of repeated simulations of a chosen sample column using random selections of the magnitudes of variables based on the probability distributions mentioned previously. The theoretical strength of each simulated column is calculated by the program subroutine described in Chapter 2.

The ratio of theoretical to nominal strength was calculated for each configuration of composite beam-column studied. The resulting ratios were then analyzed statistically to determine the shape of the probability distribution and its properties for each beam-column studied. The probability distributions so generated were used to investigate the effects of different variables studied. The contribution of

variability of the properties of structural steel, concrete, and model error to the overall strength variations of a few individual columns was also examined. The computed data is discussed separately for short and for slender beam-columns in Chapter 5. A summary of the study and conclusions drawn from it are presented in Chapter 6.

The methodology of the research program is similar to, although more refined than two earlier studies for reinforced concrete beam-columns. Grant et al. (1978) studied the strength variation of short reinforced concrete columns. Mirza and MacGregor (1989) studied the strength variation of slender reinforced concrete columns. The major difference between this report and the above-noted studies are the effects of the structural steel core and of concrete confinement due to minimum ties specified in ACI Standard 318-83 (and CSA Standard CAN3-A23.3-M84) on the strength variation of beam-columns.

2 THEORETICAL BEAM-COLUMN STRENGTH

To analyze the theoretical strength of a composite beam-column, a computer program previously developed at Lakehead University (Mirza 1989) was tested and revised as required for use in this study. The changes implemented into the program for use in this study included more efficient techniques to allow for full strain hardening of steel, generalized interpolation techniques (Lagrangian), definition of maximum allowable interpolation errors, accounting for numerical discrepancies due to column behavior at extreme values, reduction of computing time required and addition of Monte Carlo simulations. A brief flow chart of the computing procedure used is shown in Figure 2.1.

The entire program consists of a main driver program, **COMPOSIT**, and two major subroutines. The main driver reads input, initiates Monte Carlo variations of input data if required, calls the major subroutines and statistically analyzes the output data. One of the two major subroutine programs, **RTHEO**, analyzes for the theoretical strength of the composite column and the other, **RNOM**, calculates the nominal strength of the column following the design requirements of ACI 318-83 or CSA A23.3-M84. The theoretical model and related subroutines are discussed in this chapter. The nominal strength model and subroutine are discussed in Chapter 3.

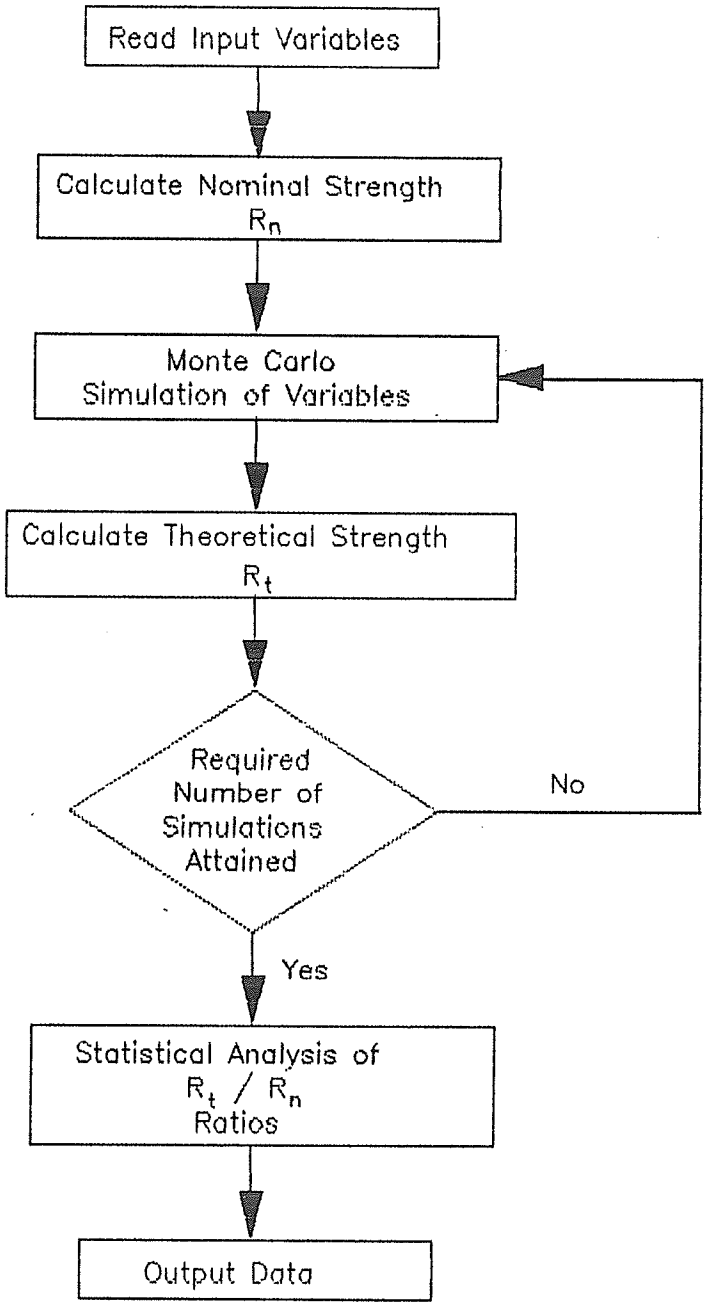

Figure 2.1 – Flow Chart of Computing Procedure

2.1 REVIEW OF PREVIOUS WORK

In order to describe the theoretical model used in this study, it was considered useful to see what techniques and assumptions have been used by others in previous studies of composite beam-columns. A review of the published work on the theoretical analysis of composite columns is briefly summarized below.

Bondale (1966 a,b,c) tested composite beam-columns and attempted to duplicate his test results by analyzing the columns with theoretical models. Strain compatibility assumptions were used to establish the cross-section relationships between axial load, bending moment and curvature. The tangent modulus theory was used to analyze the concentric load case. Slender, eccentrically loaded columns were assumed to deflect in the form of a cosine curve. Graphically solving for the equilibrium relationship between load end eccentricity and mid-height deflection established maximum eccentricities at the failure section for given axial loads. The assumptions made by Bondale are the same as described in Section 2.2 with the following exceptions: (a) tensile strength of concrete was neglected; and (b) residual stresses in the structural steel were neglected. Analysis of the test specimens showed that the tested load capacities were from 1.15 to 1.23 times the theoretical capacities.

Basu (1967) presented a computer method to approximate the capacity of pin-ended composite beam-columns subjected to equal and opposite end eccentricities and uniaxial bending. The method made efficient use of computer time since equilibrium needed to be satisfied only at the ends and at the mid-height of the beam-column. The method was similar to that of Bondale except that interpolations were made mathematically by the computer rather than graphically. Comparisons made by Basu with the test results of Bondale (1966 a,b,c) predicted the ratio of actual to predicted strength to be 1.21 to 1.33 when the maximum concrete stress was assumed to be two thirds of the cube strength. The results improved to 1.09 to 1.20 when a value of eighty percent of the cube strength was used. This shows that the stress-strain curve assumed for concrete significantly affects the results. The assumptions Basu used in his analysis are similar to those made by Bondale. Two exceptions are notable. An initial deflection of the column in the form of a cosine curve is assumed to account for some initial camber of the column. Subsequent deflections due to secondary moments are assumed to be in the form of a part cosine wave.

Basu and Hill (1968) confirmed the accuracy of Basu (1967) by developing a more precise numerical integration method of analysis. Equilibrium is satisfied at a number of points (nodes) between the mid-height and the ends of the

beam-column giving a more precise evaluation of the deflected shape of the column. Comparing runs made by the approximate method (Basu 1967) and the numerical integration method showed that the maximum error for the approximate method was five percent on the conservative side. The approximate method analysis was completed in only seven percent of the computer time required for the numerical integration analysis.

Virdi and Dowling (1973) extended the work of Basu and Hill (1968) by applying the numerical integration technique to biaxially loaded composite columns. The columns were pin-ended with equal end eccentricities. The column was assumed to be initially deflected along both axis in the form of a cosine wave, with additional second-order deflections forming a part cosine wave. Initial deflections were assumed to be less than those assumed by Basu and Hill (1968). In contrast to previous studies by others, Virdi and Dowling included the effect of residual stresses in the structural steel section. They reported that, in some cases, residual stresses enhanced the strength of long beam-columns. The column load capacities calculated by their analysis technique was compared to eight physical test specimens. A mean ratio of tested to calculated strength of 1.04 and a coefficient of variation of 10.4 percent resulted when residual stresses and an initial out-of-straightness of 0.001 times the column length were assumed.

Virdi and Dowling (1982) present a revision of their earlier work. The revised method used Gauss quadrature to integrate axial force in an element of the cross-section rather than assuming the strain at the center of gravity of an element applicable to the entire element. Residual stresses are not reported to be used in the analysis. An initial out-of-straightness of 0.001 times the length was assumed for each axis. The authors compared the revised technique against the physical tests of columns and the analysis reported earlier (Virdi and Dowling 1973). The ratio of tested to predicted strength decreased to 0.962 with a coefficient of variation of 9.7 percent. These values indicate a small overestimation of the ultimate strength although the coefficient of variation is slightly improved.

Wakabayashi (1976) proposed a superposition method of independent concrete, reinforcing bar and structural steel columns as a solution to the composite column. The summation of the tangent modulus capacity of the independent columns was proposed for use in the concentric loading case. Wakabayashi suggested that although the steel section may be initially cambered, the reinforced concrete encasement can be constructed nearly straight thereby reducing the effect of the initial camber of the steel section to the overall capacity of the composite member. This suggests that assuming the entire composite cross-section to be initially out of plumb is not required. Wakabayashi also noted that the

stress-strain relationship of concrete inside and outside the flanges of the steel section may differ due to the confining influence of the flanges.

May and Johnson (1978) reported a numerical technique designed to analyze biaxially loaded composite columns for both pin-ended and restrained end cases. The method is similar to that of Virdi and Dowling (1973) except that May and Johnson used a finite difference technique while Virdi and Dowling used a Newton-Raphson iteration scheme to converge to the equilibrium deflected shape. A comparison of their axial load - midheight deflection computations with those of Basu and Hill (1968) and Virdi and Dowling (1973) indicate very minimal differences. Assumptions used by May and Johnson are consistent with those previously mentioned for Basu and Hill (1968) and for Virdi and Dowling (1973). Residual stresses were assumed to have negligible effect. No mention is made of what was assumed for initial out-of-straightness of the beam-column.

LaChance and Hays (1980) studied the errors to be expected by making or neglecting various assumptions in the calculation of the $M-\phi-P$ (moment - curvature - axial load) relationship for composite beam-column cross-sections. A strain compatibility technique was used with assumptions similar to those used by previous authors noted above. Since only the cross-section was considered, the results are applicable only to short beam-columns. Ignoring the bending

stiffness of reinforcing bars was found to underestimate the moment capacity by only 0.05 percent. Ignoring the tensile strength of concrete caused an underestimation of moment capacity of only 0.01 percent. Neglecting to disregard the concrete area displaced by reinforcing bars and the steel I-section caused overestimations of the bending moment capacity by up to 25 percent. Using different stress-strain curves for concrete caused differences in the calculated moment capacities of up to 9 percent when bending about the major axis was considered. A stress-strain curve with a descending branch beyond the point of maximum stress yielded higher moment capacities than a curve which terminated at the peak stress. Residual stresses in the steel section did not influence the ultimate strength of the cross section. However, the authors pointed out that residual stresses may influence the strength and behavior of long beam-columns.

2.2 ASSUMPTIONS USED IN THEORETICAL STRENGTH MODEL

The theoretical strength calculations presented in this study are similar to the work of Basu (1967). A strain compatibility solution was used to compute the $M-\phi-P$ relationship of the cross-section and is discussed in Section 2.4. The capacity of the member (beam-column) was calculated by solving for the maximum eccentricity for which equilibrium could be maintained between the ends and mid-height of the beam-column. The procedure used to calculate the beam-column strength is discussed in Section 2.5.

The assumptions regarding the loading and the end conditions of the beam-columns were discussed in Section 1.1. The assumptions peculiar to the theoretical analysis are discussed here. These are:

(a) strains are compatible between concrete and steel such that no slip occurs;

(b) strain is linearly proportional to the distance from the neutral axis;

(c) deflections are small such that curvatures can be calculated as the second derivative of the deflection;

(d) shear stresses are small and their effect on strength can be neglected;

(e) effects of axial shortening are negligible;

(f) the rolled steel section is assumed to be made up of rectangular plates;

(g) residual stresses in the rolled steel section exist;

(h) the column is perfectly straight before loading;

(i) the column cross-section is symmetric about the major and minor axis; and

(j) the failure takes place due to material failure and not by local or torsional buckling;

Assumptions (a) and (b) were required for the strain compatibility solution of the cross-section $M-\phi-P$ relationship. Assumption (c) was needed for the calculation of length effects due to secondary moments. Assumptions (d) and (e) were used to simplify the calculations. Assumption

(f) simplified the discretization of the cross-section into elements and is discussed in Section 2.3. Assumption (g) acknowledges the existence of residual stresses in the rolled steel section and is discussed in Section 2.8. Assumption (h) was based on Wakabayashi's (1976) observation that the encasement of the steel section in concrete will negate any detrimental effects of initial camber of the steel section. Assumption (i) simplified the cross-section $M-\phi-P$ calculations since discretization of only one-quarter of the cross-section was required to model the entire cross-section. Assumption (j) was valid since a review of test data in the literature did not indicate any failure by local or torsional buckling. This assumption was also made by Bondale (1966 a,b,c) and would seem to be particularly valid where rectangular hoops along with surrounding concrete stiffen the compression flange of the steel section. Further assumptions directly related to the stress-strain curve for individual materials are discussed in Sections 2.6 and 2.7.

2.3 CROSS-SECTION DISCRETIZATION

The cross-section of a composite column consists of three materials (concrete, structural steel and reinforcing steel) each possessing a unique stress-strain relationship. Concrete was subdivided into three distinct types, unconfined, partially confined and highly confined as described below. Each of these concrete types had different

stress-strain characteristics. The rolled steel section was separated into the web and the flanges to model differences in their stress-strain characteristics. Hence, the cross-section was comprised of materials with six different stress-strain curves. The six distinct areas of the cross-section are shown in Figure 2.2.

The cover concrete (i.e. concrete outside of the lateral ties) was unconfined. The concrete inside the periphery of the ties but outside the flanges of the steel section was assumed to be partially confined. The concrete within an assumed parabola and between the flanges of the steel section (Fig. 2.2) was assumed to be highly confined. The assumed parabola had a vertex intersecting the edge of the web at the mid-depth of the steel section when the flange overhang was less than one-quarter of the section depth between the flanges. The vertex of the parabola was taken to be at the mid-height of the section and a distance from the web d_{vertex} dependant on the flange width b, flange thickness t, depth of steel section d, and web thickness w as shown in Figure 2.3 and in Equation 2.1.

$$d_{vertex} = \frac{b-w}{2} - \frac{d-2t}{4} \qquad (2.1)$$

$$d_{vertex} \geq 0.0$$

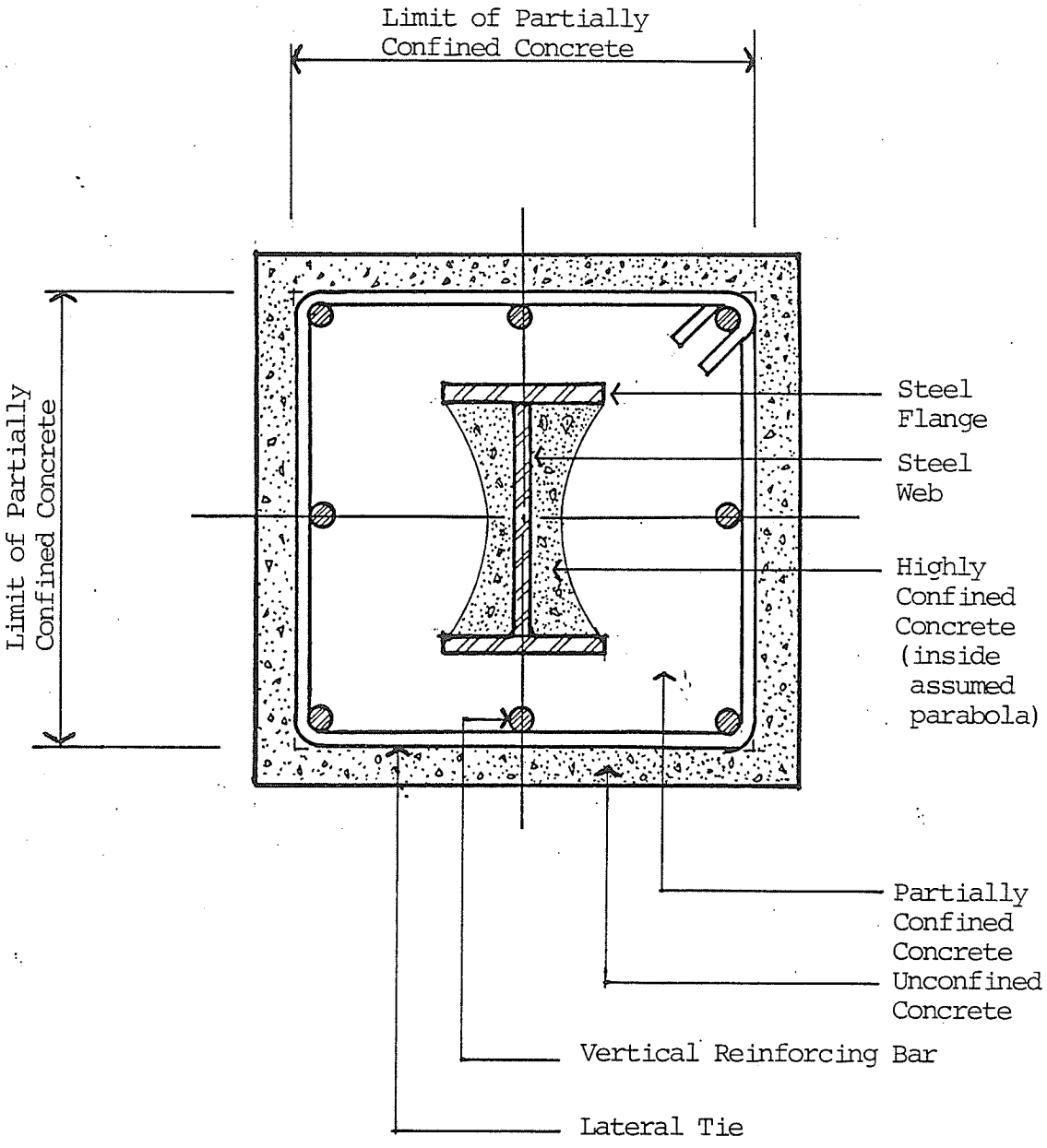

Figure 2.2 - Material Types in Composite Cross-Section

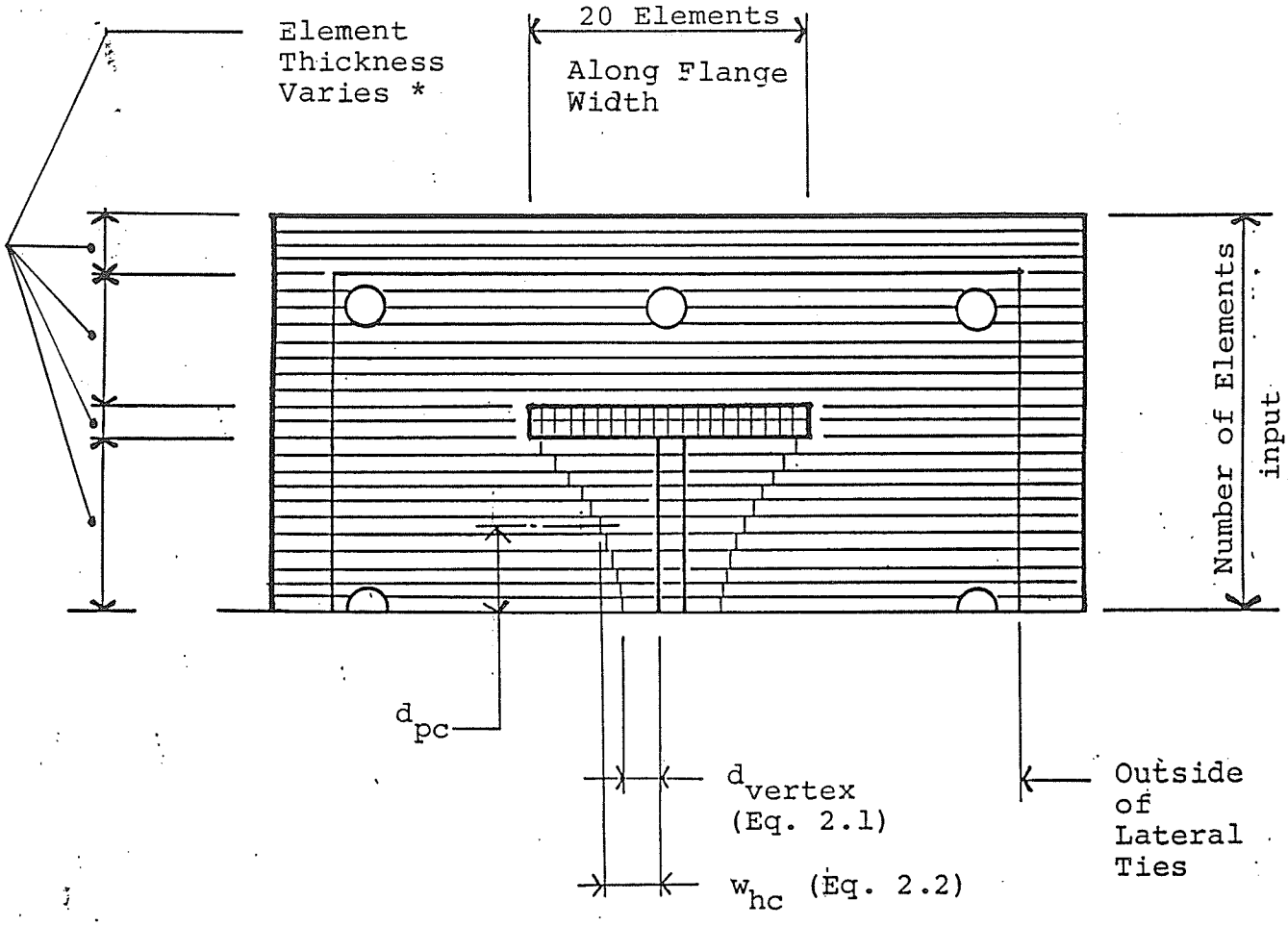

* Element thickness varies to ensure that element boundary coincides with material boundary.

Figure 2.3 - Discretization of Composite One-Half Cross-Section Used for Theoretical Strength Subroutine

The distance, parallel to the major axis, from the edge of the web to the parabola w_{hc} (Figure 2.3) for an elemental slice is computed by Equation 2.2

$$w_{hc} = d_{vertex} + \left(\frac{\left(\frac{b - w}{2} - d_{vertex} \right) d_{pc}^2}{\left(\frac{d - 2t}{2} \right)^2} \right) \qquad (2.2)$$

in which d_{pc} is measured perpendicular to the major axis from the plastic centroid of the cross-section to the centroid of the element.

The discretization between the three areas of concrete recognizes the beneficial effects of increased confinement on concrete strength and ductility. Park, Priestley and Gill (1982) used distinct boundaries between the unconfined and partially confined concrete areas in their analysis of reinforced concrete beam-columns. Potential differences in stress-strain characteristics between the partially and highly confined concrete areas were noted by Wakayabashi (1976) and Mirza (1989). This distinction is logical due to the high confining effect of the steel section as opposed to that provided by rectangular ties. The rest of the literature described in Section 2.1 made no mention of any attempt to distinguish between these concrete areas. The individual stress-strain characteristics of these three areas of concrete are discussed in Section 2.6.

The steel section was subdivided into two areas, the web and the flanges. This accounted for differences in yield strengths of the two components of the steel section as noted by Galambos and Ravindra (1978) and Kennedy and Gad Aly (1980).

In order to calculate the $M-\phi-P$ relationship the cross-section must be divided into elements small enough to allow the computer to numerically integrate the forces in each element accurately. To accomplish this the program discretizes the cross-section into finite strips parallel to the major axis. Within each strip the cross section is further discretized into the various material categories as discussed above. The width of the strip perpendicular to the major axis is determined by the number of strips requested and input to the program. The width of strips are automatically adjusted so that strip boundaries occur at the interface between two materials. Fifty elemental strips for the entire cross-section thickness were specified for the computer simulations described in Chapter 5.

To account for varying stresses along the width of the flange due to residual stresses, the flange is discretized into 20 equal width elements perpendicular to the major axis. The initial strain in each element due to residual stresses is calculated with subsequent strains being added

algebraically to each element. Figure 2.3 shows the discretization for a typical 1/2-section of a composite cross-section.

2.4 CROSS-SECTION STRENGTH MODEL

The cross-section strength model determines the relationship between bending moment, curvature and axial load ($M-\phi-P$). This information is required for establishing the cross-section axial load - bending moment ($P-M$) interaction diagram. Figure 2.4 shows typical $M-\phi-P$ relationships for several axial loads with key points marked on the diagram. In this figure, the bending moment is shown on the vertical axis with curvature shown on the horizontal axis. The peak moment on the curve for the level of axial load considered represents one point on the cross-section $P-M$ interaction diagram. Computation of these points for a sufficient number of axial load levels yields the cross-section $P-M$ interaction diagram (Figure 2.5).

The first step required in determining the $M-\phi-P$ relationships is defining the range of axial load to be examined. The maximum axial load which can be applied on the cross-section occurs when that load is applied concentric to the plastic centroid of the cross section (pure compression axial load capacity). This loading arrangement forces all elements to strain equally. Since the

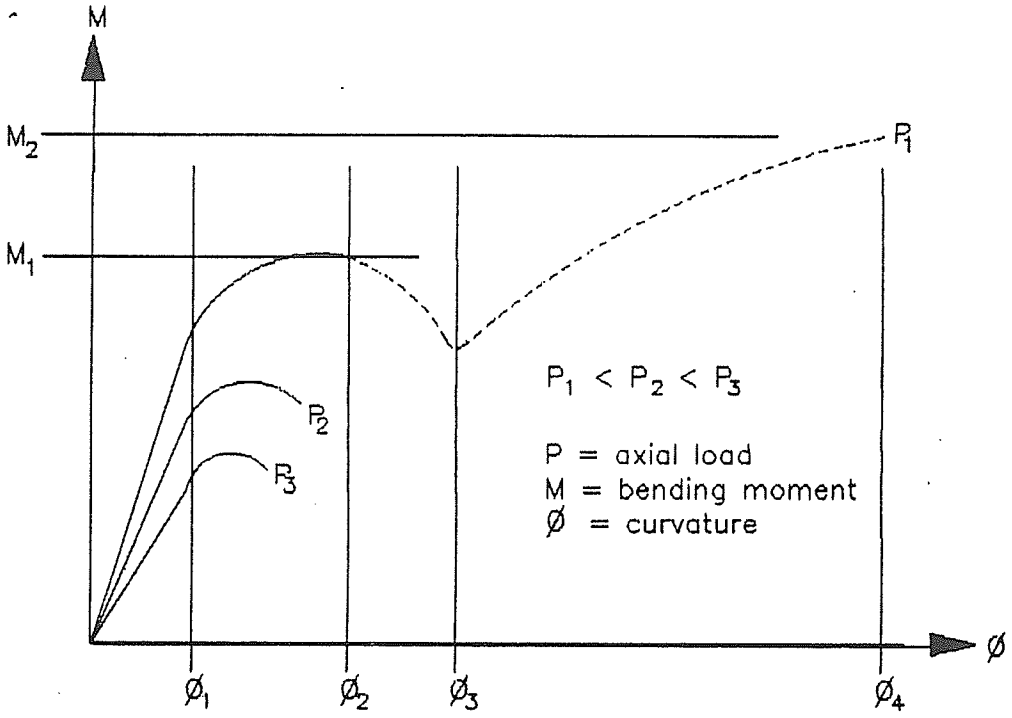

For Axial Load P_1 :

$Ø_1$ – yielding initiated in tension flange

$Ø_2$ – spalling of concrete cover begins

$Ø_3$ – concrete cover spalled off
– strain–hardening initiated in tension flange

$Ø_4$ – rupture of tension flange

M_1 – maximum bending moment
(strain–hardening neglected)

M_2 – maximum bending moment
(strain–hardening considered)

Figure 2.4 – Typical M–Ø–P Relationships for Composite Cross–Sections

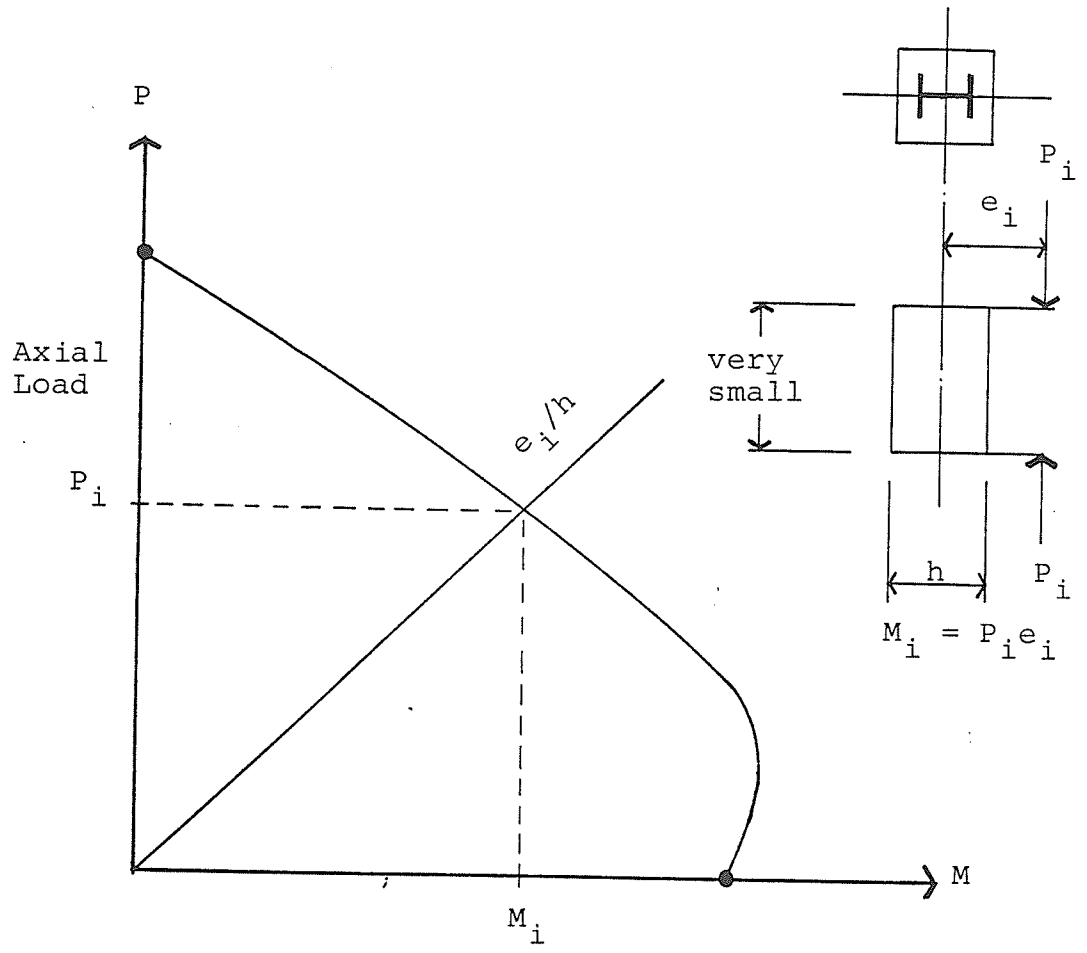

Figure 2.5 - Typical Composite Cross-Section
P-M Interaction Diagram

cross-section is doubly symmetric, the plastic centroid is coincident with the intersection of the major and minor axis.

The following procedure was used to calculate the concentric axial load corresponding to a given strain:

(a) Determine the stress in each element from the stress-strain relations corresponding to the given strain;
(b) determine the force in each element by multiplying the stress by the area of the element; and
(c) sum the forces from each element to obtain the total axial load.

An iterative technique was used to solve for the pure compression axial load capacity. The axial load was calculated at a strain that corresponded to the material with the lowest strain at peak stress from the stress-strain relationships (Sections 2.6 and 2.7). For structural and reinforcing steel, the strain corresponding to the yield point was used. The strain is incremented and the axial load level calculated until the strain corresponded to the material with the highest strain at peak stress. Since the maximum axial force lies between these two strain limits, the maximum axial load calculated during these iterations was taken as the cross-section concentric axial load capacity. This established a point on the $P-M$ interaction curve that corresponded to the axial load capacity at zero bending moment.

To determine other points on the $P-M$ interaction curve, the bending moment capacities corresponding to axial load levels between zero and the pure compression axial load capacity were calculated. The subroutine determines the $M-\phi-P$ relationship for axial loads of 0, 2, 4, 6, 8, 10, 12, 16, 20, 24, 28, 32, 36, 40, 44, 48, 52, 56, 60, 64, 70, 76, 82 and 86 percent of the concentric axial load capacity. The bending moment calculated for each axial load level was plotted on the $P-M$ interaction diagram.

To determine an $M-\phi-P$ relationship one additional term must also be known. This is the distance DNA between the neutral axis and the major axis as shown in Figure 2.6. For a given value of axial load, there are a number of corresponding moments possible depending on the location of the neutral axis and the value of the curvature. This is shown in Figure 2.4. A unique relationship exists between the axial load P, the bending moment M, the curvature ϕ and the location of the neutral axis DNA. Fixing a value for either DNA or ϕ defines the value of the other term since only a unique pair of values for DNA and ϕ will satisfy equilibrium of forces for the given axial load. Once the axial load, the curvature and the location of the neutral axis are known, the bending moment can be calculated. By

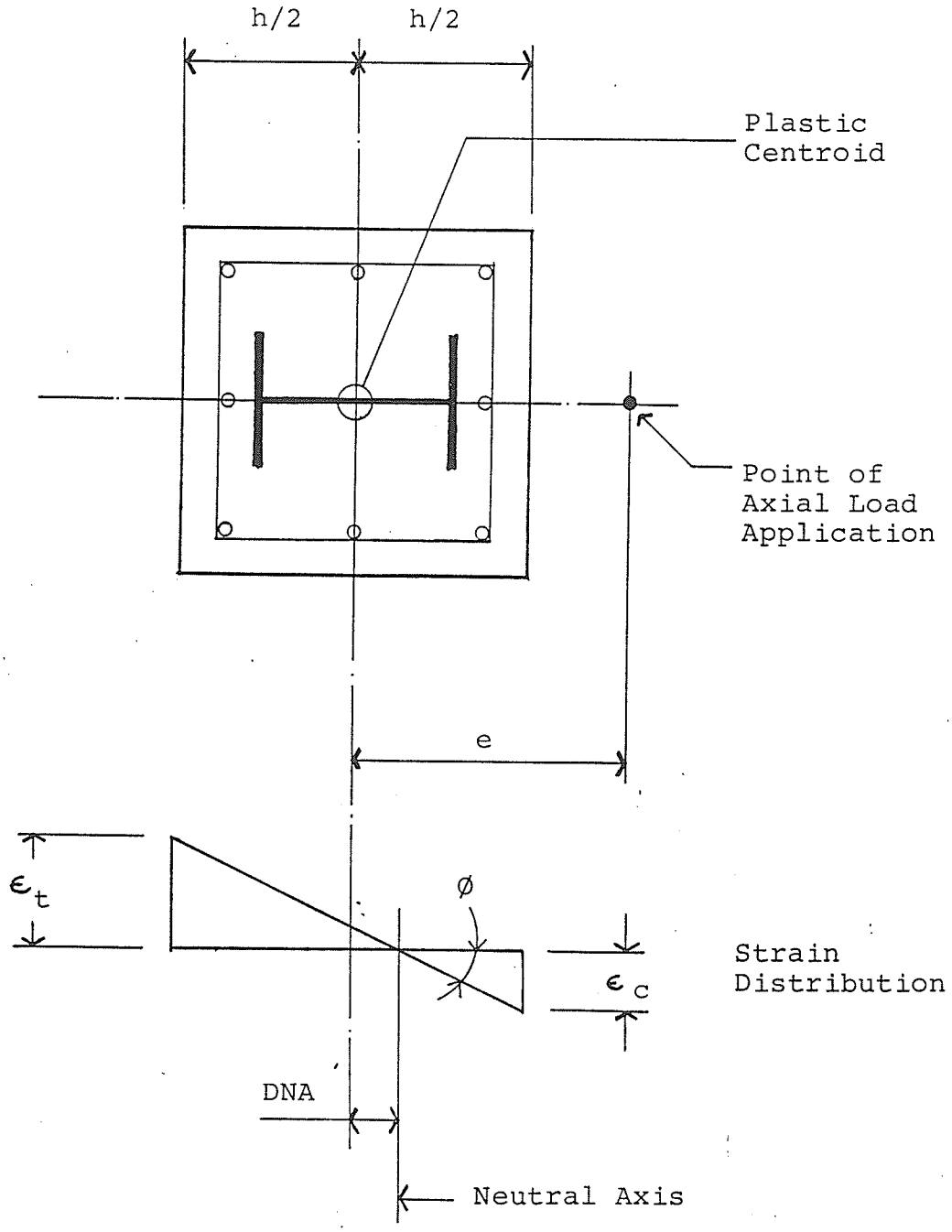

$$\phi = \frac{\epsilon_c}{(\frac{h}{2}-DNA)}$$

Figure 2.6 - Strain Gradient in Composite Cross-Section

calculating a number of these unique relationships for each axial load level, the maximum bending moment for each axial load level can be found.

To reduce computing time, the $M-\phi-P$ relationships for all axial load levels were calculated and analyzed simultaneously. A starting curvature value was assumed. Holding this value constant, the distance from the plastic centroid to the neutral axis (DNA) was varied and the corresponding axial force was calculated at each DNA value selected. The DNA was varied in such a way that all calculated values of the axial force were within the required range. This creates a matrix of P versus DNA values.

A linear interpolation of values from the P versus DNA matrix provided an approximate DNA value for each given level of P. Using the approximate DNA value, the Extended Newton-Raphson Technique (Kikuchi, Mirza and MacGregor 1978) was then used to converge to the correct DNA value for the given level of axial force. Since both the starting curvature and the position of the neutral axis corresponding to the required axial load were now known, the bending moment could be calculated easily. This procedure was then repeated for all given values of P.

With bending moments for the starting curvature known, the curvature was incremented, a new P versus DNA curve was plotted and new bending moments were calculated.

This procedure created the required $M-\phi-P$ relationships. An outline of the method by which the $M-\phi-P$ relationships were calculated for the composite cross-section is shown in Figure 2.7. The data, when plotted, is similar to the data plotted in Figure 2.4.

The maximum bending moment for a given level of axial force calculated by this method yields one point on the $P-M$ interaction curve (Figure 2.5). To ensure that the maximum bending moment for a given axial force was calculated, the curvature was incremented until the concrete cover on the compressive side of the cross-section had spalled off. Review of $M-\phi$ curves showed that the maximum bending moment occurred prior to spalling off of the concrete cover except for low axial load levels when strain-hardening of steel was considered. When the concrete cover has spalled off at a particular axial load level, the program ceases to calculate any further points on the moment versus curvature graph for that axial load level except when strain-hardening of steel is considered as described below.

When strain hardening of the steel is considered, at low levels of axial load (less than 20 percent of the pure compression axial force capacity), the maximum moment may not be reached until several hundred curvature increments have been completed. To save computing time, the curvature

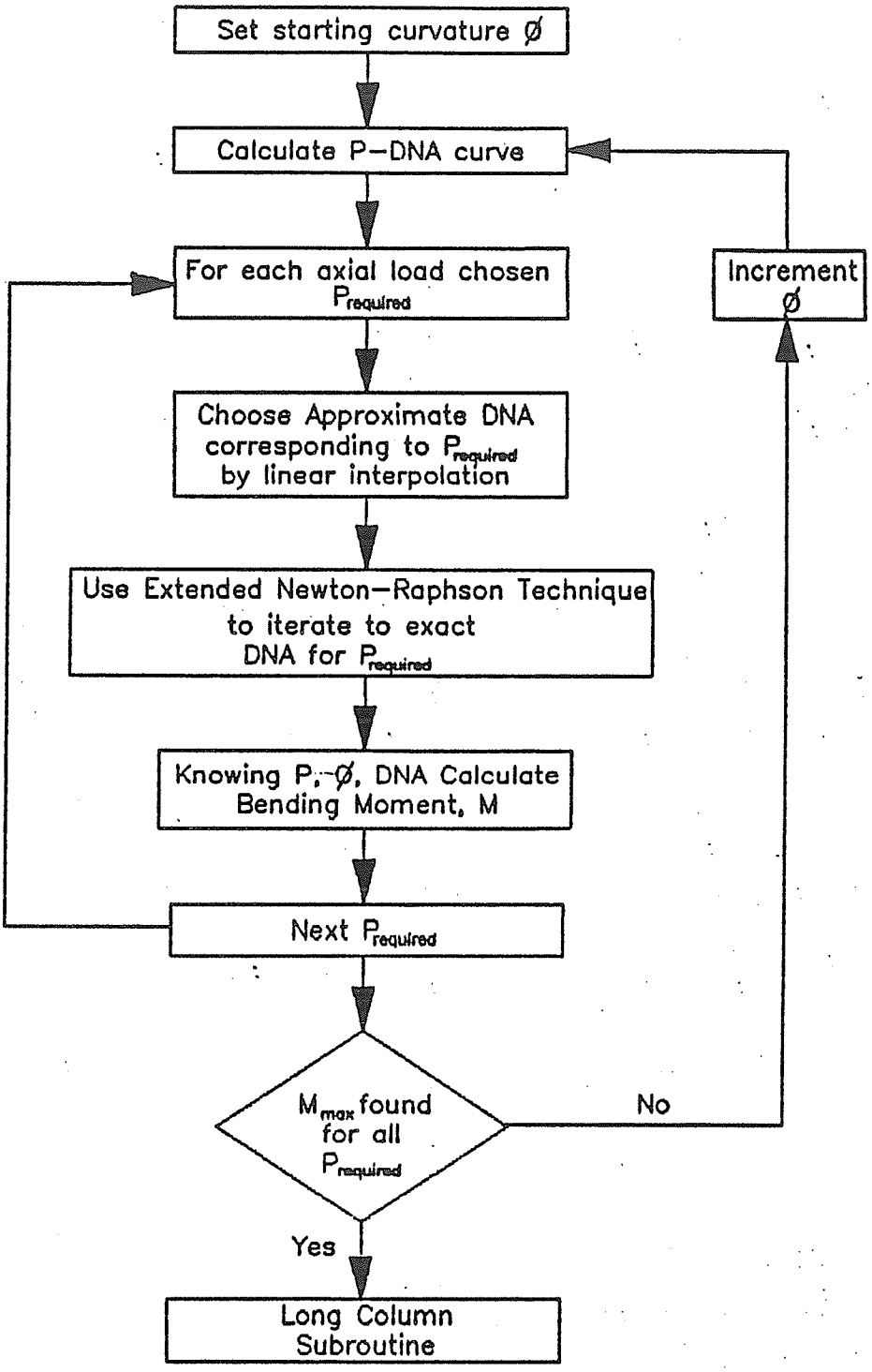

Figure 2.7 – Flow Chart of Calculation of M–∅–P Relationship for Composite Cross–Section

increment was increased to 10 and then to 100 times the original increment for only the cases in which strain-hardening of steel at low axial forces was considered.

At very high curvature values, it is theoretically possible that the tension flange of the rolled steel section may fracture. The strain in the tension flange of the steel section is monitored at each curvature increment. If rupture of the tension flange is imminent, no further points are calculated for that axial load level.

When the moment versus curvature diagrams have been completed for all axial load values to be considered, the maximum bending moment for each axial load level is stored. These bending moments paired with the corresponding axial loads form the $P-M$ interaction diagram. If the column has an input length greater than zero, the program proceeds to the slender column subroutine. If a cross-sectional study is all that is required, an input length equal to zero will make the computer return to the main program without executing the slender column subroutine.

2.5 SLENDER BEAM-COLUMN STRENGTH MODEL

A beam-column, due to its length, has less strength than its cross-sectional strength. When an eccentric axial load is applied to the beam-column, the transverse deflection of the column increases the effective eccentricity of the load at all points along the length. Therefore, the maximum end moment is controlled by the transverse deflection of the

column and the effective eccentricity at the point of maximum deflection. The purpose of the slender beam-column strength model is to calculate the maximum end moment corresponding to a particular axial load in order to construct the slender beam-column $P-M$ interaction diagram.

In this study, the maximum deflection occurs at the mid-height of the beam-column due to the assumption of equal end moments and single curvature as shown in Figure 2.8. For a beam-column to be stable, the internal and external forces acting on it must be in equilibrium at every section along its length. This condition yields an equilibrium deflected shape for a given combination of axial load and end eccentricity. Increasing the end eccentricity causes greater deflections and thus greater effective eccentricities until failure of the material at mid-height causes the collapse of the column. The maximum bending moment acting at the ends prior to collapse of the column subjected to a given axial load is the long column bending moment capacity.

Two methods to calculate the maximum end eccentricity and, hence, maximum end moment have been developed by Basu (1967) and Basu and Hill (1968) as previously discussed in Section 2.1 for the type of beam-column studied in this thesis. The numerical integration method (Basu and Hill 1968) requires that the column length be divided into a number of nodes or stations. Equilibrium must be satisfied at each node. This is achieved by iterating the deflection at each

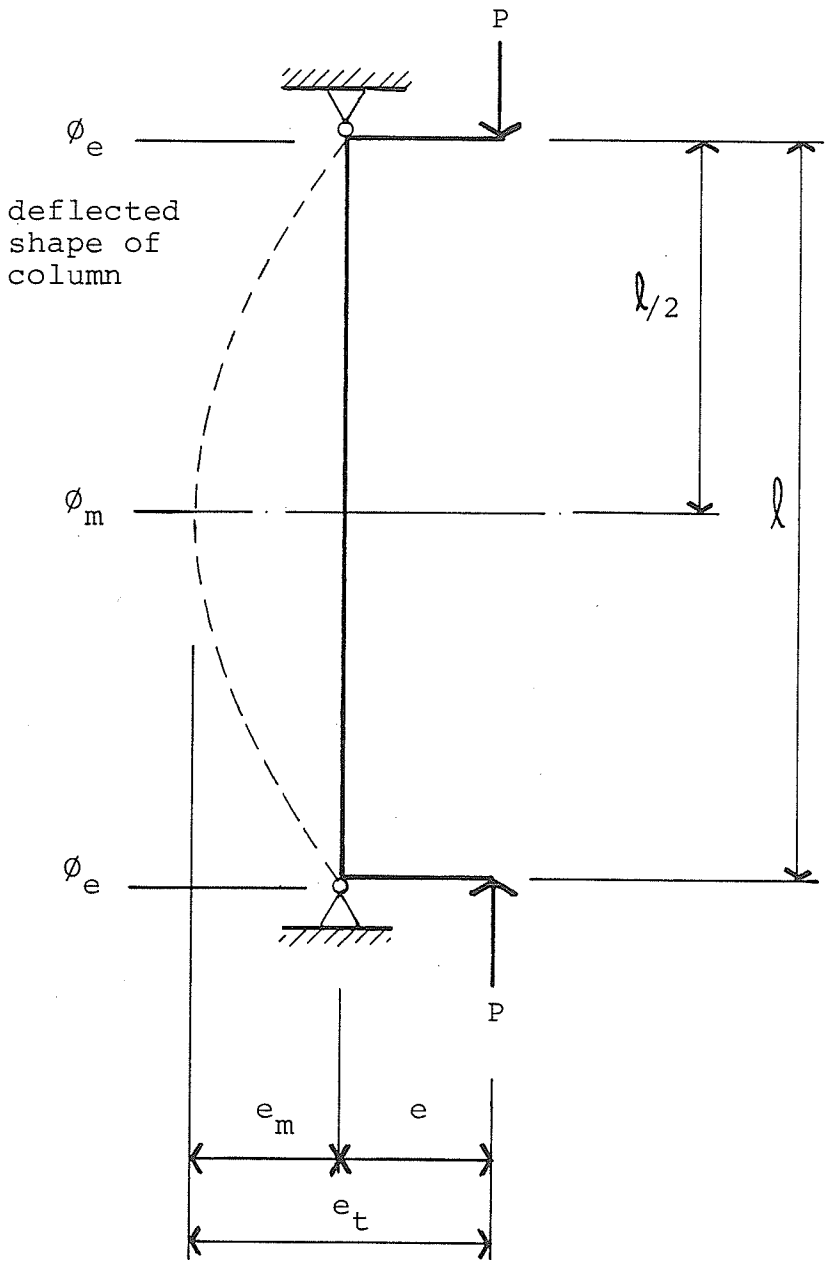

Figure 2.8 - Deflected Shape of Slender Composite Beam-Column under Eccentric Axial Load

station until all stations are in equilibrium, yielding an equilibrium deflected shape. Increasing the number of stations improves the accuracy of the solution but also increases computing time required. For the approximate method (Basu 1967), the equilibrium deflected shape is assumed to follow the shape of a part cosine curve. The deflection at the mid-height of the column can then be estimated quickly by simply solving a single equation. In both methods, an end eccentricity is assumed, a deflected shape is found and the cross-section is checked at the point of maximum deflection to check whether failure has taken place. If failure has not occurred, then the end eccentricity is increased and the process is repeated. The largest end eccentricity before failure at the point of maximum deflection is used to calculate the maximum end bending moment for the beam-column at that axial load level. The approximate method was found to calculate column capacities up to 5 percent more conservative than the numerical integration method (Basu and Hill 1968). Basu's approximate method (1967) with some modifications was used in this study. These modifications are discussed in detail in this section.

As for the case of the cross-sectional study (Section 2.4), the first requirement for creating the slender beam-column $P-M$ interaction diagram is calculation of the concentric axial load capacity. The tangent modulus theory was used to calculate this load. The tangent modulus method has

been used by Wakayabashi (1976) for his composite design proposals and is also recommended by Basu (1967) for initially straight columns.

Previous analytical studies of composite columns (Basu 1967, Basu and Hill 1968, Virdi and Dowling 1973) assumed an initial out-of-straightness of the composite column. Basu and Hill (1968) showed concentric axial load reductions of 3 to 30 percent for length to overall depth ratios of 10 to 40, respectively, when initial out-of-straightness was considered. Basu assumed an initial out-of-straightness at mid-height of the column equal to $0.00006l^2/d$, where l is the length of the column and d is the depth of the steel section, which was meant to estimate both the effect of initial out-of-straightness and the effect of residual stresses in the steel section on the column strength. This method assumes initial mid-height deflections of the steel section greatly in excess of allowable tolerances in North America.

Virdi and Dowling (1973) compared the effect of assuming no imperfections, residual stresses only, out-of-straightness of $l/1000$, residual stresses plus an assumed out of straightness of $l/1000$, and the use of only an assumed out-of-straightness of $0.00006l^2/d$ as assumed by Basu. Assuming no imperfections showed the highest strengths and the use of Basu's assumptions the lowest strengths, especially for long columns. The differences between an assumption of residual stresses only and residual

stresses with an initial out-of-straightness of $l/1000$ were very slight. The residual stress only assumption averaged a 2.6 percent greater capacity than that when residual stresses were combined with the initial deflection of $l/1000$ for the 9 columns tested by Virdi and Dowling (1973) over a number of biaxial eccentricities. These results show that assuming an initially straight column will not be in serious error, as long as residual stresses are accounted for.

The assumption of initial out-of-straightness made by the authors mentioned above considered the entire composite cross-section to have an initial out-of-straightness. Wakayabashi (1976) recognized that while the steel shape may be assumed to have initial camber, the concrete encasement is likely to be constructed straight. Since the concrete encasement gives lateral support to the steel section, he argued that the effect of the initial camber of the steel section would be negligible.

To exactly account for the geometry of the beam-column as described by Wakayabashi (1976), the program would have had to be able to be capable of calculating the strength of cross-sections symmetric about the minor axis only, since the cross-section geometry with respect to the major axis would change at every point along the length of the beam-column. This would greatly increase the complexity and computing time as $M-\phi-P$ relations would have to be calculated for a number of different sections along the column height.

Due to the small effect reported by Virdi and Dowling (1973) of initial out-of-straightness of $l/1000$ for the entire composite cross-section and the fact that the concrete encasement is not likely to be subjected to significant initial out-of-straightness, it was decided not to assume any initial camber of the steel section for this study. This assumption also allows the use of the tangent modulus theory, which cannot be correctly applied to columns that are not perfectly straight.

The concentric axial capacity of a long column is dependant on the buckling strength of the column and not the material strength as is the case for the cross-section. This means the column fails by buckling before the material strength is exceeded. The ultimate buckling stress for a column of homogeneous material is given by the tangent buckling formula:

$$f_{cr} = \frac{\pi^2 E_t}{(kl/r)^2} \tag{2.3}$$

Substituting the value of 1.0 for the effective length factor k and recalling that the radius of gyration, r, can be calculated as the square root of the moment of inertia divided by the area ($\sqrt{I/A}$), Equation 2.3 can be rewritten as:

$$f_{cr} A = \frac{\pi^2}{l^2} E_t I \qquad (2.4)$$

The column buckling load, P_{cr}, is equal to either side of Equation 2.4 and may be calculated directly.

Since a composite column is made up of materials with 6 independent stress-strain curves, Equation 2.4 is not directly applicable. Instead, Equation 2.4 was applied independently to each individual material and the sum of the tangent buckling strength for all materials gave the column tangent buckling load. This procedure is comparable to that proposed by Wakayabayshi (1976). Hence, Equation 2.4 can be modified to account for the six independent materials:

$$\sum_{i=1}^{i=6} (f_{cr_i} A_i) = \frac{\pi^2}{l^2} \sum_{i=1}^{i=6} (E_{t_i} I_i) \qquad (2.5)$$

The buckling load, P_{cr}, which simultaneously satisfies both sides of Equation 2.5 is the composite column buckling load capacity (maximum concentric axial load). Equation 2.5 cannot be solved directly since the tangent elastic modulus of an element is a function of the stress in the element. Therefore, an iterative solution was used. The axial strain of the column was adjusted until the difference in buckling load calculated by each side of Equation 2.5 is less than 1

pound (4.45 N). This established the point on the slender column $P-M$ interaction curve corresponding to maximum concentric load and zero bending moment.

To establish the points of the beam column $P-M$ interaction curve due to eccentric loading, a modified version of the approximate method of Basu (1967) was used. For each axial load level investigated less than the slender column concentric axial load capacity for which the cross-section $M-\phi-P$ relationship was previously calculated (Section 2.4), a maximum end eccentricity was sought. The method for calculating the maximum end eccentricity (and, hence, maximum end bending moment) can be described as follows:

(a) assume a mid-height deflection of the column;

(b) find the end curvature which corresponds to the desired deflected shape;

(c) find the bending moment corresponding to the end curvature from the cross-section $M-\phi-P$ relationships and calculate the end eccentricity;

(d) add the end eccentricity to the assumed mid-height deflection and calculate a new bending moment at the mid-height of the column; and

(e) if the bending moment calculated in (d) is less than the maximum bending moment from the cross-section $M-\phi-P$ relationship, increase the mid-height deflection and

repeat the process starting from item (a). If the bending moment calculated in (d) is greater than the maximum bending moment from the cross-section $M-\phi-P$ relationship, the previous end eccentricity calculated in item (d) is used to compute the maximum end bending moment.

Basu (1967) and Basu and Hill (1968) used a part cosine curve for the assumed deflected shape of the composite column and showed this method was only slightly more conservative than the numerical integration method with a maximum difference of only 5 percent. Quast (1970) studied the deflected shape of pin-ended reinforced concrete columns uniaxially loaded in single curvature. After comparing a number of theoretical deflected shapes, including a part cosine curve, against more elaborate and time consuming numerical integration techniques he concluded that the best approximation of the deflected shape was a 4th order parabola with the mid-height deflection given by Equation 2.6.

$$e_m = \frac{l^2}{10}\left(\Phi_m + \frac{\Phi_e}{4}\right) \tag{2.6}$$

where ϕ_m and ϕ_e are the curvatures at mid-height and the column ends, respectively; l is the length of the column; and e_m is the mid-height deflection of the column as shown in Figure 2.8.

Quast found that this deflected shape produced a maximum unconservative error of 2 percent and a maximum conservative error of 6 percent. The reinforced concrete columns he simulated had eccentricity ratios of between 0.1 and 1.0 with l/h ratios of 0 to 60.

Mirza and MacGregor (1989) used Quast's method of approximating the deflected shape to study the strength variability of reinforced concrete columns. Bolin (1985) tested an earlier version of the present analytical program with both approximations and found that in general both assumptions returned similar results, with Basu's assumption being slightly more conservative. In consideration of the above, Quast's approximation to the deflected shape of the beam-column was used in this study.

The total mid-height eccentricity e_t is the sum of the assumed mid-height deflection e_m from Equation 2.6 and the end eccentricity e as shown in Equation 2.7.

$$e_t = e + e_m \tag{2.7}$$

Substitution of Equation 2.6 into 2.7 and rearranging to solve for the end eccentricity yields Equation 2.8.

$$e = e_t - \left(\frac{l^2}{10}\right)\left(\Phi_m + \frac{\Phi_e}{4}\right) \tag{2.8}$$

The mid-height eccentricity e_t can be calculated by dividing the mid-height bending moment by the axial load as shown in Equation 2.9.

$$e_t = \frac{M_m}{P} \tag{2.9}$$

Substitution of Equation 2.9 into 2.8 gives the simple relationship between the end eccentricity (e), mid-height moment (M_m) , the mid-height curvature (ϕ_m) and the end curvature (ϕ_e) shown in Equation 2.10.

$$e = \left(\frac{M_m}{P}\right) - \left(\frac{l^2}{10}\right)\left(\Phi_m + \frac{\Phi_e}{4}\right) \tag{2.10}$$

The program uses Equation 2.10 and the cross-section $M-\phi-P$ relations previously calculated to solve for a combination of end eccentricity, mid-height deflection and mid-height curvature in equilibrium. Figure 2.9 outlines

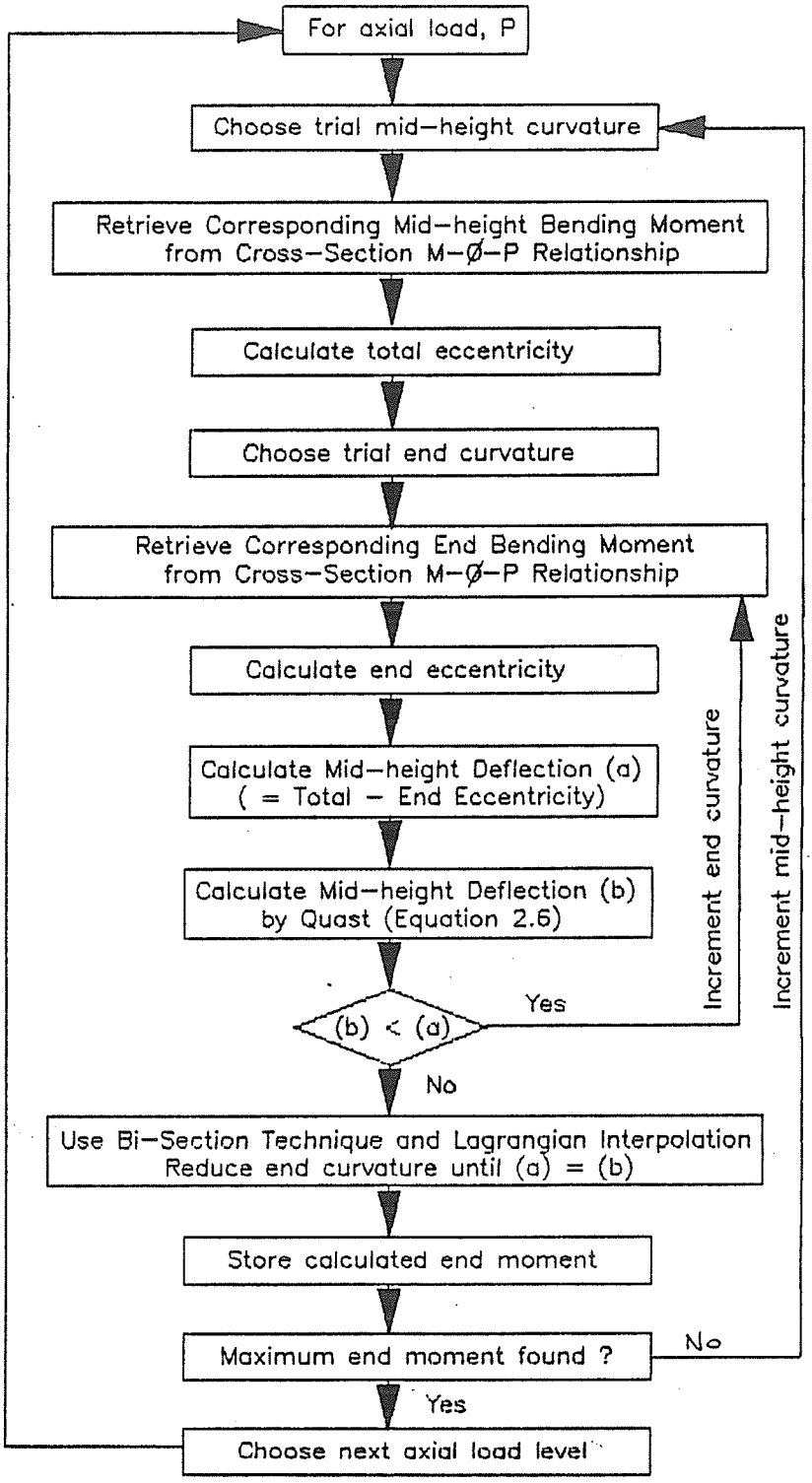

Figure 2.9 – Flowchart for Calculating Slender Column M-Ø-P Relationship

the procedure. Values for the mid-height curvature are incremented from a minimum value until a maximum end bending moment is calculated. For each mid-height curvature value assumed, values of the end curvature are tested and incremented from a minimum until an equilibrium combination is found. The largest curvature that can be attained at mid-height is the one that corresponds to the maximum moment from the $M-\phi-P$ diagram for the axial load. Once all possible mid-height curvatures have been investigated, the largest end bending moment calculated becomes one point on the slender beam-column $P-M$ interaction curve. The process is then repeated to complete the entire slender beam-column $P-M$ interaction curve.

2.6 STRESS-STRAIN CURVES FOR CONCRETE

As outlined in Section 2.3, three distinct concrete areas have been assumed in the discretization of the composite column cross-section. These distinctions are meant to account for dissimilarities in the stress-strain relationship of the concrete due to confining action of the vertical reinforcing bars, the rectangular lateral ties and the rolled steel section. Confinement of concrete increases the compressive strength and ductility of concrete in reinforced concrete columns and methods to compute its effect on the stress-strain relationship have been developed by Park, Priestly and Gill (1982), Sheikh and Uzumeri (1982), Sheikh and Yeh (1986), Mander et al. (1988). Confinement effects

on the compressive strength of concrete in composite columns were not considered by any of the previous studies on composite columns reviewed in Section 2.1. Compressive stress-strain curve characteristics for different degrees of concrete confinement are given in Sections 2.6.1, 2.6.2, and 2.6.3. The effect of confinement on the tensile stress-strain relationship of concrete is not available in the literature searched. It was, therefore, decided to assume identical tensile stress-strain relations for all types of concrete confinements. A discussion of the tensile strength of concrete is given in Section 2.6.4. Finally, all stress-strain curves used for concrete are summarized in Section 2.6.5. It should be noted that the stress-strain relations presented in this chapter are based on static loading conditions.

2.6.1 Unconfined Concrete

The two curves considered of interest for describing the stress-strain characteristics of the compressive strength of unconfined concrete are those of Hognestad (1951) and Kent and Park (1971).

The Hognestad curve (Figure 2.10) consists of a second order parabola from the origin to the peak stress. The strain at peak stress is a function of the initial tangent modulus and the concrete strength. Beyond the peak stress the curve descends linearly to a stress of 85 percent of the peak stress at a strain of 0.0038. The equations describing

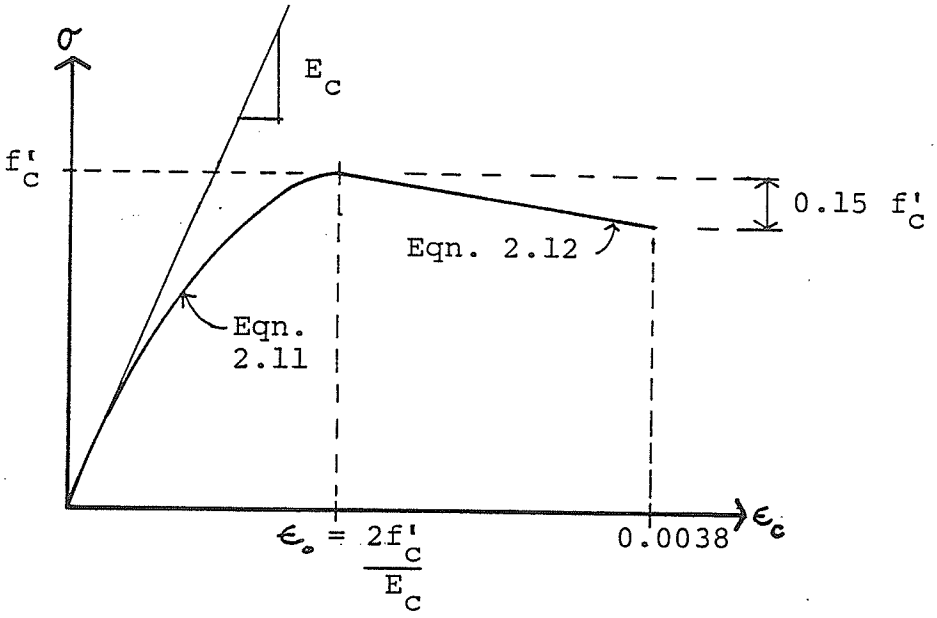

Figure 2.10 - Hognestad (1951) Stress-Strain Relationship for Unconfined Concrete

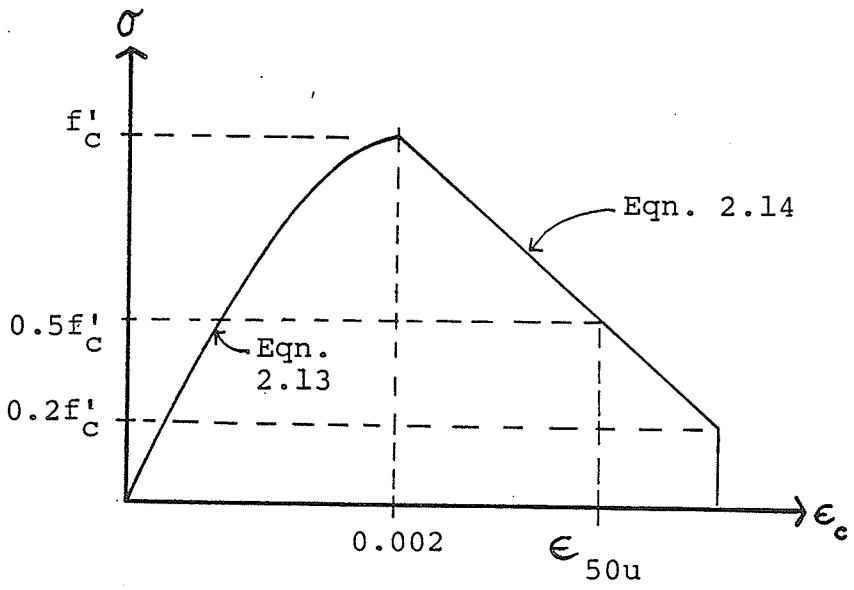

Figure 2.11 - Kent and Park (1971) Stress-Strain Relationship for Unconfined Concrete

the portion of the curve between the origin and the peak stress and between the peak stress and the stress corresponding to the ultimate strain are given in Equations 2.11 and 2.12, respectively.

$$f_c = f'_c \left[\frac{2\epsilon_c}{\epsilon_0} - \left(\frac{\epsilon_c}{\epsilon_0} \right)^2 \right] \qquad (2.11)$$

$$f_c = f'_c - \left[\frac{\epsilon_c - \epsilon_0}{0.0038 - \epsilon_0} \right] 0.15 f'_c \qquad (2.12)$$

where $\epsilon_0 = \frac{2f'_c}{E_c}$

The Kent and Park curve (Figure 2.11) is similar to the Hognestad curve except that the strain at peak stress is set at a value of 0.002. The descending branch is linear and assumed to fall from the peak stress to a value of 20 percent of the peak stress. The slope of the descending branch is a function of the concrete strength with lower strength concrete modelled to be less brittle. The equations describing the portion of the curve between the origin and the peak stress and between the peak stress and the stress corresponding to the ultimate strain are given in Equations 2.13 and 2.14, respectively.

$$f_c = f'_c \left[\frac{2\epsilon_c}{0.002} - \left(\frac{\epsilon_c}{0.002} \right)^2 \right] \qquad (2.13)$$

$$f_c = f'_c \left[1 - Z \left(\epsilon_c - 0.002 \right) \right] \qquad (2.14)$$

where $Z = \dfrac{0.5}{\epsilon_{50u} - 0.002}$

and $\epsilon_{50u} = \dfrac{3 + 0.002 f'_c}{f'_c - 1000}$

For SI conversion replace 3 by 0.0207 MPa and 1000 by 6.895 MPa.

Llewellyn (1986) compared results of using the stress-strain curves by Hognestad and Kent and Park. Essentially, no difference was found in the results obtained from the two stress-strain curves. However, the Hognestad curve occasionally produced higher strength for unconfined concrete than that obtained for confined concrete based on modified Kent and Park confined concrete stress-strain curve (Section 2.6.2). The Kent and Park curve for unconfined concrete presented no such conflict for obvious reasons.

The Kent and Park curve for unconfined concrete was used for the stress-strain curve adopted in this study. Two modifications were made. First, the strain at peak stress was

allowed to vary as a function of the concrete strength, similar to the method of the Hognestad curve as shown in Equation 2.15.

$$\epsilon_0 = \frac{2f'_c}{E_c} \qquad (2.15)$$

The second modification was to assume that the concrete loses all strength at a strain of 0.004. This assumption has previously been used by Park, Priestly and Gill (1982) to model the spalling off of the concrete cover. The stress-strain curve used in the theoretical analysis of this study for the unconfined compressive strength of concrete is shown in Figure 2.12.

2.6.2 Partially Confined Concrete

Confinement enhances the strength and ductility of concrete. Past efforts to model the behavior of the confined concrete core of reinforced concrete columns reinforced with rectangular hoops are summarized by Sheikh (1982) and Mander (1983). In a reinforced concrete column, the concrete core strains both axially and transversely under loading. As loading progresses, the transverse strains cause hoop tension in the horizontal ties. The horizontal ties thus contribute passive confinement to the core. The vertical

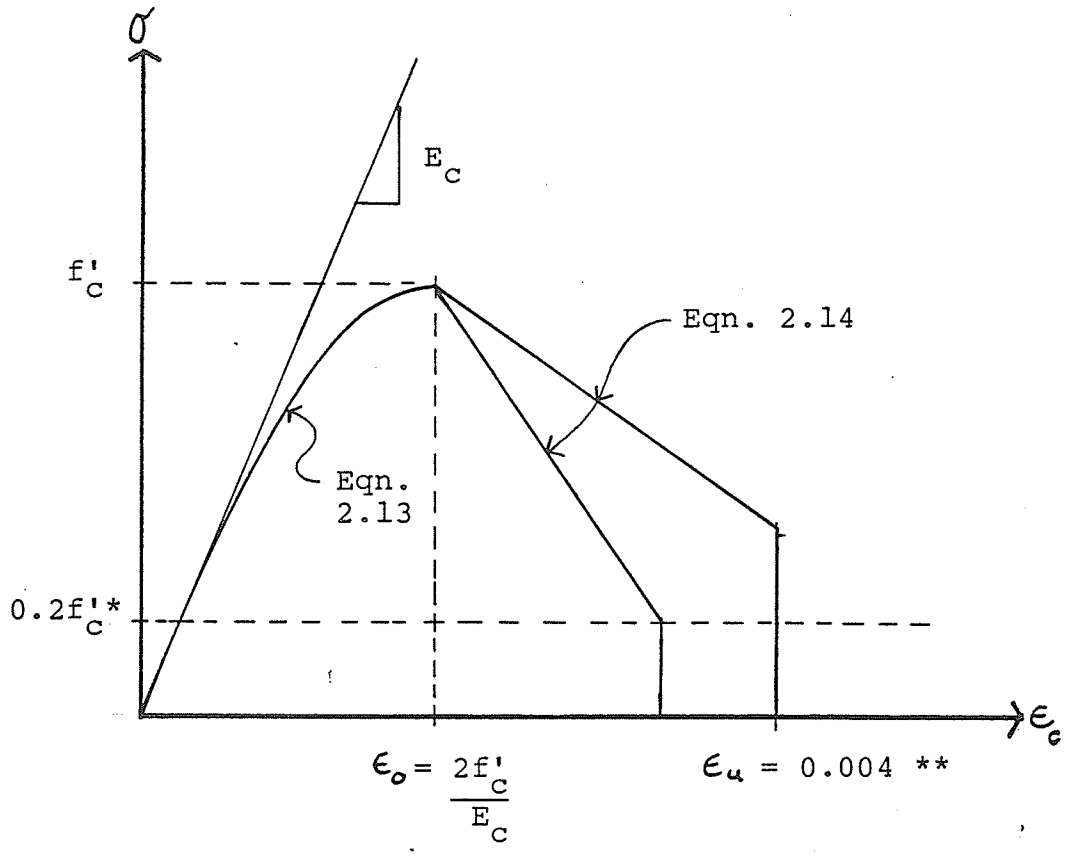

* minimum concrete stress

** maximum compressive concrete strain

Figure 2.12 - Unconfined Concrete Compressive Stress-Strain Relationship used in Theoretical Strength Subroutine

reinforcing similarly confines the core since the vertical bars are prevented from bowing out by the horizontal ties (Park and Paulay 1975).

Confinement of the core concrete in a composite steel-concrete column is expected to occur in a similar fashion. In addition, the component plates of the structural steel shape inside the core provide additional confinement. Wakayabashi (1976) recognized that stress-strain relations of concrete may differ depending on its location in the composite section. He did not, however, try to incorporate these differences into his proposed design procedure.

To account for enhancement of strength and ductility of the concrete core, two stress-strain relations were considered. The Modified Kent and Park Curve (Park, Priestly and Gill 1982) and the Sheikh - Uzumeri Curve (1982) were both developed for the confined cores of reinforced concrete columns. Since no model directly applicable to composite columns was found in the literature searched, these two curves were investigated for their compatibility and accuracy to the composite column. A third method proposed by Mander et al. (1988) was briefly reviewed but not considered for adoption since a significant amount of work for this thesis had been completed by the time the Mander paper was published.

The Modified Kent and Park Curve is a modification of an earlier Kent and Park Curve for concrete confined by rectangular hoops (Kent Park 1971). The original version of the

curve allowed an increase in the ductility of the confined concrete but not an increase in strength. Later tests on column specimens by Park, Priestley and Gill (1982) quantified the increase in concrete strength which was included into the stress-strain relationship. The degree of confinement is a function of the vertical spacing of horizontal ties, the ratio of volume of horizontal ties to volume of concrete core and the yield strength of the horizontal ties. Increasing the confinement increases both the concrete strength and the ductility. The Modified Kent and Park stress-strain curve for concrete confined by rectangular hoops is shown in Figure 2.13. Equation 2.16 describes the portion of the curve between the origin and the peak stress. Equation 2.17 describes the descending branch of the curve.

$$f_c = K f'_c \left[\frac{2\epsilon_c}{0.002K} - \left(\frac{\epsilon_c}{0.002K} \right)^2 \right] \qquad (2.16)$$

where $K = 1 + \frac{\rho_s f_{yh}}{f'_c}$

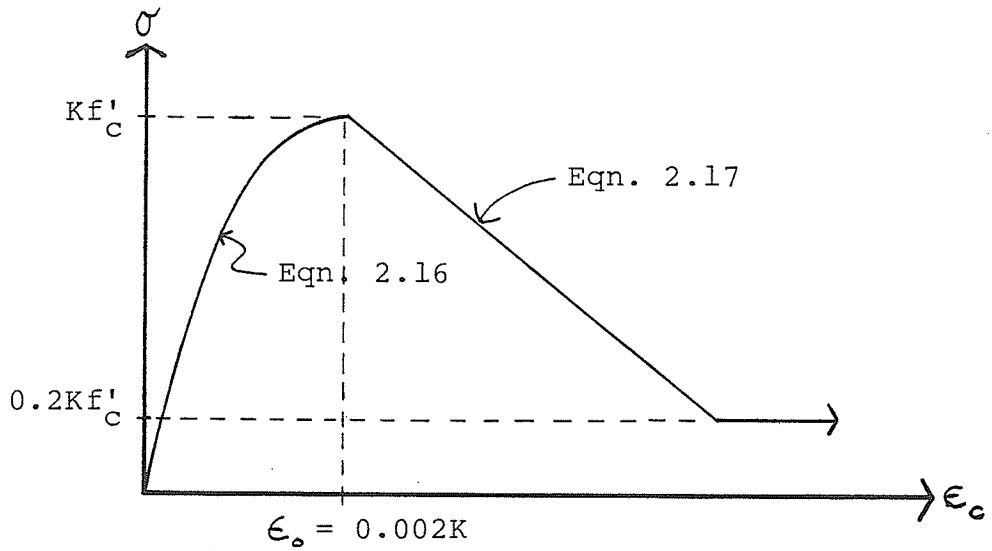

Figure 2.13 - Modified Kent and Park Stress-Strain Relationship for Concrete Confined by Rectangular Ties (Park, Priestley and Gill 1982)

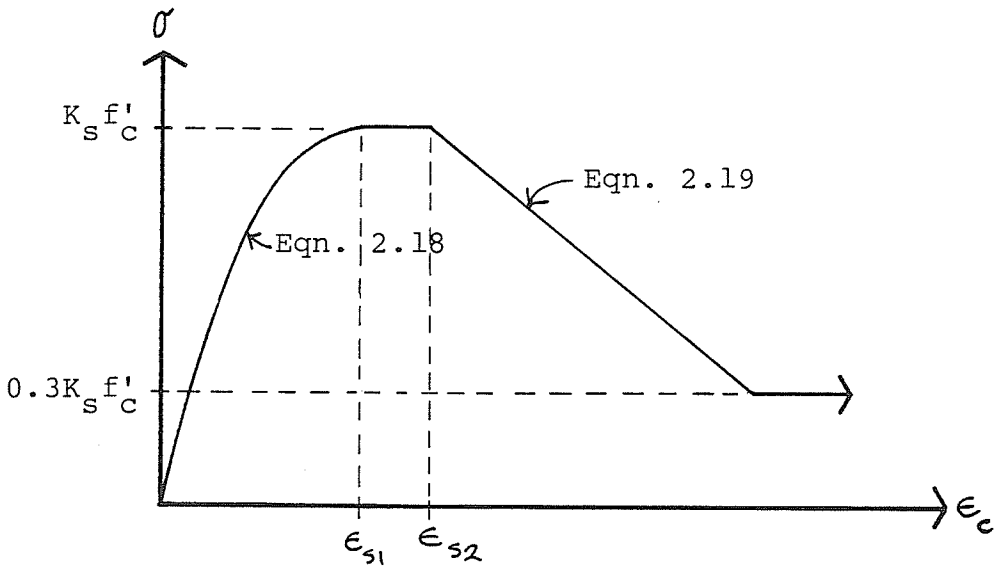

Figure 2.14 - Sheikh-Uzumeri (1982) Stress-Strain Relationship for Concrete Confined by Rectangular Ties

$$f_c = Kf'_c\,[1 - Z(\epsilon_c - 0.002K)] \geq 0.2Kf'_c \qquad (2.17)$$

where $$Z = \frac{0.5}{\epsilon_{50u} + \epsilon_{50h} - 0.002K}$$

and $$\epsilon_{50u} = \frac{3 + 0.002f'_c}{f'_c - 1000}$$

and $$\epsilon_{50h} = \frac{3}{4}\rho_s\sqrt{\frac{h''}{s_h}}$$

In the above Equations f'_c is the concrete cylinder strength, ρ_s is the ratio of volume of lateral ties to volume of concrete contained within the lateral ties, f_{yh} is the yield stress of the lateral hoops, h'' is the out to out width of the lateral hoops and s_h is the spacing of the lateral hoops. For SI conversion replace 3 and 1000 by 0.0207 MPa and 6.895 MPa respectively, for computing ϵ_{50u}.

Further tests by Scott, Park and Priestley (1982) showed that at high strain rates the enhancement of the core strength by the confinement was further increased. They conservatively chose a factor of 1.25 to account for the gain in strength in a confined core due to high strain rates. The tests also demonstrated an increase in the slope of the descending branch of the stress-strain curve. An increase of 1.25 in the slope of the descending branch was attributed to the high strain rate. This may result in a slight reduction in total ductility. The study described in this thesis involves short term loading, but the rate of

loading is assumed to be slow enough that dynamic effects are negligible (i.e. quasi-static). This will lead to conservative description of strength if the results of this study are used for dynamic loads. The tests by Scott et al. (1982) also indicated that presence of a strain gradient increased the ductility of the confined core, but the effect was not quantified.

The Sheikh - Uzumeri curve (1982) was developed from their earlier experimental tests of reinforced concrete columns (1980). The development of their analytical model recognized the importance of tie spacing, volumetric ratio of tie steel to concrete core, and tie yield strength to the degree of confinement of the core. They also found that the configuration of the vertical bars in the cross-section and the way they were tied to the horizontal hoops was also a factor. The Sheikh - Uzumeri (1982) curve describing the stress-strain relation of concrete confined by rectangular hoops is shown in Figure 2.14. Equation 2.18 describes the portion of the curve between the origin and the peak stress and Equation 2.19 describes the descending branch.

$$f_c = K_s f_c' \left[\frac{2\epsilon_c}{\epsilon_{00}} - \left(\frac{\epsilon_c}{\epsilon_{00}} \right)^2 \right] \qquad (2.18)$$

where $$K_s = 1.0 + \frac{2.73B^2}{P_{occ}} \left[\left(1 - \frac{nC^2}{5.5B^2} \right) \left(1 - \frac{s}{2B} \right)^2 \right] \sqrt{\rho_s f_s'}$$

$$f_c = K_s f_c' \left[1 - Z(\epsilon_c - \epsilon_{00})\right] \qquad (2.19)$$

where $Z = \dfrac{0.5}{\frac{3}{4}\rho_s\sqrt{B/s}}$

The Sheikh and Uzumeri (1982) curve partly accounts for the increase in ductility by assuming a horizontal plateau in the curve from the strain at peak stress to the start of the descending branch as shown in Figure 2.14. The minimum strain corresponding to the maximum stress ϵ_{s1} and the maximum strain corresponding to the maximum stress ϵ_{s2} are given by Equations 2.20 and 2.21, respectively.

$$\epsilon_{s1} = 0.55 K_s f'_c \times 10^{-6} \qquad 2.20$$

$$\epsilon_{s2} = \epsilon_{00}\left(1 + \frac{0.81}{C}\left(1 - 5.0\left(\frac{s}{B}\right)^2\right)\frac{\rho_s f'_s}{\sqrt{f'_c}}\right) \qquad 2.21$$

In Equations 2.18 to 2.21 ϵ_{00} = strain in plain concrete at maximum compressive stress; B = core concrete width measured to the center line of the lateral tie; C = the clear distance between laterally supported longitudinal reinforcing bars; P_{occ} = the area of core concrete multiplied the compressive strength of plain concrete; n = number of laterally supported longitudinal reinforcing bars; s = spacing of

lateral ties; ρ_s = ratio of volume of lateral ties to volume of core concrete and, f'_s = stress in lateral ties. Linear dimensions are in inches and stresses are in ksi.

Sheikh and Yeh (1986) confirmed an earlier finding by Park, Priestley and Gill (1982) that ductility of the confined concrete core increased when a strain gradient (i.e. a bending moment) was present. The strain gradient did not increase the maximum strength of the core concrete. For simplicity, the effect of strain gradient on the stress-strain relationship of partially confined concrete was neglected.

In order to decide which of the stress-strain curves best suited the theoretical analysis of composite columns reported in this study, three criteria were examined. These are:

1. Suzuki et al. (1983) provided the results from a series of tests conducted on composite column specimens similar to those chosen for this thesis. The ratio of structural steel section to gross column section was 3 percent for the LH series and 6 percent for the RH series. The volumetric ratio of lateral ties to concrete core varied from 0.6 to 3 percent. All specimens were concentrically loaded. By applying the stress-strain curve assumptions for the steel portion of the cross-section, as described in this thesis, the stress-strain curves for the concrete portions were computed. The method of determining the column strength

attributable to the core and to that of the cover was based on the work of Moehle and Cavanagh (1985). The core strength curves were compared to predictions made by both the Modified Kent and Park and the Sheikh - Uzumeri curves. The Modified Kent and Park curve better predicted the peak strength of the RH series while the Sheikh and Uzumeri curve was found to better predict the strength of the LH series. Strain at peak stress was estimated better by the Sheikh - Uzumeri curve. Both curves estimated greater ductility than the data indicated in most instances, although the shape of the descending branch was basically accurate. Since the results were inconclusive, further investigation was done to establish which of the stress-strain curves would be better suited for composite columns.

2. Calibration of the computer model against physical test results is described in Section 2.9. Before final calibration, the two confined concrete stress-strain curves were compared with some of the experimental data to investigate which one gave the more accurate predictions. Only the specimens with length to overall depth ratio less than 6.6 were used for this purpose. Both stress-strain curves produced about the same results. The results are shown in Table 2.1.

3. In Section 2.6.1, it was stated that the Kent and Park model (1971) was used to describe the stress-strain characteristics of the unconfined concrete. Since the Modified

Table 2.1 – Comparison of Strength Ratios*
Calculated using Modified Kent and Park and Sheikh and Uzumeri
Stress-Strain Relations for Concrete Confined by
Rectangular Lateral Ties

Stress-strain Curve Used (1)	Mean Value (2)	Coefficient of Variation (3)
Modified Kent and Park **	1.026	0.0763
Sheikh-Uzumeri (1982)	1.029	0.0767

*Based on all columns with $\ell/h \leq 6.6$ in Table 2.3

** (Park et al. 1982)

Kent and Park curve uses the Kent and Park (1971) model as a starting point, there is apparently no possibility of an overlap between the two models. The Sheikh - Uzumeri (1982) model for partially confined concrete was compared to the Kent and Park (1971) model for unconfined concrete for some of the test specimens discussed in Section 2.9. It was found that in some cases, the Sheikh - Uzumeri model for partially confined concrete predicted a lower initial tangent elastic modulus (Figure 2.15) than the Kent and Park model for unconfined concrete. It was also found that, in some cases, the slope of the descending branch of the Sheikh - Uzumeri curve for partially confined concrete was so steep that its strength was less than that of the unconfined concrete, with a strain at peak stress significantly less than that of the unconfined concrete. This behavior has been neither documented nor expected.

In order to maintain compatibility between the stress-strain curves of the unconfined and confined portions of the concrete, it was decided to use the Modified Kent and Park curve (Park, Priestley and Gill 1982) to model the partially confined portion of the concrete in the composite cross-section. As discussed in Section 2.6.1, the strain at peak stress was allowed to vary as a function of the initial elastic modulus of the concrete (Equation 2.15). The

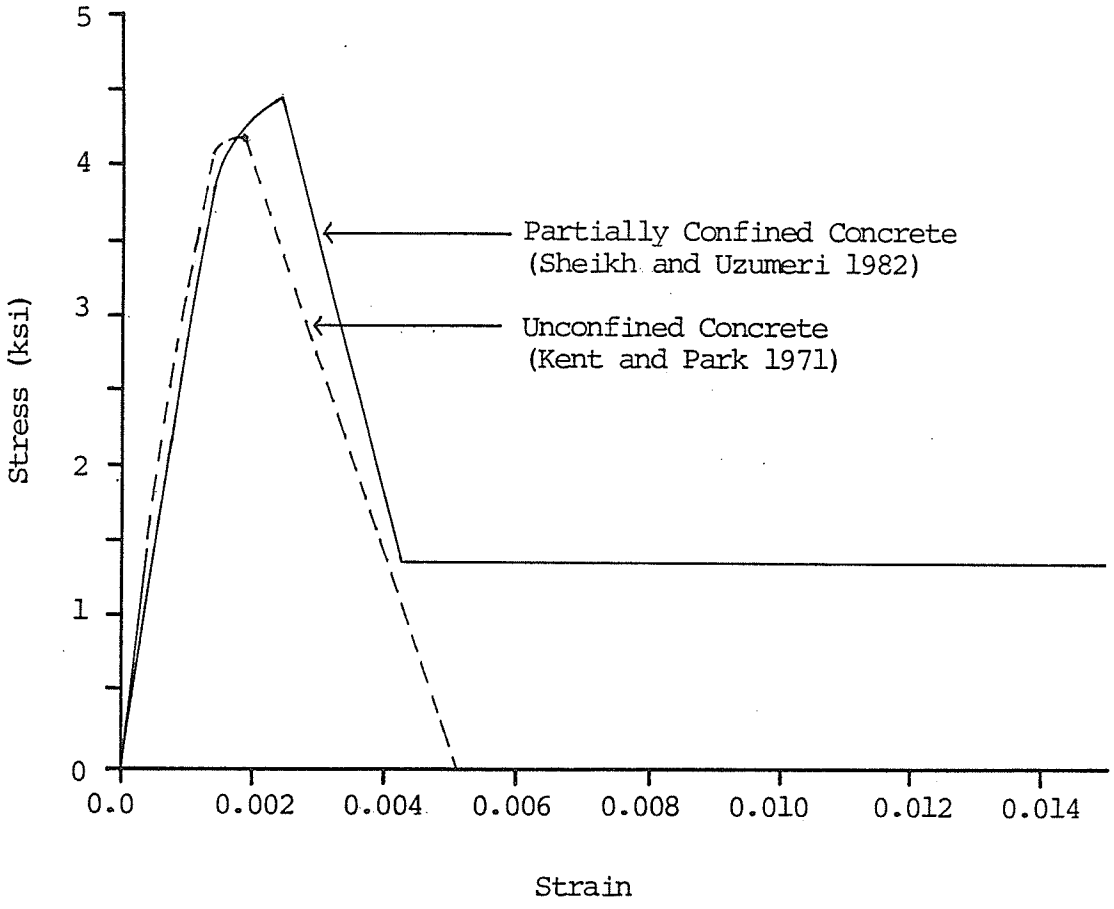

Figure 2.15 - Comparison of Unconfined and Partially Confined Concrete Compressive Stress-Strain Relationships for Column LH-100-B (Table 2.3)

stress-strain curve used in the theoretical analysis for the compressive strength of partially confined concrete is shown in Figure 2.16.

2.6.3 Heavily Confined Concrete

In the previous discussion of partially confined concrete it was noted that an increase in the amount of confinement provided to the core is accompanied by an increase in concrete strength and ductility. Both the Sheikh - Uzumeri and the Modified Kent and Park models increase both concrete strength and ductility when confinement is increased. In this study, a portion of the concrete between the flanges of the structural steel section has been assumed to be heavily confined as indicated in Figure 2.2. This area is confined by the rolled steel section on three sides and by the partially confined concrete and lateral ties on the fourth side. It is reasonable to assume that the concrete in this area is under a higher degree of confinement than the concrete outside the influence of the flanges. To account for this higher confinement, the concrete in this area has been assumed to follow the same stress-strain relationship as the partially confined concrete (Modified Kent and Park model in Figure 2.16), but does not have a descending branch. The concrete stress is assumed to remain at the peak stress throughout all strains past the strain at which the peak stress was first attained. Since the peak stress is predicted from a model for concrete confined by

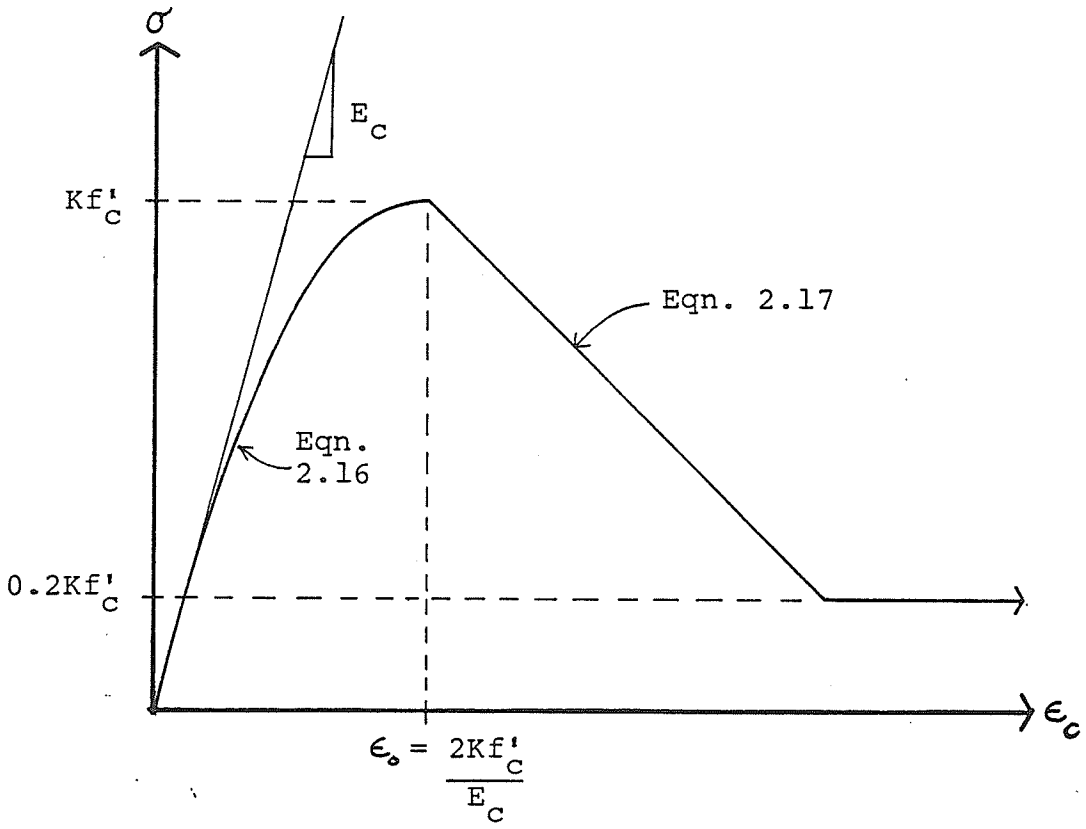

Figure 2.16 - Partially Confined Concrete Compressive Stress-Strain Relationship used in Theoretical Strength Subroutine

rectangular hoops, the prediction for the heavily confined concrete peak stress is expected to be on the conservative side. The assumed stress-strain curve for heavily confined concrete is shown in Figure 2.17.

2.6.4 Tensile Stress-Strain Relationship Of Concrete

Park and Paulay (1975) state that the tensile stress-strain relationship of concrete may be assumed to be linear up to the tensile strength (i.e. modulus of rupture) with a modulus of elasticity equal to the modulus of elasticity in compression. The tensile stress beyond the peak stress is assumed to be zero. The assumption of equal initial modulus of elasticity for tension and compression was also suggested by Mirza et al. (1979c). This stress-strain relationship was used by Mirza and MacGregor (1989) for reinforced concrete columns.

Recent work on this subject has focused on the shape of the stress-strain curve after the peak tensile stress is reached. Hwang and Rizkalla (1983), Carreira and Chu (1986) and Zhen-hai and Xiu-qin (1987) all report a descending branch to the tensile stress-strain curve after the peak stress. In all cases the stress drops sharply at strains beyond the strain at peak stress, retaining only a small percentage of the peak strength at larger strains.

LaChance and Hays (1980) assumed that the relationship between concrete tensile stress and strain was a continuation of a polynomial curve describing the entire stress-

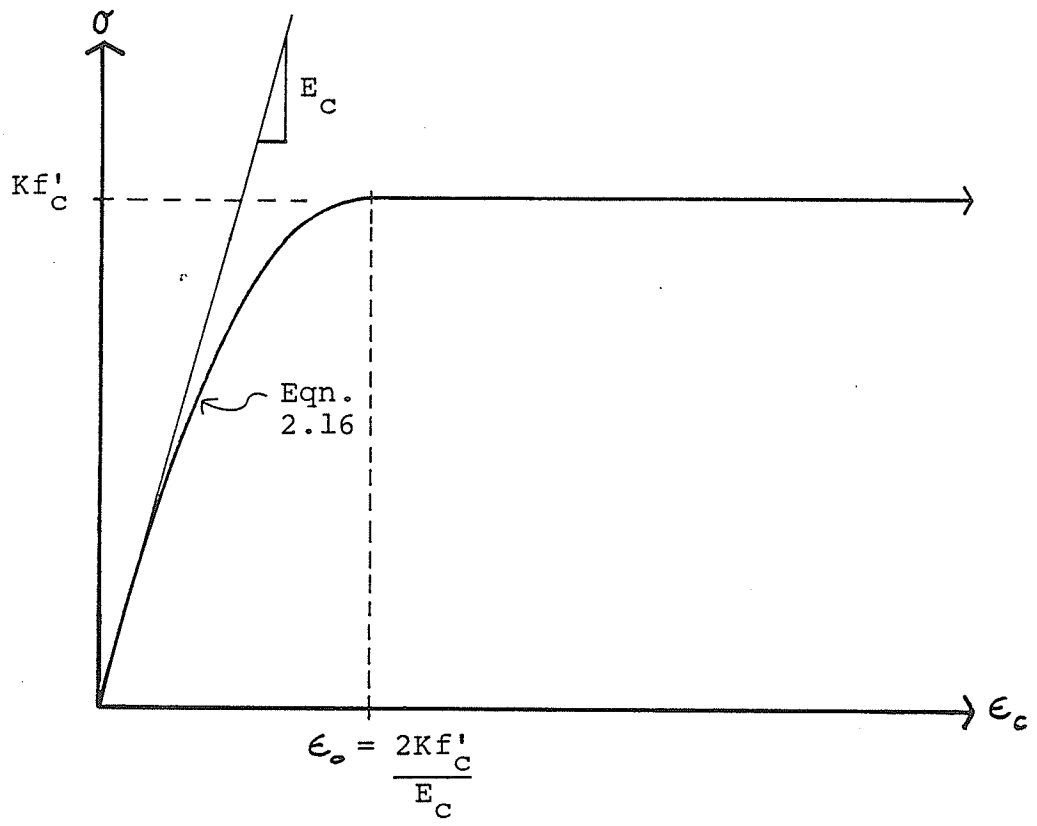

Figure 2.17 - Heavily Confined Concrete Compressive Stress-Strain Relationship used in Theoretical Strength Subroutine

strain relationship both in tension and compression. The peak tensile stress was assumed to be 10 percent of the specified concrete cylinder strength and the ultimate tensile strain was set at 0.000125 for 5000 psi (34.5 MPa) concrete. The peak stress and the ultimate strain were assumed to occur at the same point. They found that this assumption added only 0.01 percent to the strength of a composite column cross-section as opposed to ignoring it all together.

For simplicity, it was assumed in this study that the tensile portion of the concrete stress-strain curve is as suggested by Park and Paulay (1975) and by Mirza and MacGregor (1989). The work of LaChance and Hays (1980) suggests that the contribution of concrete tensile strength to the overall column strength is so small that it could be considered negligible and, therefore, a simple model was considered to be sufficient. The assumed stress-strain curve for the tensile strength of concrete is shown in Figure 2.18.

2.6.5 Summary Of Stress-Strain Relationships For Concrete

In this study, the stress-strain relationship for unconfined concrete was based on the Kent and Park (1971) curve with slight modifications, the major difference being that the strain at peak stress was assumed to be a function of the modulus of elasticity and the strength of the concrete (Equation 2.15) instead of being a constant value. The portion of the composite section considered unconfined is the

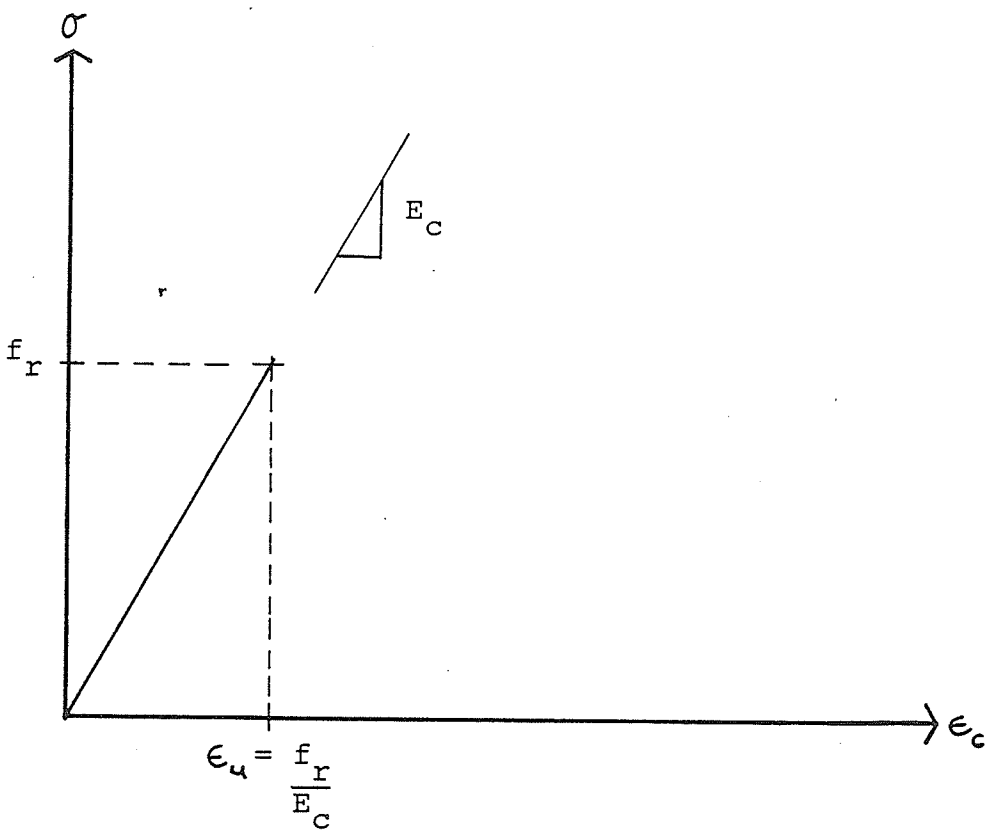

Figure 2.18 - Concrete Tensile Stress-Strain Relationship used in Theoretical Strength Subroutine

concrete outside the perimeter of the lateral ties. The Modified Kent and Park curve (Park, Priestley and Gill 1982) was used to model the partially confined concrete. However, the strain at the peak stress was calculated as noted above. Partially confined concrete is considered to be within the lateral ties but outside the confining influence of the steel section flanges. The Modified Kent and Park curve was also used to model the heavily confined concrete between the flanges except that the peak stress was assumed to be maintained at all strains beyond the strain at which the peak stress was first attained. The concrete areas of the composite cross-section assumed to be unconfined, partially confined and heavily confined are shown in Figure 2.2. The assumed stress-strain curves for unconfined, partially confined and heavily confined concrete are shown in Figures 2.12, 2.16 and 2.17, respectively.

The stress-strain curve of the tensile strength of concrete is shown in Figure 2.18. The stress-strain relationship was assumed to be linear from the origin to the modulus of rupture. The modulus of elasticity for tension is assumed to be equal to the compressive modulus of elasticity.

2.7 STRESS-STRAIN CURVES FOR STEEL

Two types of steel are used in the composite cross-section. These are the rolled structural steel shape and the reinforcing bars. The assumptions regarding the shape

of the stress-strain curve are similar for both materials. The differences occur because different variables are used to define the stress-strain curve for each type of steel. It was assumed that the stress-strain curves for all steel components were identical in tension and compression. This assumption is consistent with previous works reviewed in Section 2.1. The variables for which the data were available to define the stress-strain curves for the rolled steel section and for the reinforcing steel are given in Section 2.7.1 and 2.7.2, respectively.

2.7.1 Structural Steel

The stress-strain curve used for structural steel was assumed to be bilinear to the onset of strain-hardening. From the origin to the attainment of the yield stress, stress was assumed proportional to strain according to Hooke's law. Between the attainment of the yield stress and the onset of strain hardening the stress was assumed to be constant at the yield stress level. The strain-hardening portion of the curve is assumed to be a second order parabola. The slope of the strain-hardening portion of the stress-strain curve at the ultimate strain was assumed to be equal to zero. The variables used to define the entire stress-strain curve are the elastic modulus E_s, the yield stress f_{ys}, the strain at onset of strain hardening ϵ_{sstrn}, the initial tangent slope of the strain hardening curve E_{sstrn} and the ultimate stress f_{us}. The yield strain ϵ_{ys} and ultimate

strain ϵ_{us} are calculated by the program. The schematic stress-strain curve for structural steel is shown in Figure 2.19.

The curve used is similar to what has been assumed in previous studies. Basu (1967) and Wakayabashi (1976) assumed a slight curvature at the transition from the elastic to the plastic condition. Only LaChance and Hays (1980) and Virdi and Dowling (1982) considered the strain-hardening portion of the curve. LaChance and Hays (1980) used a non-linear curve similar to a parabola. Virdi and Dowling (1982) assumed a linear strain-hardening portion to the stress-strain curve.

2.7.2 Reinforcing Steel

The shape of the stress-strain curve used for reinforcing steel is virtually identical to that used for structural steel. The difference is in the variables which must be specified to establish the stress-strain curve. The modulus of elasticity E_r, the yield stress f_{yr}, the strain at onset of strain hardening ϵ_{rstrn}, the ultimate stress f_{ur} and the ultimate strain ϵ_{ur} must all be specified. The slope of the initial tangent to the strain hardening curve E_{rstrn} is calculated by the program, as is the yield strain ϵ_{yr}. The schematic stress-strain curve for reinforcing bars is shown in Figure 2.20.

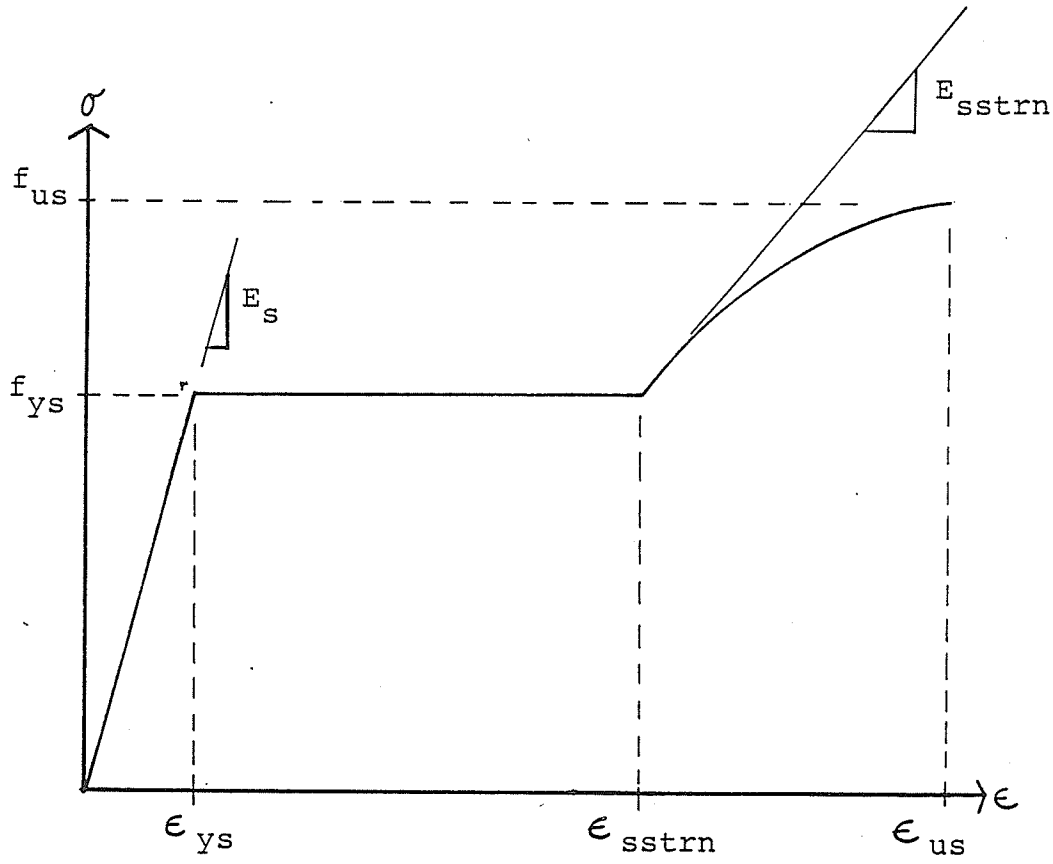

Figure 2.19 - Structural Steel Stress-Strain Relationship in Tension or Compression used in Theoretical Strength Subroutine

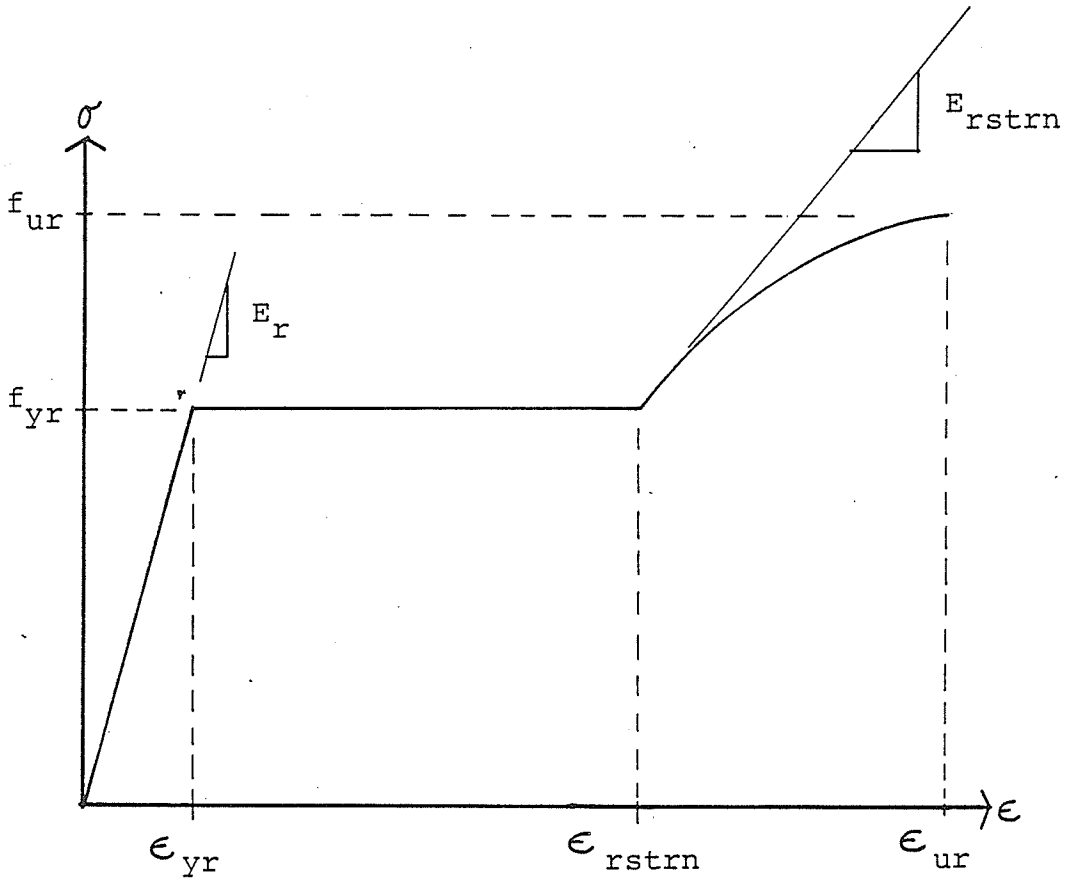

Figure 2.20 - Reinforcing Steel Stress-Strain Relationship in Tension or Compression used in Theoretical Strength Subroutine

The differences in the specified variables required for structural steel and reinforcing steel is due solely to the information available in the literature for these steels. Hardly any useful data was found on the ultimate strain of structural steel. However, some data was available for reinforcing steel ultimate strain (Allan 1972). Galambos and Ravindra (1978) published data on the initial strain-hardening modulus for structural steel. No similar data was available for reinforcing steel. Thus, the structural steel stress-strain curve required that the initial strain-hardening modulus be specified in order to calculate the ultimate strain. For reinforcing bars, the ultimate strain is specified in order to calculate the initial strain-hardening modulus.

2.8 RESIDUAL STRESSES IN ROLLED STRUCTURAL STEEL

Residual stresses form in rolled structural steel members due to uneven cooling of their component parts during the manufacturing process. Parts cooling first resist contraction and become stressed in compression. Parts cooling last become stressed in tension in order to maintain equilibrium. Heat treating can reduce the magnitude of the stresses but is usually not done. Residual stresses in composite columns, the various theories for predicting their magnitude and distribution and how they were accounted for in this study are discussed in this section.

LaChance and Hays (1980) stated that residual stresses in the structural steel had no effect on the ultimate strength of composite cross-sections. Virdi and Dowling (1973) reported that, in some cases, residual stresses may enhance the strength of beam-columns. Mirza (1989) found that residual stresses were detrimental to the composite beam-column strength at end eccentricity ratios less than 1.0 but could have a beneficial effect for larger end eccentricity ratios. Beedle and Tall (1960) reported that residual stresses reduced the strength of concentrically loaded bare steel columns.

It is evident that the effect of residual stresses on the strength of a composite beam-column can vary significantly and, therefore, was accounted for in this study.

Alpsten (1968) used a time-stepped finite difference technique to simulate the cooling of a rolled structural steel shape as it is manufactured. By modelling the rate of cooling of the component parts of the rolled shape he was able to accurately duplicate measured values. To do this, the cooling and manufacturing history of the shape had to be known. Alpsten demonstrated how factors such as restrictions to heat flow affected the residual stresses and their distribution. Alpsten stated that, in general, the flange tips and mid-depth of the web will have a compressive residual stress and that the juncture of the flange and web will have a tensile residual stress. If the rolled shapes are

placed on the cooling table in such a manner that the webs are prevented from cooling quickly, the mid-depth of the web will be in tension instead of compression.

Measured values of residual stresses have a high variation especially at the mid-depth of the web (Alpsten 1968). These variations are due to different cooling rates and manufacturing processes. After a rolled shape has cooled, it often has to be straightened by rollers or by "gagging" (mechanical bending). This process usually reduces the residual stresses at a cross-section but since all cross-sections are not treated in the same manner, this should not be considered to increase the overall strength of the steel section (Alpsten 1968). Alpsten also found that the residual stresses varied considerably across the depth of very thick flanges [3 inch (75 mm) thick]. Thinner flanges showed little variation.

The flange thicknesses used in this study were less than 1.5 inch (38 mm). Therefore, residual stresses across the depth of the flange were assumed constant. The residual stresses were assumed identical at every section along the length of the beam-column with no allowance for reductions due to mechanical straightening. Alpsten's method of calculating the residual stresses requires knowledge of the specific manufacturing process a structural shape is subjected

to and, therefore, is not applicable to a general study where the structural shapes are drawn from several manufacturers.

Several schemes have been proposed in the literature to model the distribution and magnitude of residual stresses in rolled I-shapes. Of these, two models are of interest. Both models assume compressive residual stresses at the flange tips and tensile stresses at the juncture of the flange and web. One model assumes compressive stresses at the mid-depth of the web [Figure 2.21(a)] while the other model assumes tensile stresses [Figure 2.21(b)]. The distribution of the residual stresses between these points is assumed either linear or parabolic, as indicated on Figures 2.21(a) and 2.21(b).

LaChance and Hays (1980) tried both models described above but gave no details of the assumed distribution or magnitude of the residual stresses. Trahair and Kitipornchai (1972) studied inelastic buckling of steel I-shaped beams and used a distribution similar to Figure 2.21(a). A magnitude of 50 percent of the steel yield stress for the residual stress at the flange tips (compression), 30 percent at the juncture of the flange and the web (tension) and 30 percent at the mid-depth of the web (compression) was assumed. Nethercot (1974) also studied lateral buckling of steel I-shaped beams. He examined how the different assumptions of residual stress magnitude and distribution affected

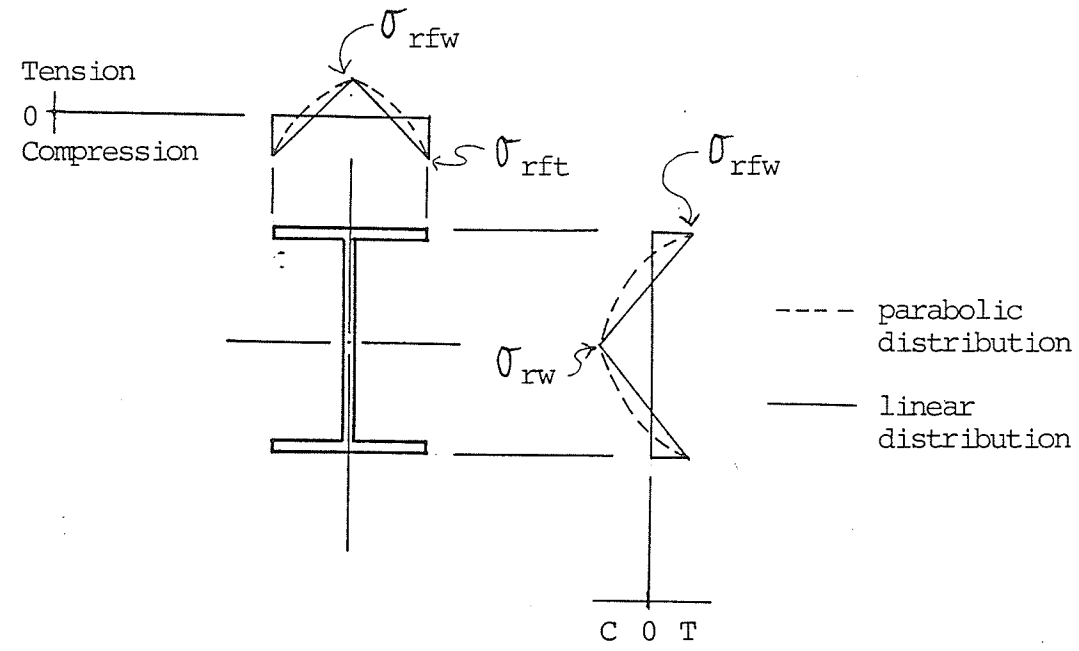

(a) Residual Stresses in Flange and Web (Young 1971)

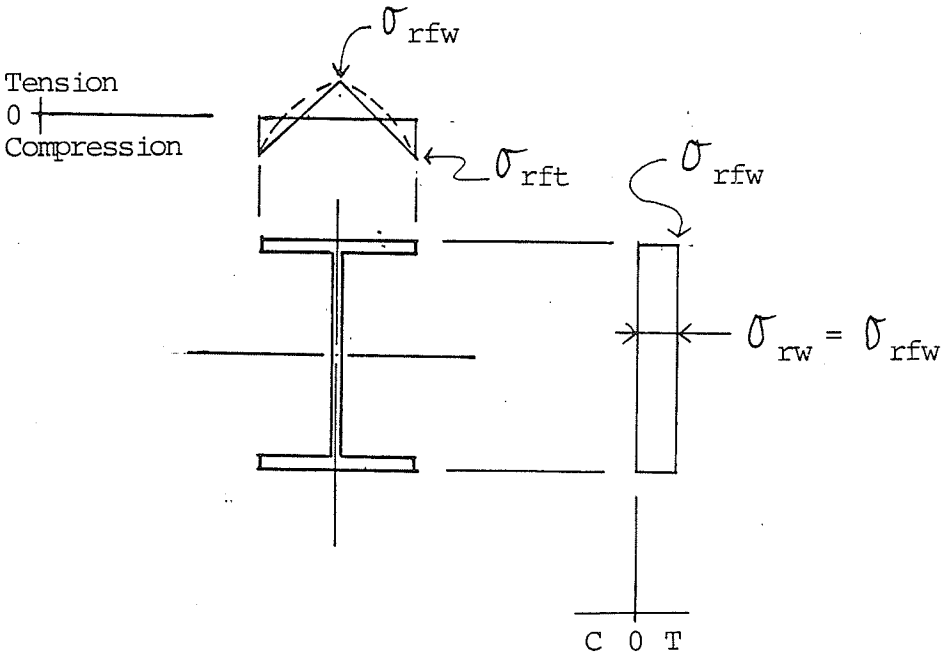

(b) Residual Stresses in Flange and Web (Galambos 1963)

Figure 2.21 - Residual Stresses in Wide Flange Shapes

the ratio of experimental to calculated bending moment capacity. He compared the distributions of Galambos (1963), Massey (1964), and Young (1971). Poorest correlation was found with the distribution by Massey. This was expected since Massey's distribution, which was based on test results of Australian rolled joist sections, assumed that the flanges were entirely in uniform tension and the web in uniform compression with a short linear transition assumed at each end of the web. Because of this very different residual stress distribution and the results reported by Nethercot (1974), Massey's model was not investigated any further. The models from Galambos (1963), Young (1971) and Trahair and Kitipornchai (1972) were examined further and are discussed below.

Galambos (1963) proposed a residual stress distribution based on measurements of American I-shapes, mostly used as columns. The distribution he proposed is shown in Figure 2.21(b). The magnitude of the residual stress at the flange tip was assumed to be 30 percent of the yield strength for mild steel. The residual stress at the juncture of the flange and web was assumed equal to the stress at the mid-depth of the web. The residual stress at the mid-depth of the web was calculated as a function of the residual stress at the flange tip and the geometry of the section. The residual stress in the web (σ_{rw}) is given by Equation 2.22.

$$\sigma_{rw} = \sigma_{rft} \left[\frac{bt}{bt + w\ (d - 2t)} \right] \qquad (2.22)$$

In Equation 2.22 σ_{rft} is the residual stress at the tip of the flanges, b is the flange width, t is the flange thickness, w is the web thickness and d is the depth of the structural steel shape.

Nethercot (1974) found that use of the Galambos' (1963) distribution (also known as Lehigh distribution) consistently gave conservative results in his analysis of I-beams.

Young (1971) collected previously published data on residual stress measurements and measured residual stresses in British beam and column shapes manufactured from mild steel. His proposed distribution is shown in Figure 2.21(a). The residual stresses at the flange tip, at the flange-web juncture and at the mid-depth of the web are all calculated as functions of the geometry of the section. The distribution of stress between these points is described by a polynomial. Young's equations for the residual stresses at the flange tip, at the juncture of the flange and web; and at the mid-depth of the flange are given by Equations 2.23, 2.24 and 2.25 respectively.

$$\sigma_{rft} = -165 \left(\frac{1 - A_w}{1.2 A_f} \right) \text{ MPa} \qquad (2.23)$$

$$\sigma_{rfw} = 100 \left(0.7 + \frac{A_w}{A_f} \right) \text{ MPa} \qquad (2.24)$$

$$\sigma_{rw} = -100 \left(1.5 + \frac{A_w}{1.2 A_f} \right) \text{ MPa} \qquad (2.25)$$

In the above Equations σ_{rft} is the residual stress at the flange tips, σ_{rfw} is the residual stress at the juncture of the flange and web, σ_{rw} is the residual stress at the mid-depth of the web, A_w is the area of the web and A_f is the area of one flange of the steel section.

Young (1971) also suggested that since his proposals were based on geometric considerations, they would be applicable to various grades of steel and not limited to mild steel.

Nethercot (1974) concluded that the use of Young's model provided a reasonably accurate method of incorporating residual stresses into the analysis of the moment capacity of beams failing by lateral buckling. He also found that the predictions of bending moment capacity were accurate and nearly identical when the Young's model and the Alpsten's (1968) finite difference technique were used to predict the residual stresses. Nethercot further concluded that correct prediction of the magnitude of the residual stresses at the

flange tips and the juncture of the flange and web was more important than the actual stress distribution assumed (i.e. linear or non-linear distribution).

Beedle and Tall (1960) reported measurements of residual stresses in various American mild steel sections. Stresses were found to vary significantly at each cross-section tested along the length of a member. Distributions similar to both those in Figures 2.21(a) and 2.21(b) were found. Attempts to correlate the dimensions of the test section sizes and the residual stresses were unsuccessful. However, it was found that the residual stresses in the flange influenced column strength to a greater degree than the residual stresses in the web.

Average magnitudes of measured residual stress at the flange tip and at the juncture of the flange and web were estimated from Figure 1 of Beedle and Tall (1960) for the nine steel section sizes included in that figure. These measured averages were compared against estimates made using the models of Trahair and Kitipornchai (1972), Galambos (1963) and Young (1971). The resulting comparison is shown in Table 2.2. Young's (1971) model predicts greater residual stresses at the tip of the flange as the ratio of flange to web area increases as indicated by Table 2.2. The section sizes in Table 2.2 are, therefore, arranged in ascending order of flange to web area for simplicity of comparisons.

Table 2.2 - Comparison of Measured and Calculated Residual Stresses in W Shapes

Shape	$\frac{A_f}{A_w}$	Residual Stresses (ksi)									
		Measured Values		Calculated Values							
		Beedle and Tall (1960)		Proposed Model		Young (1971)		Galambos (1963)		Trahair & Kitipornchai (1972)	
		*	**	*	**	*	**	*	**	*	**
(1)	(2)	(3)	(4)	(5)	(6)	(7)	(8)	(9)	(10)	(11)	(12)
36W150	1.038	-10.0	12.0	-4.72	1.64	-4.72	24.12	-10.2	3.53	-17.0	10.2
14W43	2.054	-10.0	18.0	-14.22	7.46	-14.22	17.21	-10.2	5.35	-17.0	10.2
12W50	2.373	-8.0	10.0	-15.52	8.72	-15.52	16.26	-10.2	5.73	-17.0	10.2
4W13	2.724	-12.0	4.0	-16.60	9.80	-16.60	15.47	-10.2	6.02	-17.0	10.2
8W24	2.758	-15.0	-4.0	-16.70	9.98	-16.70	15.41	-10.2	6.10	-17.0	10.2
12W65	3.170	-15.0	14.0	-17.64	11.12	-17.64	14.72	-10.2	6.43	-17.0	10.2
8W31	3.199	-15.0	5.0	-17.67	11.17	-17.69	14.68	-10.2	6.44	-17.0	10.2
8W67	3.672	-8.0	-5.0	-18.50	12.13	-18.50	14.10	-10.2	6.69	-17.0	10.2
14W426	4.283	-20.0	5.0	-19.27	13.14	-19.27	13.54	-10.2	6.96	-17.0	10.2

* Residual stress at flange tips.
** Residual stress at the flange-web juncture.

Note: (+) stands for tension and (-) stands for compression.
1 ksi = 6.895 MPa

The Trahair and Kitipornchai (1972) model is entirely based on the yield strength of the steel and therefore no variation of residual stresses for different shapes is calculated. This results in generally conservative predictions of the residual stresses at the flange tips. The prediction of the residual stress at the flange tip by the Galambos' (1963) model is also based on the yield strength of the steel. In this case the predicted value is often less than the measured value. The Galambos' estimates at the flange-web juncture are not significantly different from the measured data in most cases.

The predictions made using Young's (1971) model provided the best comparison to the flange tip residual stress data reported by Beedle and Tall. A trend of larger flange tip residual stresses as the ratio of flange to web area increases is seen in both the measured (Beedle and Tall 1960) and estimated (Young 1971) values. A trend towards lower tensile stresses at the juncture of the flange and web as the flange to web area increases may be hypothesized by examining the measured data. This trend is followed by the values generated from Young's model as indicated in Table 2.2. However, the Young's estimates for the residual stress at the flange-web juncture are significantly greater than the measured values in most cases.

The yield strength of the steel is not believed to be a major variable in determining the magnitude of residual stresses (Alpsten 1972). The model by Trahair and Kitipornchai (1972) and the flange tip stress prediction of Galambos (1963) are based solely on the yield stress of the material and, therefor, were not considered useful. On the other hand, Young's (1971) model predicts residual stresses based on the dimensional properties of the I-sections as does the flange-web juncture model of Galambos (1963). At the same time, the combination of the Young's model for predicting the residual stress at the flange tip (Equation 2.23) and the Galambos' model for predicting the residual stress at the flange-web juncture (Equation 2.22) provided the best overall prediction to the measured values reported by Beedle and Tall (1960). This combination is defined as the proposed model in Table 2.2 where it is compared with other procedures of computing residual stresses. It was decided to use the combination of the Young and Galambos models (proposed model) to estimate the residual stresses in the rolled steel section of the composite beam-columns investigated in this study. The distribution of residual stresses was assumed to be linear.

The proposed model described above gave the residual stress at the flange tip (Equation 2.23) and at the flange-web juncture (Equation 2.22). The program calculates the

required residual stress at the mid-depth of the web to maintain force equilibrium of the steel section by a trial and error method. The following steps were made:

(a) determine the net force in the flanges due to residual stresses;

(b) determine whether the mid-depth of the web is in tension or compression in order to achieve equilibrium;

(c) calculate the mid-depth residual stress assuming a triangular stress distribution in the web (Figure 2.22(a)(i) or 2.22(b)(i));

(d) if the residual stress computed in (c) exceeds 50 percent of the web yield stress, try a trapezoidal distribution (Figure 2.22(a)(ii) or 2.22(b)(ii)) assuming a value of 50 percent of the web yield stress as the mid-depth stress, incrementing the zone of mid-depth stress to a maximum of 90 percent of the web depth (Figure 2.22(a)(iii) or 2.22(b)(iii)) or until equilibrium is achieved;

(e) if equilibrium is not reached in (d) increase the mid-depth stress by 5 percent of the web yield stress and repeat the trapezoidal distribution.

Item (e) is repeated until equilibrium is achieved. This procedure balanced the residual stresses in the steel shape cross-section before the residual stress in the web reached the yield stress level. The theoretical program can

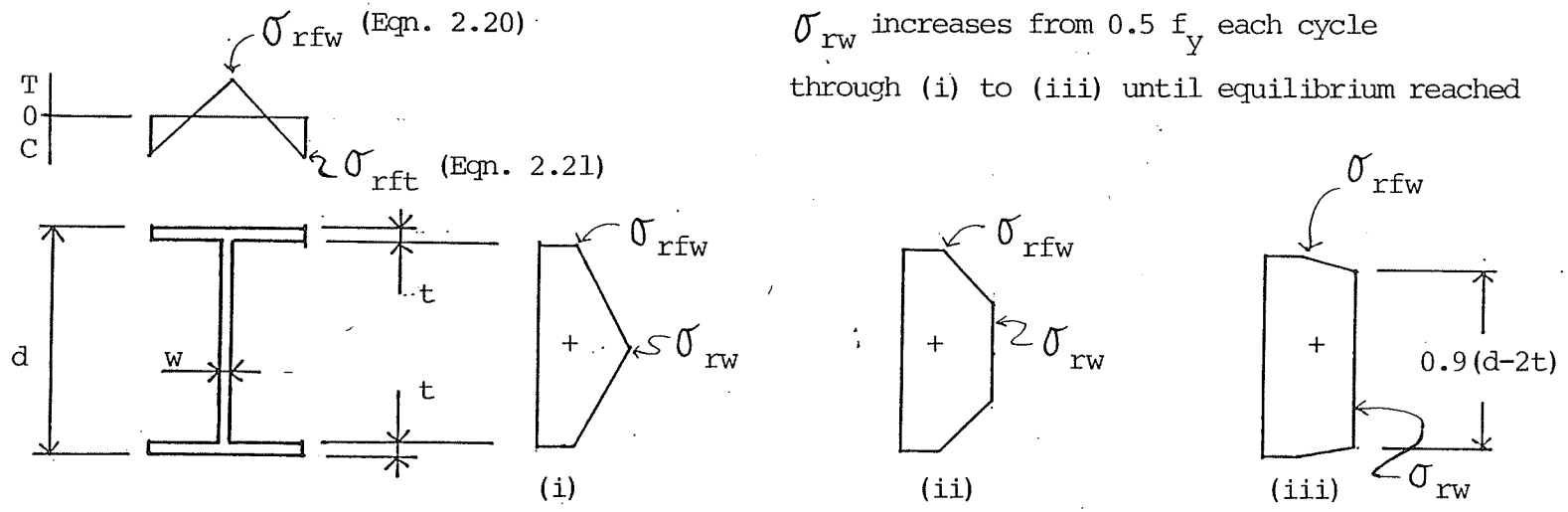

(a) Tensile Residual Stress at Mid-depth of Web (+) indicates tension

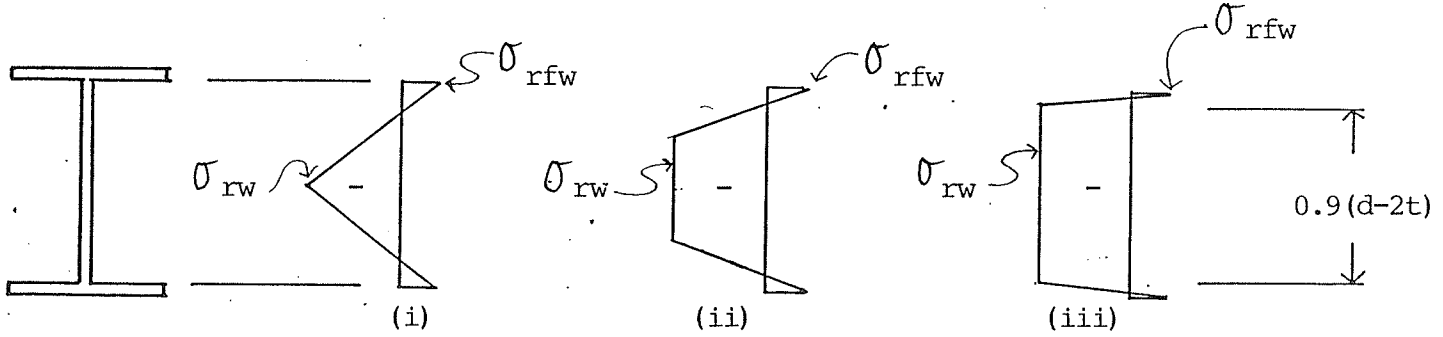

(b) Compressive Residual Stress at Mid-depth of Web (-) indicates compression

Figure 2.22 - Residual Stress Distribution in Wide Flange Steel Shapes
Used in Theoretical Strength Subroutine

be used with or without the above-noted residual stresses in the rolled steel section depending on the specified input option.

2.9 COMPARISON OF EXPERIMENTAL RESULTS TO THEORETICAL MODEL

To check the accuracy of the theoretical model, the ultimate strengths of column physical tests published in the literature were compared to the ultimate strengths predicted by the theoretical subroutine. No new physical tests were conducted for this study. Load cases examined consisted of concentric loads, eccentric loads creating bending moment about the major axis, and pure bending about the major axis. Length to overall depth (l/h) ratios varied from 2.2 to 30.0. The sources of the physical tests and a brief description of the specimen configurations are given in this section. Finally, the comparisons of measured and calculated beam-column strengths are discussed.

Bondale (1966 a, b, c) tested 16 composite column specimens with various configurations. Four of the sixteen tests (RS120.0, RS100.1, RS80.2 and RS60.3) were applicable to this study. Of these, the data for RS120.0 was rejected due to premature failure which was attributed by Bondale to improper placement in the testing apparatus. The specimens consisted of a 4-inch (101.6 mm) deep British RSJ shape, four 0.21-inch (5.3 mm) diameter rods and 0.125-inch (3 mm) diameter rectangular ties spaced at 2 inches (50.8 mm) center to center. Concrete encased the section and provided a

cover of one inch around the steel section for an overall cross-section of 6 inches (152.4 mm) deep by 3.75 inches (95 mm) wide. Length to overall depth ratios were between 10.0 and 16.7 with end eccentricity ratios between 0.17 and 0.5.

Procter (1967) tested concrete encased British RSJ sections. The overall dimensions of the composite cross-sections were 11 inches by 8 inches (280 mm by 200 mm) and 12 inches by 8 inches (305 mm by 200 mm). The RSJ sizes were 7 inches by 4 inches (178 by 100 mm) (depth by flange width) and 8 inches by 4 inches (200 by 100 mm). No vertical reinforcing bars or lateral ties were used. Twelve specimens (numbered 1 to 12) had length to depth ratios of 11 to 12. Four specimens (S1, S2, S3 and S4) had length to depth ratios of 2.0 to 2.2. The end eccentricity ratio for the 12 longer columns ranged from zero (concentric) to 0.8. All four shorter columns were concentrically loaded. To account for the lack of reinforcing, all concrete was considered to be unconfined in the computer analysis used in this report.

May and Johnson (1978) tested 8 composite beam-column specimens with restrained ends. Of the specimens tested, only 3 (RC1, RC2 and RC4) were applicable to this study. May and Johnson calculated an effective length (equivalent length of a pin-ended column) which was used as an input to the theoretical subroutine. The overall dimension of the cross-section was 8 inches by 8 inches (200 mm by 200 mm).

The structural steel section was a 6 inch by 6 inch (150 mm by 150 mm) British UC section. The vertical reinforcing consisted of four 0.25-inch (6 mm) diameter rods with 0.16-inch (4 mm) diameter rectangular hoops spaced at 6 inches (150 mm). The time of testing was noted to be approximately 4 hours. The effective length to depth ratios ranged from 8.1 to 14.8. The end eccentricity ratios were 0.11, 0.14 and 0.2.

Suzuki et al. (1983) tested 16 beam-column specimens in each of concentric and pure bending loading conditions with an additional 2 columns loaded eccentrically causing bending about the major axis. The concentric and pure bending specimens had a length to depth ratio of 2.9. The eccentrically loaded columns had a length to depth ratio of 3.8 and end eccentricity ratios of 0.87 and 1.06. The overall dimensions of the cross-section were 8.3 inches by 8.3 inches (210 mm by 210 mm). The steel sections were 6 inches (150 mm) deep with a flange width of 4 inches (100 mm) and various flange and web thicknesses. Four grades of steel were tested. Vertical reinforcing consisted of four 0.25 inch (6 mm) diameter wires. The wires were greased. Hence, the vertical reinforcement did not contribute to the strength of the column but provided support to the rectangular hoops. The hoops were also 0.25 inch (6 mm) diameter and were spaced at 0.8, 1.6 and 4 inches (20, 40 and 100 mm) center

to center. Columns without hoops were also tested. The vertical reinforcing was modelled in the computer analysis of this study by specifying a yield strength of zero.

Morino et al. (1984) tested 8 composite beam-column specimens applicable to this study. The data from one of these tests was not included because it had an unreasonably high strength which was not consistent with the rest of the data reported by Morino et al. All columns were of identical geometry. The overall dimensions of the cross-section were 6.3 inches by 6.3 inches (160 mm by 160 mm). The steel section was 4 inches by 4 inches (100 mm by 100 mm) with a flange thickness of 0.3 inches (8 mm) and a web thickness of 0.25 inches (6mm). Four 0.25 inch (6 mm) diameter bars were used as vertical reinforcing. Rectangular hoops were made of 0.15 inch (4 mm) diameter wire and spaced at 6 inches (150 mm) center to center. Length to overall depth ratios ranged from 6.0 to 30.0. End eccentricity ratios ranged from 0.25 to 0.47.

The physical tests noted above provided ultimate strengths of 63 beam-columns specimens which were used to measure the accuracy of the theoretical model. The dimensions, material properties and other pertinent data supplied by the authors noted above was used as input wherever applicable. Strain-hardening of both structural and reinforcing steels and residual stresses in the structural steel section were also included in the analysis. In some cases,

estimates were made regarding certain geometric or material properties not provided in the source literature. These estimates were, however, believed to be of sufficient accuracy for the purposes of this study. Time-to-failure is a required input to the program to estimate concrete properties as indicated in Section 4.1. The loading period of the test specimens was assumed to be 2 hours, except for the May and Johnson (1978) specimens where the authors noted a loading time of 4 hours. Table 2.3 shows the ratios of test to calculated ultimate strengths (strength ratios) for all 63 beam-column specimens.

The mean, standard deviation and coefficient of variation were calculated for the strength ratios listed in Table 2.3. For the purposes of this study, the test specimens were sub-divided into two categories with respect to l/h ratio. Short columns are assumed to be those with l/h less than 6.6 and long columns have l/h greater than or equal to 6.6. The data was further categorized into 3 ranges of end eccentricity ratio (e/h): (a) e/h of 0.0 to 0.2 inclusive; (b) e/h greater than 0.2 but less than infinity; and (c) e/h equal to infinity (pure bending case). The mean, standard deviation and coefficient of variation calculated for each of these categories and for the overall sample are shown in Table 2.4.

Table 2.3 - Description of Specimens Used for Ratio of Tested to Calculated Strength

Author	Column Designation	e/h	ℓ/h	b x h (in. x in.)	ρ_{ss}	Volumetric Ratio*	f'_c (psi)	f_y web (psi)	f_y flange (psi)	Tested Strength**	Calculated Strength**	Tested/Calculated Strength
Bondale (1966)	RS 60.3	0.50	10.0	3.75 x 6.0	0.0700	0.0074	4480	44800	44800	55.8	47.4	1.1768
	RS 80.2	0.33	13.3	3.75 x 6.0	0.0700	0.0074	4480	44800	44800	70.1	56.8	1.2343
	RS 100.1	0.17	16.7	3.75 x 6.0	0.0700	0.0074	4480	44800	44800	92.3	74.3	1.2417
May et al. (1978)	RC1	0.11	8.1	7.87 x 7.87	0.0746	0.0018	4308	42050	41630	310.5	281.9	1.1013
	RC3	0.14	8.1	7.87 x 7.87	0.0746	0.0018	3390	42050	41630	306.0	238.3	1.2841
	RC4	0.20	14.8	7.87 x 7.87	0.0746	0.0018	5191	42050	41630	191.3	218.8	0.8741
Morino et al. (1984)	B4-90	0.25	15.0	6.3 x 6.3	0.0789	0.0012	3393	50750	41615	114.6	97.3	1.1775
	C4-90	0.25	22.5	6.3 x 6.3	0.0789	0.0012	3378	45675	44660	93.9	80.4	1.1675
	D4-90	0.25	30.0	6.3 x 6.3	0.0789	0.0012	3074	52055	42485	64.7	59.2	1.0924
	A8-90	0.47	6.0	6.3 x 6.3	0.0789	0.0012	4872	53360	43935	116.1	94.3	1.2320
	B8-90	0.47	15.0	6.3 x 6.3	0.0789	0.0012	4828	53360	45095	94.0	79.9	1.1765
	C8-90	0.47	22.5	6.3 x 6.3	0.0789	0.0012	3567	53505	44225	68.0	58.3	1.1664
	D8-90	0.47	30.0	6.3 x 6.3	0.0789	0.0012	3320	53360	43790	50.1	45.9	1.0920
Procter (1967)	S1	0.00	2.2	8.0 x 11.0	0.0482	n/a*	4722	42112	42112	470.4	524.4	0.8970
	S2	0.00	2.2	8.0 x 11.0	0.0482	n/a	4722	42112	42112	481.6	524.4	0.9184
	S3	0.00	2.0	8.0 x 12.0	0.0522	n/a	5407	42560	42560	698.9	645.4	1.0829
	S4	0.00	2.0	8.0 x 12.0	0.0522	n/a	5407	42560	42560	703.4	645.4	1.0899
	1	0.53	11.7	8.0 x 11.25	0.0402	n/a	4722	42112	42112	132.2	128.5	1.0287
	2	0.80	11.7	8.0 x 11.25	0.0402	n/a	4722	42112	42112	87.4	87.3	1.0011
	3	0.00	11.7	8.0 x 11.25	0.0402	n/a	4722	42112	42112	470.4	503.5	0.9343
	4	0.53	11.7	8.0 x 11.25	0.0402	n/a	4722	42112	42112	143.4	128.5	1.1159
	5	0.80	11.7	8.0 x 11.25	0.0402	n/a	5407	42112	42112	91.8	90.7	1.0122
	6	0.75	11.0	8.0 x 12.0	0.0522	n/a	5407	42560	42560	129.9	117.3	1.1072
	7	0.50	11.0	8.0 x 12.0	0.0522	n/a	5407	42560	42560	199.4	169.8	1.1741
	8	0.00	11.0	8.0 x 12.0	0.0522	n/a	5407	42560	42560	560.0	614.9	0.9107
	9	0.27	12.0	8.0 x 11.25	0.0402	n/a	6007	42112	42112	268.8	234.3	1.0706
	10	0.27	12.0	8.0 x 11.25	0.0402	n/a	6007	42112	42112	250.9	234.3	1.1471
	11	0.00	11.0	8.0 x 12.0	0.0522	n/a	6007	42560	42560	533.1	660.7	0.8069
	12	0.25	11.0	8.0 x 12.0	0.0522	n/a	6007	42560	42560	315.8	288.7	1.0939

Table 2.3 (cont.)

Author	Column Designation	e/h	ℓ/h	b x h (in. x in.)	ρ_{ss}	Volumetric Ratio*	f'_c (psi)	f_y web (psi)	f_y flange (psi)	Tested Strength**	Calculated Strength**	Tested/Calculated Strength
Suzuki et al. (1983)	LH-000-C	0.00	2.9	8.27 x 8.27	0.0194	n/a*	4741	45135	45586	380.6	365.4	1.0416
	LH-020-C	0.00	2.9	8.27 x 8.27	0.0194	0.0274	4741	45135	45586	374.0	441.7	0.8468
	LH-040-C	0.00	2.9	8.27 x 8.27	0.0194	0.0137	4741	45135	45586	374.0	404.0	0.9258
	LH-100-C	0.00	2.9	8.27 x 8.27	0.0194	0.0055	4741	45135	45586	385.0	381.0	1.0105
	RH-000-C	0.00	2.9	8.27 x 8.27	0.0439	n/a	4840	55355	48159	550.0	458.4	1.1997
	RH-020-C	0.00	2.9	8.27 x 8.27	0.0439	0.0274	4840	55355	48159	561.0	536.0	1.0467
	RH-040-C	0.00	2.9	8.27 x 8.27	0.0439	0.0137	4840	55355	48159	517.0	499.4	1.0353
	RH-100-C	0.00	2.9	8.27 x 8.27	0.0439	0.0055	4840	55355	48159	517.0	475.4	1.0875
	HT60-000-C	0.00	2.9	8.27 x 8.27	0.0600	n/a	4840	83600	83600	594.0	562.1	1.057
	HT60-020-C	0.00	2.9	8.27 x 8.27	0.0600	0.0274	4840	83600	83600	653.4	685.7	0.953
	HT60-040-C	0.00	2.9	8.27 x 8.27	0.0600	0.0137	4840	83600	83600	660.0	644.6	1.024
	HT60-100-C	0.00	2.9	8.27 x 8.27	0.0600	0.0055	4840	83600	83600	620.4	614.4	1.010
	HT80-000-C	0.00	2.9	8.27 x 8.27	0.0633	n/a	4840	113406	113406	708.4	530.1	1.3364
	HT80-020-C	0.00	2.9	8.27 x 8.27	0.0633	0.0274	4840	113406	113406	726.0	808.1	0.8985
	HT80-040-C	0.00	2.9	8.27 x 8.27	0.0633	0.0137	4840	113406	113406	723.8	764.8	0.9464
	HT80-100-C	0.00	2.9	8.27 x 8.27	0.0633	0.0055	4840	113406	113406	704.0	725.1	0.9709
	HT80-000-CB	0.87	3.8	8.27 x 8.27	0.0429	n/a	4409	110568	110568	110.0	97.1	1.1326
	HT80-020-CB	1.06	3.8	8.27 x 8.27	0.0429	0.0274	4409	110568	110568	110.0	109.6	1.0036
	LH-000-B	∞	2.9	8.27 x 8.27	0.0194	n/a	4741	45135	45586	27.1	26.9	1.0077
	LH-020-B	∞	2.9	8.27 x 8.27	0.0194	0.0274	4741	45135	45586	29.6	32.4	0.9133
	LH-040-B	∞	2.9	8.27 x 8.27	0.0194	0.0137	4741	45135	45586	28.9	30.6	0.9435
	LH-100-B	∞	2.9	8.27 x 8.27	0.0194	0.0055	4741	45135	45586	28.9	28.4	1.0165
	RH-000-B	∞	2.9	8.27 x 8.27	0.0439	n/a	4840	55355	48159	49.1	50.0	0.9816
	RH-020-B	∞	2.9	8.27 x 8.27	0.0439	0.0274	4840	55355	48159	54.9	56.8	0.9658
	RH-040-B	∞	2.9	8.27 x 8.27	0.0439	0.0137	4840	55355	48159	53.4	52.4	1.0193
	RH-100-B	∞	2.9	8.27 x 8.27	0.0439	0.0055	4840	55355	48159	50.2	50.9	0.9855

Table 2.3 (cont.)

Author	Column Designation	e/h	ℓ/h	b x h (in. x in.)	ρ_{ss}	Volumetric Ratio*	f'_c (psi)	f_y web (psi)	f_y flange (psi)	Tested Strength**	Calculated Strength**	Tested/Calculated Strength
Suzuki et al. (1983) (cont.)	HT60-000-B	∞	2.9	8.27 x 8.27	0.0600	n/a*	4840	83600	83600	69.7	72.9	0.9549
	HT60-020-B	∞	2.9	8.27 x 8.27	0.0600	0.0274	4840	83600	83600	78.0	80.7	0.9658
	HT60-040-B	∞	2.9	8.27 x 8.27	0.0600	0.0137	4840	83600	83600	76.5	76.4	1.0020
	HT60-100-B	∞	2.9	8.27 x 8.27	0.0600	0.0055	4840	83600	83600	71.8	75.5	0.9513
	HT80-000-B	∞	2.9	8.27 x 8.27	0.0633	n/a	4840	113406	113406	93.8	95.9	0.9787
	HT80-020-B	∞	2.9	8.27 x 8.27	0.0633	0.0274	4840	113406	113406	102.5	105.9	0.9682
	HT80-040-B	∞	2.9	8.27 x 8.27	0.0633	0.0137	4840	113406	113406	101.1	103.3	0.9778
	HT80-100-B	∞	2.9	8.27 x 8.27	0.0633	0.0055	4840	113406	113406	97.4	100.3	0.9714

*Ratio of volume of lateral hoops to gross volume of confined concrete core. Concrete core is measured to outside of lateral hoops. Columns without lateral hoops are indicated by n/a.

** Strength (measured or calculated) is axial load at failure in kips, except when e/h = ∞ where strength (measured or calculated) is bending moment at failure in foot-kips.

1 in. = 25.4 mm; 1000 psi = 6.895 MPa; 1 kip = 1000 pounds = 4.448 KN; 1 foot-kip = 1.356 KN-m.

Notes:

1. Ratio of area of vertical reinforcing bars to gross cross-section area was 0.0062, 0.0028 and 0.0044 for Bondale (1966), May et al. (1978) and Morino et al. (1984), respectively. All other columns had no vertical reinforcing.

2. Yield strength for reinforcing bars (vertical and/or lateral ties) was assumed to be 71000 psi for Bondale (1966) and May et al. (1978). Yield strength was 56115 psi for Morino et al. (1984) and 48400 psi for Suzuki et al. (1983).

Table 2.4 - Statistical Analysis of Ratios of Test to Calculated Strength

Column Type (1)	(2)	all e/h (3)	$0 \leqslant e/h \leqslant 0.2$ (4)	$0.2 < e/h < \infty$ (5)	$e/h = \infty$ (6)
Short ($\ell/h < 6.6$)	No.	39	20	3	16
	$\bar{X}$	1.009	1.019	1.123	0.975
	V	9.34	11.04	10.2	2.86
Long ($\ell/h \geqslant 6.6$)	No.	24	7	17	0
	$\bar{X}$	1.091	1.022	1.12	-
	V	10.96	18.37	5.9	-
All ℓ/h	No.	63	27	20	16
	$\bar{X}$	1.04	1.02	1.12	0.975
	V	10.69	12.93	6.35	2.86

The ratio of test to calculated ultimate strength was 1.04 with a coefficient of variation of 10.69 percent when all 63 specimens were considered (Table 2.4 - Column 3). This is comparable with the mean value of 1.042 and coefficient of variation of 10.4 percent obtained by Virdi and Dowling (1973) for their analysis of 8 biaxially loaded composite columns. The differences in statistics for short and long columns drawn from the overall sample was considered negligible as indicated by Column 3 in Table 2.4.

There were significant differences in the statistics for different ranges of end eccentricity ratio (Table 2.4 Columns 4,5, and 6). The mean strength ratio was very close to 1.0 and no effect due to slenderness was noticed on mean strength ratios of columns in the low eccentricity range (Table 2.4 - Column 4). In the second eccentricity range (Table 2.4 - Column 5), the mean value of the strength ratio was significantly greater than 1.0. Hence, the theoretical model seems to be conservative in this range of end eccentricity. Again, no length effect on the mean value was noticed. For the pure bending condition (Table 2.4 - Column 6), the mean strength ratio was slightly lower than 1.0. This was probably due to the strain-hardening assumptions used for the theoretical strength model.

In summary, the mean strength ratios in Table 2.4 are consistent for short and long column specimens and for the combined sample. The coefficients of variation, however,

show some differences between short and long column specimens although a definite trend to lower coefficients of variation as the end eccentricity ratio increases is apparent in Table 2.4 (Columns 4, 5, and 6). Considering the wide range of column sizes, configurations, loadings and sources, and the small sample sizes for some categories, the accuracy of the theoretical strength model seems acceptable.

To examine the probability distribution of the strength ratios calculated above, the data for each range of end eccentricity ratio was plotted on normal probability paper. A normal distribution was calculated from each set of data using the statistics of overall sample given in Table 2.4 (Columns 4, 5, and 6). Figures 2.23, 2.24 and 2.25 plot the probability distributions for the ranges of end eccentricity ratio noted in Columns 4, 5 and 6 of Table 2.4, respectively. It can be reasonably assumed that the data follows a normal probability distribution for all three ranges of end eccentricity ratio.

2.10 CALCULATION OF MODEL ERROR

The strength ratios calculated in Section 2.9 represent the overall variation between the test specimen strength and the strength predicted by the theoretical model. The coefficient of variation of the ratio of tested to calculated strength, $V_{t/c}$, is attributed to three sources: V_{model}, V_{test} and $V_{in\text{-}batch}$. V_{model} is the coefficient of variation representing the variability of the theoretical model. V_{test} is

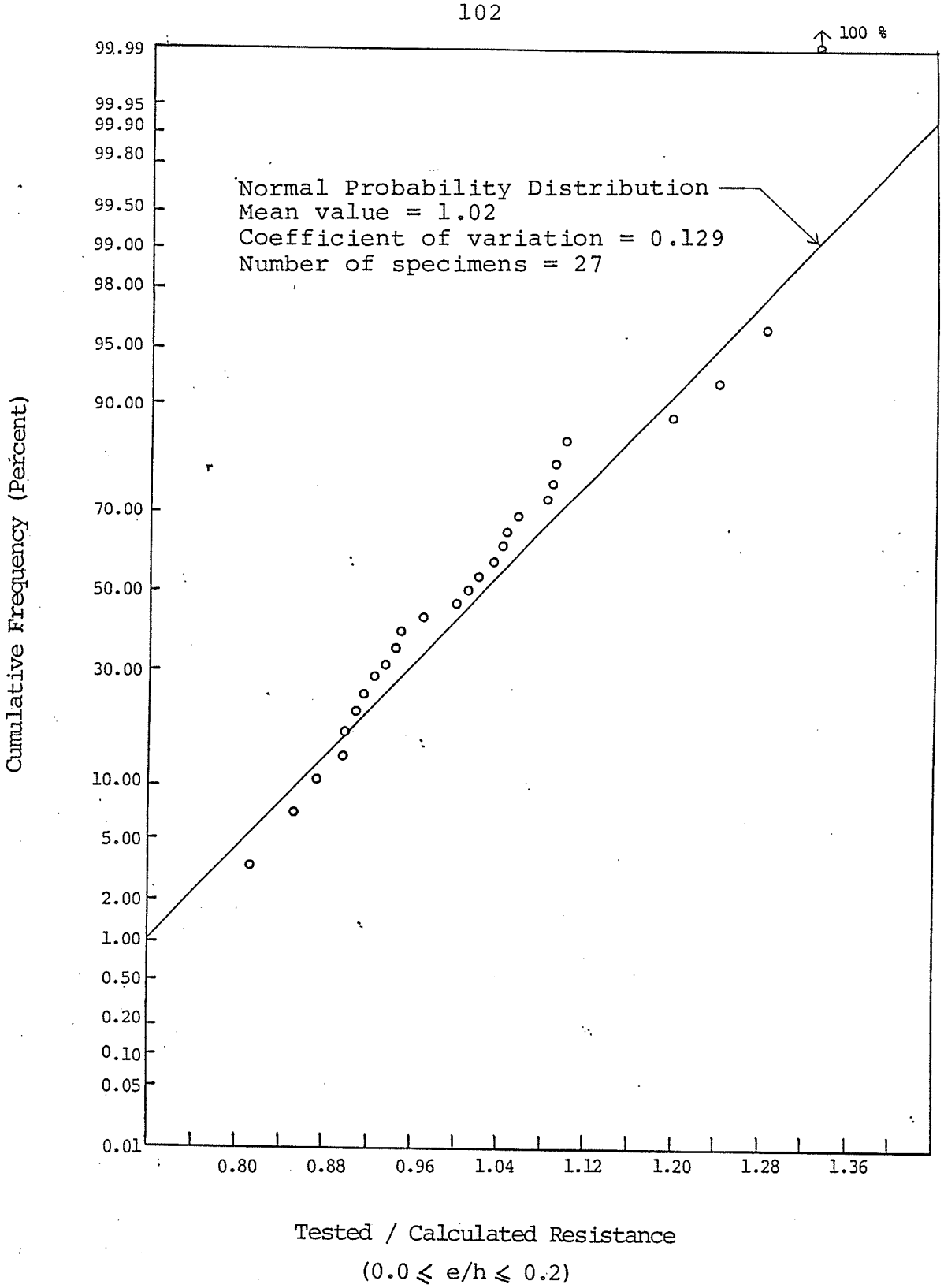

Figure 2.23 - Cumulative Frequency of Ratio of Tested / Calculated Resistance of Composite Beam-Column Specimens (Table 2.3) with $0.0 \leq e/h \leq 0.2$

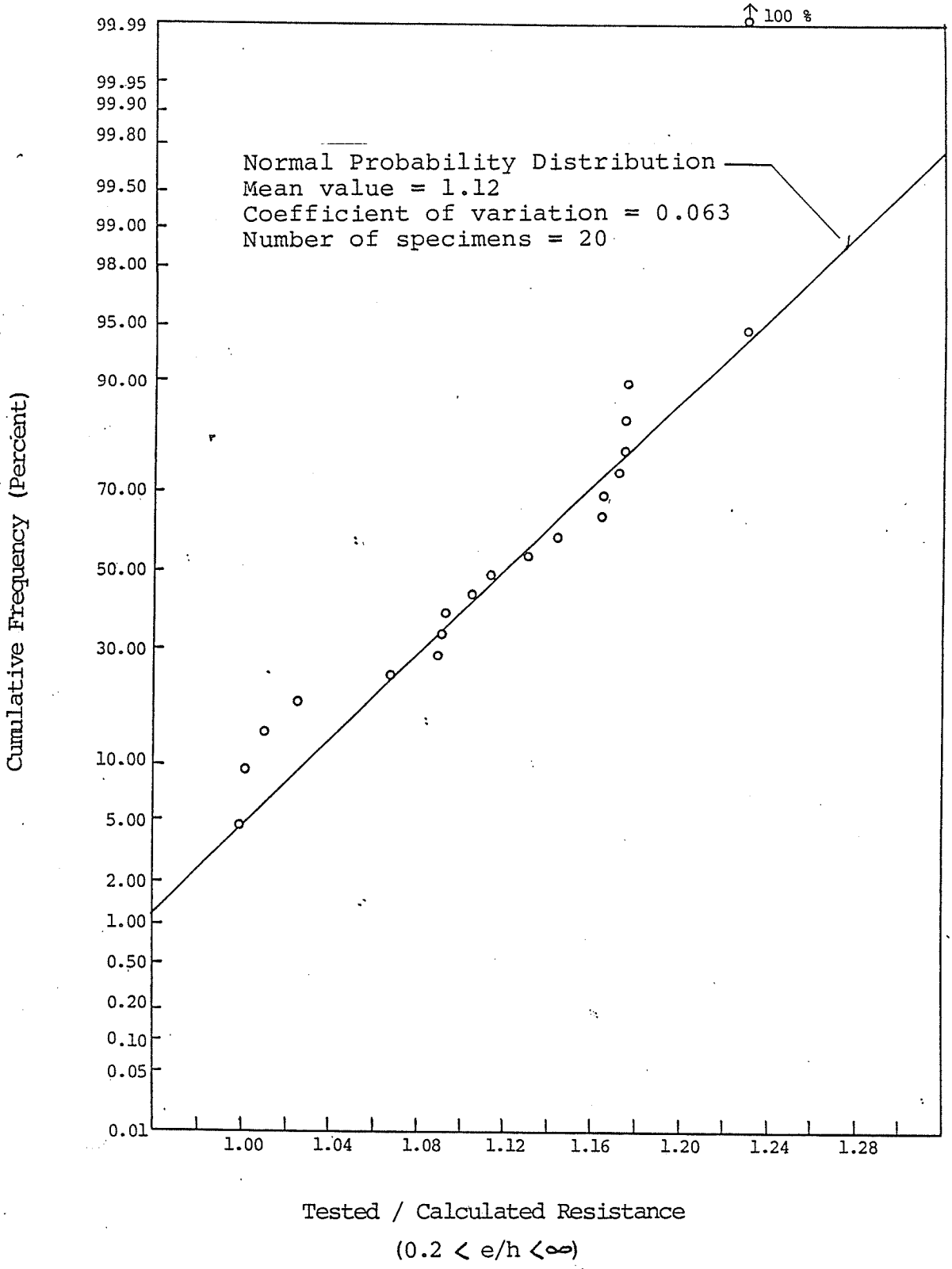

Figure 2.24 - Cumulative Frequency of Ratio of Tested / Calculated Resistance of Composite Beam-Column Specimens (Table 2.3) with $0.2 < e/h < \infty$

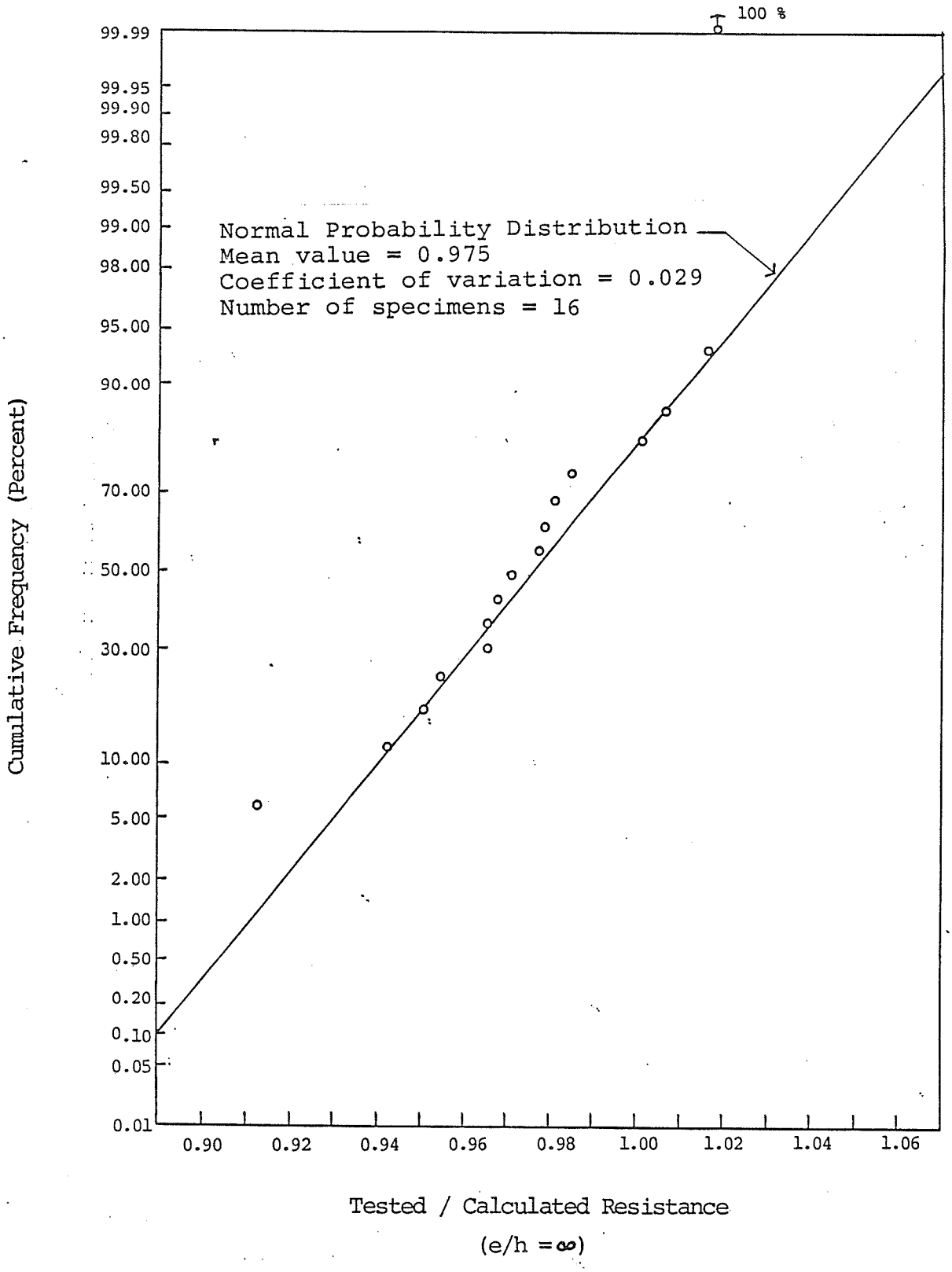

Figure 2. 25- Cumulative Frequency of Ratio of Tested / Calculated Resistance of Composite Beam-Column Specimens (Table 2.3) with e/h = ∞

the coefficient of variation representing uncertainties in recording the correct failure load during physical tests due to inaccuracies in measuring equipment, recording procedures and different definitions of failure. $V_{in\text{-}batch}$ represents the coefficient of variation that accounts for the variability of laboratory material properties as well as differences in strength between laboratory control samples and the materials in the test specimens. Mirza and MacGregor (1982) have related these four variabilities as shown in Equation 2.26.

$$V_{t/c}^2 = V_{model}^2 + V_{test}^2 + V_{in\text{-}batch}^2 \qquad (2.26)$$

To calculate V_{model}, Equation 2.26 was rearranged to Equation 2.27.

$$V_{model} = \sqrt{V_{t/c}^2 - V_{test}^2 - V_{in\text{-}batch}^2} \qquad (2.27)$$

$V_{t/c}$ was found to be significantly affected by eccentricity ratio in Section 2.9. Hence, V_{model} also depends on the eccentricity ratio of the beam-column as described below.

V_{test} was assumed to be 0.04 for end eccentricity ratios between 0.0 and 0.2 inclusive. This value was used by Mirza and MacGregor (1989) for a similar study of reinforced concrete beam-columns. V_{test} was assumed to equal 0.02 at pure

bending ($e/h = \infty$), and was arbitrarily assumed to vary linearly at end eccentricity ratios between 0.2 and infinity as shown in Equation 2.28.

$$V_{test} = 0.02 + 0.004h/e \quad \text{for} \quad e/h > 0.2 \qquad (2.28)$$

The higher value for V_{test} at low end eccentricity ratios is justified due to the involvement of a compression failure, the resulting loss of measuring accuracy, and the difficulty in defining a point of failure. V_{test} used in this study is graphically represented in Figure 2.26(a).

$V_{in\text{-}batch}$ was calculated using the Monte Carlo technique described in Chapter 5. Four beam-columns were chosen to calculate the in-batch variability. These beam-columns were selected from the test specimens listed in Table 2.3. Various e/h and l/h ratios were represented. The beam-columns selected for computing $V_{in\text{-}batch}$ are shown in Table 2.5. The theoretical strength of each column shown in Table 2.5 was simulated 200 times. Each time the values of the basic variables were randomly generated by the computer according to predefined in-batch probability distributions of each variable affecting the strength (Table 4.1). For simplicity, the material strengths and dimensions reported for each test specimen were taken as the mean values of the variables for computing the $V_{in\text{-}batch}$ for that specimen. The theoretical

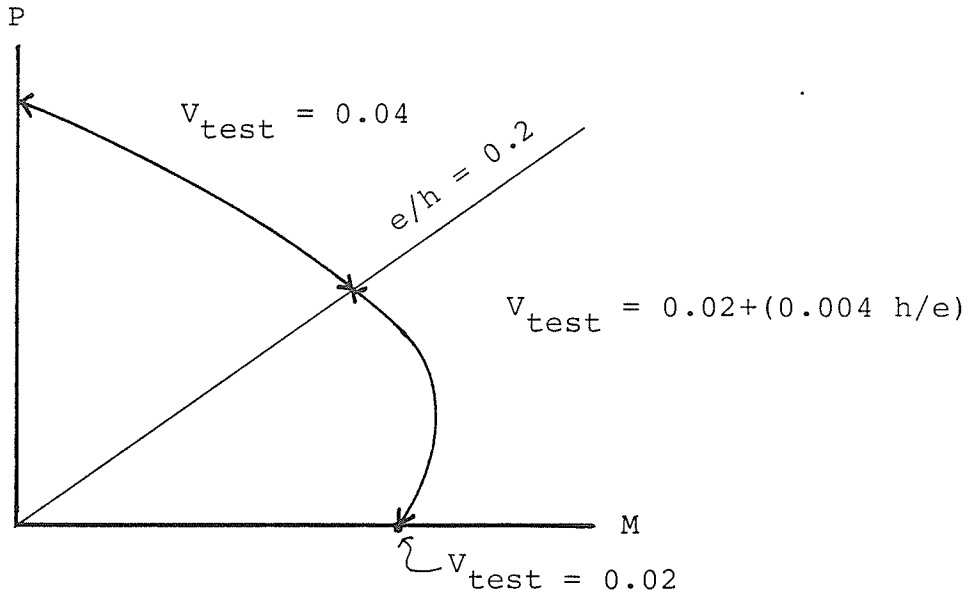

(a)

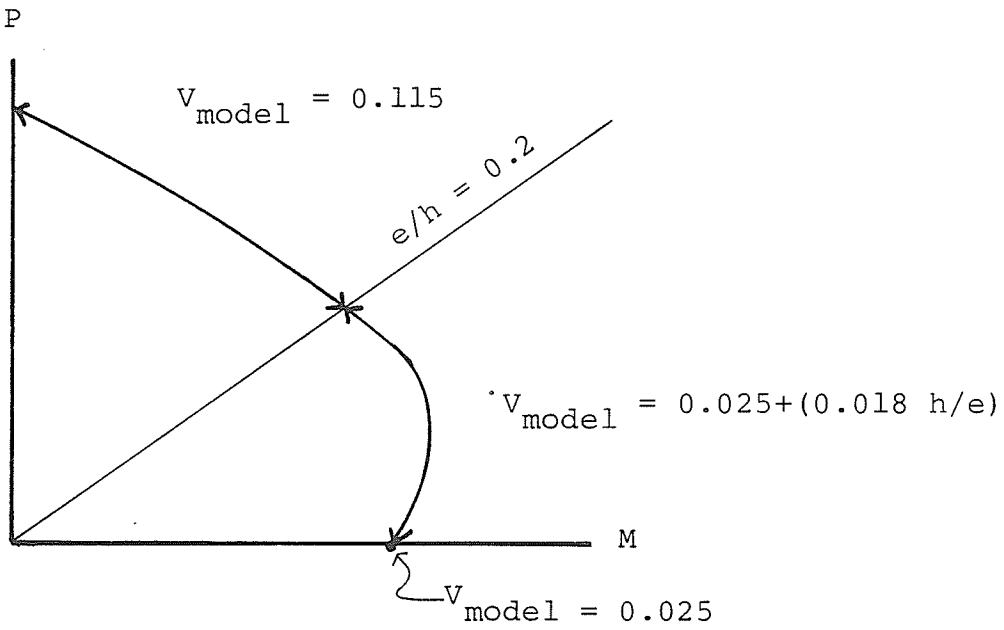

(b)

Figure 2.26 - V_{test} and V_{model} used

Table 2.5 – Variability of Theoretical Strength Model

Column Designation (Table 2.3) (1)	e/h (2)	ℓ/h (3)	$V_{t/c}$ (4)	$V_{in-batch}$ (5)	V_{test} (6)	V_{model} (calc) (7)	V_{model} (used) (8)
LH-100-C	0.0	2.9	0.129	0.039	0.040	0.116	0.115
RC1	0.11	8.1	0.129	0.028	0.040	0.119	0.115
D8-90	0.47	30.0	0.063	0.018	0.029	0.053	0.063
LH-100-B	∞	2.9	0.029	0.019	0.020	0.008	0.025

strength samples so simulated were used to compute $V_{in\text{-}batch}$ for the beam-columns listed in Table 2.5. The computed values of $V_{in\text{-}batch}$ and V_{test} are shown in the same table. The values of $V_{t/c}$ given in Table 2.5 were taken from Table 2.4. V_{model} was then calculated using Equation 2.27 for each of the beam-columns listed in Table 2.5. The resulting values are shown in Column 7 of Table 2.5. These values provided a basis for estimating the coefficient of variation associated with the theoretical strength model.

V_{model} was chosen to be constant at 0.115 for end eccentricity ratios between 0.0 and 0.2 inclusive. A value of V_{model} equal to 0.025 was assumed for the pure bending condition. V_{model} for end eccentricity ratios greater than 0.2 and less than infinity was assumed to vary inversely with respect to the end eccentricity ratio as shown in Equation 2.29.

$$V_{model} = 0.025 + 0.018h/e \qquad \text{for } 0.2 < e/h < \infty \qquad (2.29)$$

The coefficient of variation of the theoretical strength model used in this study is shown graphically in Figure 2.26(b). The values of V_{model} based on this Figure for four typical beam-column specimens are given in Column 8 of Table

2.5. A comparison of these values with the calculated values of V_{model} in Column 7 of the same Table indicates a reasonable agreement between calculated and used values of V_{model}.

A random normal variable with a mean of 1.0 and a coefficient of variation as described above was used to vary the strength ratios calculated in the Monte Carlo simulations described in Chapter 5. The mean value of 1.0 was chosen since it is a conservative estimate of the strength ratios of test to calculated strengths described in Section 2.9 and summarized in Table 2.4. At the pure bending condition, this assumption for the mean value appears slightly unconservative when strain-hardening of steel is used (Table 2.4). However, it is expected to be conservative when strain-hardening of steel is not allowed. A normal probability distribution of the strength ratios was assumed based on Figures 2.23, 2.24 and 2.25.

3 NOMINAL BEAM-COLUMN STRENGTH

A computer subroutine was used to calculate the design code strength (referred to as nominal strength) of a composite beam-column. This strength was then compared to the corresponding theoretical strength of the beam-column. The subroutine calculates the design code strength according to the assumptions and methods of ACI Standard 318-83 or CSA Standard CAN3-A23.3-M84. In this study, the comparisons of the theoretical strengths were done primarily with the strengths computed according to ACI Standard 318-83.

This chapter describes how the nominal strength of the composite beam-column is calculated. The assumptions made by the design codes regarding material strength and strength analysis of the beam-column are discussed first. The nominal strength program, **RNOM**, is then described. The differences between ACI 318-83 and CSA CAN3-A23.3-M84 are discussed in the final section of this chapter.

3.1 ASSUMPTIONS

The North American design standards make certain assumptions regarding the characteristics of the materials used and the behavior of the composite beam-columns in order to simplify the design. The assumptions discussed here are common to both ACI 318-83 and CSA CAN3-A23.3-M84 and have been incorporated into the nominal strength subroutine.

Assumptions regarding the behavior of the composite beam-column are:

(a) perfect bond exists between steel and concrete, i.e. no slip;

(b) strain in the composite cross-section is proportional to the distance from the neutral axis;

(c) composite columns with a slenderness ratio, kl/r, less than ([34 - 12 M_1/M_2) where M_1 is the lesser and M_2 is the greater column end bending moment, were considered short columns and length effects were neglected.

Assumptions regarding the behavior of the materials are:

(a) the maximum useable concrete strain at the extreme compression fibre is 0.003;

(b) the tensile strength of concrete was neglected;

(c) the shape of the concrete stress-strain curve was assumed to be an equivalent rectangular stress block with a maximum stress equal to 85 percent of the specified 28-day cylinder strength;

(d) the uniformly distributed compressive stress in the concrete is bounded by the limits of the section and at a line parallel to the neutral axis and a distance $\beta_1 c$ from the extreme compression fibre (Figure 3.1) where c is the distance from the neutral axis to the extreme compression fibre and β_1 has a value of 0.85 for specified concrete strengths up to 4000 psi (30 MPa) and decreases linearly by 0.05 for each 1000 psi (0.08 for each 10 MPa) to a minimum value of 0.65;

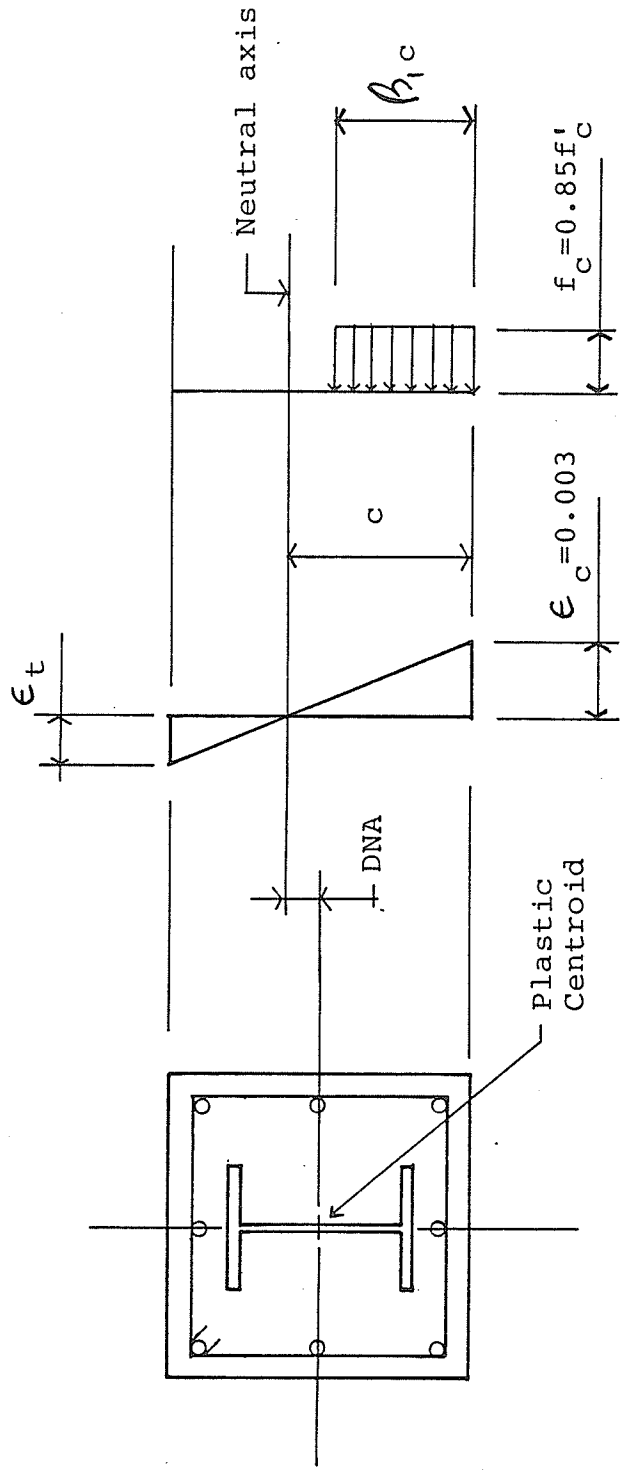

Figure 3.1 - Code Stress and Strain Distribution for Concrete

(e) the stress-strain relation of steel (structural shapes and reinforcing bars) was assumed to be elastic-plastic with the maximum stress equal to the specified yield stress (see Figure 3.2);

(f) the stress-strain relation of steel is identical in compression and tension; and

(g) residual stresses in the steel section are neglected.

The above assumptions were applied to all composite beam-columns. In addition several assumptions were made which were applicable only to the beam-columns investigated in this study. These assumptions are:

(a) the beam-columns were pin-ended so that the effective length was equal to the actual length;

(b) the column ends were prevented from translation (sideway prevented);

(c) no transverse loads were applied to the columns;

(d) end moments were equal and opposite such that the beam-column bent in single curvature and that the ratio of the end moments was equal to 1; and

(e) the loading time to failure was short so that the effect of creep were neglected ($\beta_d = 0$).

The ACI and CSA design codes specify limitations on the maximum material strengths as well as on ratios of structural steel and reinforcing bars to the total cross sec-

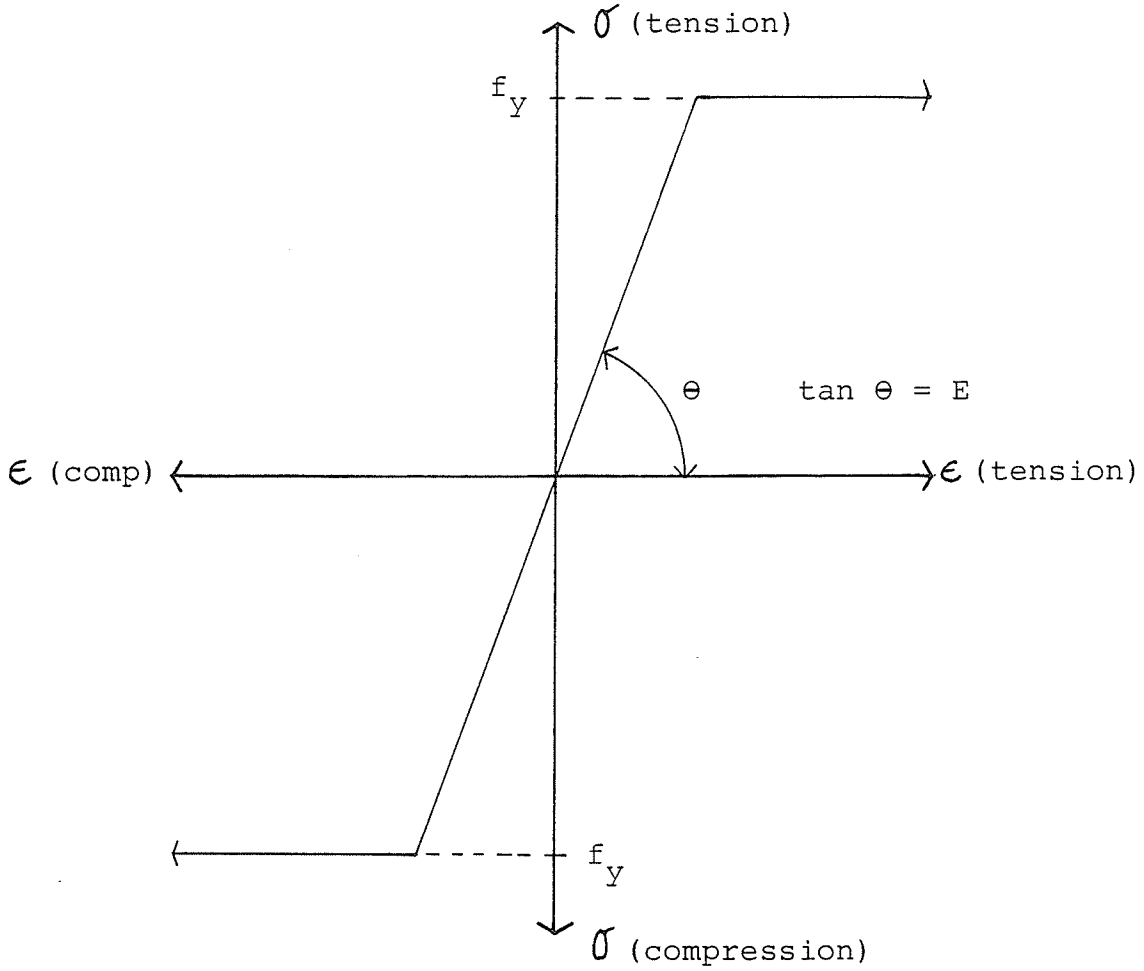

Figure 3.2 - Code Stress-Strain Relationship for Steel

tional area. These limitation were observed when designing the beam-columns used in this study and described in Chapter 5.

Another requirement of the design codes is that all load assigned to the concrete portion of the composite section must be transferred to the concrete by members or brackets attached to the steel core and in direct bearing with the concrete. Although not specifically addressed in the strength calculations, this requirement ensures the validity of the assumption of no slip between steel and concrete.

To calibrate the nominal strength model and to provide data in a form that is easily useable for future probabilistic assessment of understrength factors, all understrength factors in this study were assigned a value of 1.0.

3.2 NOMINAL STRENGTH PROGRAM

Calculation of the nominal beam-column strength requires the following procedures:

(a) input of nominal dimensions, nominal material strengths, selection of design code (ACI Standard 318-83 or CSA Standard CAN3-A23.3-M84);

(b) discretization of the structural steel section;

(c) calculation of the cross-section axial load - bending moment ($P-M$) interaction diagram;

(d) calculation of the composite slenderness ratio to determine whether the beam-column is considered short or long; and, if needed,

(e) calculate the long column $P-M$ interaction diagram by evaluating the concentric capacity and the bending moment modifier for long column effect.

All specified dimensions, areas and geometric properties of the column as well as the components are read into the program. The specified concrete 28-day cylinder strength and the specified yield strength of the structural and reinforcing steel are required inputs. The modulus of elasticity of the concrete is calculated by the design code expression shown in Equation 3.1.

$$E_c = 57,000\sqrt{f'_c} \text{ psi} \qquad (3.1)$$
$$= 5000\sqrt{f'_c} \text{ MPa}$$

The modulus of elasticity for steel was assumed to be 29,000,000 psi (200,000 MPa). The program is designed to include the specified values of the understrength (ϕ) factors and the sustained load factor (β_d). As stated earlier, the understrength factors were all assigned a value of 1.0 and β_d was assigned a value of 0.0 for this study.

All concrete areas were assumed to behave in a similar fashion, with no distinction made between unconfined and confined concrete. Discretization of the concrete in the cross-section was not required because the stress in all stressed parts of the concrete was assumed to be uniform

(rectangular stress block). The stress in vertical reinforcing bars was determined by multiplying the strain calculated at the centroid of the bar by the modulus of elasticity of the reinforcing bar. Discretization of the structural steel section was done since the stress varied significantly along the depth of the section. The steel section was discretized into 20 elements with boundaries parallel to the neutral axis. The stress in each element was calculated by multiplying the strain at the centroid of each element by the modulus of elasticity of steel. The stresses so calculated were reduced by $0.85f'_c$ for reinforcing bars and parts of the steel section that fell within the concrete stress block. Residual stresses in the structural steel were neglected.

The development of the nominal cross-section $P-M$ interaction diagram is much simpler than that used for the theoretical analysis. The strain at the compression face of the concrete was set at the maximum value allowed by the code (0.003). The location of the neutral axis was fixed at a distance from the compression face and the corresponding axial load and bending moment capacities calculated. This locates one point on the cross-section $P-M$ interaction curve (Figure 3.3).

The location of the neutral axis was varied between the pure bending and the pure compression conditions and the

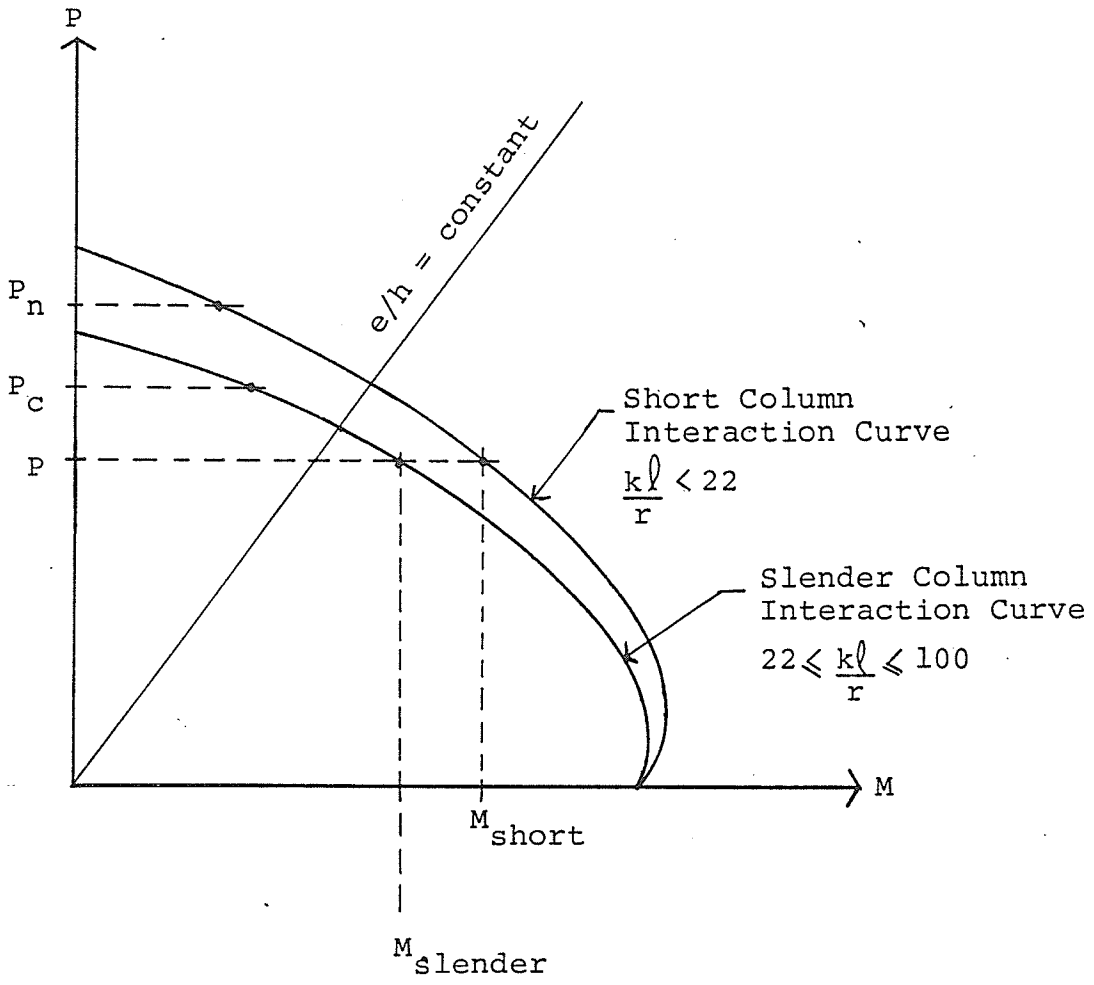

$$\delta_b = \frac{M_{short}}{M_{slender}} \geqslant 1.0$$

Figure 3.3 - Axial Load-Bending Moment Interaction Diagram for Nominal Strength Subroutine

corresponding axial load and bending moment capacities were calculated, creating sufficient points to accurately define the entire $P-M$ diagram. These points were then used to interpolate the axial load and bending moment capacities for the specified end eccentricity ratios.

After the completion of the cross-section $P-M$ interaction diagram, the program determines whether slenderness effects are required to be accounted for. If the slenderness effects are to be included, the radius of gyration r of the composite section is estimated using the code expression shown in Equation 3.2 in which E_c is the modulus of elasticity of concrete (Equation 3.1), A_g and I_g are the area and moment of inertia of the gross cross-section, respectively, E_s is the modulus of elasticity of the structural steel section and, A_s and I_s are the area and moment of inertia of the structural steel section, respectively.

$$r = \sqrt{\frac{(E_c I_g/5) + E_s I_s}{(E_c A_g/5) + E_s A_s}} \tag{3.2}$$

The slenderness ratio of the beam-column is then calculated using Equation 3.3.

$$\text{slenderness ratio} = kl/r \tag{3.3}$$

In this study, the effective length factor k in Equation 3.3 had a value of 1.0 due to the assumption of pinned ends. ACI 318-83 and CAN3-A23.3-M84 specify that the slenderness effects may be neglected if the slenderness ratio calculated by Equation 3.3 has a value less than that calculated by Equation 3.4.

$$kl/r < 34 - 12(M_1/M_2) \tag{3.4}$$

In this study, the ratio of the end moments (M_1/M_2) is equal to 1.0. Therefore, beam-columns with a slenderness ratio of 22 or less were classified as short columns and the slenderness effects were neglected, i.e. the member strength was considered to be the same as the cross-section strength.

Slenderness effects must be considered for columns for which kl/r exceeds 22. For such cases, the critical strength of the slender beam-column P_c must be calculated by Equation 3.5.

$$P_c = \frac{\pi^2 EI}{(kl)^2} \tag{3.5}$$

To determine the critical strength by Equation 3.5, the flexural stiffness (EI) of the beam-column was first calculated by Equation 3.6.

$$EI = \frac{(E_c I_g / 5)}{1 + \beta_d} + E_s I_s \qquad (3.6)$$

In this study the value of β_d in Equation 3.6 was taken equal to 0.0 as stated earlier. It is interesting to note that the design codes allow the stiffness of the vertical reinforcing bars to be considered for reinforced concrete columns, but not for composite columns even though the requirements for percentage of vertical reinforcing bars are identical for both cases.

Slenderness effects reduce the bending moment capacity of a beam-column associated with a particular axial load. Hence, for axial loads lower than the long column concentric capacity, these effects were accounted for through a bending moment modifier δ_b (Equation 3.7) applied to the cross-section bending moment capacity obtained at the same load level of axial load.

$$\delta_b = \frac{C_m}{1 - \frac{P}{\phi P_c}} \geq 1.0 \qquad (3.7)$$

The modifier has a value of 1.0 for the pure bending case and increases until the long column concentric capacity is reached. The ϕ factor in Equation 3.7 was taken equal to

1.0 as explained earlier and the C_m factor is defined as the equivalent uniform bending moment diagram factor and was calculated from Equation 3.8.

$$C_m = 0.6 + 0.4\frac{M_1}{M_2} \geq 0.4 \tag{3.8}$$

In this study, C_m had a value of 1.0 due to the uniform primary bending moment diagram resulting from the assumption of equal and opposing end moments.

Dividing the cross-section bending moment capacity at a given axial load by δ_b yielded the slender column bending moment capacity at the same axial load as shown in Equation 3.9.

$$M_{slender} = M_{short} / \delta_b \tag{3.9}$$

This yielded one point on the slender beam-column $P-M$ interaction diagram (Figure 3.3). Calculating the slender beam-column bending moment capacities for several levels of axial load provided the data points required to construct the entire slender beam-column $P-M$ interaction diagram.

These points were then used for interpolating the long column moment and axial load capacities for specified end eccentricity ratios.

3.3 COMPARISON OF DESIGN CODES

ACI 318-83 and CSA CAN3-A23.3-M84 both impose limits on the geometry, material behavior, strength assumptions and the nominal strength of structural members designed in accordance with these codes. Generally, the two design codes are similar in their limitations. The limitations and the differences between the two codes are discussed below.

The most obvious difference in the ACI and CSA codes is with respect to the application of understrength factors. The ACI code calculates the nominal design strength of a composite beam-column using all specified material strengths and cross-section dimensions. An overall understrength factor ($\phi < 1.0$) is applied to the nominal axial and moment capacities. The magnitude of the understrength factor depends on the failure mode of the beam-column which is defined by the strain state relative to the balanced strain condition (balance point). ACI 318-83 defines the balanced strain condition as the point on the cross-section $P-M$ interaction diagram corresponding to the strain condition in which the strain at the compressive face of concrete reaches 0.003 as the tensile stress in the vertical reinforcing reaches its yield point. Failures at axial loads greater

than the balance point load are compression failures. Failures at axial loads less than the balance point load are tension failures. Tension failures can be predicted accurately and, therefore, the understrength factor for tension failures is greater than that for compression failures. The definition of the balance strain condition as it applies to composite beam-columns is discussed in detail in Section 5.3.1. The nominal strength program assumes the point corresponding to maximum moment on the cross-section $P-M$ interaction curve as the transition point between the tension and compression failures and the related understrength factors. In this study, the definition of the balance point does not affect the results since all understrength factors were set to 1.0.

CSA Standard CAN3-A23.3-M84 applies material understrength factors directly to the specified strengths of the constituent materials. Different values are applied to each material. No difference between compression or tension failure is made. This method has been used by the CSA code since the 1984 edition. Prior to this, the method used by ACI was also used by the CSA code.

Both design codes restrict the cross-section axial load capacity by imposing a ceiling on the axial load level. In the preceding section it was stated that the nominal strength subroutine calculates the cross-section concentric capacity on the basis of strain compatibility. The design

codes calculate the concentric axial load capacity by assuming that each material in the cross-section contributes to strength in proportion to its area and its maximum permissible stress (Note this assumes all materials reach their maximum permissible stress at the same strain). ACI 318-83 assumes that the concrete maximum stress is 85 percent of the specified 28-day cylinder strength and the steel stress is the specified yield stress of the material. The strength from each component is summed and multiplied by the compression failure understrength factor. The strength is reduced further by multiplying it by 0.85 as shown in Equation 3.10.

$$\phi P_n = 0.85\phi[0.85f'_c(A_g - A_{st}) + f_{ys}A_{st}] \qquad (3.10)$$

CSA CAN3-A23.3-M84 uses a similar technique by reducing the factored concentric axial load by 20 percent for composite columns with rectangular horizontal ties as shown in Equation 3.11.

$$P_n = 0.80[0.85\phi_c f'_c(A_g - A_s - A_r) + \phi_s f_{ys}A_s + \phi_r f_{yr}A_r] \qquad (3.11)$$

The ceilings on axial load described herein were not considered in the Monte Carlo study described in Chapter 5. How-

ever, the maximum axial load given by Equation 3.10 (Equation. 3.11 for CSA) is recorded in the output of the program for the reader's information.

Both codes apply an understrength factor to the calculated long column critical strength as shown in Equation 3.7. The value for the understrength factor is different for the two codes. However, for this study, the ϕ factor in Equation 3.7 was taken equal to 1.0.

Limitations on material strengths are similar in both codes. The minimum specified concrete strength is 2500 psi (17.2 MPa) for ACI 318-83 and 2900 psi (20 MPa) for CSA CAN3-A23.3-M84. The maximum structural steel yield strength permitted is 50,000 psi (345 MPa) for ACI 318-83 and 50,750 psi (350 MPa) for CSA CAN3-A23.3-M84. These criteria were taken into consideration when designing the beam-columns studied in Chapter 5.

Geometric limitations refer to percentage of steel area and to placement of vertical reinforcing bars and spacing of horizontal, rectangular ties. The ACI code limits the amount of vertical reinforcing bars to a minimum of 1.0 and a maximum of 8.0 percent of the net concrete area. No limit is indicated for the structural steel core. The CSA code requires that 1.0 to 8.0 percent of the gross area be vertical reinforcing bars. The maximum percentage of all steel (structural and reinforcing) is limited to 20 percent of the gross area for the CSA code. These limitations were also

included in the Monte Carlo analysis described in Chapter 5. Requirements for spacing of vertical reinforcing bars and lateral hoops is similar for both codes and will not be discussed further here.

4 PROBABILITY MODELS OF BASIC VARIABLES

The strength variation of a composite beam-column is due to the individual variations of strength and size of all elements of the beam-column. The statistics (probability models) of the basic variables were compiled and used in the Monte Carlo simulations (Chapter 5). Probability distributions of all variables were derived as part of this study from data available in the literature or were taken from previous studies. No new testing of materials was performed.

Two distinct probability distributions were used for each basic variable. One probability distribution described the in-batch variation of the variable and the other one described the global variation. In-batch variations represent expected variations within one production run of a manufacturer. Hence, in-batch probability distributions were used to calculate the in-batch variation ($V_{in\text{-}batch}$) of the strength of laboratory specimens as discussed in Section 2.10. Global probability distributions represent expected variations in material strength and dimensions due to differences in manufacturing practices between manufacturers of an item. They also represent variations in construction practice between different contractors. The global probability distributions were used in Monte Carlo simulations to calculate the strength variation of the composite

beam-column on an industry wide scale (Chapter 5). The global variations derived were based on North American data where possible.

Twenty-four basic variables affecting the strength of a composite beam-column were accounted for. The variables describe material stress-strain relations, size and geometry of individual components of the column cross-section, and overall column dimensions and geometry. The basic variables specific to concrete, structural steel, reinforcing bars and column dimensions are discussed in this chapter. Table 4.1 summarizes the in-batch probability distributions used in Section 2.10. Table 4.2 summarizes the global probability distributions used for the study described in Chapter 5.

4.1 CONCRETE

Three mechanical properties of concrete most affecting the strength of composite beam-columns are compressive strength, tensile strength (modulus of rupture) and modulus of elasticity. Descriptions of the probability distributions of these properties have been presented by Mirza et al. (1979c) and were used in this study. Summaries of these probability distributions are presented in this section. These probability models have been used by Mirza and MacGregor (1982 and 1989) for strength variation studies of reinforced concrete members.

Table 4.1 - In-batch Variations of Basic Variables*

Property	Mean	Standard Deviation	Coefficient of Variation
Concrete in Structure (loaded to failure in 2 hr.)			
Compressive Strength (psi)	3320	166	0.05
Modulus of Rupture (psi)	462	23	0.05
Modulus of Elasticity (ksi)	3084	108	0.035
Structural Steel			
Modulus of Elasticity (ksi)	29000	290	0.01
Static Yield Strength of Web (psi)	53360	1067	0.02
Initial Tangent Modulus of Strain Hardening Curve (ksi)	600	150	0.25
Reinforcing Steel			
Modulus of Elasticity (ksi)	29200	292	0.01
Static Yield Strength (psi)	56115	1403	0.025
Strain at Start of Strain-hardening	0.015	0.0015	0.10
Ultimate Strain	0.15	0.015	0.10
Deviation of Overall Dimensions from Specified Values			
Cross Section depth and width	0.0	0.08	-
Concrete Cover to Lateral Hoops	0.0	0.055	-

*Notes: (1) Data for in-batch variations of basic variables shown are only for Column D8-90 taken from Table 2.3. Other columns used in determination of in-batch variations [Columns LH-100-C, LH-100-B, and RC1 (Table 2.3)] used the same coefficients of variation as shown for concrete, structural steel and reinforcing steel and the same standard deviation for deviation of dimensions from specified values. Mean values for the basic variables of those columns were determined from the test data and were different from those shown in this table.

(2) All probability distributions were assumed to be normal except for static yield strength of structural steel and reinforcing steel where modified lognormal probability distributions were used with lower boundaries of 0.75 times the static yield strength.

(3) 1000 psi = 1 ksi = 6.895 MPa; 1 in. = 25.4 mm.

Table 4.2 - Overall Variations of Basic Variables

Property	Mean	Standard Deviation	Coefficient of Variation
Concrete in Structure (Loaded to Failure in 1 hr.)			
Compressive Strength (psi)			
-Average Quality Control			
f'_c = 4000 psi	3388	596	0.176
f'_c = 6000 psi	4640	817	0.176
-Excellent Quality Control			
f'_c = 6000 psi	4640	631	0.136
Modulus of Rupture (psi)			
-Average Quality Control			
f'_c = 4000 psi	445	97	0.218
f'_c = 6000 psi	523	114	0.218
-Excellent Quality Control			
f'_c = 6000 psi	523	111	0.211
Modulus of Elasticity (ksi)			
-Average Quality Control			
f'_c - 4000 psi	3260	388	0.119
f'_c - 6000 psi	3800	452	0.119
-Excellent Quality Control			
f'_c = 6000 psi	3800	399	0.105
Structural Steel			
Modulus of Elasticity (ksi)	29000	580	0.02
Static Yield Strength of Web f_{yws} (psi)			
f_y = 36000 psi	39240	3375	0.086
f_y = 44000 psi	47960	4125	0.086
f_y = 50000 psi	54500	4687	0.086
Static yield strength of flange - f_{yfs}	0.95 f_{yws}	n/a*	n/a*
Static ultimate strength of web - f_{uws}	1.5 f_{yws}	n/a*	n/a*
Static ultimate strength of flange - f_{ufs}	1.5 f_{yfs}	n/a*	n/a*
Strain at Start of Strain-Hardening	0.017	0.004	0.24
Initial Tangent Modulus of Strain Hardening Curve (ksi)	600	150	0.25
Residual Stresses (psi)			
- W10 x 54 (W250 x 80)			
at flange tip	-18576**	2786	0.15
at flange-web juncture	12089	8825	0.73
- W10 x 112 (W250 x 167)			
at flange tip	-19311**	2897	0.15
at flange-web juncture	16240	11855	0.73

Table 4.2 (continued)

Ratio of Actual to Nominal Dimensions			
- section depth	1.0	0.0	0.0
- flange width	1.005	0.0136	0.0135
- flange thickness	0.976	0.0407	0.0417
- web thickness	1.0167	0.039	0.038
Reinforcing Steel			
Modulus of Elasticity (ksi)	29000	957	0.033
Static Yield Strength - f_{yrs} f_{yr} = 60,000 psi	66800	5520	0.083
Static Ultimate Strength - f_{urs}	1.55 f_{yrs}	n/a*	n/a*
Strain at Start of Strain-hardening	0.015	0.004	0.267
Ultimate Strain	0.15	0.03	0.2
Deviation of Overall Column Dimensions from Specified Values			
Length (in.)	0.0	0.67	-
Cross Section depth (in.)	+0.0625	0.25	
Cross Section width (in.)	+0.0625	0.25	
Concrete Cover to lateral hoops (in.)	+0.33	0.166	
Spacing of lateral hoops (in.)	0.0	0.53	-

* Value of this variable is assumed dependent on the value of another variable.

** (-) indicates compressive stress.

Notes: (1) All columns had nominal cross-section of 20 x 20 in. with 1.5 in. clear concrete cover to lateral hoops. Lateral hoop nominal spacing was 10 in.

(2) Yield strength of reinforcing bars was assumed to follow a beta probability distribution, whereas the yield strength of structural steel, the ratio of actual to specified flange width, and the ratio of actual to nominal web thickness were represented by modified lognormal probability distributions with lower limits of 0.75 times the specified yield stress, 0.884, and 0.813, respectively. All other variables were assumed to follow normal probability distributions.

(3) 1000 psi = 1 ksi = 6.895 MPa; 1 in. = 25.4 mm.

4.1.1 Compressive Strength

The in-situ compressive strength of concrete differs from the specified strength due to factors including variations in materials, mixing, placing and curing techniques, quality control and rate of loading (Mirza et al. 1979c). The mean value of compressive strength of in-situ concrete is lower than that indicated by standard cylinder tests. This is recognized in both ACI 318-83 and CSA CAN3-A23.3-M84 as only 85 percent of the specified 28-day cylinder strength is allowed for design use. To relate the specified 28-day cylinder strength to the mean 28-day in-situ strength loaded at a similar rate (35 psi or 0.241 MPa per second), Mirza et al. (1979c) proposed the expression given in Equation 4.1.

$$\begin{aligned} \bar{f}_{cstr35} &= 0.675 f_c' + 1{,}100 \quad \leq 1.15 f_c' psi \\ &= 0.675 f_c' + 7.58 \quad \leq 1.15 f_c' MPa \end{aligned} \tag{4.1}$$

Rate of loading affects the strength of concrete. Mirza et al. (1979c) studied experimental tests by others in order to relate the compressive strength of concrete in a structure at a given rate of loading to concrete in a structure loaded at the standard cylinder test rate. This relation is given in Equation 4.2.

$$\bar{f}_{cstrR} = \bar{f}_{cstr35}[0.89(1 + 0.08\log_{10}R)] \quad psi \qquad (4.2)$$
$$= \bar{f}_{cstr35}[0.89(1 + 0.08\log_{10}145R)] \quad MPa$$

The loading rate R was calculated by dividing the mean concrete strength calculated by Equation 4.1 by the loading time to failure.

The coefficient of variation of the in-situ compressive strength, V_{cstrR}, was calculated by Equation 4.3 (Mirza et al. 1979c).

$$V^2_{cstrR} = V^2_{creal} + V^2_{in-situ} + V^2_R \qquad (4.3)$$

V_{creal} represents the variation in the relation between real cylinder strength and the specified design strength. $V_{in-situ}$ represents the variation in the relation between in-situ strength and real cylinder strength. V_R represents the variation in the relation between concrete loaded at R psi/sec and concrete loaded at 35 psi/sec (0.241 Mpa/sec). Jones and Richart (1935) found only a small dispersion in concrete strength due to rate of loading effects. Allen (1970) suggested that dispersion of concrete strength is unaffected by the speed of testing. Therefore, V_R can be considered negligible (Mirza et al. 1979c). $V_{in-situ}$ has been assumed to equal 10 percent by Mirza et al. (1979c) based on

the work by Davis (1976) and was used in this study as well.

The strength of concrete in test cylinders varies due to the real variations, V_{creal}, and in-batch variations, $V_{in-batch}$. This relation is shown in Equation 4.4.

$$V_{ccyl}^2 = V_{creal}^2 + V_{in-batch}^2 \qquad (4.4)$$

$V_{in-batch}$ was estimated as 4 percent by Mirza et al. (1979c) and was used in this study. This roughly corresponds to the suggestions of American Concrete Institute Committee 214 (ACI 1965) which recommend $V_{in-batch}$ values of 4-5 percent for good quality control, 5-6 percent for average quality and above 6 percent for poor quality control.

By combining equations 4.3 and 4.4 the variation of the in-situ compressive strength is given by Equation 4.5.

$$V_{cstrR}^2 = V_{ccyl}^2 - V_{in-batch}^2 + V_{in-situ}^2 + V_R^2 \qquad (4.5)$$

Substituting a value of 4 percent for $V_{in-batch}$, 10 percent for $V_{in-situ}$, and zero for V_R, as discussed above, into Equation 4.5 yields Equation 4.6:

$$V_{cstrR}^2 = V_{ccyl}^2 - 0.04^2 + 0.10^2 \qquad (4.6)$$

The variation in the strength of test cylinders V_{ccyl} was found to be dependant on the degree of quality control for a particular job. Combining data from a variety of sources, Mirza et al. (1979c), found that for specified concrete strengths up to 4000 psi (27.6 MPa), the average V_{ccyl} was roughly constant with values of 10, 15 and 20 percent for excellent, average and poor quality control, respectively. For specified compressive strengths greater than 4000 psi, V_{ccyl} decreases due to the higher degree of care used in the manufacture of higher strength concrete (Mirza et al. 1979c). In the Monte Carlo simulations described in Chapter 5, quality control of concrete was assumed to be average for specified design strengths of 4000 psi (V_{ccyl} = 15 percent) and excellent (except where noted) for 6000 psi concrete (V_{ccyl} = 10 percent). Data studied by Mirza et al. (1979c) suggested a normal distribution for the compressive strength of in-situ concrete which was also assumed for this study.

4.1.2 Tensile Strength

Mirza et al. (1979c) studied data from the literature to establish the relationship between compressive cylinder strength and tensile strength (modulus of rupture). The relationship given by Equation 4.7 was found to most closely fit the regression line calculated from the data (Mirza et al. 1979c).

$$f_r = 8.3\sqrt{f_c} \quad psi \qquad (4.7)$$
$$= 0.689\sqrt{f_c} \quad MPa$$

This value is only slightly larger than the value suggested by ACI 318-83 for modulus of rupture shown in Equation 4.8.

$$f_r = 7.5\sqrt{f_c} \quad psi \qquad (4.8)$$
$$= 0.623\sqrt{f_c} \quad MPa$$

The in-situ tensile strength of concrete may differ from control specimens due to effects of volume, rate of loading and effect of concrete being cast-in-situ and not into a specified control test form. Bolotin (1969) found that the volume of the test specimen did not significantly effect the minimum tensile strength of the concrete, although mean strengths were. Since the minimum values are unaffected, the volume effect can be neglected for understrength studies (Mirza et al. 1979c). Wright (1952) showed that the tensile strength of concrete increased with increasing rate of loading. McNeely and Lash (1963) suggested a logarithmic relation between the tensile strength and the rate of stress application. Data on the effect of in-situ casting as opposed to control specimen casting was not found by Mirza et al. (1979c) and they chose to assume the effect as negligible. Using the results of their analysis of data and the

relation suggested by McNeely and Lash, Mirza et al. (1979c) proposed that the relation given in Equation 4.9 be used to calculate the mean value of the modulus of rupture for a given loading rate.

$$\bar{f}_{rstrR} = 8.3\bar{f}^{1/2}_{cstr35}[0.96(1 + 0.11\log_{10}R)] \quad psi \qquad (4.9)$$

$$= 8.3\bar{f}^{1/2}_{cstr35}[0.96(1 + 0.11\log_{10}145R)] \quad MPa$$

Calculating tensile strength from a relation based on a calculation of compressive strength results in considerably larger dispersions than for compressive strength alone. The total variation of the tensile strength calculated from Equation 4.9 combines the variations due to the calculation of the compressive strength as discussed in the previous section and the variability of the ratio of observed to calculated (Equation 4.7) tensile strength. Mirza et al. (1979c) calculated the coefficient of variation of the ratio of modulus of rupture calculated by Equation 4.7 to actual tested modulus of rupture calculated to be 20 percent. The total variation may, therefore, be expressed as shown in Equation 4.10.

$$V^2_{rstrR} = \frac{V^2_{cstr35}}{4} + 0.2^2 \quad \geq V^2_{cstrR} \qquad (4.10)$$

V_{cstr35} was taken equal to V_{cstrR} and calculated from Equation 4.6 since the effect of loading rate on the coefficient of variation was assumed negligible. Substituting Equation 4.6 into Equation 4.10 yields Equation 4.11.

$$V^2_{rstrR} = \frac{V^2_{ccyl}}{4} + 0.0421 \geq V^2_{cstrR} \qquad (4.11)$$

The probability distribution of the tensile strength was assumed to be normal although some deviation from normality may be expected (Mirza et al. 1979c).

4.1.3 Modulus Of Elasticity

Mirza et al. (1979c) studied data from 139 standard cylinder tests of normal weight concrete from the University of Illinois. This data provided measurements of cylinder strength and initial tangent modulus of elasticity in compression. The relationship of compressive cylinder strength to initial tangent modulus was found to have a high degree of correlation. The relationship given in Equation 4.12 was proposed for the mean value of elastic modulus at a loading rate of 35 psi/sec (0.241 Mpa/sec).

$$E_{ci35} = 60,400\sqrt{f_c} \quad psi \qquad (4.12)$$
$$= 5,016\sqrt{f_c} \quad MPa$$

This relationship yields slightly higher values for the tangent elastic modulus than the ACI 318-83 recommendation shown in Equation 4.13.

$$E_c = 57,000\sqrt{f_c} \quad psi \qquad (4.13)$$
$$= 4,734\sqrt{f_c} \quad Mpa$$

The ratio of modulus of elasticity calculated by Equation 4.12 and the observed elastic modulus from the test data was found to have a mean value of 1.0 and a coefficient of variation of 8 percent. A normal probability distribution was found to adequately approximate the above-noted ratios (Mirza et al. 1979c).

The effect of the rate of loading on the elastic modulus was studied by Allen (1970). Equation 4.14 was proposed to relate the elastic modulus at any loading rate to the standard cylinder test rate of 35 psi/sec (0.241 Mpa/sec).

$$\overline{E}_{cR} = (1.16 - 0.08\log_{10} t)\overline{E}_{c35} \qquad (4.14)$$

where t = loading duration in seconds.

As Equation 4.14 indicates, an increase in the loading time results in a softening of the concrete to the peak stress. Combining the results of the Illinois test data and Allen,

Mirza et al. (1979c) proposed the following equation for the mean value of initial tangent modulus of elasticity of concrete in structure.

$$\bar{E}_{cistrR} = 60,400\bar{f}^{1/2}_{cstr35}(1.16 - 0.08\log_{10}t) \quad psi \qquad (4.15)$$

$$= 5,016\bar{f}^{1/2}_{cstr35}(1.16 - 0.08\log_{10}t) \quad Mpa$$

The coefficient of variation of the modulus of elasticity calculated by Equation 4.15 must include all of the variations associated with the compressive strength as well as the variations inherent to Equation 4.12. Combining these factors, the coefficient of variation of the initial tangent modulus of in-situ normal weight concrete can be calculated by Equation 4.16 (Mirza et al. 1979c).

$$V^2_{cistrR} = \frac{V^2_{cstr35}}{4} + 0.08^2 \qquad (4.16)$$

Substituting the value of V^2_{cstr35} from Equation 4.6 into Equation 4.16 related the in-situ coefficient of variation of initial tangent modulus in compression to the coefficient of variation of test cylinders as shown in Equation 4.17.

$$V^2_{cistrR} = \frac{V^2_{ccyl}}{4} + 0.0085 \qquad (4.17)$$

In this study, Equation 4.15 and 4.17 were used to compute the mean value and the coefficient of variation of the modulus of elasticity of in-situ concrete. The probability distribution of the modulus of elasticity was assumed to follow a normal distribution after Mirza et al. (1979c).

Mirza et al. (1979c) found little data on the modulus of elasticity of concrete in tension, but what was found showed little difference between compressive and tensile elastic moduli. They concluded that the tensile and compressive elastic moduli may be assumed to have equal magnitude.

4.2 STRUCTURAL STEEL

Variations in the mechanical and geometric properties of the rolled steel section effect the variation of the overall strength of the composite beam-column. The mechanical properties that define the stress-strain curve of structural steel described in Section 2.7.1 are the modulus of elasticity, the yield stress, the strain at the start of strain hardening, the initial tangent slope of the strain hardening curve and the ultimate stress. The yield strain and the ultimate strain can be calculated from the above properties and the assumptions described in Section 2.7.1. Variations in residual stresses in the rolled steel section also influence the overall strength variation of the beam-column. Variation of the dimensions of the depth, flange width, flange thickness and web thickness affect the cross sectional area and the stiffness (moment of inertia) of the

steel section. To properly model the basic variables noted above for use in the theoretical program (Chapter 2) and for the Monte Carlo analysis (Chapter 5), the mean value, coefficient of variation (or standard deviation) and the type of probability distribution were defined for each basic variable. These definitions were taken from the literature or derived from data existing in the literature. No new test data was generated in this study. A description of the statistical distributions used for each variable is given below.

4.2.1 Modulus of Elasticity

Galambos and Ravindra (1978) studied existing experimental data of mechanical properties of rolled structural steel sections to determine the statistical properties. They recommended that a value of 29,000,000 psi (200,000 MPa) be used as the mean value for the modulus of elasticity for structural steel shapes and the coefficient of variation be taken as 6 percent. Kennedy and Gad Aly (1980) considered only the data from North American sources compiled earlier by Galambos and Ravindra and recommended that a value of 1.9 percent be used for the coefficient of variation. Bjorhovde (1972) found very small variations of the modulus of elasticity in the data he studied (0.1 to 0.5 percent) and he, therefore, considered the modulus of elasticity to be constant.

The mean values and the coefficients of variation of the data collected by Galambos and Ravindra (1978) is shown in Table 4.3 (Rows 1 to 6). The data in Rows 1 to 5 in the same table was collected from North American sources and in Row 6 from a European source. The weighted means and coefficients of variation were calculated and are presented for all of the data (Row 7) and for the data from only the North American sources (row 8).

Based on above-noted discussions and Table 4.3 (Row 8), it was decided to use a value of 29,000,000 psi (200,000 MPa) as the mean value for the modulus of elasticity with a coefficient of variation of 2 percent. None of the authors referenced above commented on the shape of the probability distribution curve for modulus of elasticity of structural steel. Mirza et al. (1979b) assumed a normal distribution for the modulus of elasticity of reinforcing steel. Since no other data was found, a normal probability distribution was used for the modulus of elasticity of structural steel.

4.2.2 Yield Strength

The yield strength of a rolled structural steel shape is dependant on the rate of loading, the location of the specific element on the cross-section and the thickness of the material. The influence of each of these three factors is discussed below.

Table 4.3 - Elastic Modulus of Structural Steel

Row No. (1)	Reference (2)	No. of Test Specimens (3)	Mean Value (ksi) (4)	Coefficient of Variation (5)
1	Lyse & Keyser (1934)	7	29360	0.010
2	Rao et al. (1964)	56	29437	0.014
3	Julian (1957)	67	29540	0.010
4	Julian (1957)	67	29550	0.010
5	Johnston and Opila (1941)	50	29774	0.038
6	Tall and Alpsten (1969)	94	31200	0.060
7	*	341	30013	0.044
8	**	247	29562	0.020

* Row 7 combines all data from Rows 1 to 6 inclusive.

** Row 8 combines data from North American sources only (Rows 1-5).

Notes: (1) All data from tension tests except Row 4 which is for compression tests.
(2) 1 ksi = 6.895 MPa.

Generally, the strength reported by steel mills is either the upper (f_{yu}) or lower (f_{yl}) yield strength as shown on Figure 4.1. The strain rates (about 1,000 micro in. per in. per second) used for mill tests are significantly higher than those expected under normal loading conditions (Beedle and Tall 1960). Under normal loading applications, the load may be applied at a very low rate. Therefore, the "static" yield stress, defined as the yield stress at a zero rate of strain f_{ys}, is the yield stress of interest (Figure 4.1). The static yield stress f_{ys} is measured by halting the plastic strain until the stress drops from the dynamic yield stress (f_{yd}) to stabilize at the static yield stress as shown in Figure 4.1. Rao et al. (1964) proposed that the static yield stress may be calculated from the relationship:

$$f_{ys} = f_{yd} - (3.2 + 0.001\dot{\epsilon}) \quad \text{ksi} \qquad (4.18)$$

$$= f_{yd} - (22.07 + 0.001\dot{\epsilon}) \quad \text{MPa}$$

where $\dot{\epsilon}$ is measured in micro in. per in. per sec. or micro mm per mm per sec.

Kennedy and Gad Aly (1980) used Equation 4.18 to calculate the difference between the dynamic and static yield stress for the CSA Standard G40.20-1974 maximum test strain rate of 1/16 in. per in. per minute (1040 micro in./in./sec.). The dynamic yield stress was calculated to

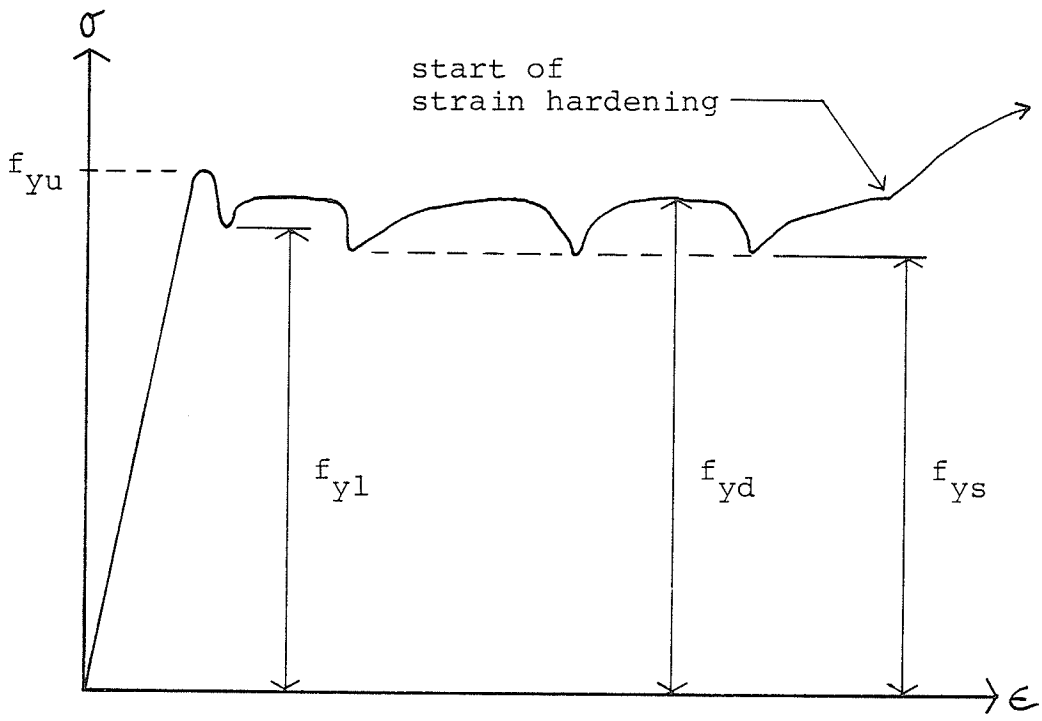

f_{yu} = upper yield stress
f_{yl} = lower yield stress
f_{yd} = dynamic yield stress
f_{ys} = static yield stress

Figure 4.1 - Definitions of yield stress of steel

be 4.2 ksi (29 Mpa) greater than the static yield stress. As shown in Figure 4.1, the lower yield stress (f_{yl}) lies between the dynamic and static yield stress levels. Kennedy and Gad Aly (1980) assumed that the static yield stress was 2 ksi (13.8 MPa) less than the lower yield point.

Beedle and Tall (1960) found that the original location of the test coupon on the rolled wide flange shape affected the yield strength of the specimen. Coupons cut from the web were found to have yield strengths greater than coupons cut from the flange. Generally, mill tests are performed on web specimens (Beedle and Tall 1960). Kennedy and Gad Aly (1980) attributed the higher strength of the web to increased work hardening during the rolling process due to the smaller thickness of webs.

Alpsten (1972) found a tendency for thicker plates to have lower yield strengths. He attributed this to a coarser grain structure due to a longer cooling period. He also commented that during the manufacture of thick plates, steel producers may alter the chemical composition to account for lower strengths. It should be noted that the plate sizes investigated by Alpsten exceeded one inch (25.4 mm) in thickness. Kennedy and Gad Aly (1980) neglected any variation in yield strength directly due to component plate thickness since the data they analyzed included this variation. The same assumption was made in this study.

Mill test data is based only on tensile tests. However, it has been found that there is no difference in static yield stress level for tension or compression tests (Galambos and Ravindra 1978). Hence, the properties derived from tensile tests have been assumed to apply to the compressive loading case as well in this study.

4.2.2.1 Web yield strength - Tension tests on web coupons from North American rolled shapes were summarized by Lay (1965), American Iron and Steel Institute (1972) and Kennedy and Gad Aly (1980). The mean values and coefficients of variation of mill tests tabulated by Lay and American Iron and Steel Institute for steel with a specified yield strengths of 33 ksi (228 MPa) are shown in Columns 2 and 3 of Table 4.4, respectively. These mill tests report dynamic yield stress and were also used by Galambos and Ravindra (1978) for statistical analysis of web yield strength. Kennedy and Gad Aly reported mill test measurements of lower yield point stress for Canadian steel grade CSA G40.21-44W. The mean value and coefficient of variation of this data are given in Column 4 of Table 4.4.

To determine the mean value and coefficient of variation of the ratio of web static yield stress to specified yield stress, the data reported by Lay (1965), American Iron and Steel Institute (1972) and Kennedy and Gad Aly (1980) were statistically pulled together. First, the mean value, standard deviation and coefficient of variation of the reported

Table 4.4 - Web Yield Stress Measurements

Property (1)	Lay (1965) (2)	American Iron and Steel Institute (1972) (3)	Kennedy and Gad Aly (1980) (4)
No. of Tests	3794	3124	4507
Specified yield stress f_y (ksi)	33	33	44
Measured Values			
-Mean yield stress f_{yw} (ksi)	40.0	39.4	50.6
V	0.09	0.08	0.064
σ (ksi)	3.6	3.15	3.24
-Mean static yield stress f_{yws} (ksi)	36.0	35.4	48.6
V	0.10	0.089	0.067
σ (ksi)	3.6	3.15	3.24
-Mean static yield stress ratio f_{yws}/f_y	1.091	1.073	1.105
V	0.10	0.089	0.067
σ	0.109	0.095	0.074

Note: 1 ksi = 6.895 MPa.

mill strengths were calculated for the three sets of data as shown in Columns 2, 3 and 4 of Table 4.4. The mean static yield stress ($\bar{f}_{ys}$) was then computed from Equation 4.18 assuming a strain rate $\dot{\epsilon}$ of 800 micro in./in./sec. (800 micro mm/mm/sec.) for the data given in Columns 2 and 3 of Table 4.4. The strain rate assumed was previously used by Galambos and Ravindra (1978) when they studied the same data and was, therefore, considered applicable in this study. For the data shown in Column 4 of the same table, $\bar{f}_{ys}$ was taken as 2 ksi (13.8 MPa) lower than the mill test mean lower yield stress as previously assumed by Kennedy and Gad Aly (1980). The new coefficients of variation were calculated based on $\bar{f}_{ys}$. The mean value of the ratio of static to specified yield stress (mean stress ratio) was then calculated by dividing the mean static yield stress value for each data set by the specified yield stress for that data set. Multiplying the mean stress ratios by the coefficients of variation gave the standard deviation of the mean stress ratio for each data set.

The weighted mean stress ratio was calculated by combining the data from all three data sets using Equation 4.19 and was calculated to be 1.092.

$$\overline{X} = \frac{\sum_{i=1}^{k} N_i \overline{x}_i}{\sum_{i=1}^{k} N_i} \qquad (4.19)$$

The weighted standard deviation of the stress ratio was calculated by Equation 4.20 to be 0.094.

$$\sigma = \sqrt{\frac{\sum_{i=1}^{k} N_i \sigma_i^2 + \sum_{i=1}^{k} N_i (\overline{x}_i - \overline{X})^2}{\sum_{i=1}^{k} N_i}} \qquad (4.20)$$

The ratio of this weighted standard deviation and the mean stress ratio gave the coefficient of variation of the ratio of web static yield stress to specified yield stress and was calculated to be 0.086. In the Monte Carlo analysis described in Chapter 5, the mean web static yield stress was assumed as 1.09 times the specified yield stress with a coefficient of variation of 8.6 percent. Galambos and Ravindra recommended that the mean value be taken as 1.10 times the specified value with a coefficient of variation of 11 percent, while Kennedy and Gad Aly proposed that the mean strength of the web was 1.11 times the specified value with a coefficient of variation of 6.5 percent. These values are somewhat different from those used for this study.

4.2.2.2 **Flange yield strength** - Beedle and Tall (1960) reported that flange static yield stress was 4 to 7 percent lower than that for the web. Galambos and Ravindra (1978) recommended that the mean value for the static yield strength of the flange be taken as 1.05 times the specified yield stress with a coefficient of variation of 10 percent. Kennedy and Gad Aly (1980), based on the report of Beedle and Tall (1960), assumed that the flange static yield stress was 95 percent of the web static yield stress. The assumptions made by Kennedy and Gad Aly were also used in this study. The flange strength was assumed to be directly in proportion with the web strength and no further variation was applied.

4.2.2.3 **Probability distribution of yield strength** - Frequency histograms of the yield strength of test specimens were reported as positively skewed (Alpsten 1972). This is reasonable since any heat (manufacturing run) of steel not meeting the minimum specified criteria will be rejected, truncating the lower end of the strength probability distribution. Since the frequency distribution is not symmetrical, a normal distribution is not valid. Alpsten (1972) recommended a modified lognormal distribution for yield strength of structural steel.

To define a distribution for the yield strength, a modified lognormal distribution was fitted to the web data provided by Kennedy and Gad Aly (1980) for CSA G40.21 Grade 44W

steel. The histogram and statistical parameters for the data are given in Figure 4.2. A modified lognormal distribution was derived using the mean value and standard deviation of the data and Equations 4.21, 4.22 and 4.23.

$$\bar{x}_{10} = \frac{1}{2}\log_{10}\left[\frac{(\bar{x}-X_o)^4}{(\bar{x}-X_o)^2+\sigma_x^2}\right] \tag{4.21}$$

$$\sigma_{10} = 0.4342945\sqrt{\log_{10}\frac{\sigma_x^2+(\bar{x}-X_o)^2}{(\bar{x}-X_o)^2}} \tag{4.22}$$

$$PDF = \frac{0.4342945}{(x-X_o)\sigma_{10}\sqrt{2\pi}}\exp\left\{-\frac{1}{2}\left[\frac{\log_{10}(x-X_o)-\bar{x}_{10}}{\sigma_{10}}\right]^2\right\} \tag{4.23}$$

Equations 4.21, 4.22 and 4.23 give respectively the mean value, standard deviation and cumulative frequency of a modified lognormal distribution. Lower boundary values (X_o) of 36, 38 and 40 ksi (248.3, 262, and 275.9 MPa) were tested for the data reported by Kennedy and Gad Aly. The best fit to the data was with a lower boundary of 36 ksi as shown in Figure 4.3.

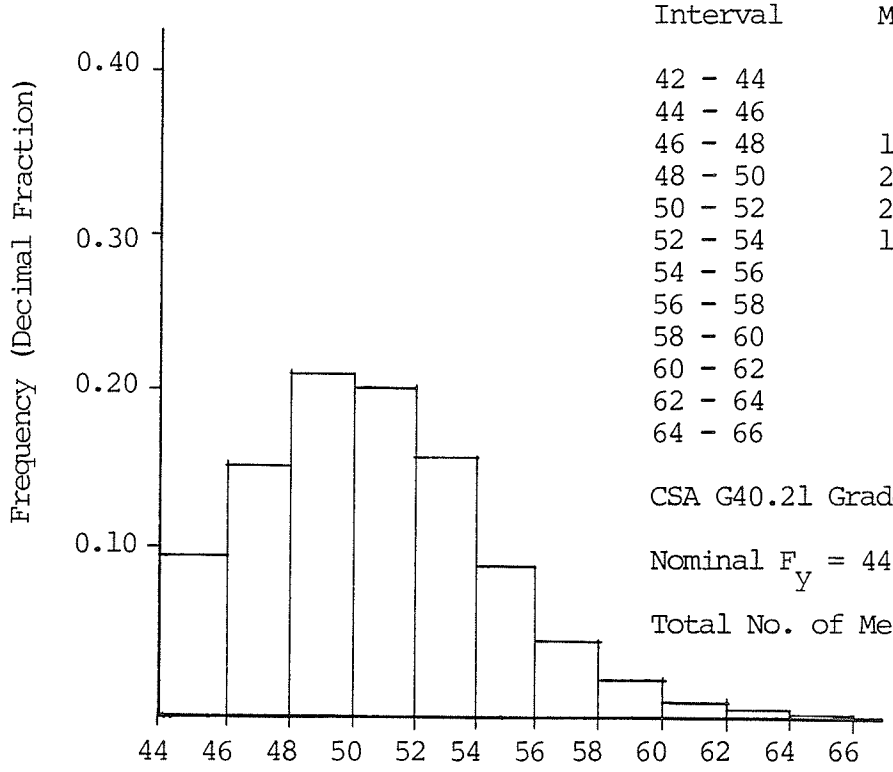

Class Interval	% of Measurements
42 - 44	0.00
44 - 46	9.56
46 - 48	15.73
48 - 50	21.19
50 - 52	20.59
52 - 54	16.04
54 - 56	9.25
56 - 58	4.53
58 - 60	2.06
60 - 62	0.80
62 - 64	0.16
64 - 66	0.09

CSA G40.21 Grade 44W

Nominal F_y = 44 ksi (303.4 MPa)

Total No. of Measurements = 4507

$\overline{F}_{yl}$ = 50.61 ksi = 348.9 MPa

$V_{F_{yl}}$ = 0.064

Figure 4.2 - Variation of Web Lower Yield Strength (F_{yl})
(Kennedy and Gad Aly 1980)

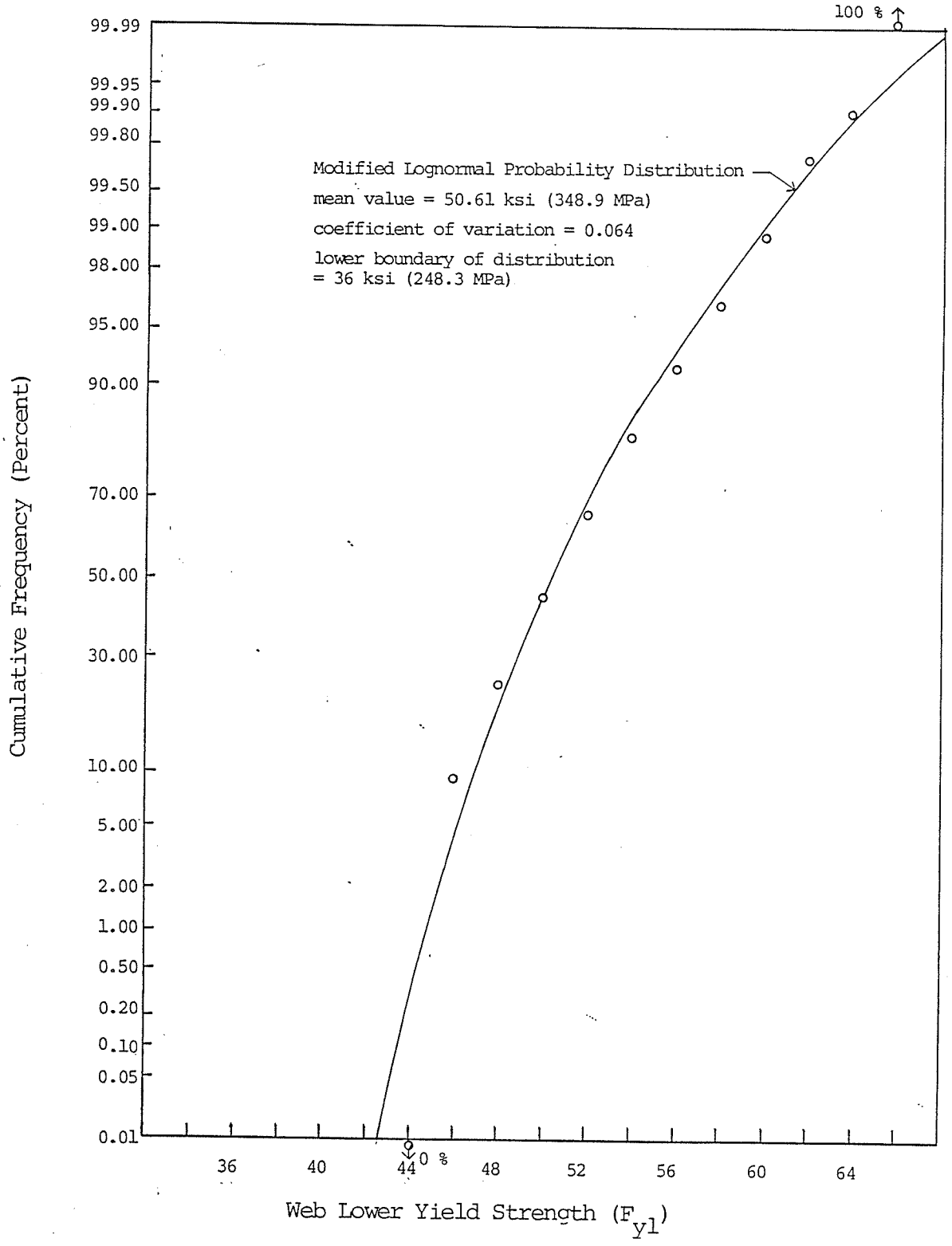

Figure 4.3 - Cumulative Frequency of Web Lower Yield Strength (F_{yl})

To adjust the web data in Figure 4.2 from mill yield stress to static yield stress the mean values and the lower boundary were reduced by 2 ksi (13.8 MPa) as noted previously. Thus, a lower boundary value (X_o) of 34 ksi (234.5 MPa) was calculated for the web static yield stress or 77 percent of the specified yield strength. For simplicity, however, a value of 75 percent of the specified yield strength was taken as the lower boundary for the web. The cumulative frequency of the web static yield strength was, therefore, computed from Equation 4.23 with X_o taken as 0.75 times the specified yield stress. The static yield strength of the flange was assumed as 95 percent of the web static yield strength at any point along the cumulative frequency curve.

4.2.3 Ultimate Stength

Little data was found on the ultimate strength of a rolled structural steel shape. Alpsten (1972) presented data indicating the ratio of ultimate strength to yield strength ranged from 1.36 to 1.89 with an average value of 1.59 for 41 samples taken from a single rolled section. Specifications for structural steel indicate minimum ultimate tensile strength requirements ranging from 1.28 times the specified yield strength for CSA G40.21-M 350W steel to 1.61 for ASTM A36 steel. For this study, the static ulti-

mate stress was arbitrarily chosen to be 1.5 times the static yield stress. No further variation was defined for this parameter.

4.2.4 Strain At Initiation Of Strain-Hardening

Alpsten (1972) reported values for the strain at the end of the plastic plateau (initiation of strain-hardening) for various grades of structural steel. These values range from 1.1 percent for ASTM A572 steel to 2.0 percent for ASTM A36 steel. The average value recommended by Alpsten for ASTM steels was 1.72 percent. No information on the variability of this strain was found. For this study, a mean value of 0.017 was chosen with a coefficient of variation of 26 percent for the strain at initiation of strain-hardening for structural steel. Note the coefficient of variation used for structural steel is the same as that measured for reinforcing steel (Section 4.3.4).

4.2.5 Strain Hardening Modulus

The strain hardening modulus defines the initial tangent slope of the strain-hardening portion of the structural steel stress-strain relationship. Alpsten (1972) reported values of 450 to 720 ksi (3,103 to 4,965 MPa) for tension and 700 to 820 ksi (4,828 to 5,655 MPa) for compression strain-hardening modulus of ASTM steels. Alpsten noted that there was very little information on the strain hardening properties of steels and that various definitions of the strain hardening modulus could result in large discrepancies

in reported values. Galambos and Ravindra (1978) studied work by Doane at the University of Texas at Austin (1969). Doane measured the strain hardening modulus for ASTM A7, A36 and A441 steels. The tensile strain hardening modulus was found to have a mean of 570 ksi (3,931 MPa) and the corresponding compressive value was 670 ksi (4,621 MPa). Galambos and Ravindra recommended a mean value of 600 ksi (4138 MPa) and a coefficient of variation of 25 percent.

In this study it was assumed that the mean value of the initial tangent strain-hardening modulus was 600 ksi and the coefficient of variation was 25 percent. The same value was used for both compressive and tensile loading conditions.

4.2.6 Dimensional Variations

Variations in the dimensions of the rolled steel shape are discussed here to distinguish them from overall column dimensional variations. Alpsten (1972) reported that measurements of approximately 5000 rolled shapes from European mills showed very little variation in section depth and flange width. More variation was noticed in the flange and web thicknesses. A tendency for flanges to be thinner and webs to be thicker than the nominal dimensions was noted.

Kennedy and Gad Aly (1980) reported measurements of flange width, flange thickness and web thickness of wide flange sections manufactured at Canadian mills. They used

these measurements along with assumptions based on code tolerance limits to evaluate the mean values and coefficients of variation of the steel section geometric properties.

In the Monte Carlo simulations (Chapter 5), the dimensions of the rolled steel section were varied according to statistics of the data reported by Kennedy and Gad Aly (1980). The remaining geometric properties of the steel section were calculated using the simulated dimensions.

4.2.6.1 Section depth - Kennedy and Gad Aly (1980) estimated the statistical parameters of the ratio of actual to nominal section depth by using the tolerance limits of CSA Standard S16.1 for Steel Structures for Buildings. This code allows the section depth to vary 0.2 inch (4 mm) maximum from the nominal value. Kennedy and Gad Aly assumed that the mean ratio of actual to nominal depth was equal to 1.0. The extreme values of the ratio of actual to nominal depth were then calculated considering the upper and lower permitted tolerances. Six standard deviations were assumed to occur between the upper and lower values. The coefficient of variation was calculated by dividing the standard deviation by the mean value. When this method was applied to a nominal 10 inch (254 mm) deep section, the coefficient of variation was computed to be less than 1 percent. Since this coefficient of variation was so small, it was assumed that the actual depth of the rolled section was equal to the nominal depth and that there was no variation.

4.2.6.2 **Flange width** - Data regarding the ratio of actual to nominal flange width for 1248 samples was presented by Kennedy and Gad Aly (1980). A histogram of the frequency distribution of the data from their report is reproduced in Figure 4.4. The mean value of the ratio is 1.005 with a coefficient of variation of 1.35 percent. The measured data was plotted on a normal probability paper (Figure 4.5). Normal and modified lognormal probability distributions were plotted using the calculated mean and coefficient of variation. The best fit to the data, especially at the lower tail, was found to be a modified lognormal distribution with lower boundary of 0.88 as shown in Figure 4.5.

Based on Figure 4.5, a modified lognormal distribution was assumed for the ratio of actual to nominal flange width. The lower boundary of the ratio was set at 0.88. The mean value was taken to be 1.005 with a coefficient of variation 1.35 percent as calculated by Kennedy and Gad Aly (1980).

4.2.6.3 **Flange thickness** - Kennedy and Gad Aly (1980) reported data on 2768 measurements of the ratio of actual to nominal flange thickness. A histogram of the frequency distribution is shown in Figure 4.6. The mean value of the ratio was 0.976 with a coefficient of variation of 4.17 percent. The data was also plotted on a normal probability paper along with a normal distribution using the reported statistical parameters (Figure 4.7). Figure 4.7 indicates

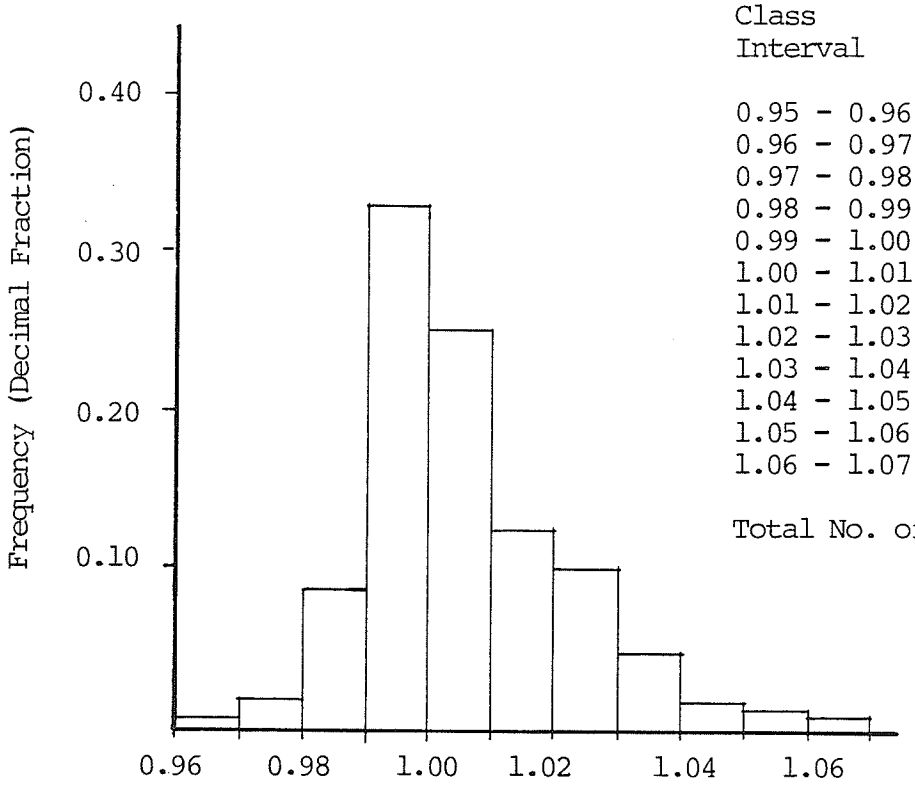

Class Interval	% of Measurements
0.95 - 0.96	0.00
0.96 - 0.97	0.24
0.97 - 0.98	1.65
0.98 - 0.99	8.47
0.99 - 1.00	32.93
1.00 - 1.01	25.32
1.01 - 1.02	12.47
1.02 - 1.03	10.00
1.03 - 1.04	4.59
1.04 - 1.05	1.88
1.05 - 1.06	1.29
1.06 - 1.07	1.18

Total No. of Measurements = 1248

Mean value of ratio = 1.005

Coefficient of Variation of ratio = 0.0135

Figure 4.4 - Variation of Ratio of Measured / Nominal Flange Width of W Sections (Kennedy and Gad Aly 1980)

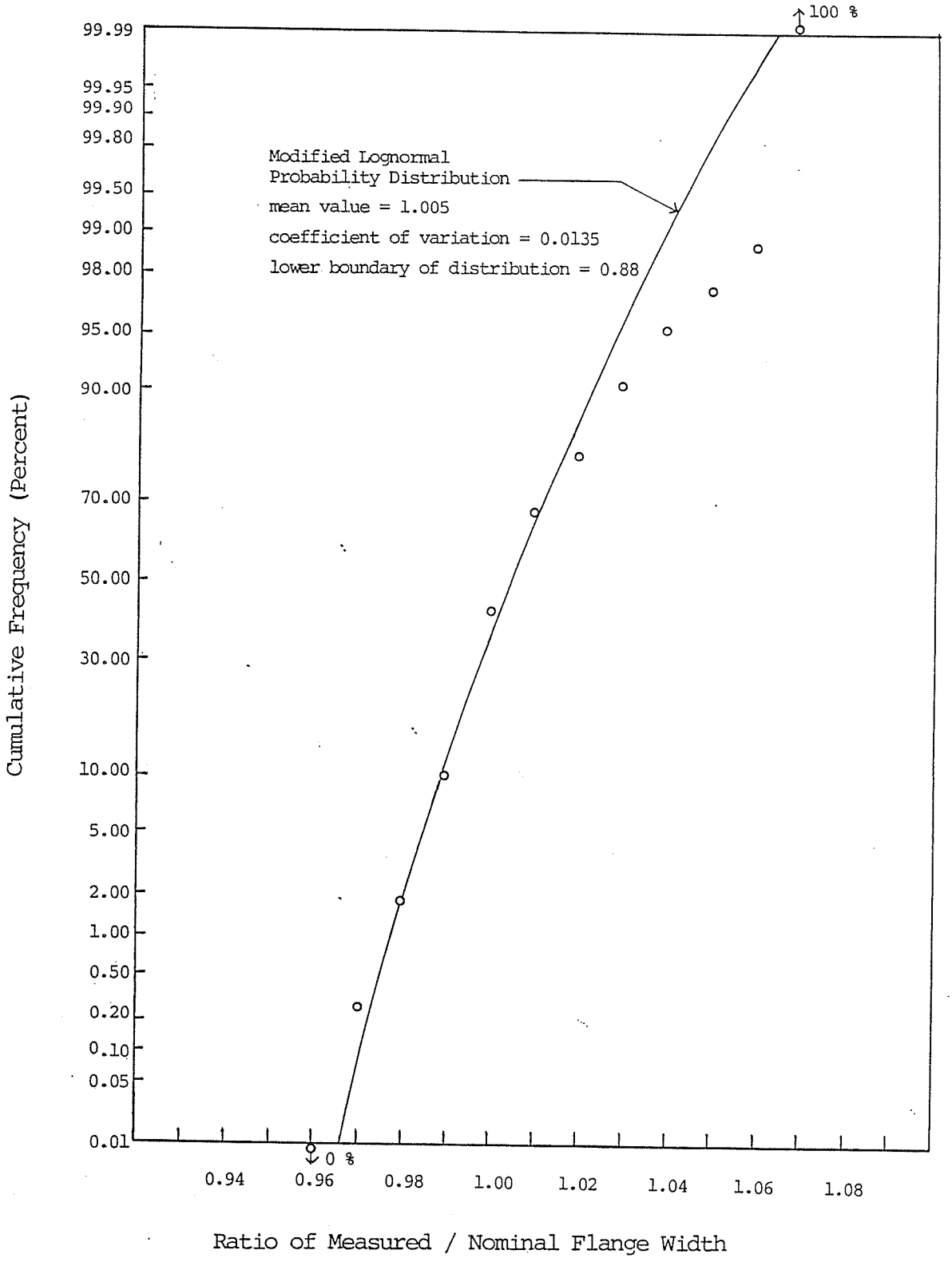

Figure 4.5 – Cumulative Frequency of Ratio of Measured / Nominal Flange Width of W Sections

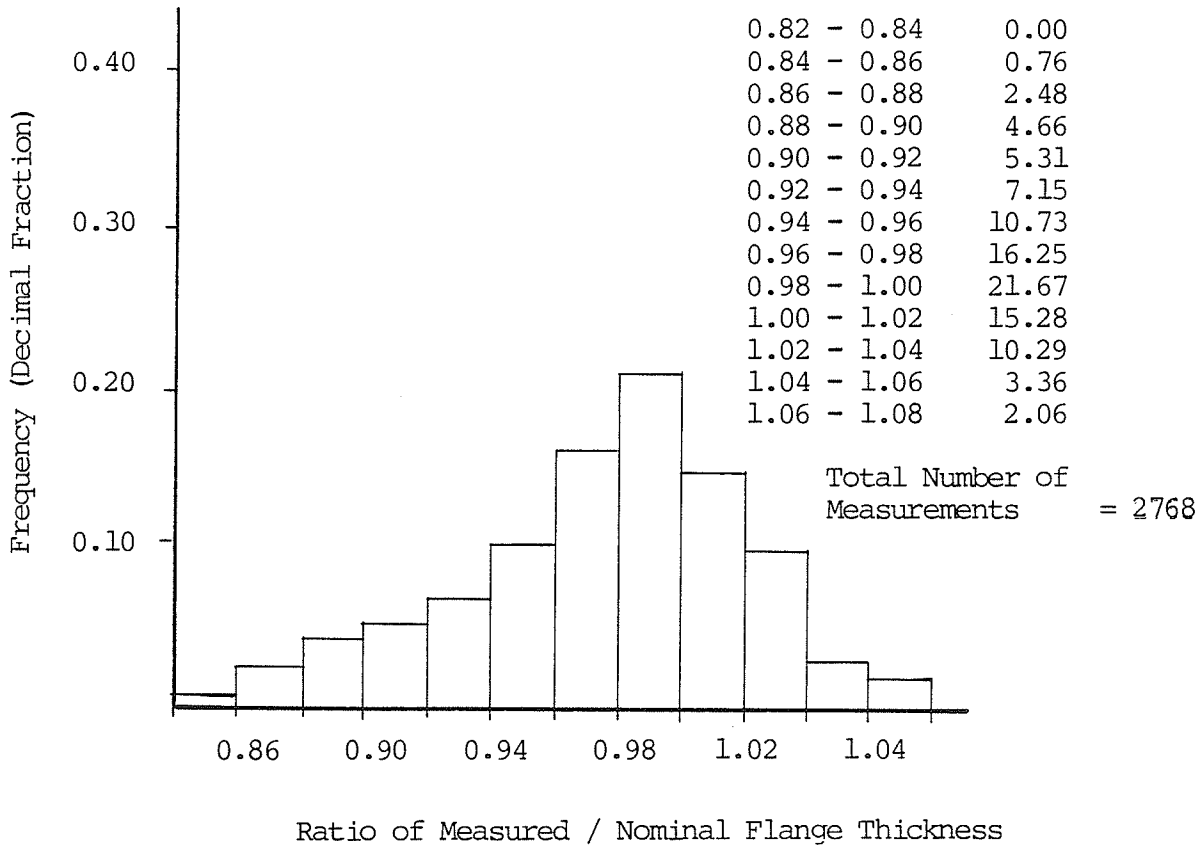

Mean value of ratio = 0.976

Coefficient of Variation of ratio = 0.0417

Figure 4.6 - Variation of Ratio of Measured / Nominal Flange Thickness of W Sections (Kennedy and Gad Aly 1980)

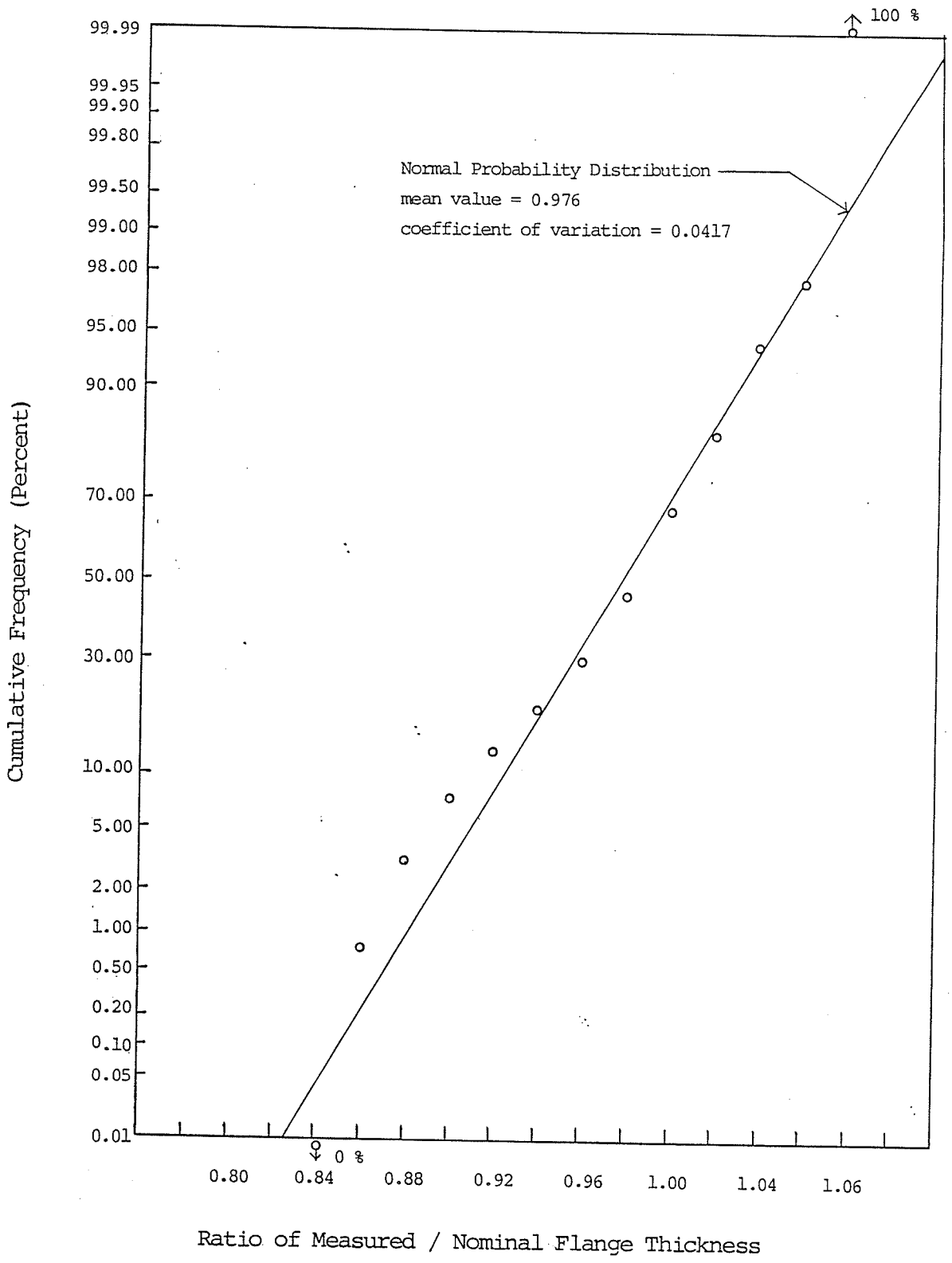

Figure 4.7 - Cumulative Frequency of Ratio of Measured / Nominal Flange Thickness of W Sections

that a normal probability distribution provides a reasonable estimate of the actual probability distribution. A normal distribution with the mean value and coefficient of variation as reported by Kennedy and Gad Aly was used in this study for the ratio of actual to nominal flange thickness.

4.2.6.4 Web thickness - Kennedy and Gad Aly (1980) reported measurements of the ratio of actual to nominal web thickness. Based on a total of 352 measurements, a mean value of 1.0167 and a coefficient of variation of 3.84 percent was calculated. A histogram of the frequency distribution of the web thickness data is shown in Figure 4.8. The data was also plotted on a normal probability paper (Figure 4.9). Normal and modified lognormal probability distributions using the reported mean and standard deviation were compared to the data. A modified lognormal distribution with a lower boundary set at 0.8 was found to provide the best fit to the data as indicated by Figure 4.9.

A modified lognormal distribution was, therefore, used in this study for the ratio of actual to nominal flange width. The lower boundary of the ratio was set at 0.8. The mean and coefficient of variation were set at the values calculated by Kennedy and Gad Aly (1980).

4.2.7 Residual Stresses

Residual stresses in steel sections have a large variation associated with them (Beedle and Tall 1960, Alpsten 1972). Sources of variation are from different cooling

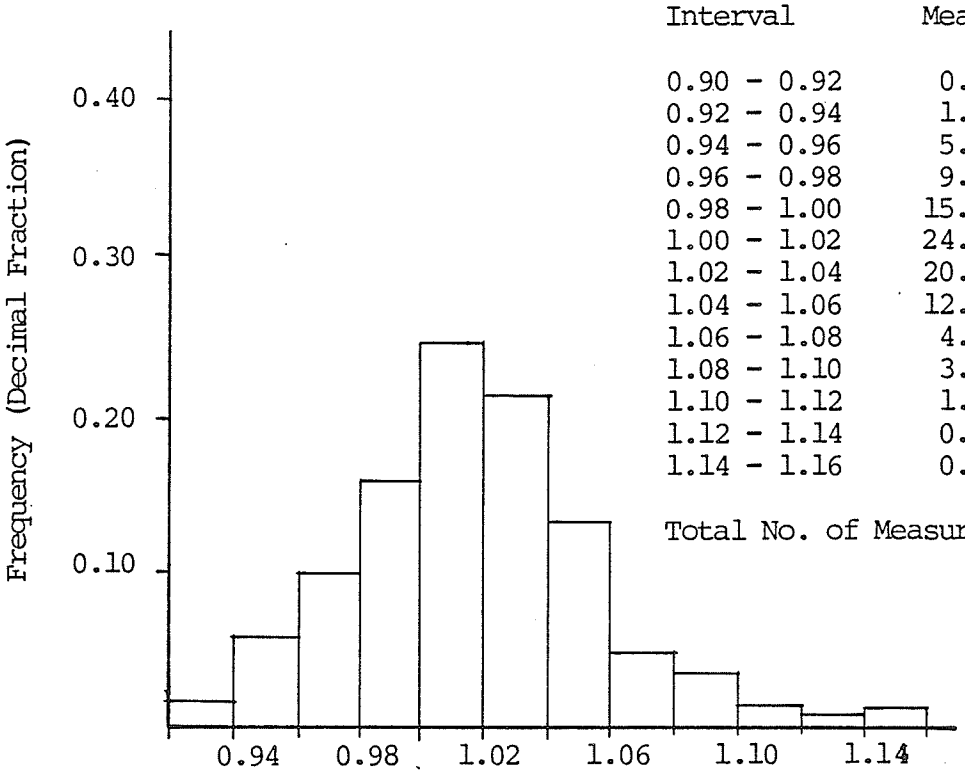

Mean value of ratio = 1.0167

Coefficient of Variation of ratio = 0.0384

Figure 4.8 - Variation of Ratio of Measured / Nominal Web Thickness of W Sections (Kennedy and Gad Aly 1980)

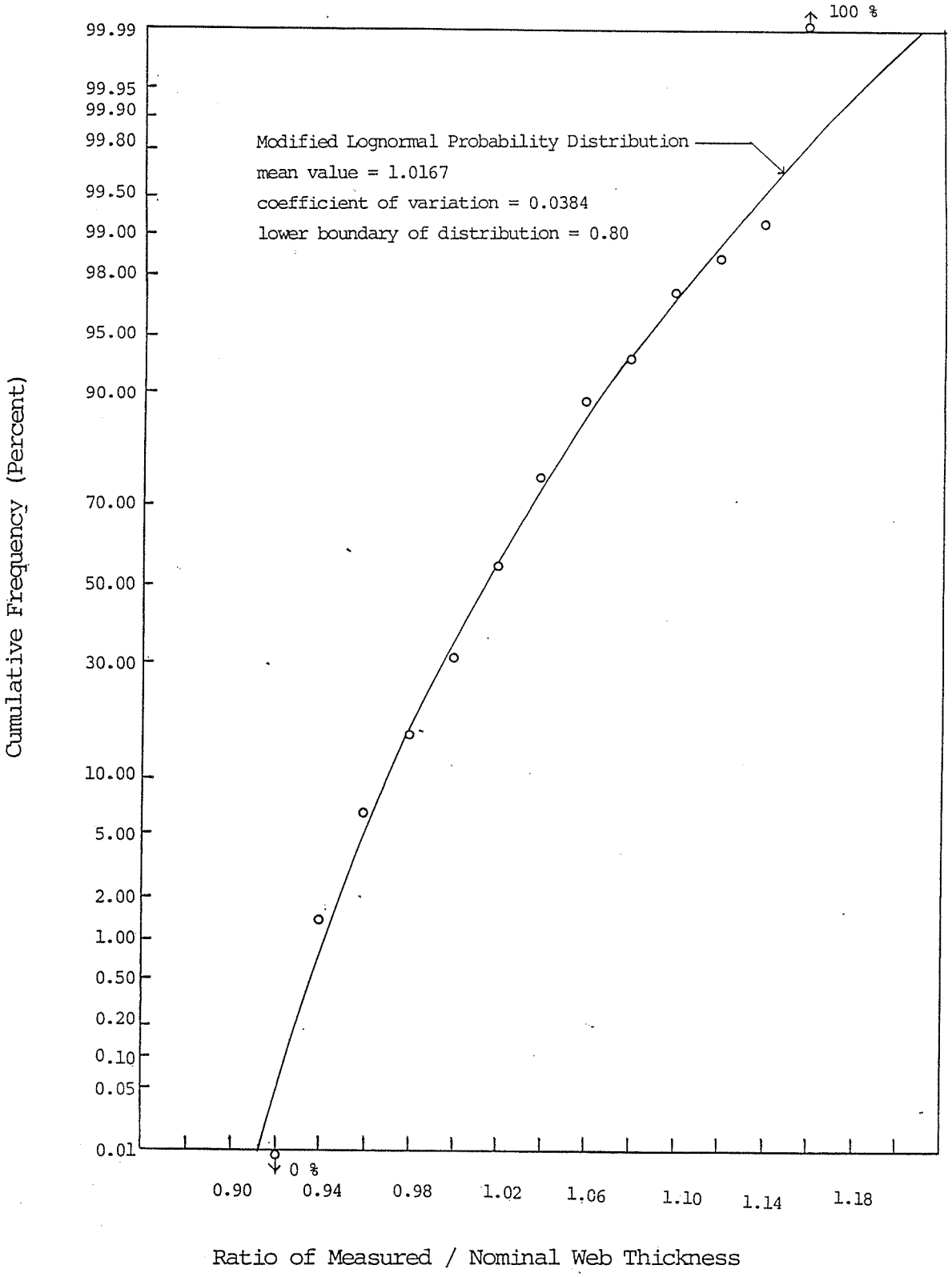

Figure 4.9 - Cumulative Frequency of Ratio of Measured / Nominal Web Thickness of W Sections

rates, different manufacturing processes (Alpsten 1968), and dimensional variations of the cross section. Further variations result from straightening of the steel section through rollers or by gagging (bending about a point) (Alpsten 1968). The combined effect of these sources of variation makes it difficult to accurately predict the variability of the residual stresses in a structural steel shape.

Beedle and Tall (1960) reported the results of residual stress measurements on a large number of American steel wide flange shapes. The maximum, minimum and average values for the residual stress at the flange tip and at the flange-web juncture for beam and column shapes were reported. The data for column shapes is summarized in Table 4.5. This data was used to estimate the coefficients of variation of residual stresses which were then used for the Monte Carlo simulations (Chapter 5). Six standard deviations were assumed to occur between the maximum and minimum values. The coefficient of variation was calculated by dividing the standard deviation by the reported average value given in Table 4.5. The coefficient of variation of the residual stress at the flange tip so calculated was 14.3 percent. For simplicity, a value of 15 percent was used in this study. Using the same procedure, the coefficient of variation of the residual stress at the flange-web juncture was calculated to be 73 percent and was used in this study. The

Table 4.5 - Measured Residual Stress in Wide Flange Column Shapes (Beedle and Tall (1960))

Residual Stress at Flange Tip (ksi)			Residual Stress at Flange-Web Juncture (ksi)		
Minimum	Mean	Maximum	Minimum	Mean	Maximum
-7.7	-12.8	-18.7	16.5	4.7	-4.1

Note: 1 ksi = 6.895 MPa; (-) indicates compressive stress.

higher coefficient of variation of the stress at the flange-web juncture is reasonable since this location is more likely to have its cooling rate affected by external influences. The mean values used for the residual stresses were calculated from Equations 2.20 and 2.21 given in Section 2.8. A normal probability distribution was arbitrarily assumed for all residual stresses.

4.3 REINFORCING STEEL

Variations in the mechanical and geometric properties of the vertical and transverse reinforcing bars affect the variation of the overall strength of the composite beam-columns. This is because the variations in the properties of vertical reinforcing bars affect the overall strength of a beam-column directly in terms of stiffness and in the development of the $M-\phi-P$ relationships. Similarly, the variations in the properties of the transverse ties affect the degree of confinement of concrete and, therefore, indirectly affect the overall strength of the beam-column. The mechanical properties that define the stress-strain relations of the reinforcing bars (described in Section 2.7.2) are the modulus of elasticity, yield stress, strain at initiation of strain hardening, ultimate stress, and ultimate strain. The only geometric variation of concern to this study is the ratio of actual to nominal cross-sectional area. Strength variations due to variation in placement of reinforcing bars is discussed in Section 4.4. To properly

model the basic variables noted above for use in the theoretical subroutine (Chapter 2) and for the Monte Carlo analysis (Chapter 5), the mean value, coefficient of variation (or standard deviation) and the type of probability distribution were defined for each basic variable. These definitions were either taken directly from the literature or derived from the data available in the literature. No new test data was generated for this study. A description of the statistical distributions used for each variable is given below.

4.3.1 Modulus Of Elasticity

The elastic modulus for steel in reinforcing bars has been found to have a small dispersion and is relatively unaffected by rate of loading (Mirza et al. 1979b). Allen (1972) found that the variability of elastic modulus was about the same for in-batch and overall variations. Variations resulting from the ratio of actual to nominal area of bar were also incorporated into the overall variation. Allen (1972) suggested a mean value of 28,500 ksi (196,550 MPa) and a coefficient of variation of 2 percent. Mirza et al. (1979b) studied Allen's data as well as data from others. They suggested that the probability distribution of elastic modulus can be considered normal with a mean value of 29,200 ksi (201,380 MPa) and a coefficient of variation of 3.3 percent.

In this study it was assumed that the elastic modulus of reinforcing steel followed a normal distribution with a mean of 29,000 ksi (200,000 MPa) and a coefficient of variation of 3.3 percent.

4.3.2 Yield Strength

Factors contributing to the variability of yield strength of reinforcing steel are the variation in the composition of the steel, variation in the actual cross-sectional area of the bar and the effect of rate of loading (Mirza et al. 1979b). As outlined for structural steel (Section 4.2.2), the static yield strength rather than the dynamic yield strength provides a better estimate of the yield strength of the bars under normal loading conditions in a building. Static loading reduces the magnitude of the yield strength and is, therefore, of more interest for reliability analysis.

Yield strengths reported from mill tests are based on strain rates of approximately 1040 micro in. per in. per sec (Mirza et al. 1979b) which is the same as that reported for mill tests of structural steel (Kennedy and Gad Aly 1980). Rao et al.'s equation (1964) presented earlier (Equation 4.18) was found to correlate well with the yield strength data at various strain rates (Mirza et al. 1979b). A value of 4 ksi (27.6 MPa) was suggested as a reasonable assumption to describe the difference between the mill test (dynamic) and the static yield strengths. By combining the

collected test data and accounting for the differences between the mill test and the static yield strength, Mirza et al. (1979b) calculated the mean static yield strength of 66.8 ksi (460.7 MPa) and a coefficient of variation of 8.3 percent for Grade 60 reinforcing bars.

The probability distribution of the static yield strength was studied by Mirza et al. (1979b) and was found to be positively skewed. This is reasonable since quality control practices limit the probability of the yield strength being less than specified. A probability density function of a beta distribution was found to provide the best fit to the static yield strength data. The probability density function suggested by Mirza and MacGregor for Grade 60 reinforcing steel is shown in Equation 4.24:

$$PDF = 7.587\left(\frac{f_{ys} - 54}{48}\right)^{2.02}\left(\frac{102 - f_{ys}}{48}\right)^{6.95} \qquad (4.24)$$

in which $54 \text{ ksi} \leq f_{ys} \leq 102 \text{ ksi}$.

For SI conversion, multiply the terms 48, 54, and 102 in Equation 4.24 by 6.895.

The probability density for static yield strength of Grade 60 reinforcing bar described by Equation 4.24 is plotted in Figure 4.10 while the cumulative frequency is plotted in Figure 4.11. These curves were used for the

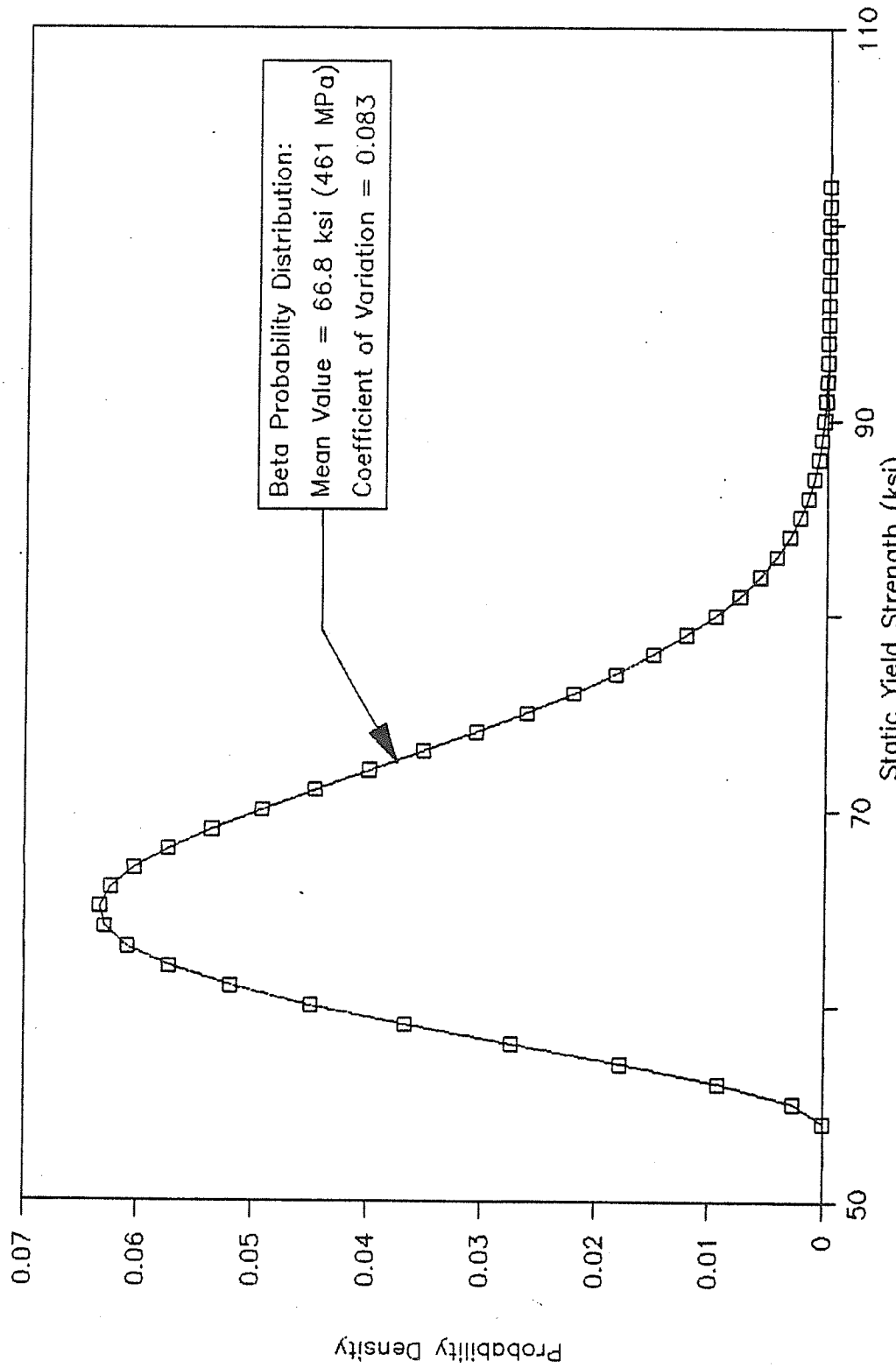

Figure 4.10 – Probability Density for Static Yield Strength of Grade 60 (414 MPa) Reinforcing Bars

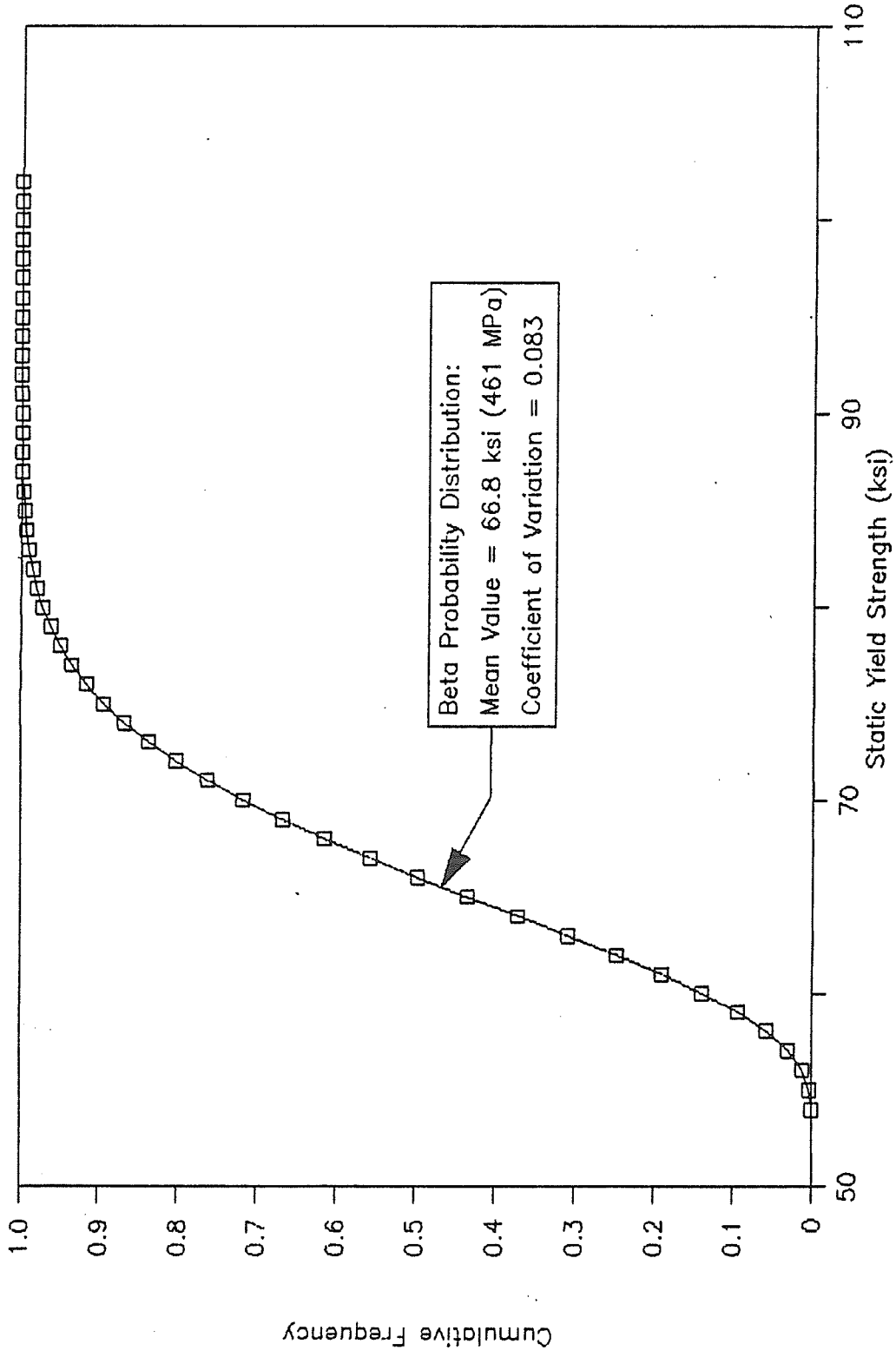

Figure 4.11 – Cumulative Frequency for Static Yield Strength of Grade 60 (414 MPa) Reinforcing Bars

Monte Carlo simulations reported in this study (Chapter 5). It should be noted that the data used to derive Equation 4.24 was based on nominal areas of bar cross-section. Therefore, the effect of variation in ratio of actual to nominal bar cross-sectional area is already included in Equation 4.24.

4.3.3 Ultimate Strength

Factors affecting the variation of ultimate strength are the same as those affecting the yield strength. Mirza et al. (1979b) reported that the ratio of ultimate to yield strength had a mean value of 1.55. The coefficient of variation was essentially unchanged from the values obtained for yield strength data (8.3 percent). Since it is reasonable to assume that reinforcing steel with a higher yield strength will also have a higher ultimate strength, the static ultimate strength of reinforcing steel was simply taken as 1.55 times the static yield strength for use in the Monte Carlo simulations (Chapter 5).

4.3.4 Strain At Initiation Of Strain Hardening

Allen (1972) performed controlled tensile tests on various sizes of reinforcing bars and determined the strain at the initiation of strain hardening. The strain value was found to vary significantly depending on the bar diameter and ranged from a minimum of 0.7 percent for No. 14 (44.5 mm diameter) bars to a maximum of 2.2 percent for No. 5 (15 mm diameter) bars. Allen calculated a strain value of 1.49

percent with a coefficient of variation of 26.6 percent for the strain at the commencement of strain hardening when all bar sizes were considered.

In this study, the mean value of the strain at the initiation of strain hardening was taken as 1.5 percent and the coefficient of variation was assumed to be 26.6 percent. Allen (1972) made no analysis of the probability distribution. A normal probability distribution was arbitrarily assumed for this study.

4.3.5 Ultimate Strain

Allen (1972) measured the ultimate strain of reinforcing bars ranging in size from No. 3 to No. 14 (9.5 mm to 44.5 mm diameter). The mean ultimate strain reported by Allen was 15.5 percent and the coefficient of variation was 20.3 percent.

In this study the ultimate strain of reinforcing bars was assumed to have a mean value of 15.5 percent. For simplicity, the coefficient of variation was taken as 20 percent. A normal probability distribution was arbitrarily assumed for ultimate strain of reinforcing bars.

4.4 COLUMN GEOMETRY

A composite column is a combination of factory made and site casted components. In this section the variations in field fabrications affecting the strength of beam-columns are discussed. The field fabrications for the construction of a composite column are similar to those for a reinforced

concrete column. Mirza et al. (1979a) studied published data to determine the statistics of the geometric variables of reinforced concrete columns. For this study, these statistics were assumed applicable to composite columns as well. The variables described are the column length, the overall column width and depth, the concrete cover to the hoop reinforcing, the spacing of rectangular hoops and the distance from the geometric centroid of the column to interior reinforcing bar layers.

To keep the theoretical strength subroutine (**RTHEO**) as efficient as possible, the cross-section of the composite beam-column was assumed to be symmetric about each axis (Chapter 2). This assumption reduces the number of variables allowed from the maximum number possible that affect the strength of a composite column. Unsymmetric variations about the minor axis do not affect the strength of the columns analyzed in this study since major axis bending, without twisting, was assumed. Unsymmetric variations about the major axis could affect the strength slightly but were neglected. A discussion of each of the variables considered is given in the following subsections.

4.4.1 Column Length

No data for variations of column length was found in the literature available. To accommodate this variable, the statistical description of beam span suggested by Mirza et al. (1979a) was assumed to be applicable to the column

length. The deviation from the specified column length used had a mean value of 0.0 and a standard deviation of 0.67 inch (17 mm). A normal probability distribution was assumed for this variable. For cross-section studies, the specified length of the column was input as 0.0.

4.4.2 Column Width And Depth

The overall column width and depth may vary due to inaccurate forming. Mirza et al. (1979a) studied data recorded by others on overall dimensions of cast-in-place columns. They recommended that for rectangular columns with face dimensions ranging from 11 to 30 inches (280 to 762 mm), mean deviation of the face dimension was 1/16 inch (1.6 mm) greater than the specified value with a standard deviation of 1/4 inch (6 mm). A normal probability distribution was recommended by Mirza et al. (1979a).

In this study, the above-noted statistical properties were used. The width and depth of the column were varied independently.

4.4.3 Concrete Cover

The concrete cover is measured from the face of the column to the exterior edge of the lateral hoops. This dimension may vary due to inaccurate fabrication of the hoop, inaccurate forming of the column, or both. Measurements of the concrete cover do not distinguish these sources. Since the variation of column face dimension is calculated separately, this variable can be considered to be a measurement

of the placement of extreme bar layers (Mirza et al. 1979a). Grant (1976) studied data of others and suggested that the deviation of the concrete cover from the specified value (C_{sp}) could be described by a normal distribution with a mean value ($\overline{C}_a$) given by Equation 4.25 and a standard deviation of 0.166 inches (4.2 mm):

$$\begin{aligned} \overline{C}_a &= C_{sp} + 0.25 + 0.004h \text{ in.} \\ &= C_{sp} + 6.35 + 0.102h \text{ mm} \end{aligned} \qquad (4.25)$$

The cover concrete is a function of the face dimension of the column (h). These values were used to vary independently the amount of concrete cover parallel to the minor and major axis.

4.4.4 Placement Of Layers Of Vertical Bars

The dimension from the major axis to the center line of the extreme bar layers was defined by the concrete cover. It was assumed that these bars were tied to the lateral hoops and, therefore, were not independently varied.

The dimension from the major axis to interior bar layers was described by a normal probability distribution with a mean value deviation from the specified dimension of +0.04 inch (1 mm) and a standard deviation given by Equation 4.26 (Mirza et al. 1979a):

$$\sigma_{ca} = 0.20 + 0.033h \quad \text{in.} \qquad (4.26)$$
$$= 5.08 + 0.838h \quad \text{mm}$$

where σ_{ca} is the standard deviation of the dimension from the major axis to the bar layer and h is the overall depth of the column. This statistical description was assumed in the Monte Carlo simulations. It should be noted that due to the double symmetry of the cross-section assumed by the theoretical strength model (Chapter 2), an interior bar layer located at the major axis was assumed to have no deviation from the specified location.

4.4.5 Spacing Of Rectangular Hoops

Spacing of the rectangular hoops affects the degree of confinement of the core concrete and, therefore, the strength of the composite beam-column (Section 2.6.2). No data on the variation of rectangular hoop spacing was found. Mirza and MacGregor (1982) assumed that the spacing of ties in concrete beams followed a normal probability distribution with a mean value equal to the specified value and standard deviation equal to 0.53 in. (13.5 mm). These values were assumed to be valid for the spacing of ties in columns as well and were used for this study.

5 SIMULATION AND ANALYSIS OF COMPOSITE BEAM-COLUMN STRENGTHS

The theoretical ultimate strengths (R_t) of a composite beam-column were simulated 500 times by a Monte Carlo technique and were based on the theoretical strength model and probability distributions of the variables affecting the strength. These strengths were divided by the nominal ultimate strength (R_n) of the beam-column which was computed using the Code procedures and the nominal properties of variables affecting the strength. This provided the simulated sample of the non-dimensionalized strength ratios (R_t/R_n) for the beam-column. A statistical analysis of the simulated sample provided the coefficient of variation and other probability distribution properties of the strength ratios for the beam-column under consideration. The beam-columns studied were of various cross-section configurations and lengths. A general description of the Monte Carlo technique is given first followed by descriptions of the beam-column configurations studied. The results of the study are then discussed with the effect of different variables on the overall strength variations examined. The discussions are given separately for short and for slender columns.

5.1 MONTE CARLO TECHNIQUE

The premise of the Monte Carlo technique is that the overall variability of the performance of a system can be

synthetically derived if a deterministic relationship between the system performance and each variable affecting the performance exists and the probability distributions of all variables affecting the performance are known (Mirza 1985b). Repeated random choosing of the value of each variable according to its individual probability distribution, calculating the performance of the system based on each set of randomly generated values of variables, and statistically analyzing the simulated sample of system performance will provide the overall variation of the performance of the system. A flowchart of the technique is given in Figure 5.1.

As the number of simulations is increased, the synthetically created probability distribution of the system performance will tend to its true distribution (Mirza 1985b). Mirza (1985b) compared sample sizes of 200, 500 and 1000 simulations in a variability analysis of reinforced concrete beam-columns. It was found that there was no significant difference in the statistical properties of the strength samples obtained for 500 and 1000 simulations. Therefore, a sample size of 500 simulations was used for all beam-columns analyzed in this study.

5.2 DESCRIPTIONS OF BEAM-COLUMNS STUDIED

The specified material properties and dimensions of the beam-columns studied were chosen to give a reasonable representation of the range of variables expected in actual construction. Figure 5.2 shows the nominal dimensions of the

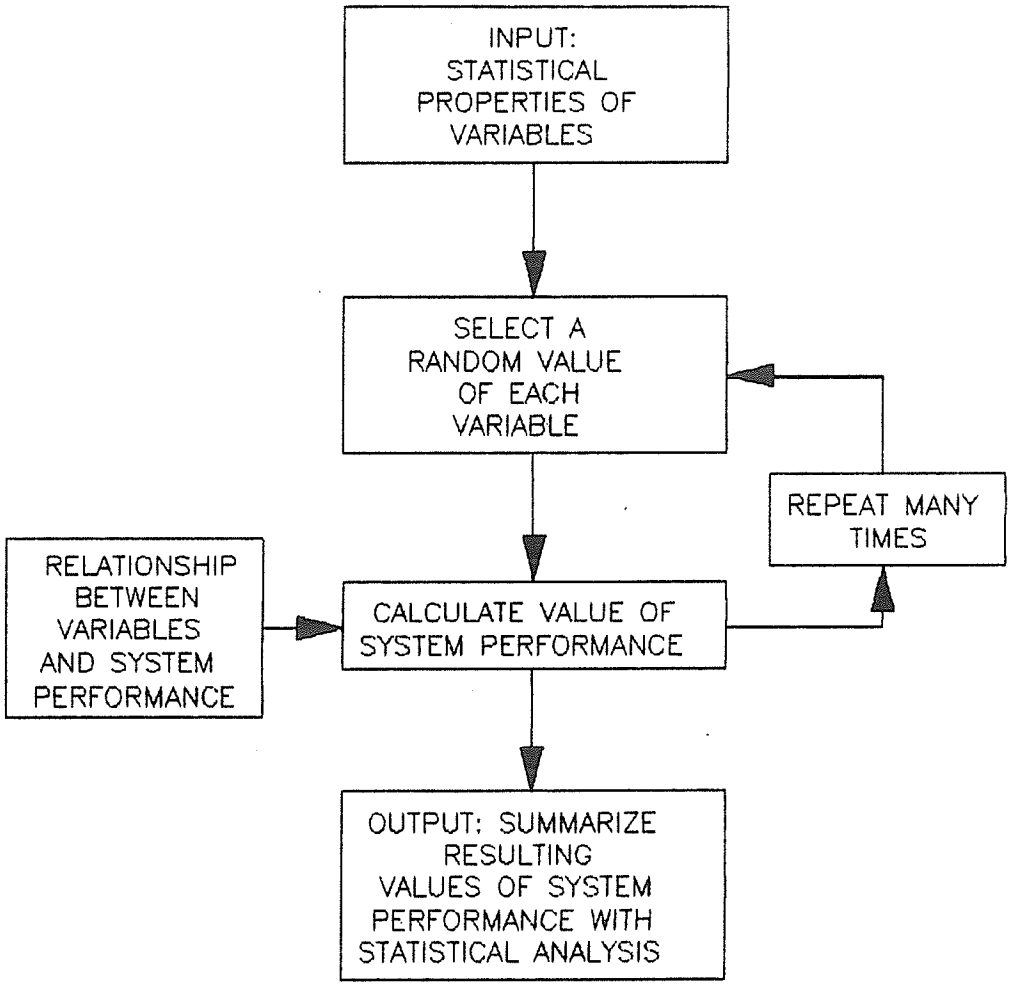

Figure 5.1 – The Monte Carlo Technique
(Mirza 1985b)

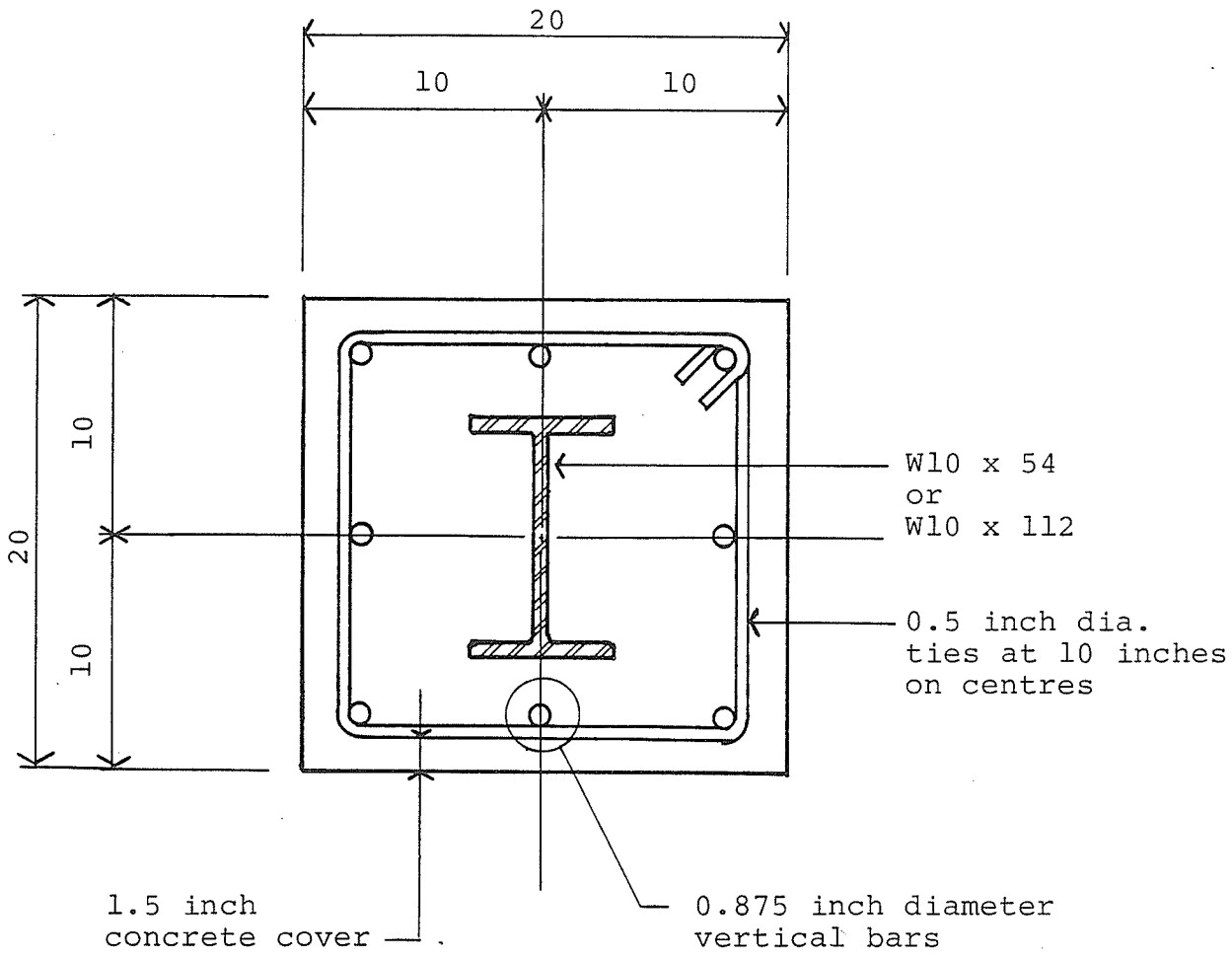

Note: 1 inch = 25.4 mm

Figure 5.2 - Nominal Column Cross-Section Details
(all dimensions are given in inches)

cross-section used. These dimensions conform to the requirements of ACI 318-83 and CAN3-A23.3-M84. The variables selected for study were the specified concrete strength, specified structural steel yield strength, ratio of structural steel area to gross area of cross-section, slenderness ratio, and end eccentricity ratio. The specified yield strength of the reinforcing bars was chosen to be 60 ksi (414 MPa) for all columns studied. The ratio of vertical reinforcing bar steel area to gross cross-section (ρ_{rs}) area was 1.2 percent. The study was divided into two parts: (a) basic study and (b) supplemental study for the short as well as for the slender beam-columns. The specified values of the variables used for these studies are discussed in the following two sections.

5.2.1 Basic Study

The basic study investigated the effects of the specified concrete strength, ratio of area of structural steel to gross area of cross-section, end eccentricity ratio, and slenderness ratio on the ratio of theoretical to nominal strength of composite beam-columns. Specified concrete strengths of 4000 and 6000 psi (27.6 and 41.4 MPa) were studied. These values were chosen to represent the commonly specified values for columns. The quality control of 4000 psi (27.6 MPa) concrete was assumed to be average (coefficient of variation of test cylinder strength = 15 percent). The quality control of 6000 psi (41.4 MPa) concrete was

assumed to be excellent, reflecting the extra care taken to mix higher strength concretes (coefficient of variation of test cylinder strength = 10 percent).

Ratios of structural steel area to gross cross-sectional area (ρ_{ss}) of 4 and 8 percent were studied. The smaller ratio was obtained by assuming a W10 x 54 (W250 x 80) rolled steel section and the larger one by using a W10 x 112 (W250 x 167) rolled steel shape. It was felt that the structural steel ratios less than 4 percent would not be practical for composite columns. Structural steel ratios larger than 8 percent are difficult to obtain without the use of built-up steel sections. The specified yield strength of the structural steel was chosen as 50 ksi (345 MPa) for the basic study. This represents the maximum allowable specified yield strength of structural steel by ACI 318-83 and CAN3-A23.3-M84 Codes.

Slenderness ratios (kl/r) of 0 and 22 were examined for the short columns. A slenderness ratio of 0 represents the cross-section. A slenderness ratio of 22 represents the upper limit for beam-columns designed without length effects by both ACI 318-83 and CAN3-A23.3-M84 Codes for the type of beam-columns studied. Slenderness ratios of 22.1, 33, 66 and 100 were chosen for the slender columns. A slenderness ratio of 22.1 nearly represents the lower limit for which the length effects must be included in design for the type

of columns studied. A slenderness ratio of 100 is the maximum slenderness ratio allowed for the evaluation of stability effects by the moment magnifier method of ACI 318-83 and CAN3-A23.3-M84.

Eccentricity ratios (e/h) of 0, 0.05, 0.1, 0.15, 0.2, 0.25, 0.3, 0.4, 0.5, 0.6, 0.7, 0.8, 1.0, 1.5, 2.0, 4.0 and infinity (pure bending) were studied for all columns. Note, for the basic study, the theoretical strength included the effects of residual stresses in structural steel and concrete confinement due to lateral ties but did not include the effect of strain-hardening of structural and reinforcing steels.

Table 5.1 lists the short columns, whereas Table 5.2 lists the slender columns used for the basic study. The column designations in these tables are made up of four elements separated by hyphens: The first element represents the specified concrete strength in kips per square inch, the second element identifies the specified structural steel yield strength in kips per square inch, the third element represents the approximate ratio of structural steel area to gross area of cross-section and the fourth element identifies the slenderness ratio.

5.2.2 Supplemental Study

Three additional variables were investigated to study their effect on the probability distribution properties of

Table 5.1 - Specified Properties of Short Beam-Columns Used for Basic Study*

Run Number (1)	Column Designation (2)	f'_c (psi) (3)	f_y (psi) (4)	$k\ell/r$ (5)	ρ_{ss} (6)
B01	4-50-4-0	4000	50000	0	0.040
B02	4-50-4-22	4000	50000	22	0.040
B07	6-50-4-0	6000	50000	0	0.040
B08	6-50-4-22	6000	50000	22	0.040
B13	4-50-8-0	4000	50000	0	0.082
B14	4-50-8-22	4000	50000	22	0.082
B19	6-50-8-0	6000	50000	0	0.082
B20	6-50-8-22	6000	50000	22	0.082

*Each beam-column listed above was studied for nominal e/h values of 0.0, 0.05, 0.1, 0.15, 0.2, 0.25, 0.3, 0.4, 0.5, 0.6, 0.7, 0.8, 1.0, 1.5, 2.0, 4.0, and ∞. All columns had cross-section size of 20 x 20 in., Grade 60 (414 MPa) reinforcing bars, and $\rho_{rs} = 0.012$. Lateral ties conformed to the minimum requirements of ACI 318-83 and CAN3-A23.3-M84. The quality control of 4000 psi (27.6 MPa) concrete was assumed to be average, whereas that for 6000 psi (41.4 MPa) concrete was taken to be excellent.

Note: 1000 psi = 6.895 MPa; 1 in. = 25.4 mm.

Table 5.2 - Specified Properties of Slender Beam-Columns Used for Basic Study*

Run Number (1)	Column Designation (2)	f'_c (psi) (3)	f_y (psi) (4)	$k\ell/r$ (5)	ρ_{ss} (6)
B03	4-50-4-22.1	4000	50000	22.1	0.040
B04	4-50-4-33	4000	50000	33	0.040
B05	4-50-4-66	4000	50000	66	0.040
B06	4-50-4-100	4000	50000	100	0.040
B09	6-50-4-22.1	6000	50000	22.1	0.040
B10	6-50-4-33	6000	50000	33	0.040
B11	6-50-4-66	6000	50000	66	0.040
B12	6-50-4-100	6000	50000	100	0.040
B15	4-50-8-22.1	4000	50000	22.1	0.082
B16	4-50-8-33	4000	50000	33	0.082
B17	4-50-8-66	4000	50000	66	0.082
B18	4-50-8-100	4000	50000	100	0.082
B21	6-50-8-22.1	6000	50000	22.1	0.082
B22	6-50-8-33	6000	50000	33	0.082
B23	6-50-8-66	6000	50000	66	0.082
B24	6-50-8-100	6000	50000	100	0.082

*Each beam-column listed above was studied for nominal e/h values of 0.0, 0.05, 0.1, 0.15, 0.2, 0.25, 0.3, 0.4, 0.5, 0.6, 0.7, 0.8, 1.0, 1.5, 2.0, 4.0, and ∞. All columns had cross-section size of 20 x 20 in., Grade 60 (414 MPa) reinforcing bars, and $\rho_{rs} = 0.012$. Lateral ties conformed to the minimum requirements of ACI 318-83 and CAN3-A23.3-M84. The quality control of 4000 psi (27.6 MPa) concrete was assumed to be average, whereas that for 6000 psi (41.4 MPa) concrete was taken to be excellent.

Note: 1000 psi = 6.895 MPa; 1 in. = 25.4 mm.

the ratio of theoretical to nominal strength of beam-columns. The three variables were the specified yield strength of structural steel, the strain-hardening of structural and reinforcing steels, and the effect of concrete quality control.

Specified structural steel yield strengths of 36 ksi (ASTM A36) ($f_y = 248$ MPa) and 44 ksi (CSA G40.21-M 44W) ($f_y = 303$ MPa) are common in the United States and Canada, respectively. To study the influence of specified structural steel yield strength on the theoretical to nominal strength ratios of beam-columns, the results of two short and two slender beam-columns selected from the basic study were compared to the results of identical columns having the specified structural steel yield strength of 36 and 44 ksi (248 and 303 MPa).

Strain-hardening provides an enhancement of the steel strength. However, the use of this enhanced strength of steel is not allowed by the ACI or CSA code. To examine the effect of strain-hardening on the ratios of theoretical to nominal strengths, the results of two short and two slender columns selected from the basic study were compared to the results of identical columns in which the strain-hardening of both structural and reinforcing steel beyond the plastic plateau was permitted for computing the theoretical strengths.

To examine the influence of concrete quality control on the variation of theoretical to nominal strength ratios, two short and two slender columns from the basic study with specified concrete strengths of 6000 psi (41.4 MPa) and excellent concrete quality control were compared to identical columns having average concrete quality control. Note the excellent quality control assumes a coefficient of variation of 10 percent for test cylinders, whereas average quality control had a test cylinder coefficient of variation of 15 percent.

The short beam-columns of the supplemental study are shown in Table 5.3, whereas the slender columns of the supplemental study are given in Table 5.4. The fifth element appearing in some column designations in these tables represents the inclusion of strain-hardening of both steels (STH) or the use of average quality control for 6000 psi (41.4 MPa) concrete (A). The first four elements of the column designation in Tables 5.3 and 5.4 are identical to those described for Tables 5.1 and 5.2 of the basic study. Note the effects of concrete confinement due to lateral ties and residual stresses in structural steel were also included in computing the theoretical strengths for the supplemental study.

5.3 SHORT COMPOSITE BEAM-COLUMNS

This section examines the overall strength variations of short composite columns. The effects of individual vari-

Table 5.3 - Specified Properties of Short Beam-Columns Used for Supplemental Study*

Run Number (1)	Column Designation (2)	f'_c (psi) (3)	f_y (psi) (4)	$k\ell/r$ (5)	ρ_{ss} (6)	Strain Hardening Included (7)	Concrete Quality Control (8)
SG1	4-36-4-22	4000	36000	22	0.040	No	Average
SG3	4-44-4-22	4000	44000	22	0.040	No	Average
SG5	6-36-4-22	6000	36000	22	0.040	No	Excellent
SG7	6-44-4-22	6000	44000	22	0.040	No	Excellent
STH1	4-50-4-0-STH	4000	50000	0	0.040	Yes	Average
STH3	6-50-4-0-STH	6000	50000	0	0.040	Yes	Excellent
CQ1	6-50-4-22-A	6000	50000	22	0.040	No	Average
CQ3	6-50-8-22-A	6000	50000	22	0.082	No	Average

*Each beam-column listed above was studied for nominal e/h values of 0.0, 0.05, 0.1, 0.15, 0.2, 0.25, 0.3, 0.4, 0.5, 0.6, 0.7, 0.8, 1.0, 1.5, 2.0, 4.0, and ∞. All columns had cross-section size of 20 x 20 in., Grade 60 (414 MPa) reinforcing bars, and $\rho_{rs} = 0.012$. Lateral ties conformed to the minimum requirements of ACI 318-83 and CAN3-A23.3-M84.

Note: 1000 psi = 6.895 MPa; 1 in. = 25.4 mm.

Table 5.4 - Specified Properties of Slender Beam-Columns Used for Supplemental Study*

Run Number (1)	Column Designation (2)	f'_c (psi) (3)	f_y (psi) (4)	$k\ell/r$ (5)	ρ_{ss} (6)	Strain Hardening Included (7)	Concrete Quality Control (8)
SG2	4-36-4-33	4000	36000	33	0.040	No	Average
SG4	4-44-4-33	4000	44000	33	0.040	No	Average
SG6	6-36-4-33	6000	36000	33	0.040	No	Excellent
SG8	6-44-4-33	6000	44000	33	0.040	No	Excellent
STH2	4-50-4-66-STH	4000	50000	66	0.040	Yes	Average
STH4	6-50-4-66-STH	6000	50000	66	0.040	Yes	Excellent
CQ2	6-50-4-33-A	6000	50000	33	0.040	No	Average
CQ4	6-50-8-33-A	6000	50000	33	0.082	No	Average

*Each beam-column listed above was studied for nominal e/h values of 0.0, 0.05, 0.1, 0.15, 0.2, 0.25, 0.3, 0.4, 0.5, 0.6, 0.7, 0.8, 1.0, 1.5, 2.0, 4.0, and ∞. All columns had cross-section size of 20 x 20 in., Grade 60 (414 MPa) reinforcing bars, and $\rho_{rs} = 0.012$. Lateral ties conformed to the minimum requirements of ACI 318-83 and CAN3-A23.3-M84.

Note: 1000 psi = 6.895 MPa; 1 in. = 25.4 mm.

ables on the strength ratios are discussed here and the major variables that affect the variability of short composite columns are identified as well. The specified properties of short composite beam-columns studied are given in Tables 5.1 and 5.3.

5.3.1 Overall Strength Variations

Figures 5.3 and 5.4 are the plots of the simulated axial load-bending moment interaction diagrams for Columns 6-50-4-22 and 4-50-8-22 taken from Table 5.1. These columns represent the extremes of the structural steel index ($\rho_{ss} f_y / f'_c = 0.33$ and 1.03) for the columns studied. The theoretical maximum, mean, one-percentile and minimum strength curves, obtained from 500 simulations are plotted. Also plotted is the ACI 318-83 ultimate strength curve which was calculated assuming a value of 1.0 for understrength factors.

The factored ACI strength curve shown in Figures 5.3 and 5.4 was obtained by dividing the ACI ultimate strengths by a safety factor that varied from $1.55/0.7 = 2.21$ to $1.55/0.9 = 1.72$. The safety factor of $1.55/0.7$ was used for axial loads that exceeded the load corresponding to the maximum bending moment on the ACI ultimate strength interaction curve. Below this axial load, the safety factor was assumed to vary linearly with the axial load from $1.55/0.7$ to $1.55/0.9$ at the pure bending condition. The value 1.55 used above represents the average of the ACI load factors for

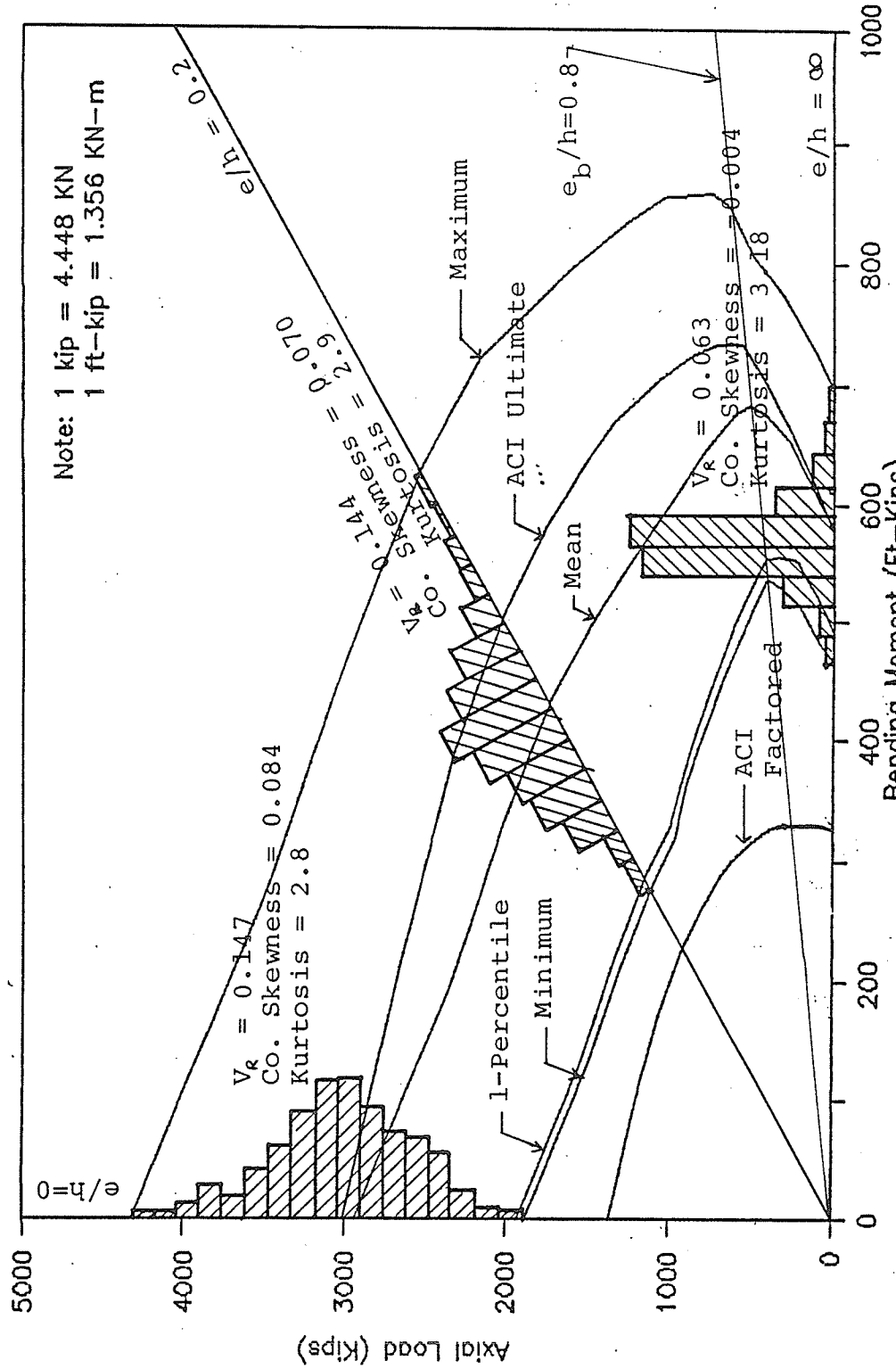

Figure 5.3 – Axial Load–Bending Moment Strength Interaction Curves of Randomly Generated Sample of 500 Short Composite Columns [Column 6–50–4–22 (Table 5.1)]

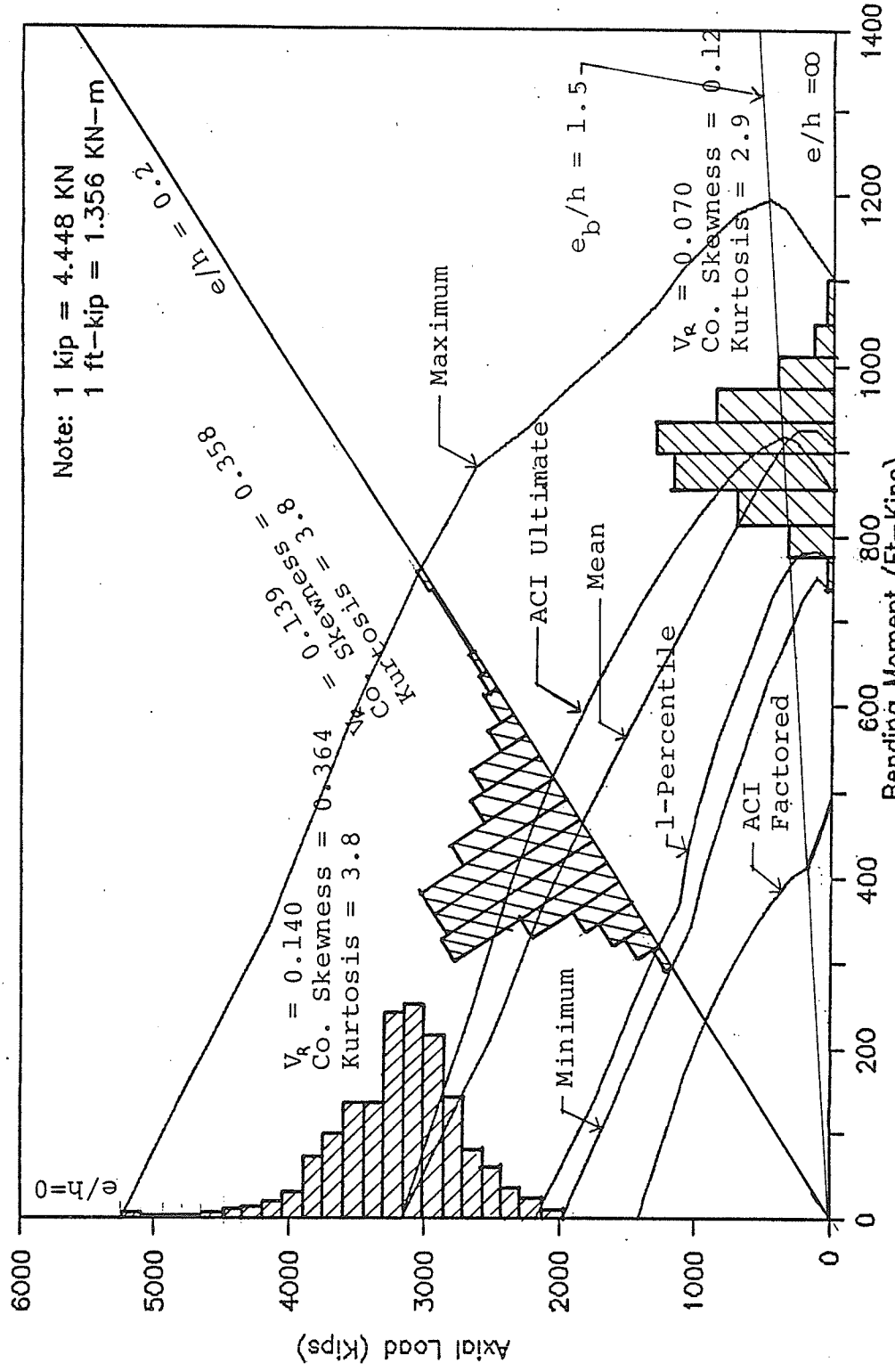

Figure 5.4 – Axial Load–Bending Moment Strength Interaction Curves of Randomly Generated Sample of 500 Short Composite Columns [Column 4–50–8–22 (Table 5.1)]

dead load (1.4) and for live load (1.7). The values 0.7 and 0.9 are the ACI 318-83 understrength factors for compression and tension failure conditions, respectively. The axial load level below which ACI 318-83 allows an increase in the understrength factor greater than 0.7 is further discussed at the end of this section.

A comparison of the ACI ultimate strength and the theoretical mean strength interaction curves shown in Figures 5.3 and 5.4 indicates that the ACI procedure overestimates the mean ultimate strength for e/h ratios less than or equal to around 1.5. However, these differences between the ACI ultimate strength and the mean theoretical strength (for $e/h \leq 1.5$) appear to decrease as the structural steel index ($\rho_{ss} f_y / f_c'$) increases. This can be seen by comparing Figures 5.3 and 5.4. For $e/h > 1.5$, the ACI prediction is nearly the same as the mean theoretical strength when $\rho_{ss} f_y / f_c' = 0.33$ (Figure 5.3). When $\rho_{ss} f_y / f_c' = 1.03$ (Figure 5.4), the ACI Code underestimates the mean theoretical strength for e/h greater than 1.5.

Comparison of the one-percentile and factored ACI interaction curves show that the factored ACI curve is well below the one-percentile strength curve. It should be noted that the factored ACI curve shown in Figures 5.3 and 5.4 is only an approximation and may rise or fall depending on loading combinations and variations.

Histograms of theoretical beam-column strength at eccentricity ratios of 0.0 (pure compression), 0.2, and infinity (pure bending) are also plotted on Figures 5.3 and 5.4. In Figure 5.3 ($\rho_{ss} f_y / f_c' = 0.33$), the histograms appear symmetric at all three eccentricity ratios. In Figure 5.4 ($\rho_{ss} f_y / f_c' = 1.03$), the histograms are slightly positively skewed, indicating the influence of the larger structural steel area. Note the probability distribution of structural steel strength was assumed to be positively skewed. A smaller coefficient of variation at higher e/h ratios is apparent in both figures.

The balance point is defined by ACI 318-83 as the strain condition which produces yielding in the tensile steel as the compressive face of the concrete reaches its maximum useable strain. In a reinforced concrete cross-section, the balance point defines the transition from compression to tension failure and occurs at the maximum bending moment on the axial load - bending moment interaction curve. ACI 318-83 specifies the lower of the axial load at the balance point or the axial load calculated by Equation 5.1 as the transition point for defining the value of understrength factors.

$$P = 0.1 f_c' A_g \qquad (5.1)$$

in which A_g = gross area of cross-section.

Four composite beam-column cross-sections were analyzed in order to see how the definition of balance point given above applies to composite columns. The axial load corresponding to the yielding of the tension reinforcing bars, incipient yielding of the tension flange of the steel section and full yielding of the tension flange was calculated for all four cross-sections ($l/h = 0.0$) shown in Table 5.1. Figure 5.5 plots the ACI ultimate strength interaction curve for a cross-section (Column 4-50-4-0 in Table 5.1) with axial load levels corresponding to the above-noted yielding conditions identified in the Figure. The maximum bending moment capacity occurs at an axial load level between those corresponding to incipient and full yielding of the tension flange. Furthermore, the axial load level at yielding of the tension reinforcing bars is significantly greater than the axial load corresponding to the maximum bending moment capacity. Thus, the definition of balance point used for reinforced concrete beam-columns does not seem to be applicable to the composite cross-section shown in Figure 5.5. Similar conclusions were drawn for the remaining three cross-sections given in Table 5.1. Hence, defining the balance point for composite column cross-sections as the strain condition at which full yielding of the tension flange occurs as the compression face of concrete reaches its maximum useable strain (0.003) will be both appropriate and conservative for

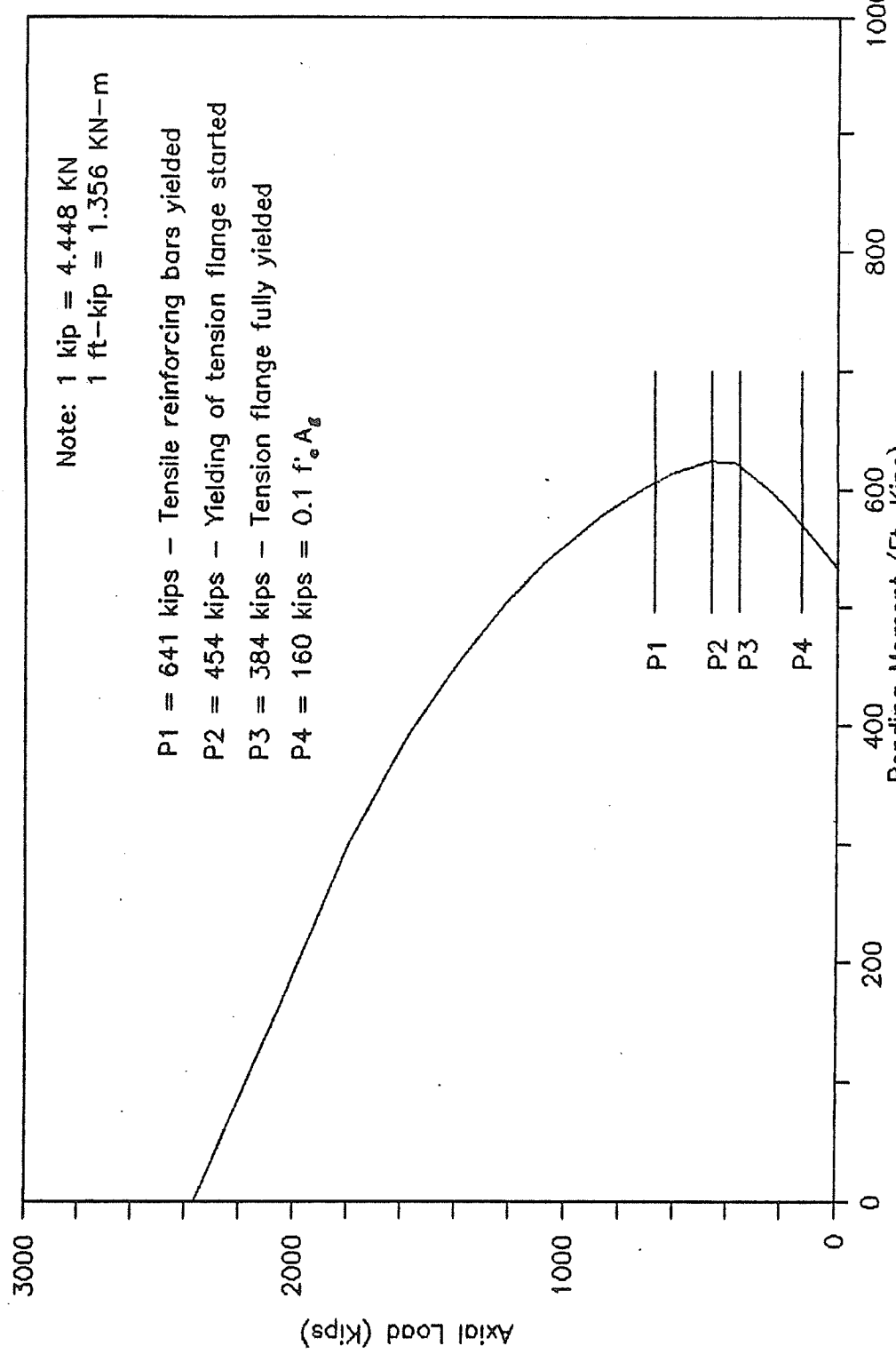

Figure 5.5 – ACI 318-83 Ultimate Strength Interaction Diagram for Column 4-50-4-0 (Table 5.1)

assigning understrength factors. This definition of the balance point has been used in this study and for Figures 5.3 and 5.4.

The axial load level corresponding to Equation 5.1 was significantly less than the axial loads discussed in the previous paragraph and is also marked in Figure 5.5. Therefore, the second ACI 318-83 condition on axial load level as given by Equation 5.1 seems to be overly conservative, particularly when applied to composite beam-columns.

5.3.2 Effects Of Variables Used For Basic Study

The eight short columns in the basic study (Table 5.1) were used to examine the effects of four variables on the probability distribution properties of the ratio of theoretical to nominal strength (strength ratio). These variables are the slenderness ratio (kl/r), specified concrete strength ($fprime_c$), ratio of structural steel area to gross area of cross-section (ρ_{ss}) and end eccentricity ratio (e/h). The comparisons for each of these variables are made at the one-percentile and five-percentile levels and at the mean value. The one-percentile level is of most concern since it pertains to the lower tail of the strength probability distribution.

5.3.2.1 Effect of slenderness ratio - Four direct comparisons of the effect of slenderness ratio (kl/r) on the probability distribution properties of the strength ratio were made. Each comparison contained two short columns having

kl/r values of 0 and 22 with all other properties being identical. The results from two of the comparisons are shown in Figures 5.6 and 5.7.

At one-percentile level, 3 out of 4 comparisons clearly showed lower strength ratios for columns with kl/r of 22 over all end eccentricity ratios. The most significant differences in one-percentile strength ratios were obtained for the column set with combination of f'_c = 4000 psi (27.6 MPa) and ρ_{ss} = 0.040 as shown in Figure 5.6(a). Exception to this behavior was the column set having f'_c = 6000 psi (41.4 MPa) and ρ_{ss} = 0.082 for which the one-percentile strength ratios for the column with kl/r = 0 were lower in regions of e/h less than 0.25. This is indicated in Figure 5.7(a). However, the differences in one-percentile strength ratios for $e/h < 0.25$ in Figure 5.7(a) seem to be small.

At the 5-percentile level and at the mean value, the column with kl/r of 22 yielded lower strength ratios than the columns having kl/r of 0.0 for all e/h ratios as shown in Figures 5.6(b) and (c) and Figures 5.7(b) and (c). From this it is reasonable to conclude that the columns with slenderness ratio of 22 are more critical for reliability analysis of short composite beam-columns.

5.3.2.2 <u>Effect of specified concrete strength</u> - Four column sets were used to investigate the effect of specified concrete strength (f'_c) on the probability distribution properties of the strength ratio. Each set had one column with

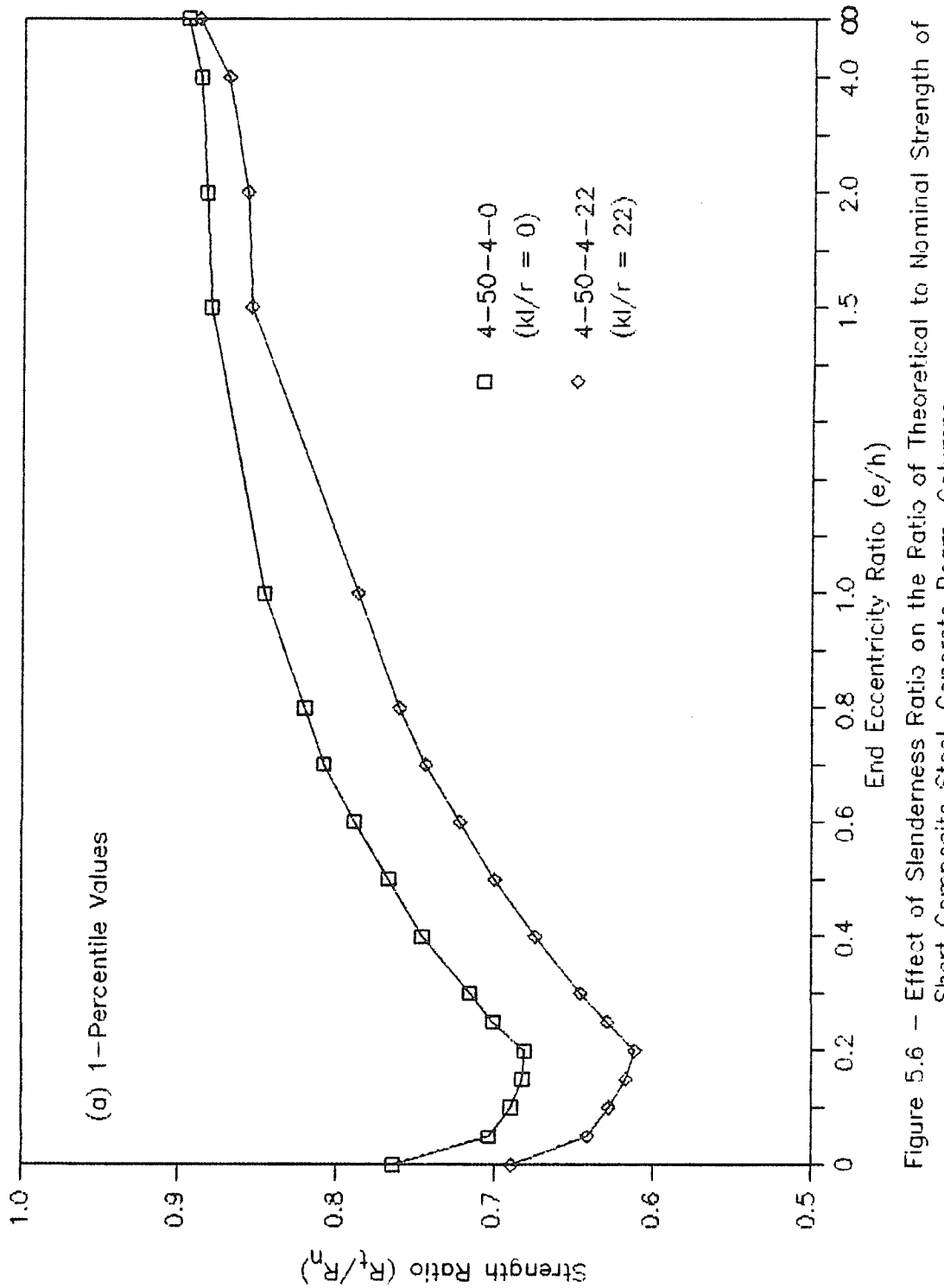

Figure 5.6 – Effect of Slenderness Ratio on the Ratio of Theoretical to Nominal Strength of Short Composite Steel–Concrete Beam–Columns

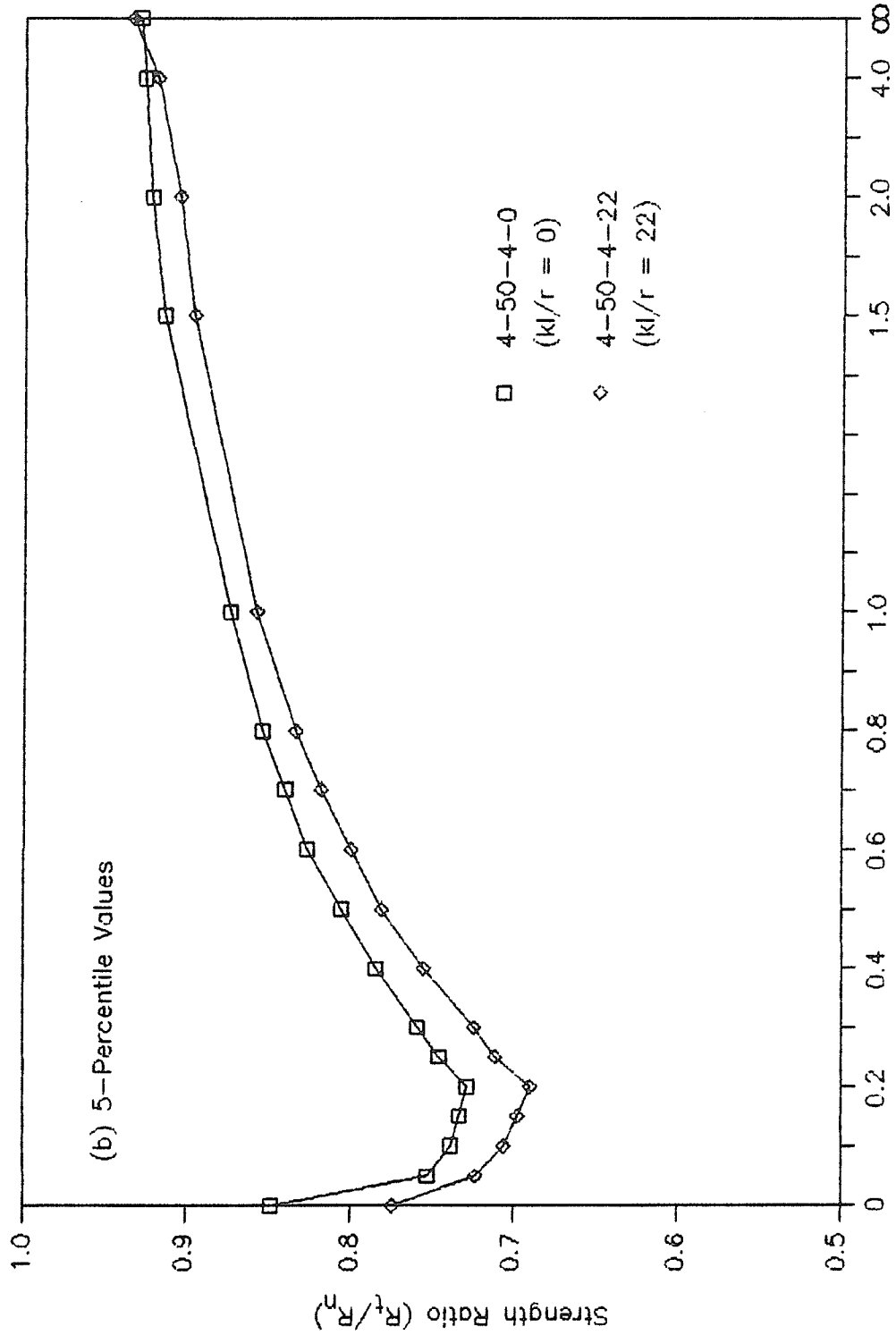

Figure 5.6 (cont.) – Effect of Slenderness Ratio on the Ratio of Theoretical to Nominal Strength of Short Composite Steel–Concrete Beam–Columns

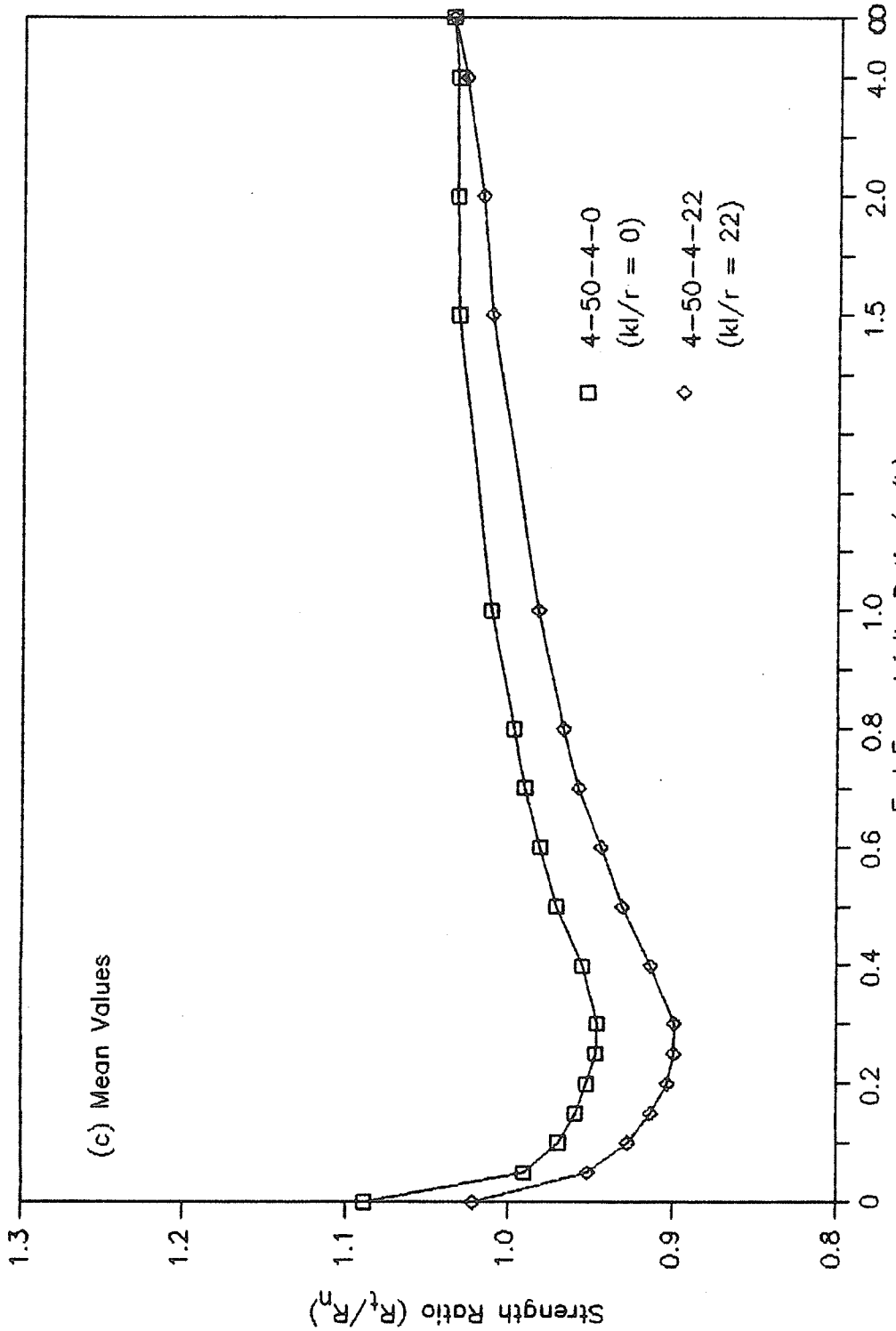

Figure 5.6 (cont.) – Effect of Slenderness Ratio on the Ratio of Theoretical to Nominal Strength of Short Composite Steel–Concrete Beam–Columns

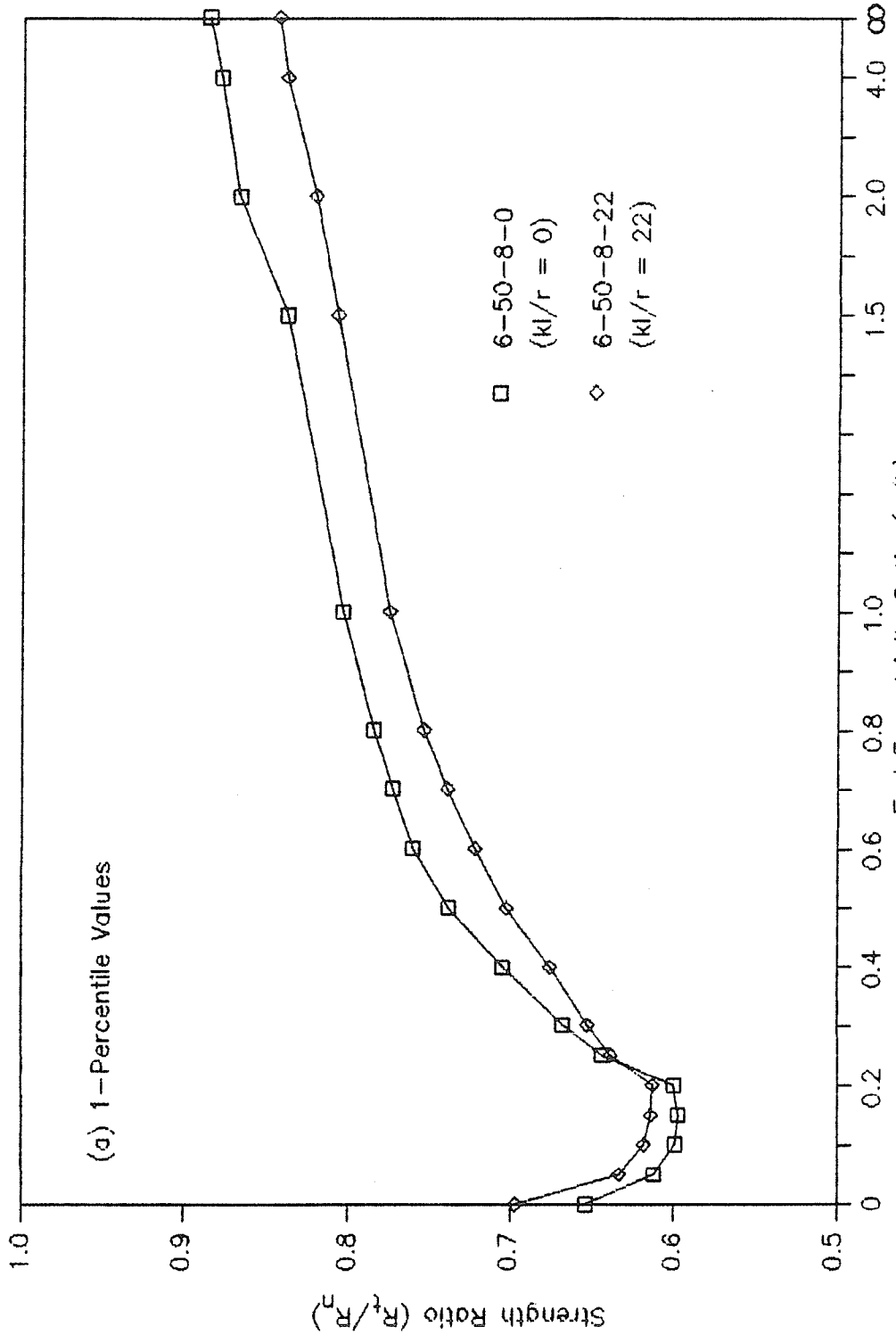

Figure 5.7 – Effect of Slenderness Ratio on the Ratio of Theoretical to Nominal Strength of Short Composite Steel–Concrete Beam–Columns

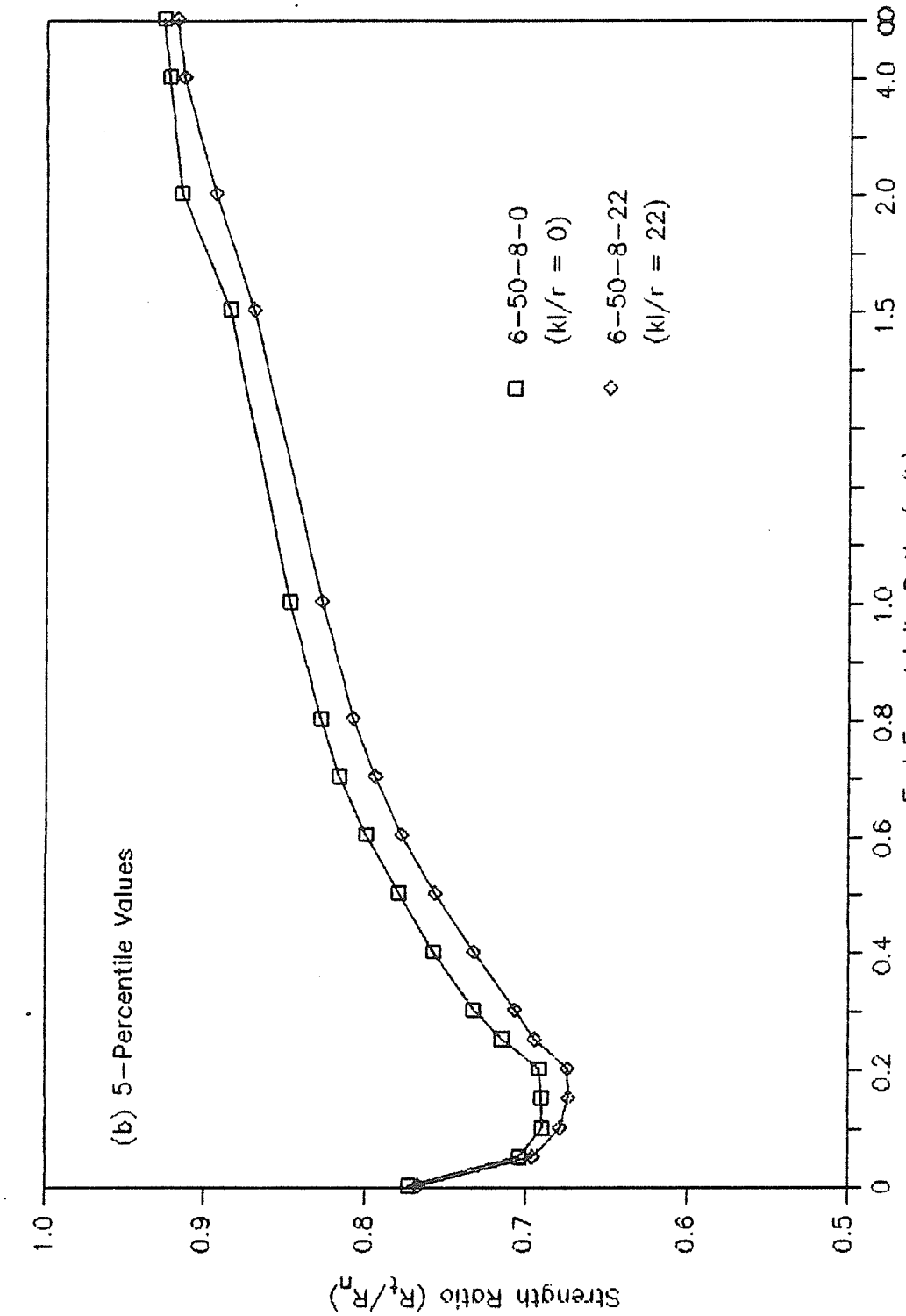

Figure 5.7 (cont.) – Effect of Slenderness Ratio on the Ratio of Theoretical to Nominal Strength of Short Composite Steel–Concrete Beam–Columns

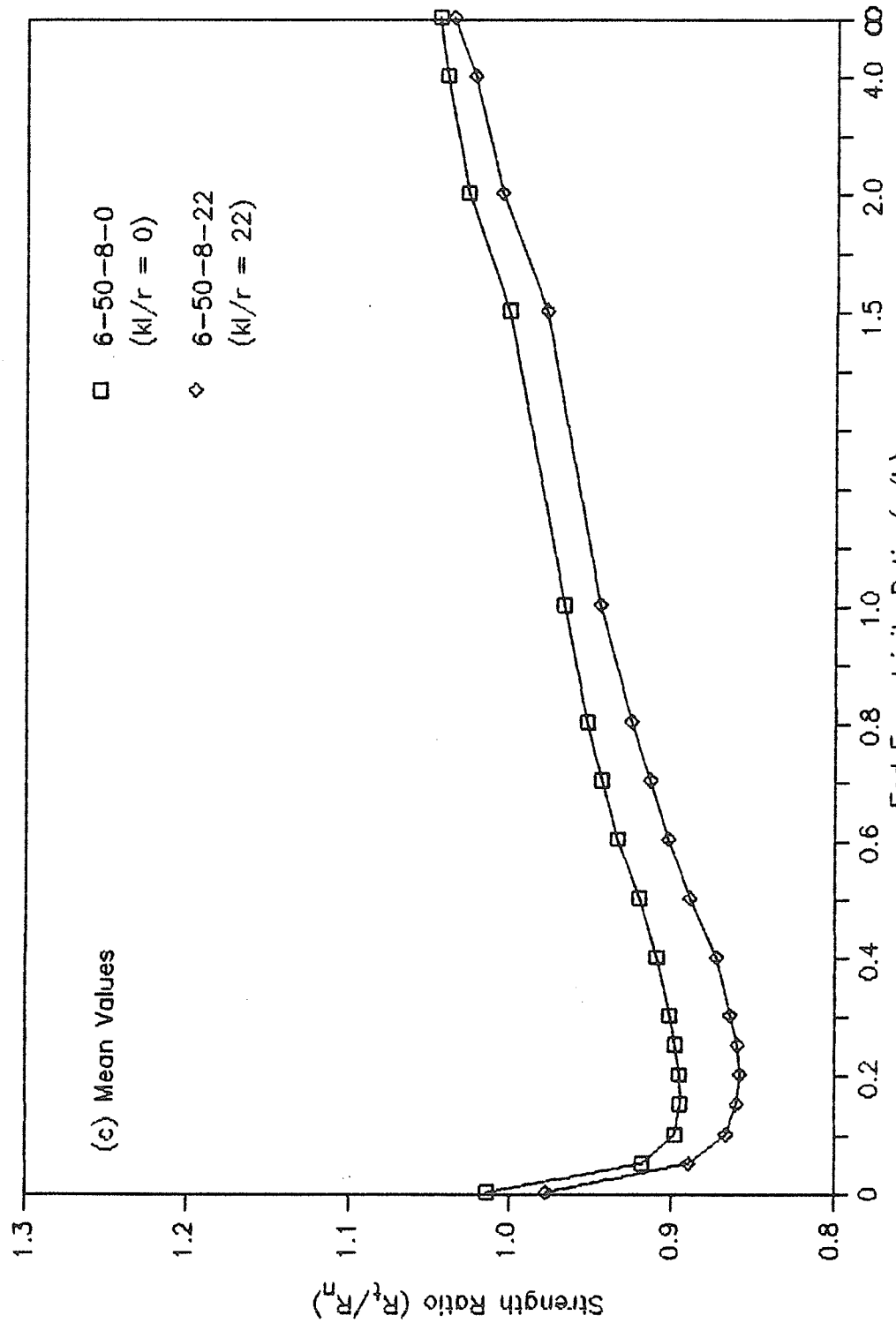

Figure 5.7 (cont.) – Effect of Slenderness Ratio on the Ratio of Theoretical to Nominal Strength of Short Composite Steel–Concrete Beam–Columns

f'_c of 4000 psi (27.6 MPa) and one column with f'_c = 6000 psi (41.4 MPa) with all other properties being identical. As noted in Chapter 4, the coefficient of variation of the strength of test cylinders was taken as 15 percent (average quality) for 4000 psi (27.6 MPa) concrete and 10 percent (excellent quality) for 6000 psi (41.4 MPa) concrete. This difference in the test cylinder coefficients of variation reflects the extra care taken in the manufacture of higher strength concrete. The results from two of the comparisons are shown in Figures 5.8 and 5.9.

At the 1-percentile level, 3 out of 4 comparisons showed significantly lower strength ratios for the column with 6000 psi (41.4 MPa) concrete. These differences were especially apparent for low eccentricity ratios when ρ_{ss} was 0.040 as shown in Figure 5.8(a). The trend appeared less significant as the structural steel ratio increased to 0.082 as shown in Figure 5.9(a) where there was no difference between the strength ratios of columns with f'_c = 4000 and 6000 psi (27.6 and 41.4 MPa) at e/h of 0.2 or less. The columns with the higher structural steel percentage have the overall strength less influenced by the concrete strength and, therefore, less difference is expected between the one-percentile strength ratios for columns with 4000 and 6000 psi (27.6 and 41.4 MPa) specified concrete strength.

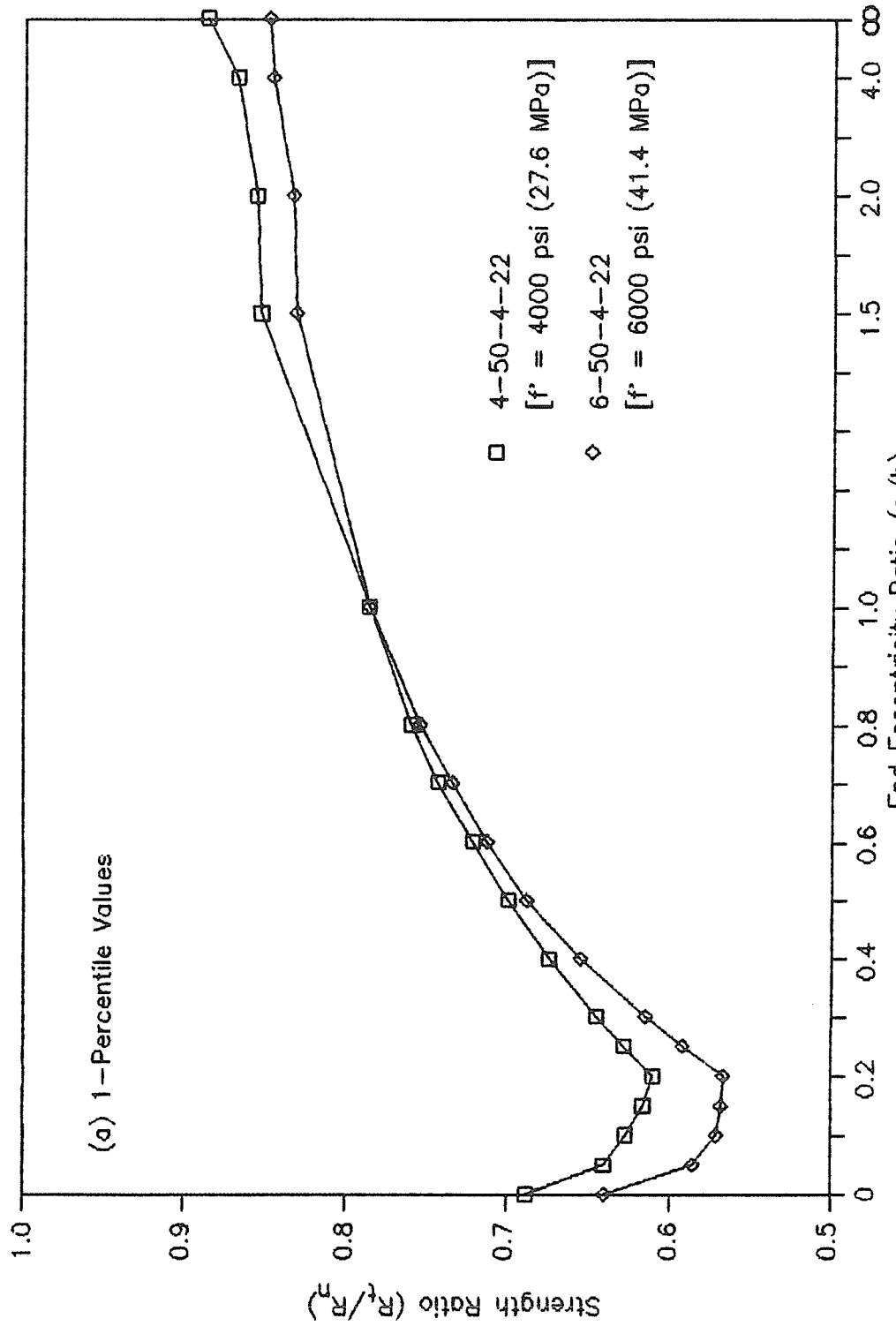

Figure 5.8 – Effect of Specified Concrete Strength on the Ratio of Theoretical to Nominal Strength of Short Composite Steel–Concrete Beam–Columns

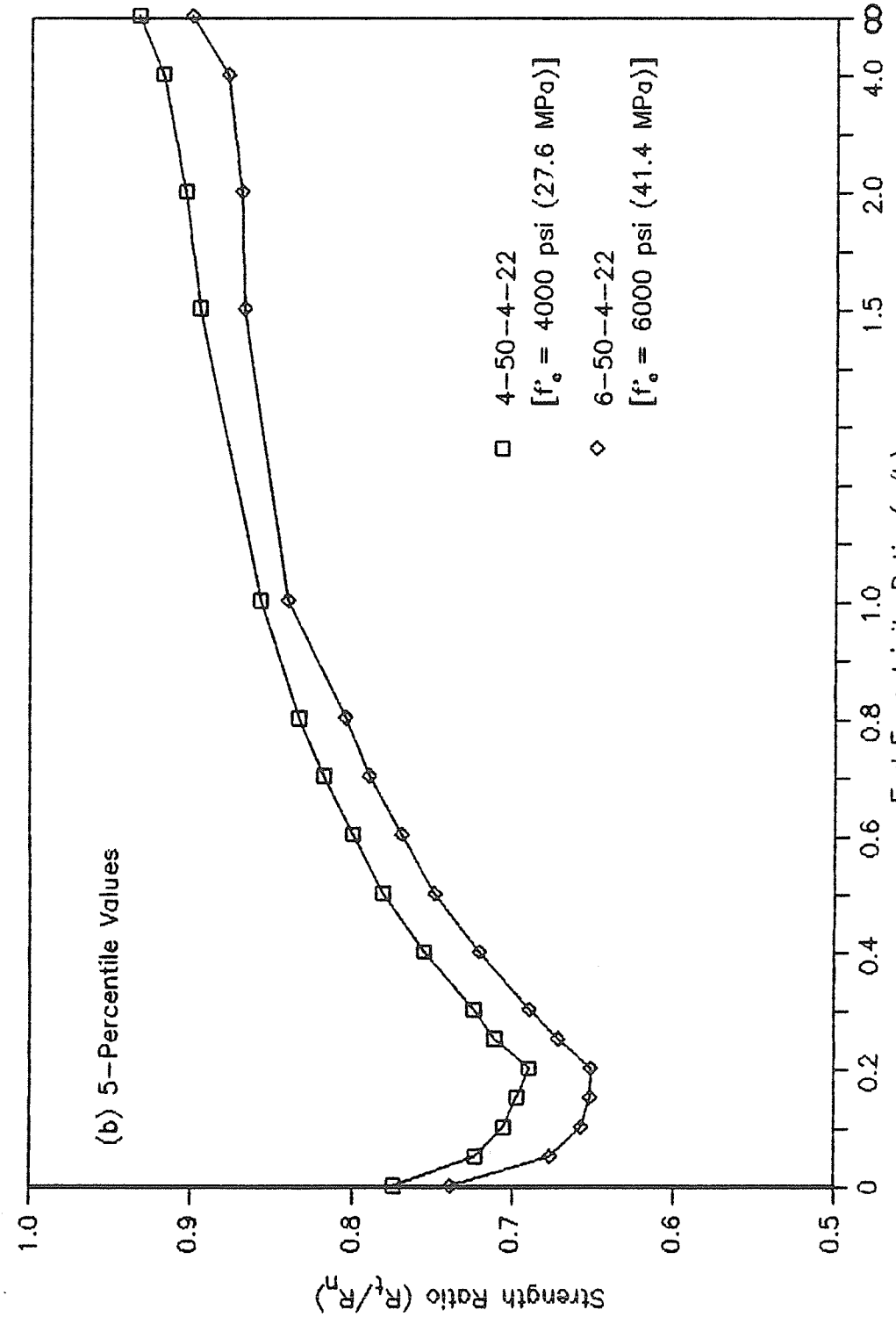

Figure 5.8 (cont.) – Effect of Specified Concrete Strength on the Ratio of Theoretical to Nominal Strength of Short Composite Steel–Concrete Beam–Columns

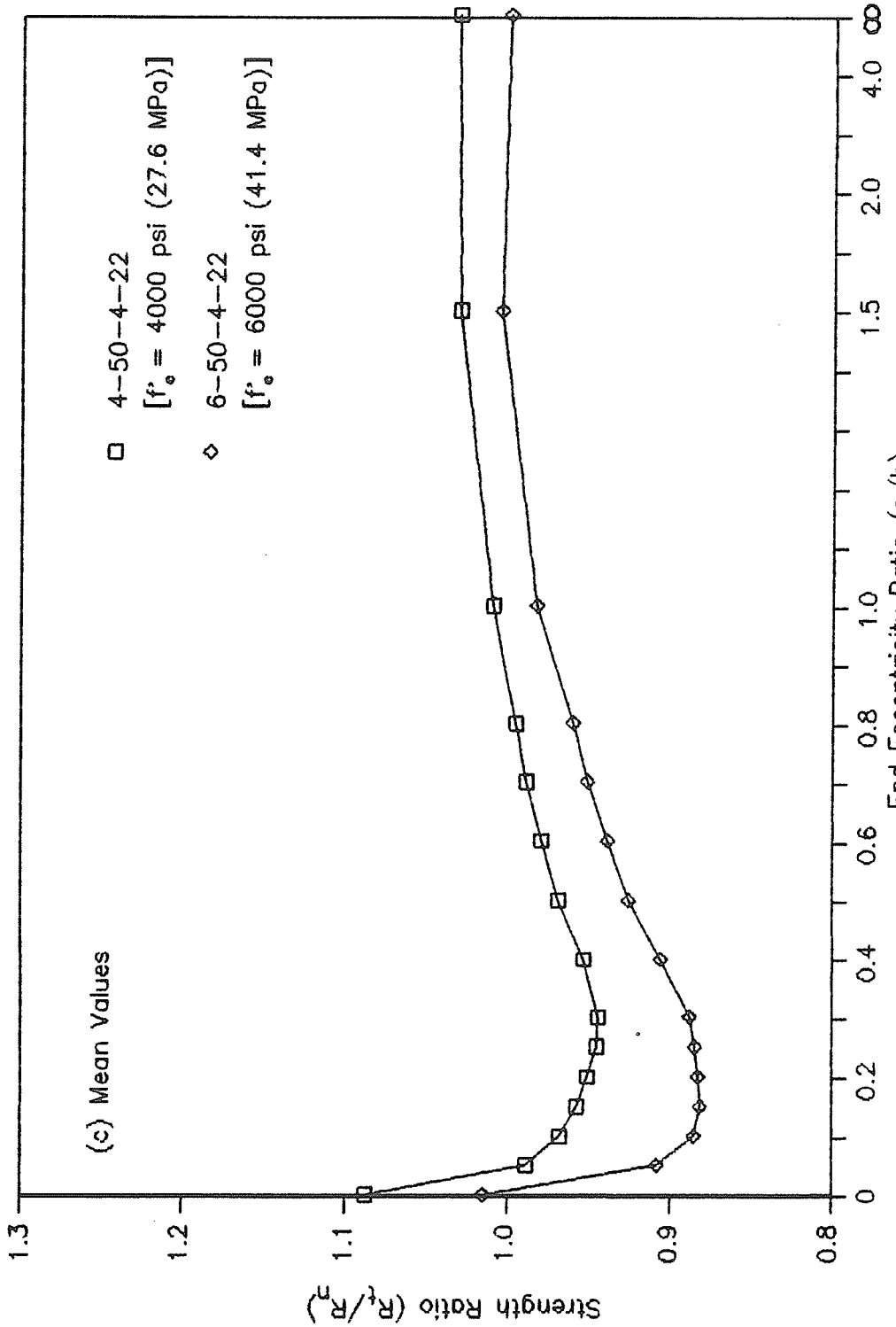

Figure 5.8 (cont.) – Effect of Specified Concrete Strength on the Ratio of Theoretical to Nominal Strength of Short Composite Steel–Concrete Beam–Columns

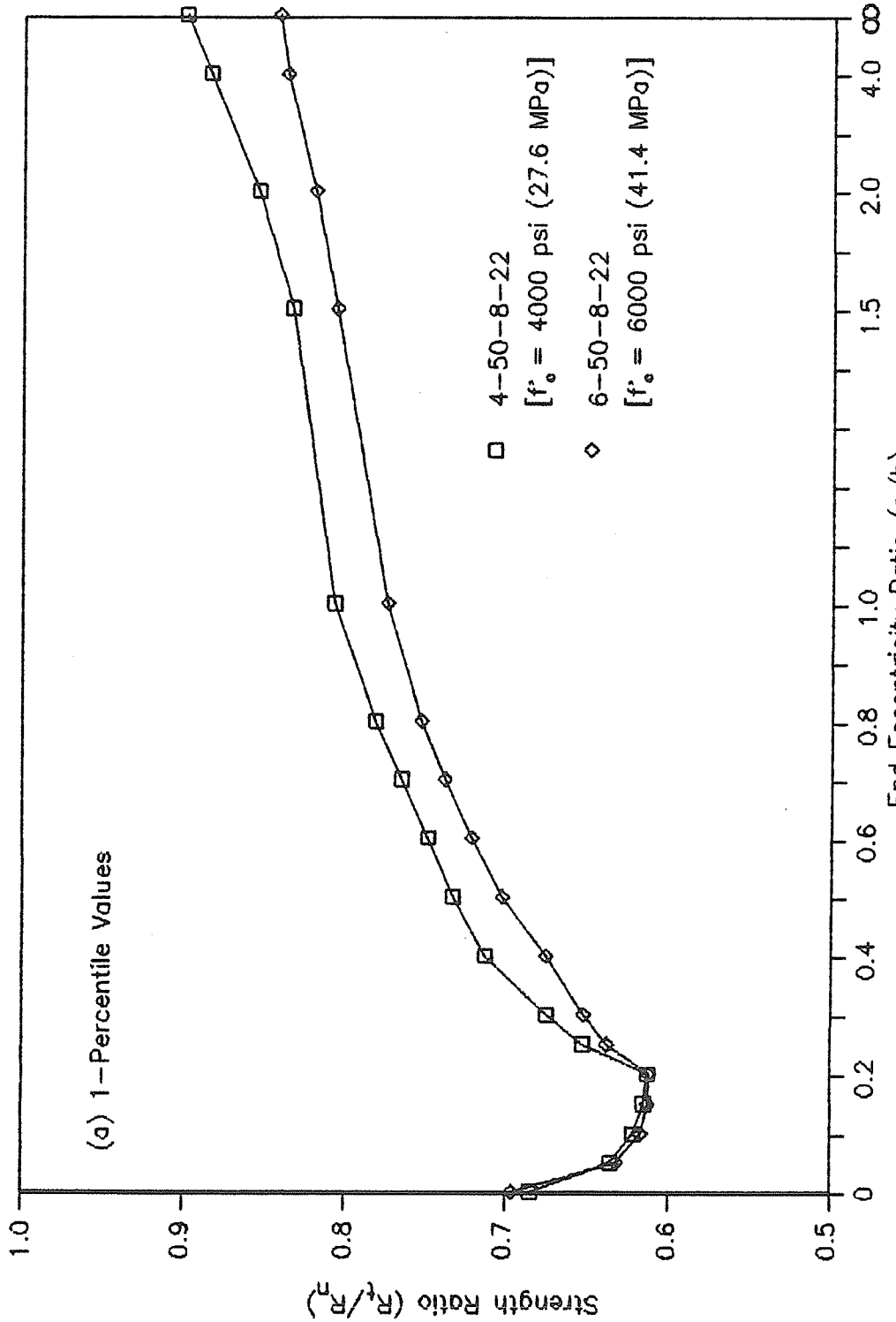

Figure 5.9 – Effect of Specified Concrete Strength on the Ratio of Theoretical to Nominal Strength of Short Composite Steel–Concrete Beam–Columns

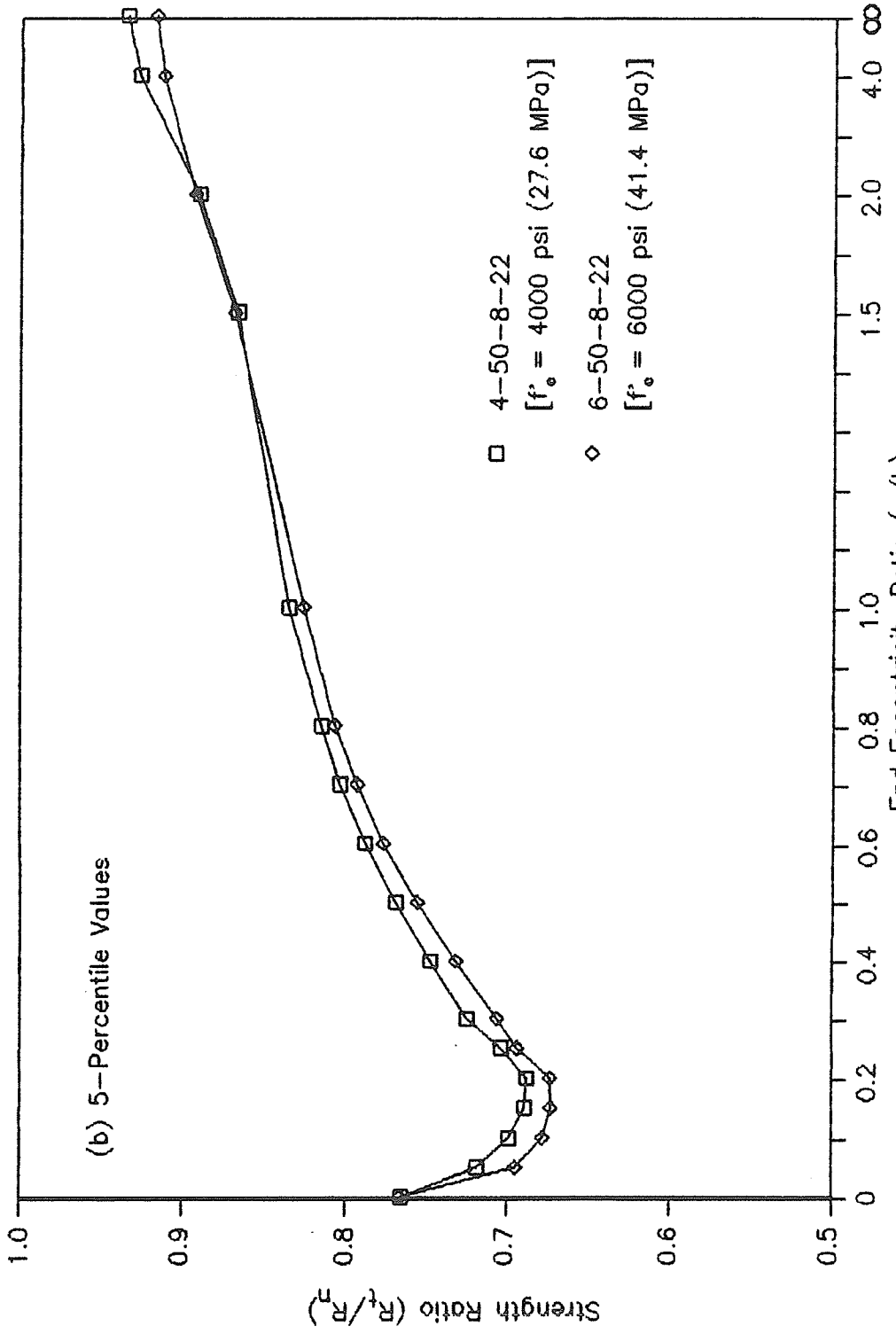

Figure 5.9 (cont.) – Effect of Specified Concrete Strength on the Ratio of Theoretical to Nominal Strength of Short Composite Steel-Concrete Beam-Columns

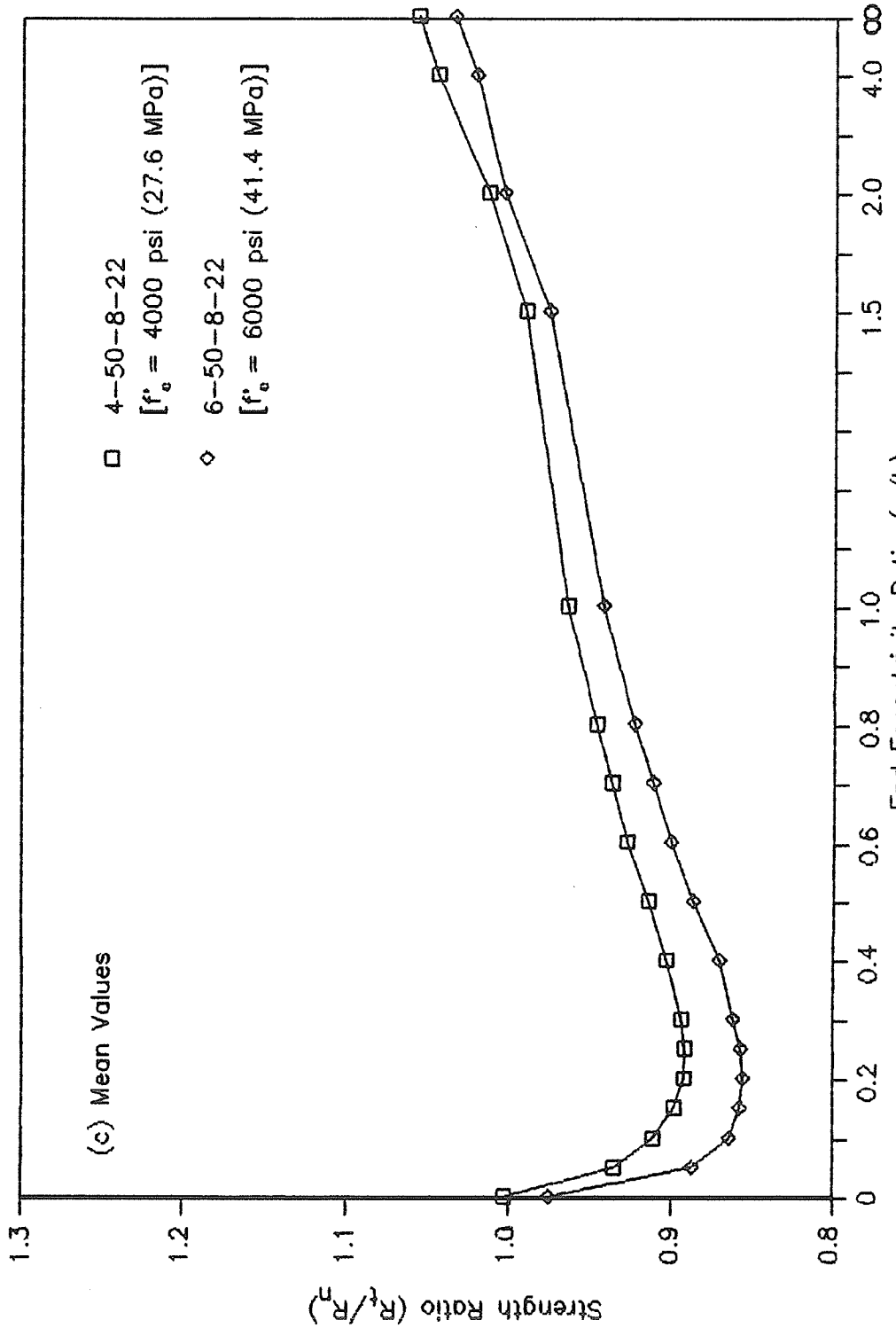

Figure 5.9 (cont.) – Effect of Specified Concrete Strength on the Ratio of Theoretical to Nominal Strength of Short Composite Steel–Concrete Beam–Columns

At the 5-percentile and mean value levels [Figures 5.8(b) and (c) and 5.9(b) and (c)] the columns having 6000 psi (41.4 MPa) concrete yielded lower values of strength ratios at all e/h ratios. Again, the trend was more significant for the columns with the lower percentage of structural steel.

The columns with 6000 psi (41.4 MPa) concrete produced lower strength ratios due to the lower value of the ratio of the mean in-situ strength to specified strength of concrete used for these columns than for those having 4000 psi (27.6 MPa) concrete. The in-situ strength is given by Equation 4.2. The ratio of mean in-situ strength to specified strength is 0.847 for 4000 psi (27.6 MPa) concrete and 0.773 for 6000 psi (41.4 MPa) concrete when it is loaded to failure in 1 hour.

From the above-noted discussions, it is concluded that the specified concrete strength significantly affects the strength ratios, especially for low structural steel percentages and, therefore, should be included in studies of reliability analysis.

5.3.2.3 Effect of structural steel ratio - Four direct comparisons were made to examine the effect of the ratio of the area of structural steel to gross area of the cross-section (ρ_{ss}) on the probability distribution properties of the strength ratios. Each comparison included two columns, one

with ρ_{ss} = 0.040 and one with ρ_{ss} = 0.082 with all other properties being identical. The results from two of the comparisons are shown in Figures 5.10 and 5.11.

Three out of four sets showed lower one-percentile strength ratios for columns with 4 percent structural steel than those obtained for columns with 8 percent structural steel. The only exception was the column set with f'_c = 4000 psi (27.6 MPa) and kl/r = 0.0 where this trend was reversed. For 4000 psi (27.6 MPa) concrete, the column with ρ_{ss} = 0.040 had strength ratios significantly lower than those for the column with ρ_{ss} = 0.082 when e/h ratio fell between 0.25 and 1.0 as shown in Figure 5.10(a). For e/h greater than 1.0 and less than 0.25, there seem to be minor differences in the one-percentile strength ratios calculated for the two columns shown in the figure. For 6000 psi (41.4 MPa) concrete [Figure 5.11(a)], the column with 4 percent structural steel produced significantly lower one-percentile strength ratios than those obtained for the column having 8 percent structural steel when $e/h < 0.6$. For $e/h > 1.0$, the trend reversed and lower one-percentile strength ratios were obtained for the columns with 8 percent steel, as indicated in Figure 5.11(a).

The 1-percentile strength ratios plotted in the above-noted figures may be explained by examination of the relative contributions of structural steel and concrete to the overall strength of the column. The concrete contributes

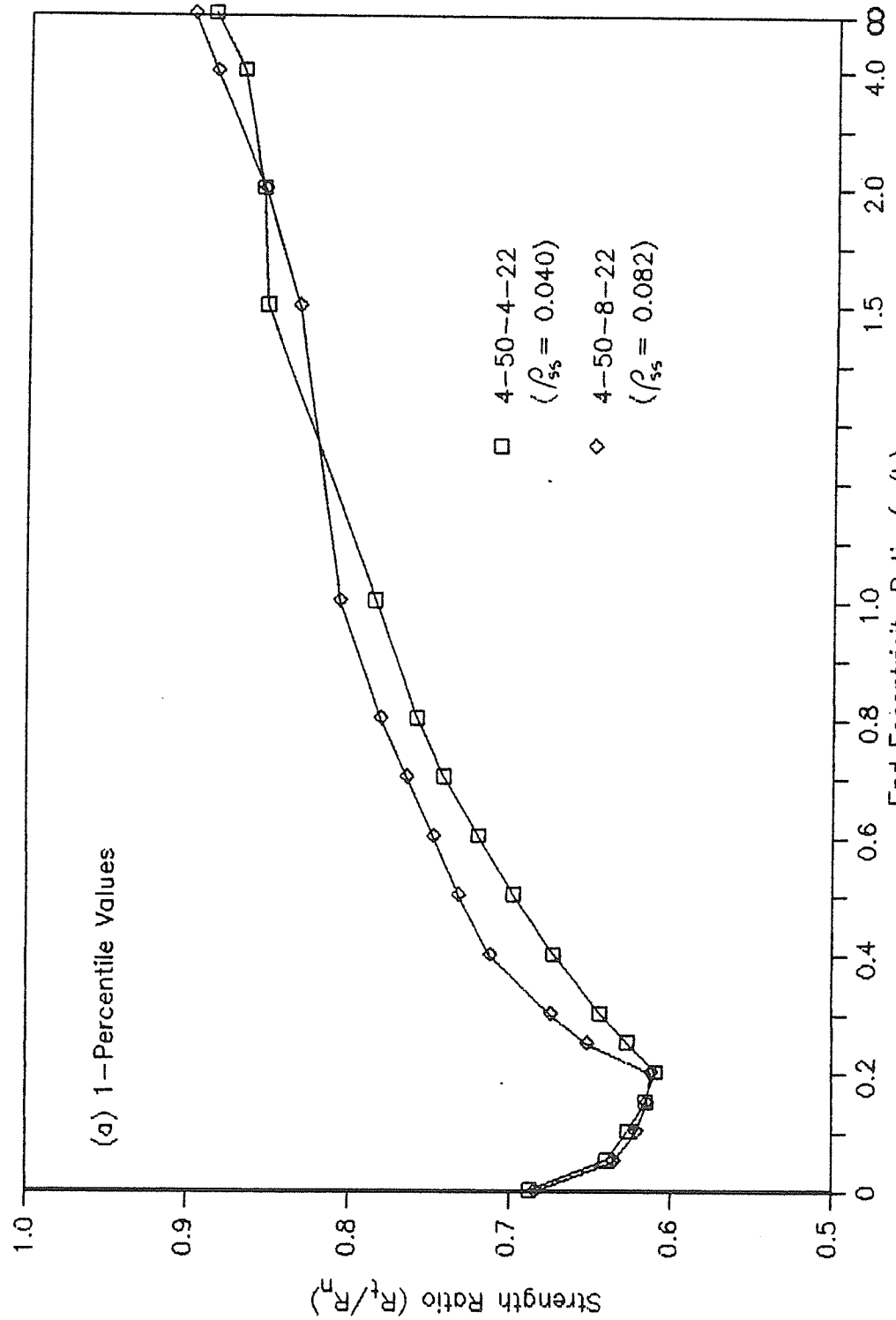

Figure 5.10 – Effect of Structural Steel Ratio on the Ratio of Theoretical to Nominal Strength of Short Composite Steel–Concrete Beam–Columns

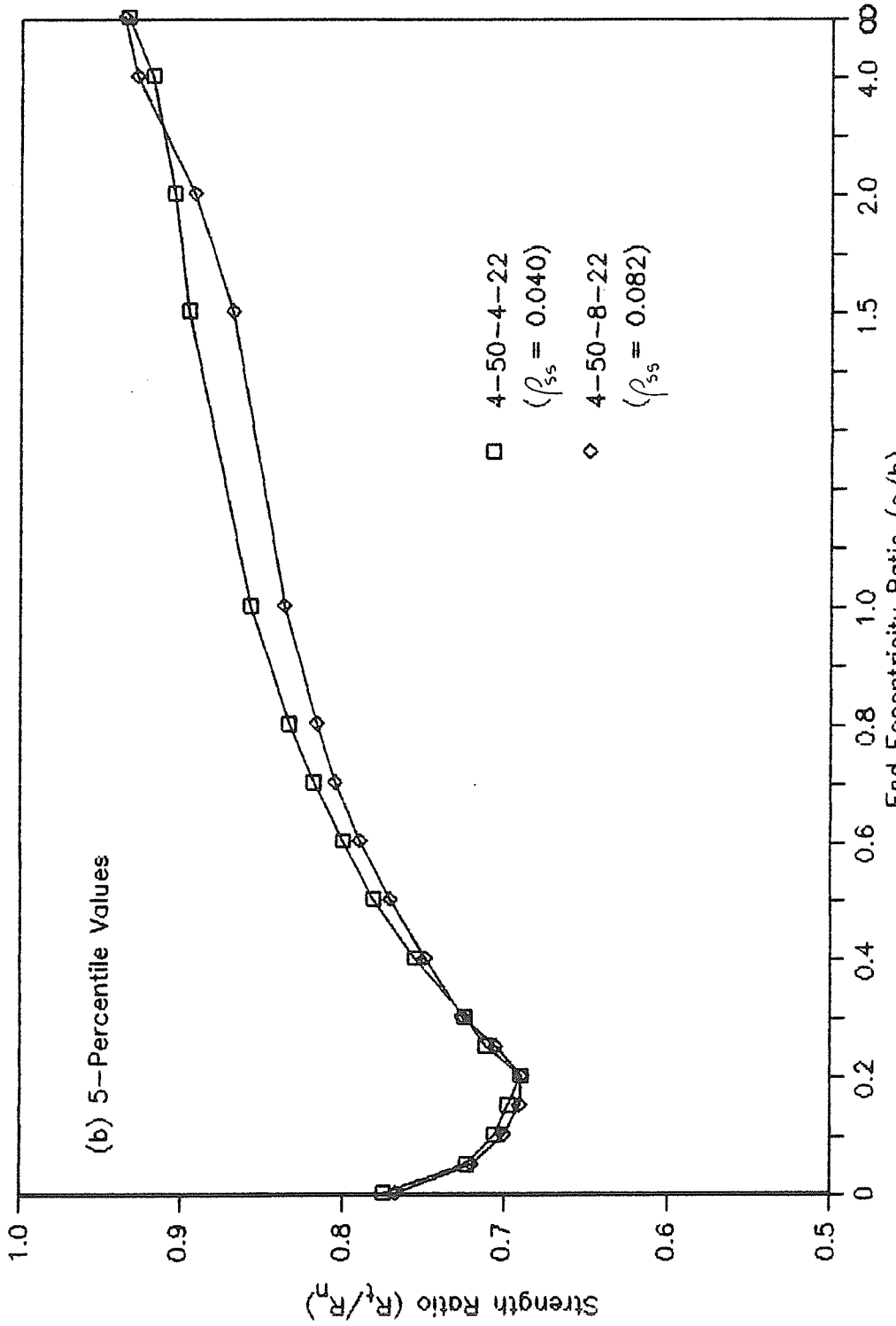

Figure 5.10 (cont.) – Effect of Structural Steel Ratio on the Ratio of Theoretical to Nominal Strength of Short Composite Steel–Concrete Beam–Columns

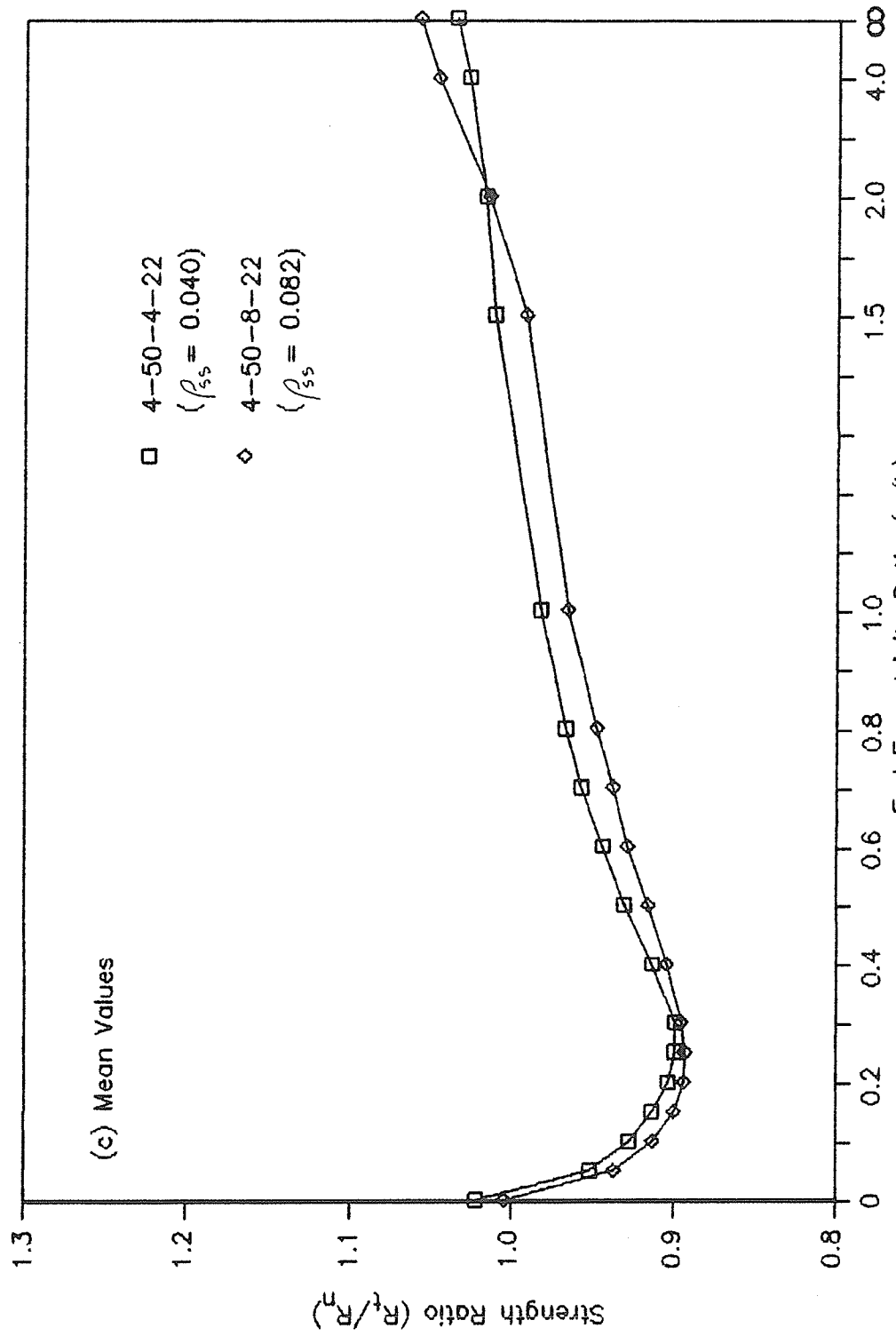

Figure 5.10 (cont.) – Effect of Structural Steel Ratio on the Ratio of Theoretical to Nominal Strength of Short Composite Steel–Concrete Beam–Columns

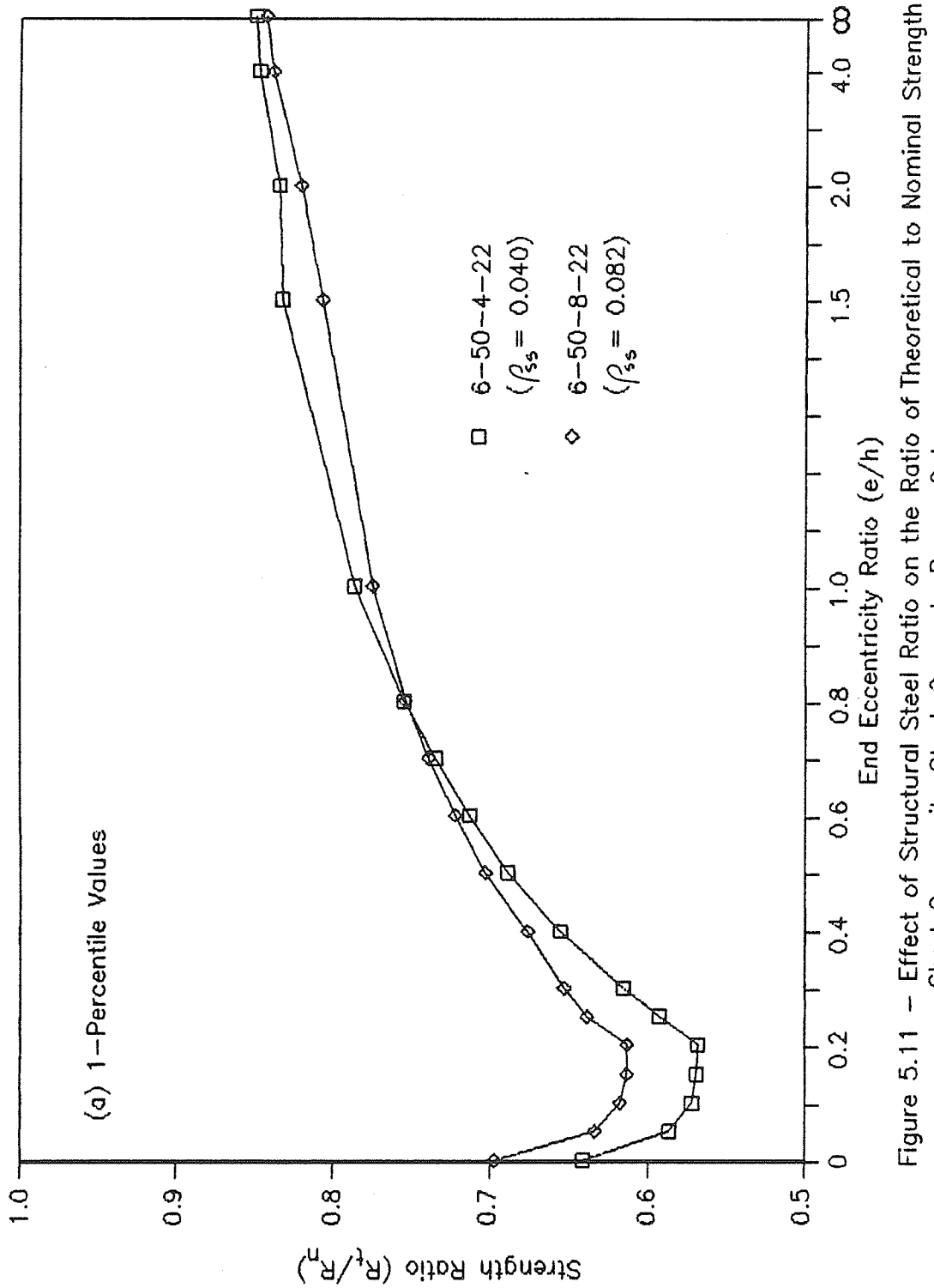

Figure 5.11 – Effect of Structural Steel Ratio on the Ratio of Theoretical to Nominal Strength of Short Composite Steel–Concrete Beam–Columns

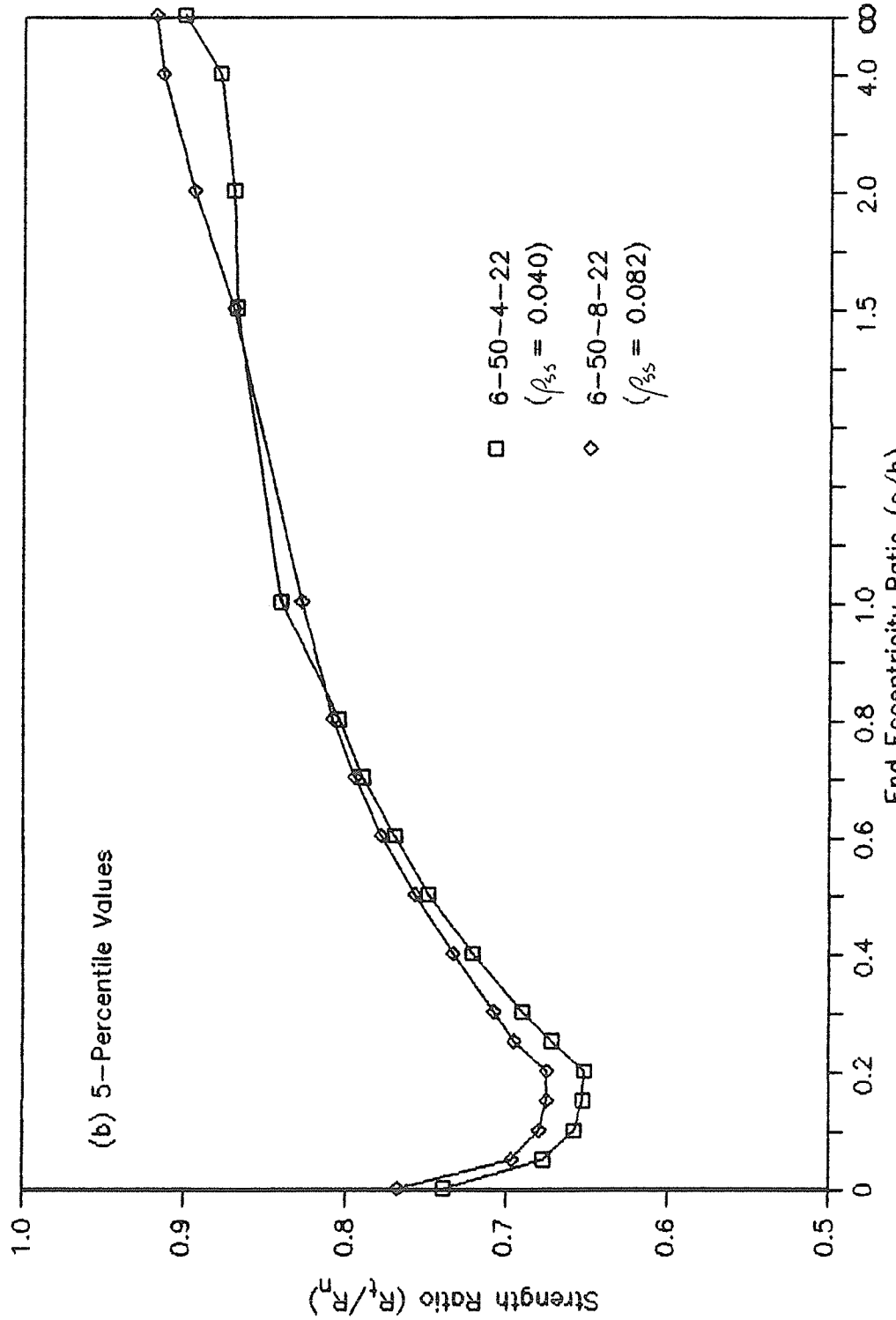

Figure 5.11 (cont.) – Effect of Structural Steel Ratio on the Ratio of Theoretical to Nominal Strength of Short Composite Steel–Concrete Beam–Columns

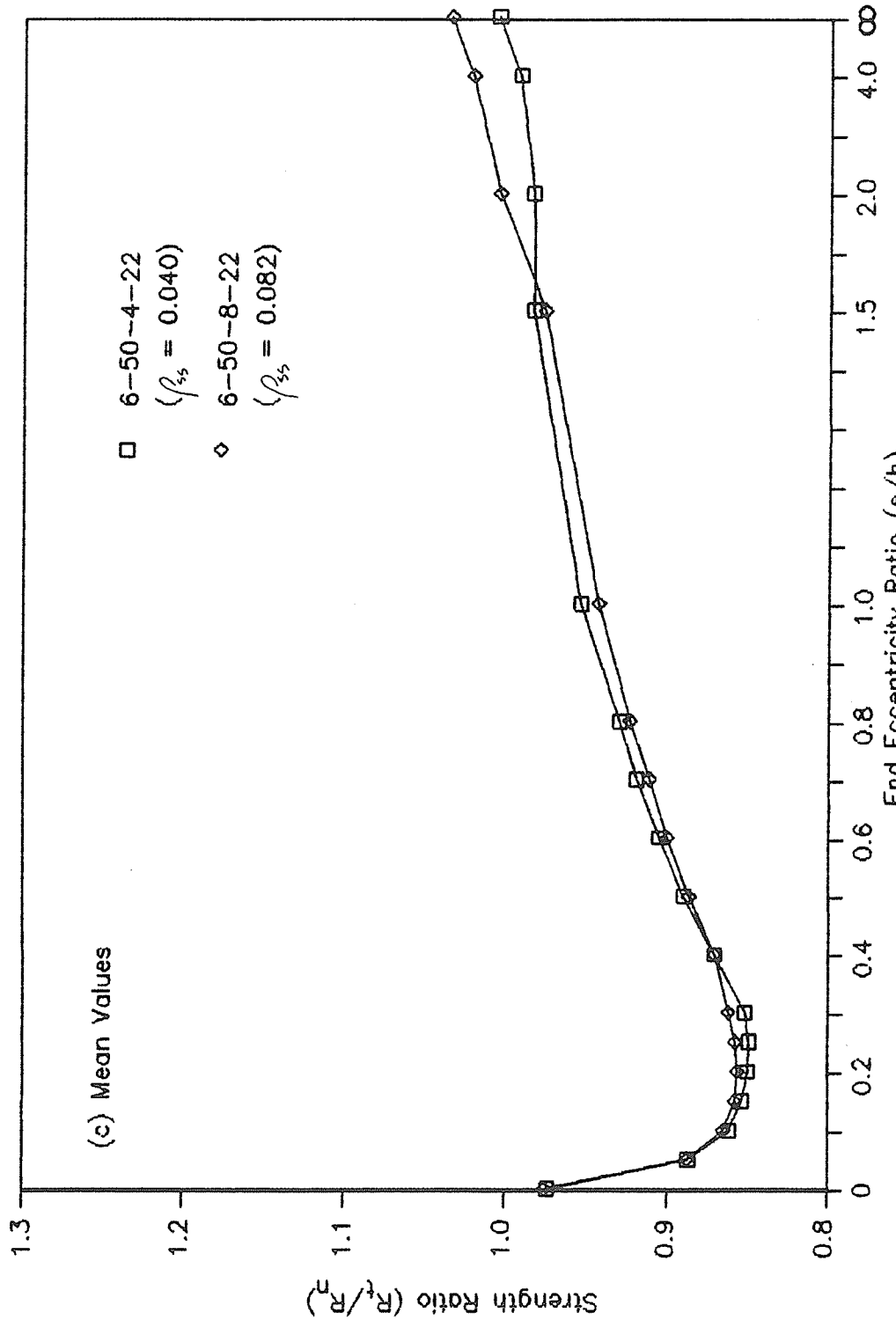

Figure 5.11 (cont.) – Effect of Structural Steel Ratio on the Ratio of Theoretical to Nominal Strength of Short Composite Steel–Concrete Beam–Columns

more to the overall strength of the column at low e/h values than at high e/h values. Hence, at low e/h larger variations take place in the overall strength of the beam-column since the concrete strength has a higher variability than the structural steel strength. Hence, lower one-percentile strength ratios are expected for smaller ρ_{ss} in regions of low e/h. At high e/h values, the contribution of the structural steel becomes predominant and the variability of steel strength is the primary cause of overall beam-column strength variations. This produces smaller overall strength variations and, hence, less spread in one-percentile values for different ρ_{ss} ratios. These results concur with earlier findings by Grant et al. (1978) where reinforced concrete columns with low steel ratios were found to have larger variations than the columns with high steel ratios.

Minor differences between the strength ratios for columns having 4 percent and for columns having 8 percent structural steel were noticed at the 5-percentile and mean value levels, as indicated by Figures 5.10(b) and (c) and 5.11(b) and (c). This seems to be particularly valid for f'_c = 6000 psi (41.4 MPa) [Figures 5.11(b) and (c)]. Since the 1-percentile level is more critical for reliability analysis, it is recommended that ρ_{ss} be included as a variable for such analyses.

5.3.2.4 Effect of end eccentricity ratio - Each column from the basic study (Table 5.1) was investigated for 17 end eccentricity ratios (e/h = 0.0, 0.05, 0.1, 0.15, 0.2, 0.25, 0.3, 0.4, 0.5, 0.6, 0.7, 0.8, 1.0, 1.5, 2.0, 4.0 and ∞). Figures 5.6 through 5.11 indicate that the strength ratios drop sharply as e/h increases from 0.0 to 0.2. The strength ratios tend to increase then at a declining rate as e/h increases from 0.2 to infinity (pure bending condition). The dip in strength ratios at e/h of 0.2 is the most significant at 1-percentile level and becomes less significant at 5-percentile and mean value levels. For 1-percentile and 5-percentile strength ratios, the maximum values were obtained at $e/h = \infty$ (pure bending condition). For mean strength ratios, however, the maximum values occurred at e/h = 0.0 and ∞ (pure compression and pure bending conditions), as indicated by Figures 5.6 - 5.11.

For further analysis, data from the eight columns of the basic study (Table 5.1) were grouped into two sets according to the specified concrete strength. For each concrete strength, the range of one-percentile, 5-percentile, and mean strength ratios at all e/h values studied is plotted in Figure 5.12 (a), (b), and (c), respectively. The trends for the effect of e/h ratio stated in the preceding paragraph are also valid for the plots shown in Figure 5.12. Additionally, it is apparent from Figure 5.12 that the upper boundary of the range of strength ratios is defined by the

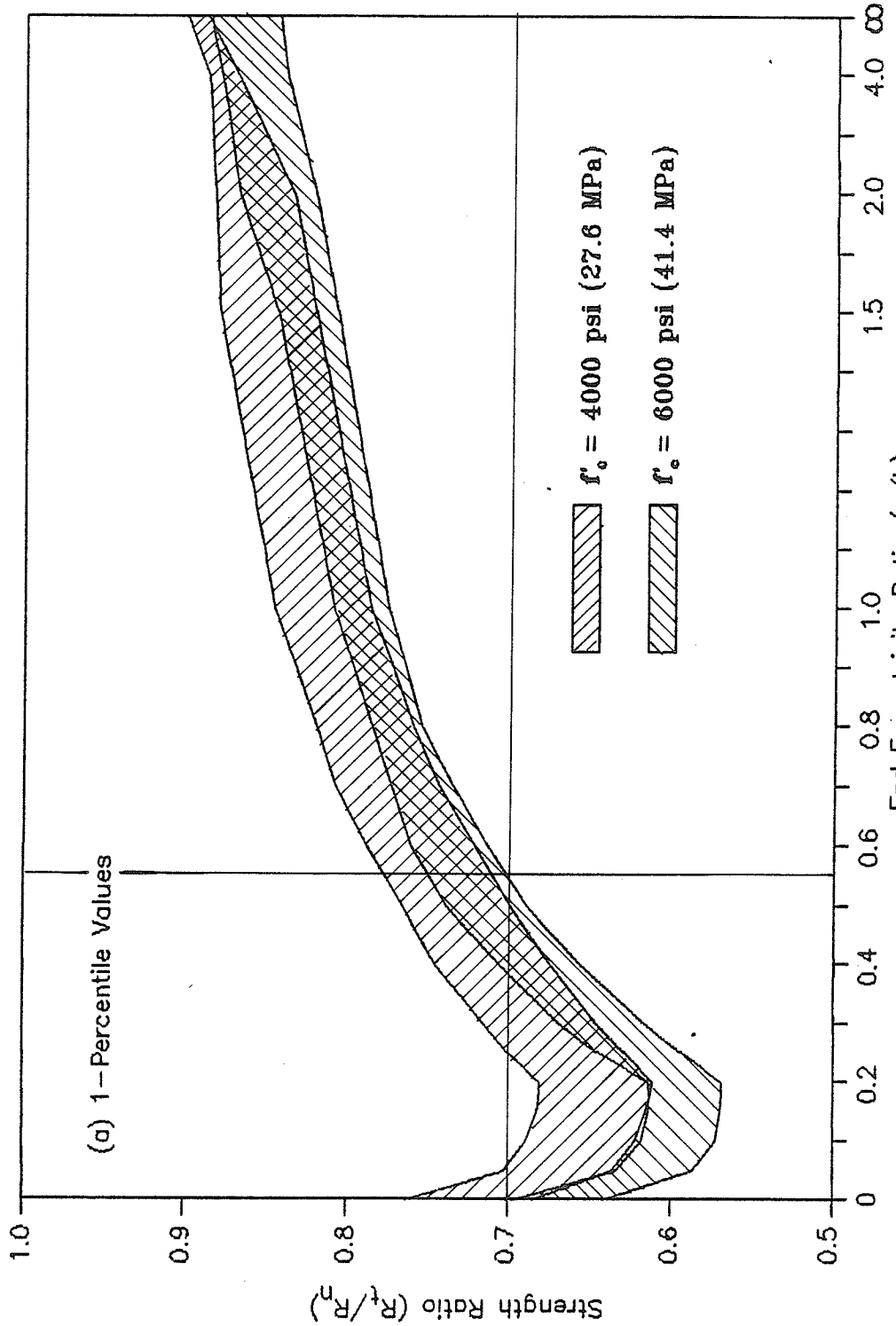

Figure 5.12 – **Range of Ratio of Theoretical to Nominal Strength of** Short Composite Steel–Concrete Beam–Columns

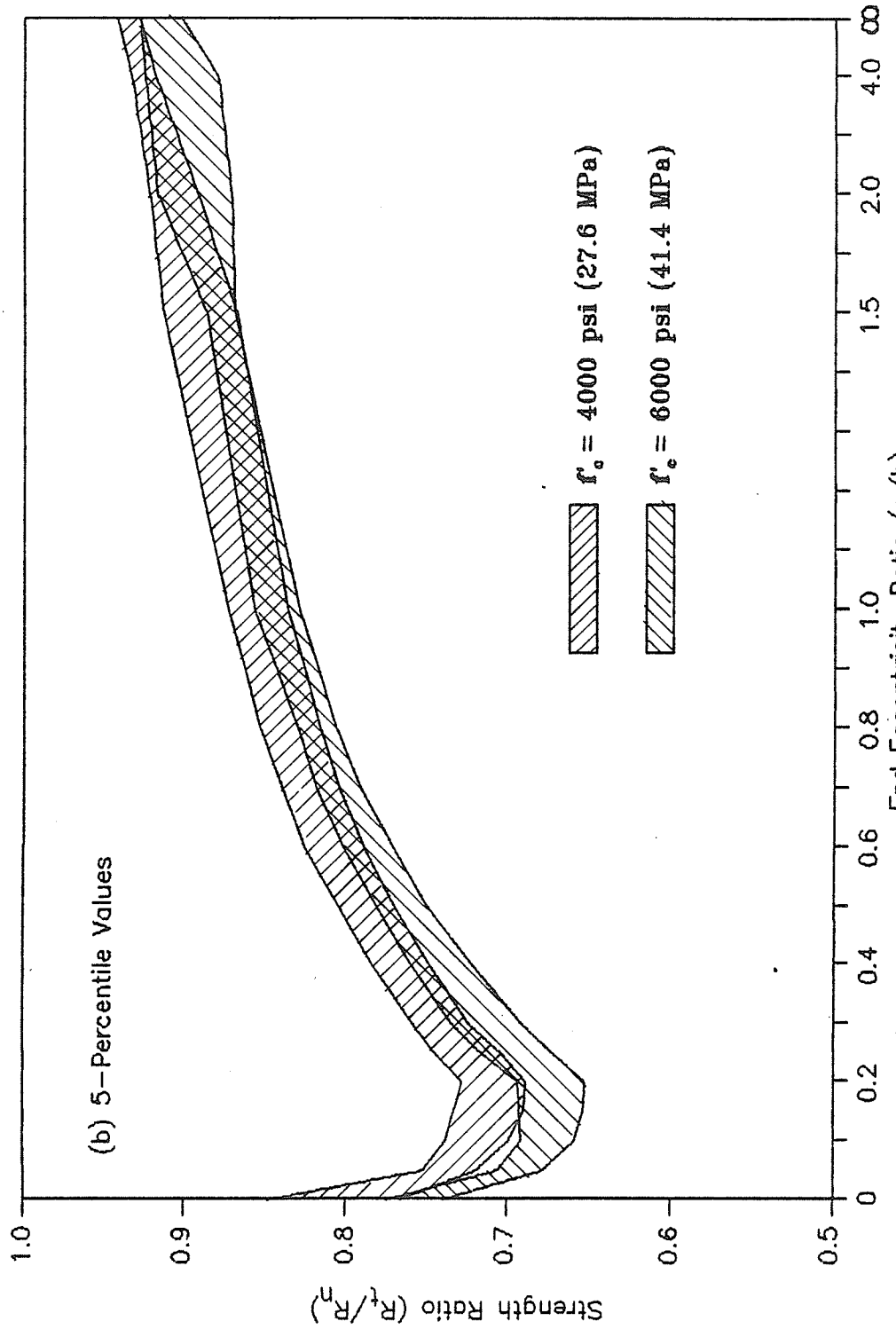

Figure 5.12 (cont.) – **Range of Ratio of Theoretical to Nominal Strength of** Short Composite Steel–Concrete Beam–Columns

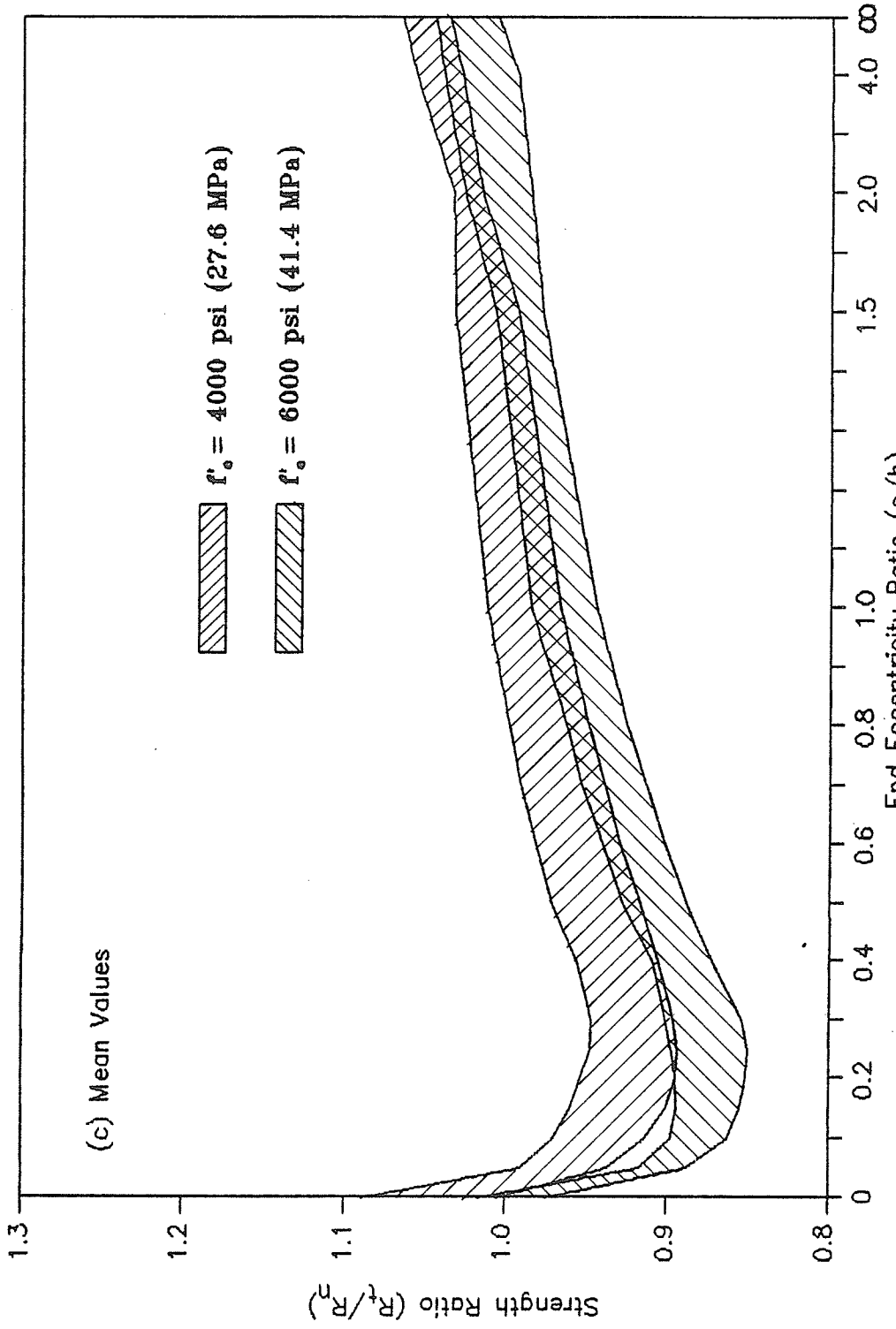

Figure 5.12 (cont.) – **Range of Ratio of Theoretical to Nominal Strength of** Short Composite Steel–Concrete Beam–Columns

columns having 4000 psi (27.6 MPa) concrete and the lower boundary is defined by the columns with 6000 psi (41.4 MPa) concrete. The maximum spread in one-percentile, 5-percentile and mean strength ratios occurs at e/h of 0 and 0.2, whereas the minimum spread in these values takes place at $e/h = \infty$ (pure bending), as indicated by Figure 5.12.

The range of the strength coefficients of variation for the two sets of columns discussed above is plotted on Figure 5.13. The coefficients of variation are the greatest at e/h of 0.0 and decrease only slightly between e/h of 0.0 and 0.2. The coefficients of variation then decline sharply at a declining rate as e/h increases from 0.2 to infinity. The largest spread between the minimum and maximum values of the coefficient of variation occurs for columns having 4000 psi (27.6 MPa) concrete when e/h lies between 0 and 0.2.

At $e/h \leq 0.7$, the range of coefficients of variation for columns having 6000 psi (41.4 MPa) concrete fall within the range of coefficients of variation for columns with 4000 psi (27.6 MPa) concrete. This is expected because the 6000 psi (41.4 MPa) concrete was assumed to have excellent quality control as opposed to average quality control for 4000 psi (27.6 MPa) concrete and because the concrete quality has an influence on variability of beam-concrete strength when e/h is not high. As expected for values of e/h higher than 0.7,

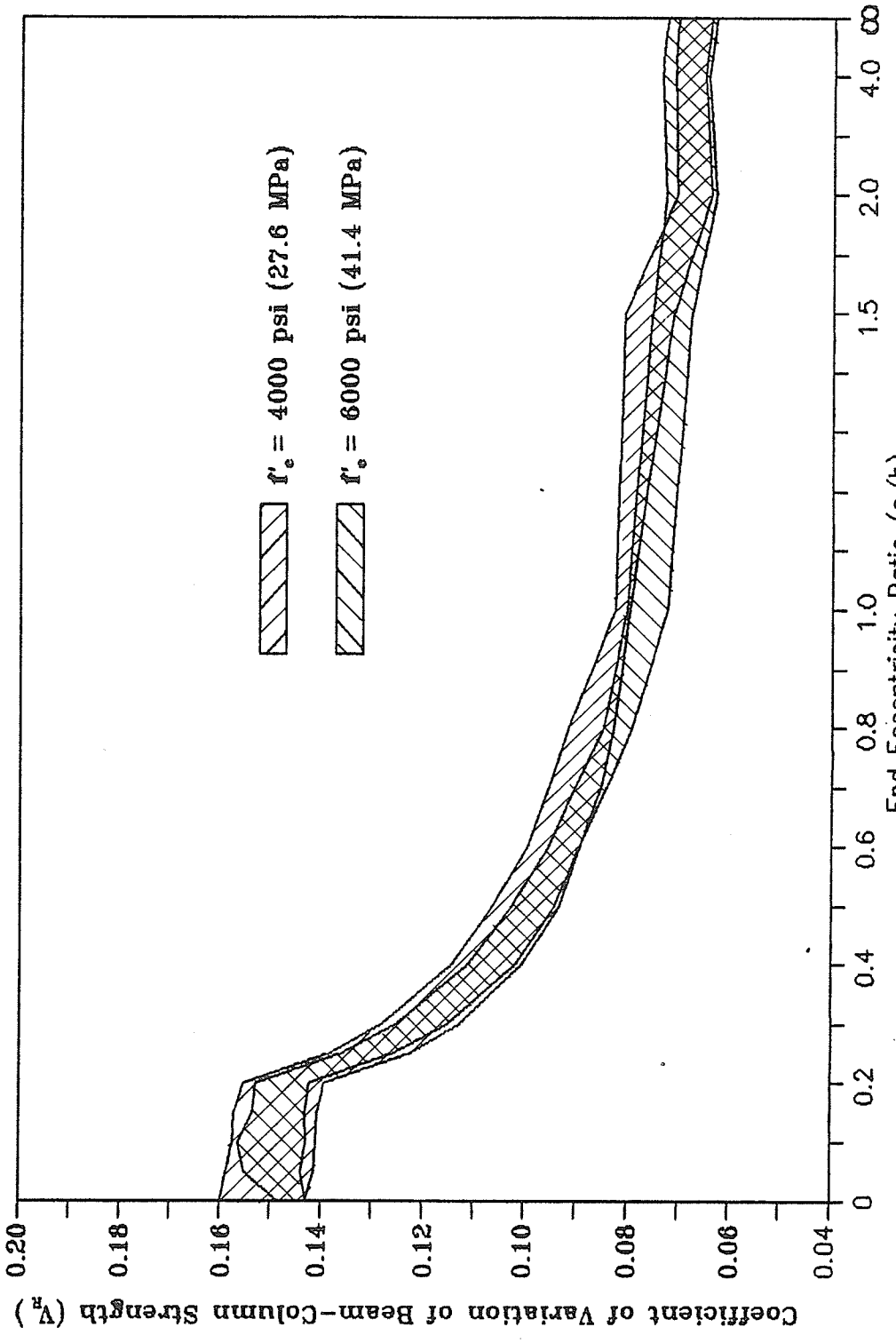

Figure 5.13 – Range of the Coefficient of Variation of the Ratio of Theoretical to Nominal Strength of Short Composite Steel–Concrete Beam–Columns

the range of the beam-column strength coefficients of variation remained practically unaffected by the specified concrete strength. This was particularly valid for pure bending condition ($e/h = \infty$), as indicated by Figure 5.13.

From the above discussions, it is obvious to conclude that the end eccentricity ratio is a variable which needs to be considered in reliability studies. End eccentricity ratio effects both the beam-column strength ratios and the coefficients of variation to a significant extent. The end eccentricity ratios below 0.55 are especially critical since these e/h ratios produce one-percentile strength ratios that fall below 0.7, as indicated by Figure 5.12(a).

5.3.2.5 Sensitivity analysis - The portions of the overall variability of the beam-column strength attributable to the variations in the mechanical properties of concrete, the mechanical and geometric properties of structural steel, and the theoretical strength model error were determined for a typical beam-column cross-section. Column 4-50-4-0 (Table 5.1) was chosen for this analysis. To determine the beam-column strength variability due to each of the three sets of variables noted above, three separate computer runs of 500 simulations each were made. For each computer run, only the variables from one of the above-noted sets were allowed to vary while the remaining variables were kept constant at their mean value. The portions of the overall variability

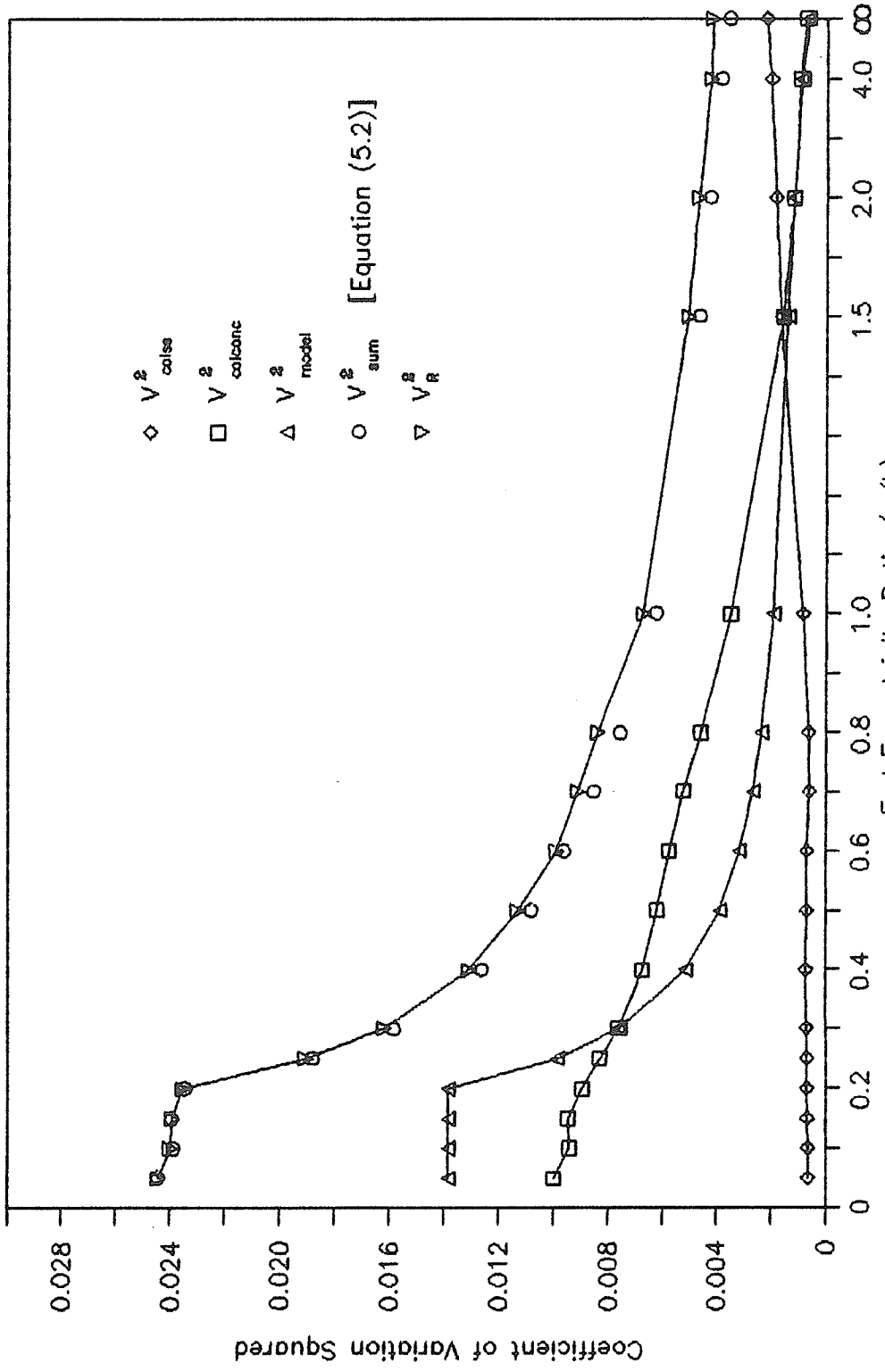

Figure 5.14 – Effect of Variabilities of Properties of Constituent Materials on Overall Strength Variability of Beam–Column Cross–Section 4–50–4–0 (Table 5.1)

of the beam-column strength so determined were respectively designated as $V_{colconc}$, V_{colss}, and V_{model} for the three sets of variables noted above.

The squares of the coefficients of variation $V^2_{colconc}$, V^2_{colss}, and V^2_{model} computed for column 4-50-4-0 at e/h values ranging from 0.05 to infinity are plotted on Figure 5.14. These plots indicate that the overall variability of the strength of the above-noted column cross-section is mostly influenced by the variations in the theoretical strength model and the concrete mechanical properties for $e/h \leq 1.0$, and by the variations in the structural steel section properties for $e/h = \infty$. For $1.0 < e/h < \infty$, all three variations ($V_{colconc}$, V_{colss}, and V_{model}) seem to contribute to the overall strength variability of column cross-section 4-50-4-0. Note the effects of the variability of the theoretical strength model and of the concrete properties decrease significantly as the end eccentricity ratio increases. The effect of the variability of the structural steel properties increases somewhat as e/h increases from 1.0 to higher values.

The values of V^2_{sum} plotted in Figure 5.14 represent the sum of the squares of the coefficients of variation of Column 4-50-4-0 strength obtained from individual variabilities of the three sets of variabilities, i.e.

$$V_{sum}^2 = V_{colconc}^2 + V_{colss}^2 + V_{model}^2 \qquad (5.2)$$

Also plotted in Figure 5.14 are the values of V_R^2 which is the square of the coefficient of variation of the beam-column cross-section strength obtained when variabilities from all sources were included simultaneously in computations. A comparison of V_{sum}^2 and V_R^2 plotted in Figure 5.14 indicates a very good correlation of these values up to e/h of 0.3. V_{sum}^2 only slightly underestimates V_R^2 for e/h greater than 0.3. This underestimation by V_{sum}^2 at e/h values higher than 0.3 is likely caused by the variations in the properties of the reinforcing steel and perhaps by the variations in cross-section geometry which were not included in V_{sum}^2 [Equation (5.2)]. This confirms an earlier finding by Mirza (1989) that the cross-section dimensions have negligible effect on composite column strength variability. Grant et al. (1978) reported similar conclusions for reinforced concrete columns. The effects of variations in properties of reinforcing bars were insignificant in this study because the reinforcing steel ratio (ρ_{rs} = 0.012) was much smaller than the structural steel ratio (ρ_{ss} = 0.040 and 0.082) used for the composite cross-section.

5.3.2.6 Summary of effects of variables used for basic study - The following summarizes the effects of variables used for the basic study of short composite beam-columns:

(a) Slenderness ratio of 22 is critical for the type of short columns studied;

(b) the specified concrete strength is a major variable;

(c) the ratio of structural steel area to gross cross-sectional area is a significant variable;

(d) the end eccentricity ratio has a very significant effect on the strength ratios and is especially critical in the range from 0.0 to 0.55; and

(e) the overall variations of the beam-column theoretical strength are primarily due to the variations in the mechanical properties of the concrete, the geometric and mechanical properties of the structural steel, and the theoretical model.

5.3.3 Effects Of Variables Used For Supplemental Study

From the short columns used for the supplemental study (Table 5.3), the effects of the specified yield strength of structural steel, the strain-hardening of structural steel section and reinforcing bars, and the quality control of concrete on the beam-column strength ratios were studied. Plots of the one-percentile, five-percentile and mean strength ratios at various values of e/h were made for each variable studied.

5.3.3.1 **Effect of specified yield strength of structural steel** - To study the effect of the specified yield strength of structural steel on the strength ratios, two short columns from the basic study (Columns 4-50-4-22 and 6-50-4-22 in Table 5.1) were compared to four columns from the supplemental study (Columns 4-44-4-22, 4-36-4-22, 6-44-4-22, and 6-36-4-22 in Table 5.3). This provided two sets of three columns, each column with structural steel f_y of 50, 44, or 36 ksi (345, 303, or 248 MPa). All other properties of the three columns in a set were identical. Figures 5.15 (a), (b), and (c) respectively plot the one-percentile, five-percentile and mean strength ratio data for one of the sets noted above.

At the 1-percentile level, the lowest strength ratios were found for the columns having 50 ksi (345 MPa) and 36 ksi (248 MPa) structural steel which plot almost identically at e/h values below 0.4. The one-percentile strength ratios for the columns with 44 ksi (303 MPa) structural steel plot somewhat higher in this range of e/h. Between e/h of 0.4 and 0.8, the one-percentile strength ratio data for the column with 50 ksi (345 MPa) structural steel rises slightly higher than the data for the columns with 36 ksi (248 MPa) structural steel. At the pure bending condition, all three beam-columns have similar one-percentile strength ratios, as indicated by Figure 5.15(a).

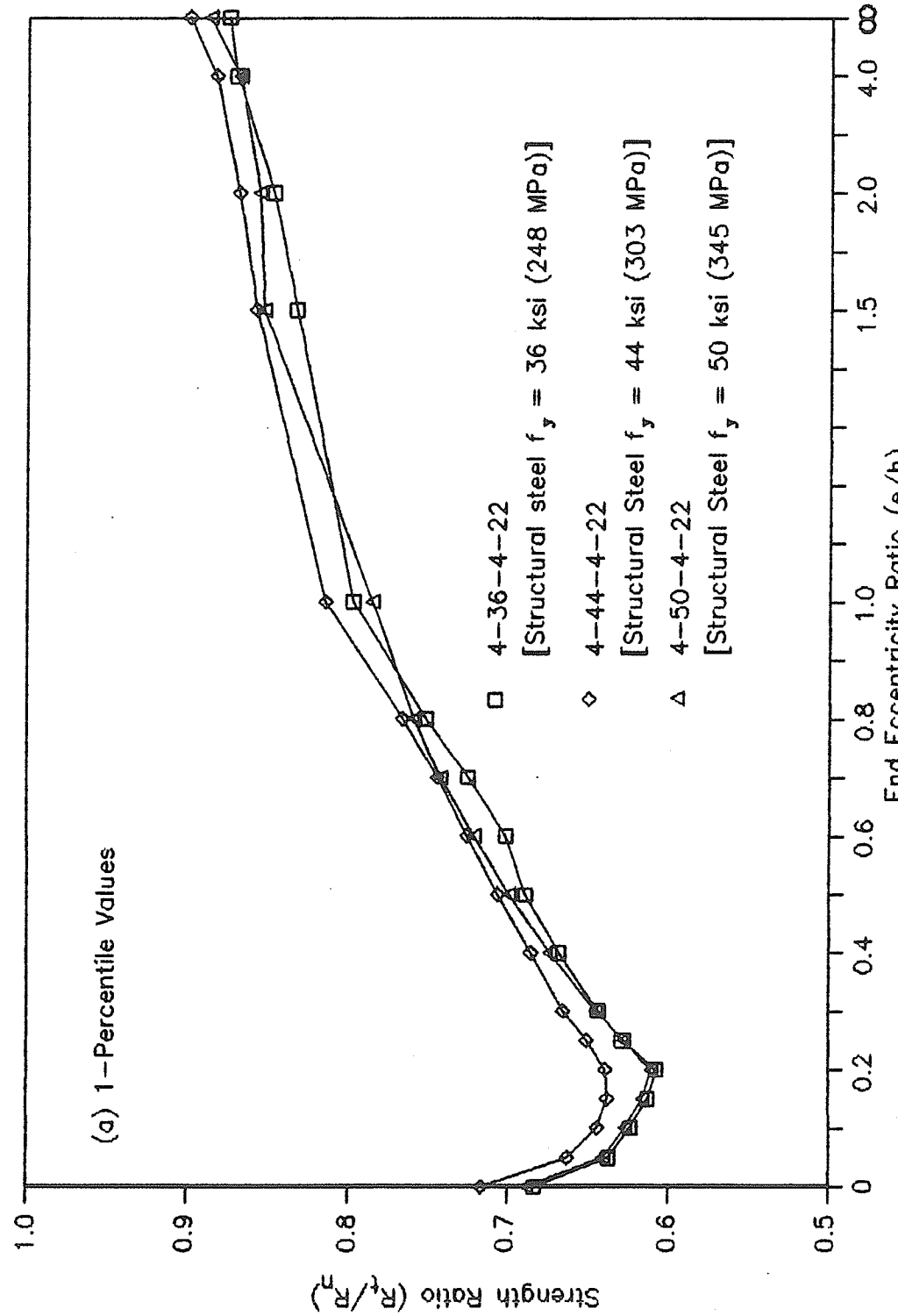

Figure 5.15 – Effect of Specified Structural Steel Yield Strength on the Ratio of Theoretical to Nominal Strength of Short Composite Steel-Concrete Beam-Columns

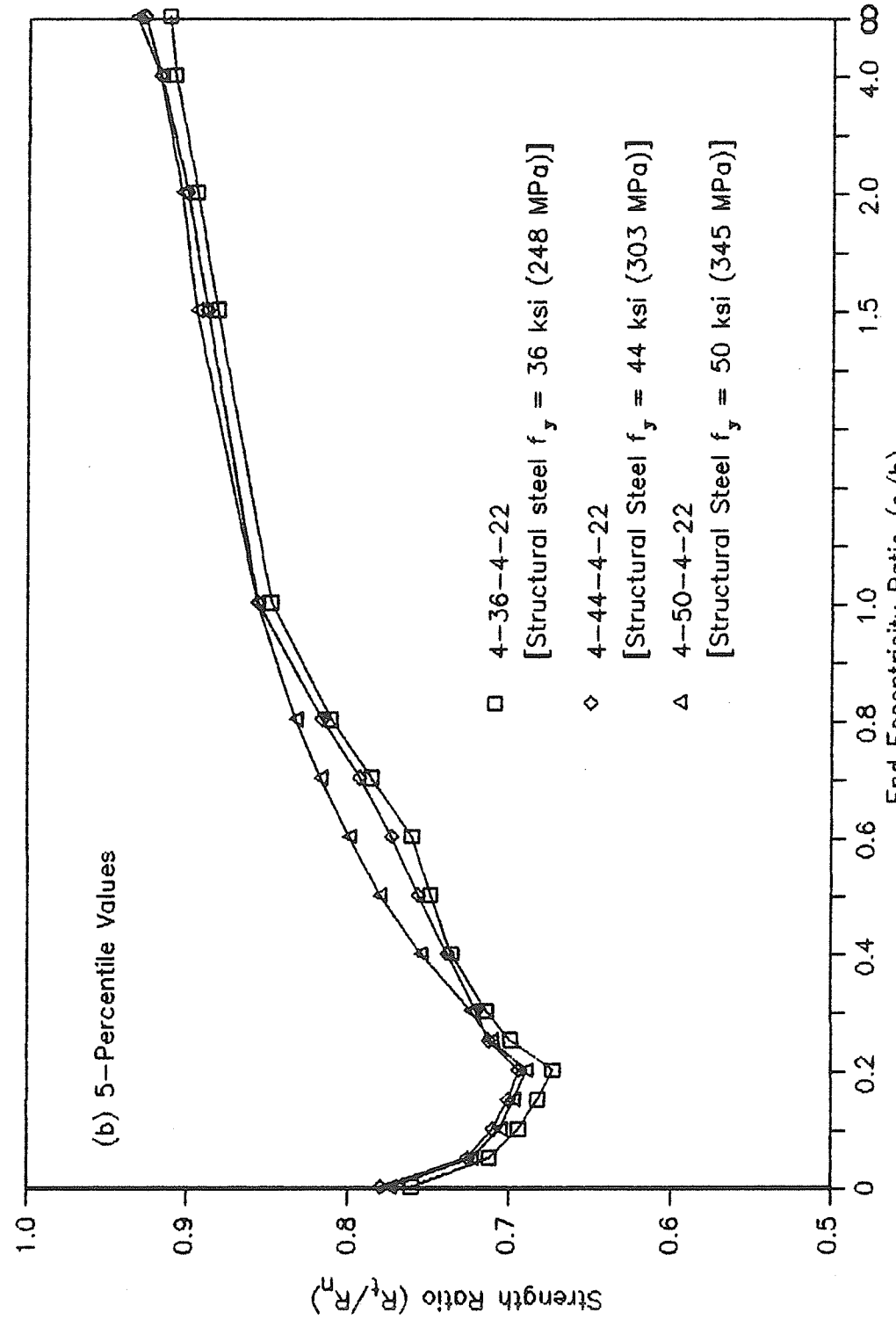

Figure 5.15 (cont.) – Effect of Specified Structural Steel Yield Strength on the Ratio of Theoretical to Nominal Strength of Short Composite Steel–Concrete Beam–Columns

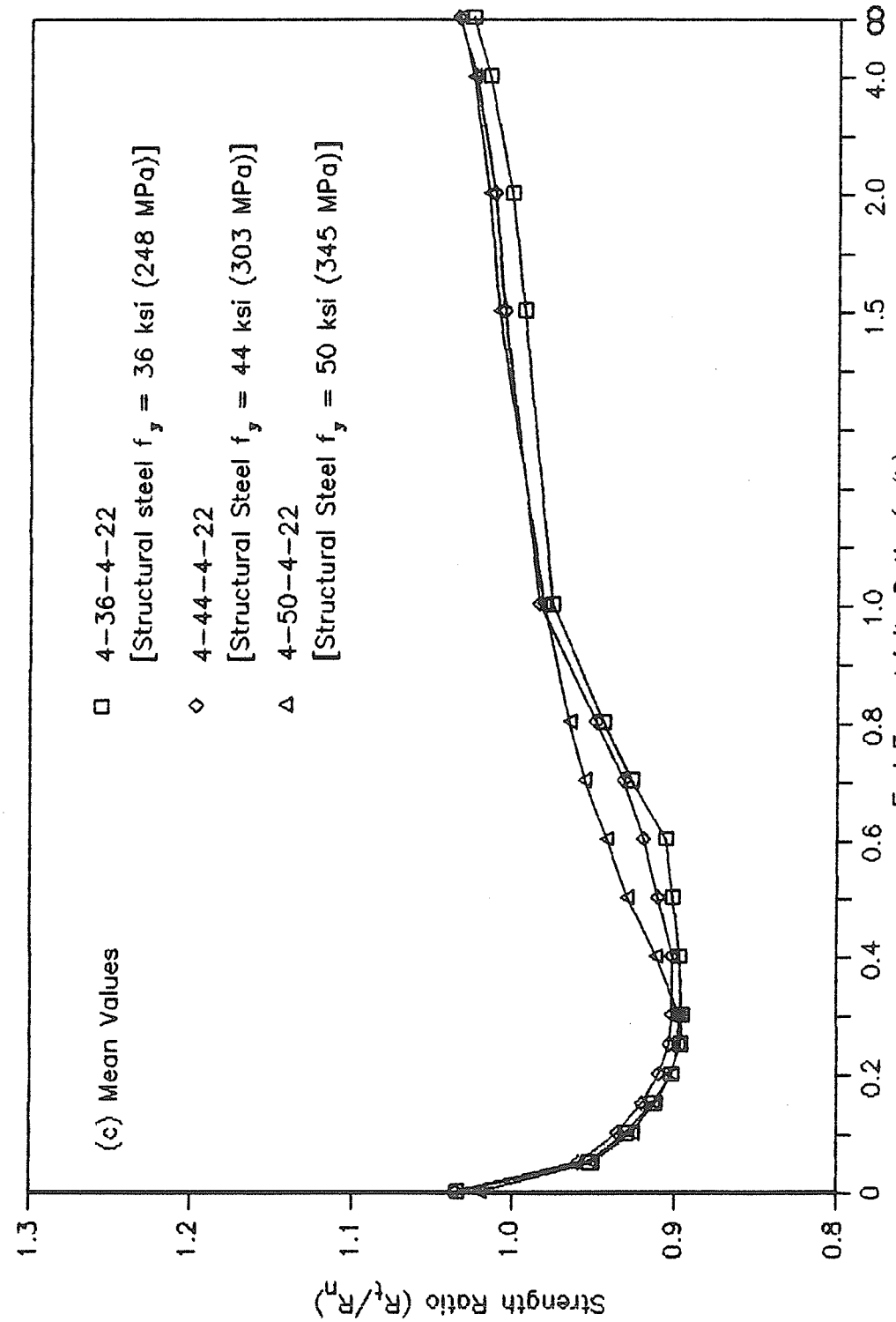

Figure 5.15 (cont.) – Effect of Specified Structural Steel Yield Strength on the Ratio of Theoretical to Nominal Strength of Short Composite Steel–Concrete Beam–Columns

At the 5-percentile and mean value levels, the data for columns with all three grades of structural steel plot close to each other [Figures 5.15 (b) and (c)]. The only noted differences were at e/h values between 0.3 and 1.0. However, these differences were not considered significant.

Similar conclusions were obtained from the strength ratio data of the remaining set of beam-columns used to investigate the effect of the specified yield strength of structural steel. Since differences between strength ratios for columns with three different grades of steel are minimal at the one-percentile level, it is recommended that 50 ksi (345 MPa) structural steel be used in future reliability analysis of composite cross-sections. The 50 ksi (345 MPa) structural steel is the highest steel grade presently allowed by the design codes (ACI 318-83 and CAN3-A23.3-M84) for composite columns and will ensure relevancy as common steel grades increase above the present values.

5.3.3.2 Effect of strain hardening of steel - To examine the effects of strain-hardening of the structural steel and of the vertical reinforcing bars on the strength ratios of composite cross-sections, the data from two columns taken from the basic study (Columns 4-50-4-0 and 6-50-4-0 in Table 5.1) were compared to the data from the corresponding columns of the supplemental study (Columns 4-50-4-0-STH and 6-50-4-0-STH in Table 5.3). Note the strain-hardening of

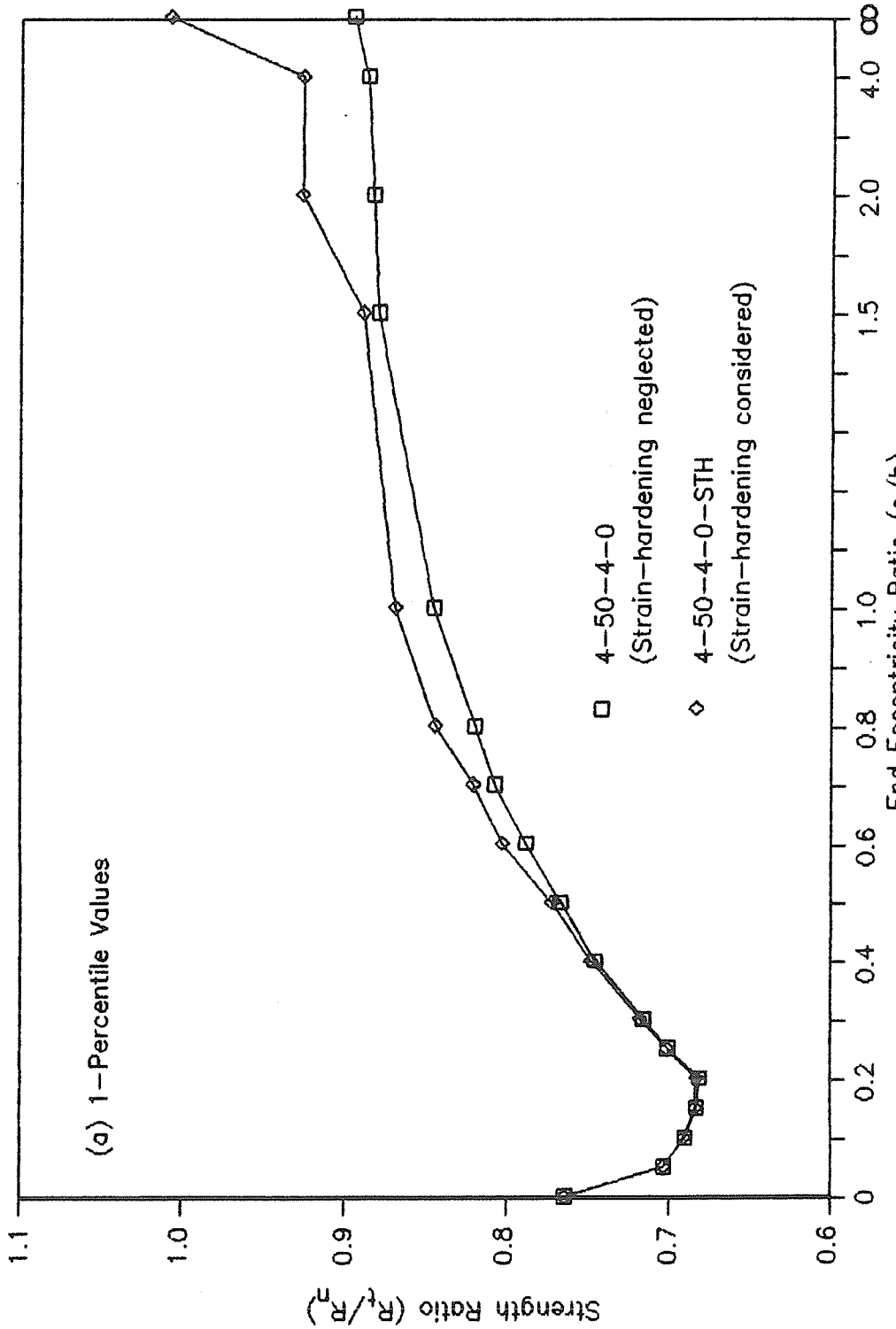

Figure 5.16 – Effect of Strain-Hardening of Steel on the Ratio of Theoretical to Nominal Strength of Short Composite Steel-Concrete Beam-Columns

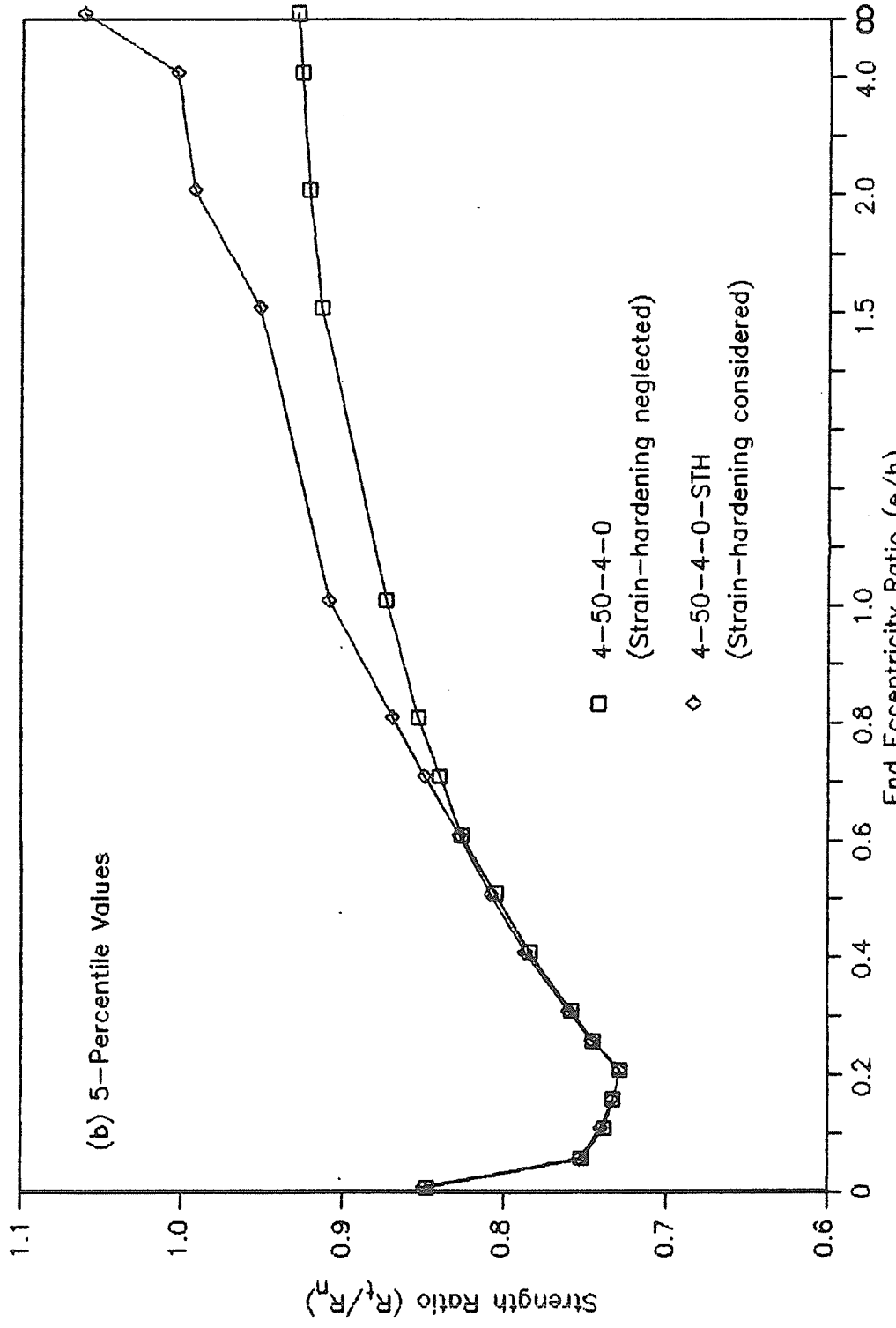

Figure 5.16 (cont.) – Effect of Strain-Hardening of Steel on the Ratio of Theoretical to Nominal Strength of Short Composite Steel-Concrete Beam-Columns

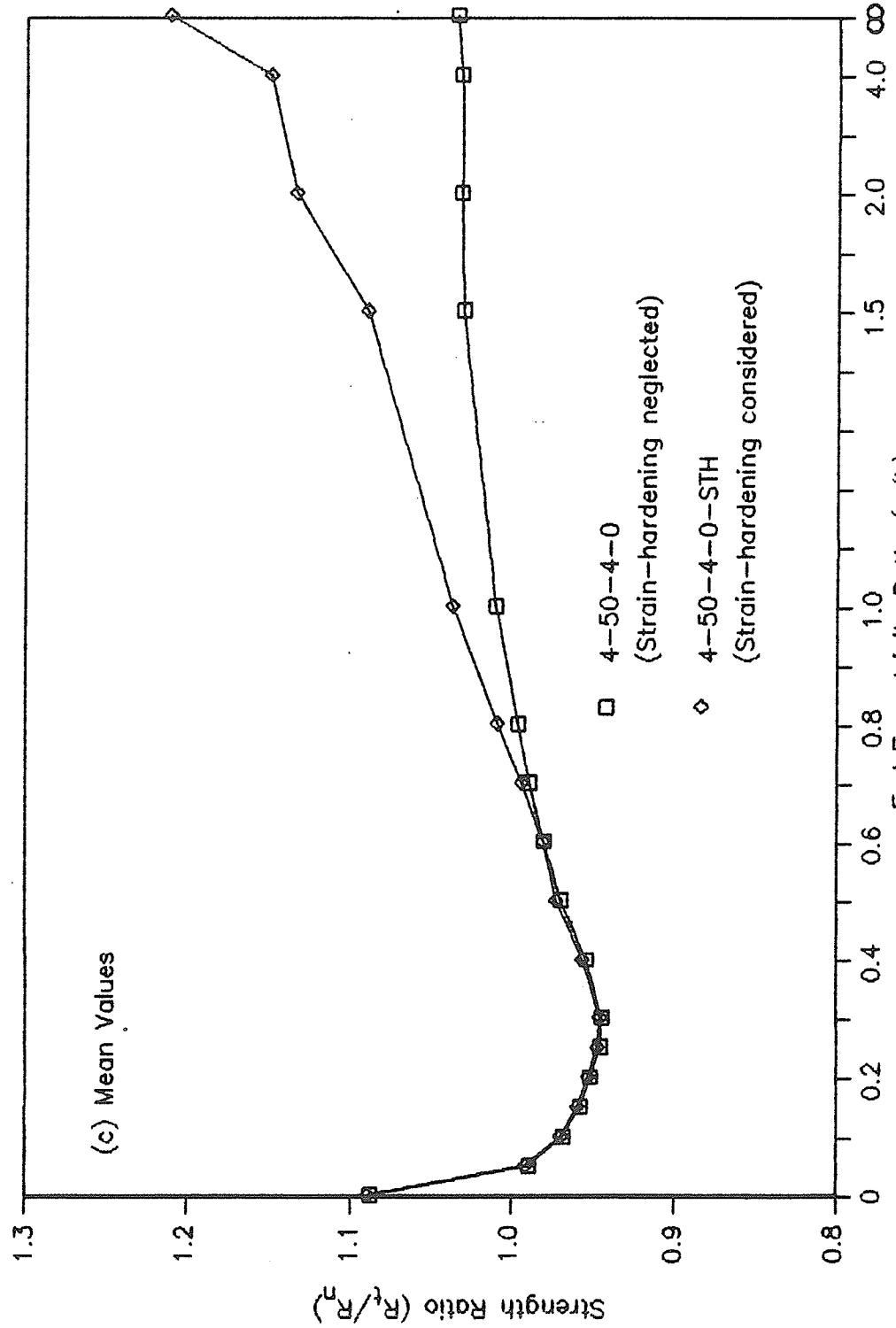

Figure 5.16 (cont.) – Effect of Strain-Hardening of Steel on the Ratio of Theoretical to Nominal Strength of Short Composite Steel-Concrete Beam-Columns

both steels was included in theoretical strength computations of Columns 4-50-4-0-STH and 6-50-4-0-STH, while the strain-hardening of steel was neglected for Columns 4-50-4-0 and 6-50-4-0. This provided two sets of columns, each set having one column in which strain-hardening was included and one column in which strain-hardening was not permitted. All other properties were identical for both columns in a set. The strength ratios for columns from one of these sets are shown in Figure 5.16.

The plots in Figures 5.16 (a), (b), and (c) show no effect of strain-hardening of steel on one-percentile, five-percentile and mean strength ratios at e/h values less than or equal to around 0.6. Between e/h of 0.6 and 1.5, there is some increase in strength ratios of the column in which strain-hardening was included in theoretical strength computations. At pure bending, however, the strain-hardening of steel produced significantly higher strength ratios (roughly in the order of 15 percent) at one-percentile, five-percentile and mean value level, as indicated by Figure 5.16.

A similar behavior was observed from the remaining set of composite cross-sections used to investigate the effect of strain-hardening of both steels. The data clearly showed that an improvement in the strength ratios for cross-sections occurred only at or near the pure bending condition when strain-hardening of steel was used. This is expected

since the steel must plastically strain to a level approximately ten times the yield strain before the beneficial effect of strain-hardening can be obtained which can only occur at high load eccentricities. It is, therefore, recommended that strain-hardening not be accounted for in future reliability analysis of short composite beam-columns.

5.3.3.3 Effect of quality of concrete - In the basic study (Table 5.1), the concrete quality for four columns with f'_c = 6000 psi (41.4 MPa) was assumed to be excellent. This corresponds to the control cylinder strength coefficient of variation of 10 percent. The average quality control of concrete assumes a coefficient of variation of 15 percent for the control cylinder strength. To study the effect of average quality control on strength of short composite beam-columns having 6000 psi (41.4 MPa) concrete, the strength ratios for Column 6-50-4-22 (Table 5.1) were compared to those for Column 6-50-4-22-A (Table 5.3). Similar comparisons were also made for the strength ratio data obtained for Columns 6-50-8-22 (Table 5.1) and 6-50-8-22-A (Table 5.3). Note Columns 6-50-4-22 and 6-50-8-22 had excellent quality concrete while Columns 6-50-4-22-A and 6-50-8-22-A employed average quality concrete. This produced two sets of columns, each set had one column with excellent and one column with average quality concrete. All other properties were identical for both columns in a set. The one-percentile,

five-percentile and mean strength ratios for columns in one of the above-noted sets are plotted in Figures 5.17 (a), (b), and (c), respectively.

Figures 5.17 (a) and (b) show that the average concrete quality control produces significantly lower one-percentile and five-percentile strength ratios over the entire range of load eccentricities than does the excellent concrete quality control. The lower one-percentile and five-percentile strength ratios can be attributed directly to the larger coefficient of variation associated with average quality concrete. The effect is significant for end eccentricity ratios up to roughly 1.5 and is negligible at the pure bending condition. This is expected since the concrete contributes little to the overall strength of the column under pure bending. At the mean value level, there is virtually no difference between the strength ratios obtained for columns with excellent and average concrete quality controls. This is expected since the mean values of the concrete strength are not affected by the quality control. Similar results were obtained from the analysis of strength ratio data for the columns in the other set used to investigate the quality control of concrete.

The comparisons of the strength ratios in Figure 5.17 show that the concrete quality control significantly affects the lower tail of the strength probability distribution and,

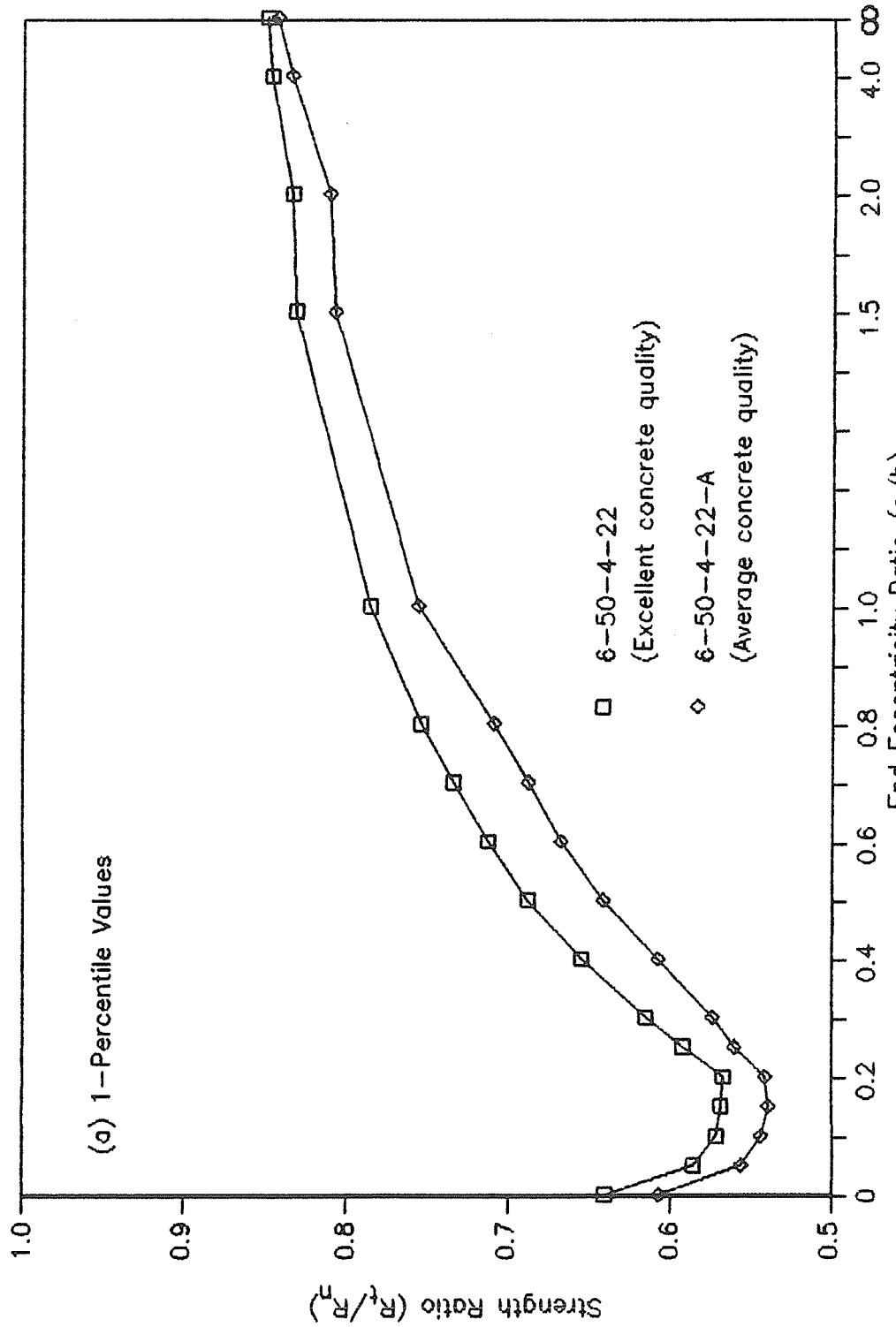

Figure 5.17 – Effect of Concrete Quality Control on the Ratio of Theoretical to Nominal Strength of Short Composite Steel-Concrete Beam-Columns

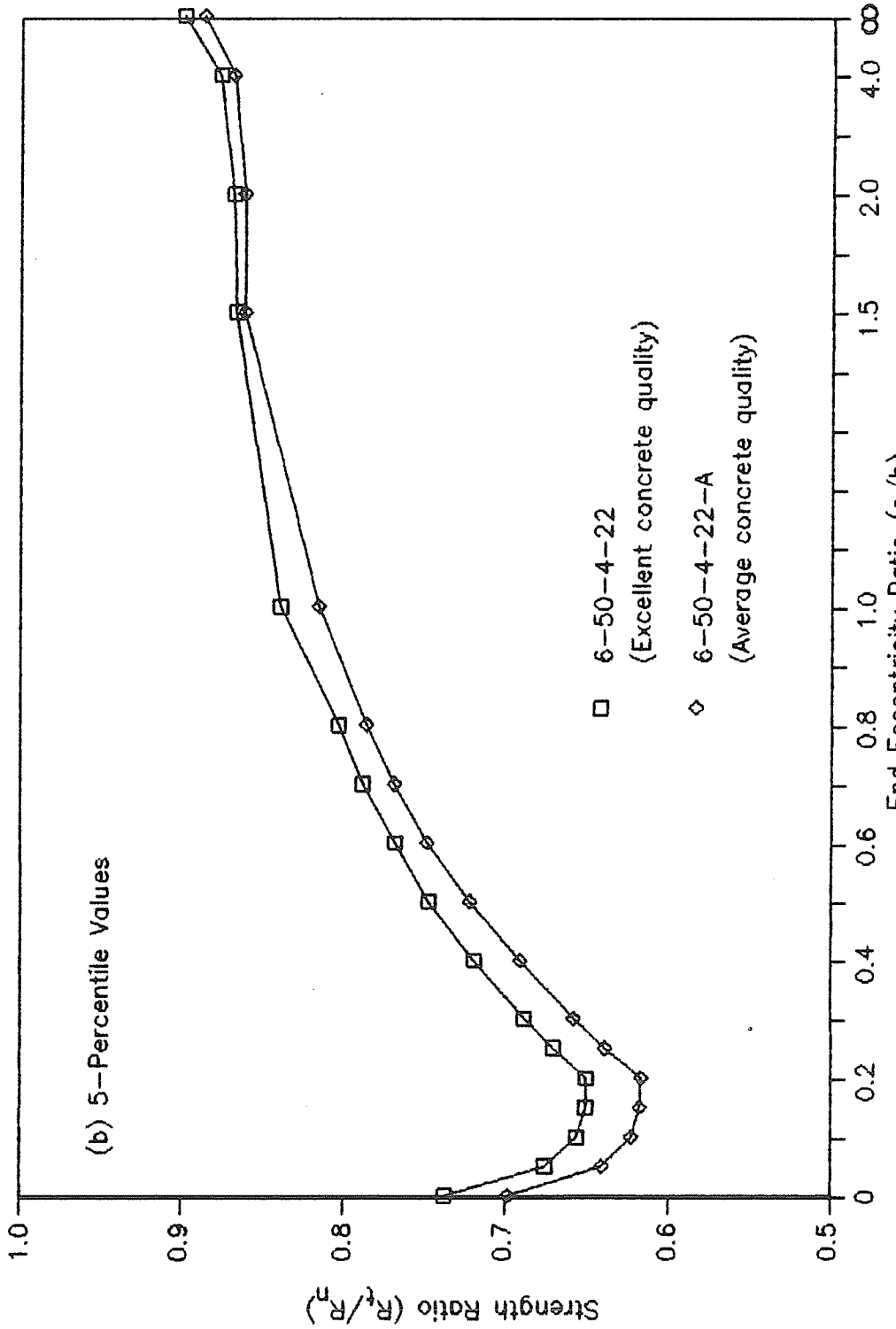

Figure 5.17 (cont.) – Effect of Concrete Quality Control on the Ratio of Theoretical to Nominal Strength of Short Composite Steel–Concrete Beam–Columns

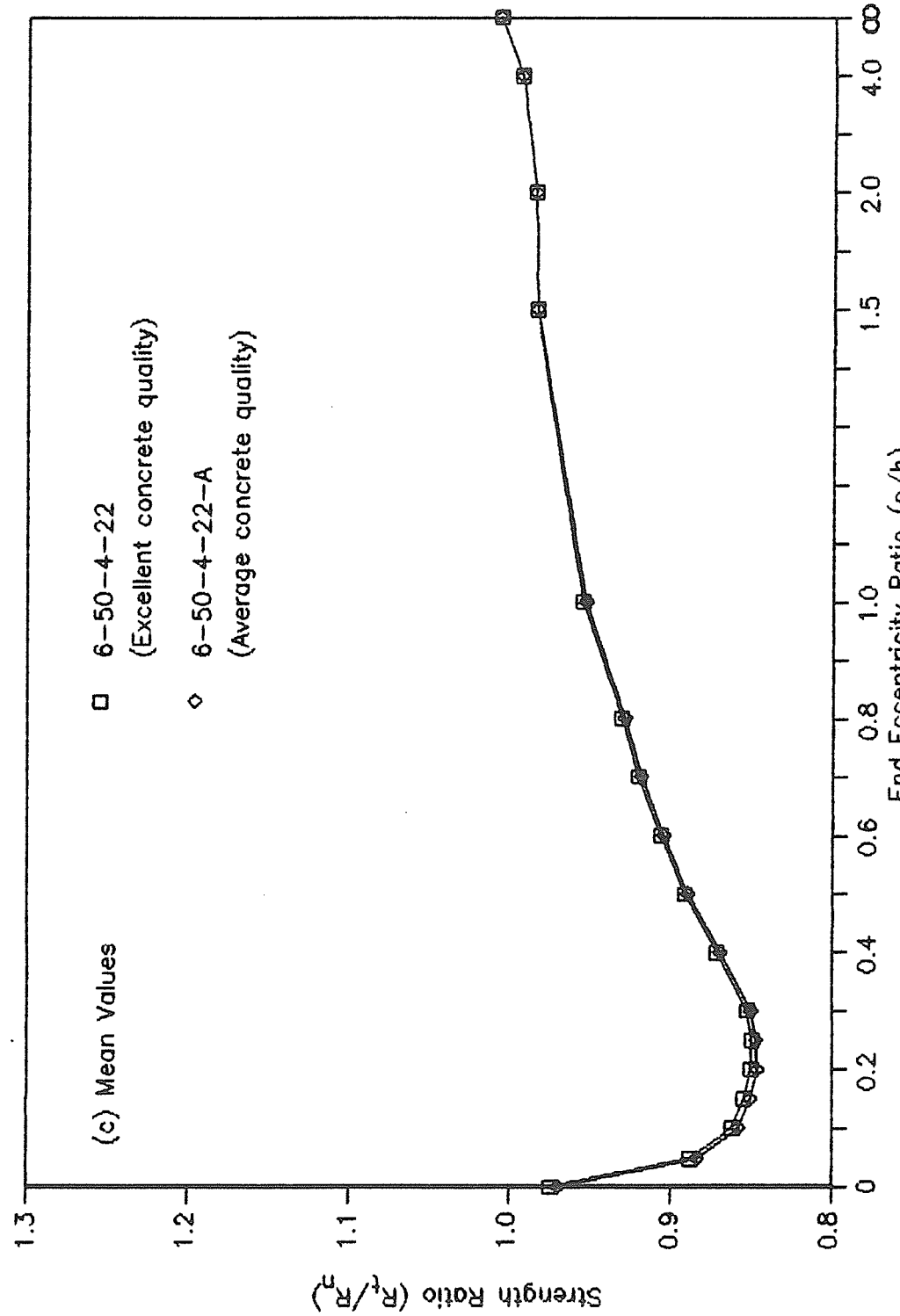

Figure 5.17 (cont.) – Effect of Concrete Quality Control on the Ratio of Theoretical to Nominal Strength of Short Composite Steel–Concrete Beam–Columns

hence, it is important that the future reliability analysis considers the concrete quality control as one of the variables.

5.3.3.4 Summary of effects of variables used for supplemental study - The following summarizes the effects of variables used for the supplemental study of short composite beam-columns:

(a) The use of 50 ksi (345 MPa) structural steel produces strength ratios not significantly different from those obtained for lesser grades of steel;

(b) the strain-hardening of steel enhances the strength ratios of the beam-columns only at very high e/h values and is not recommended for inclusion in the reliability analysis; and

(c) the quality control of concrete significantly affects the lower tail of the strength probability distribution and should be included in the reliability analysis.

5.4 SLENDER COMPOSITE BEAM-COLUMNS

This section examines the overall strength variations of slender composite beam-columns. The effects of individual variables on the strength ratios are discussed here and the major variables that affect the variability of slender composite columns are identified as well. The specified properties of slender beam-columns studied are given in Tables 5.2 and 5.4.

5.4.1 Overall Strength Variations

Axial load-bending moment interaction diagrams simulated for two slender beam-columns (Column 6-50-4-66 and Column 4-50-8-33) taken from Table 5.2 are plotted in Figures 5.18 and 5.19. These columns represent the upper and lower limits of the structural steel index studied ($\rho_{ss} f_y / f'_c$ = 0.33 and 1.03). Plots included are of the maximum, mean, one-percentile, and minimum theoretical strengths as well as the ACI 318-83 ultimate and factored strengths computed for the slender columns. The ACI ultimate strengths were based on all understrength factors being equal to 1.0. The ACI factored strengths were calculated as outlined in Section 5.3.1. Also included in these figures are the theoretical mean cross-sectional strength curves which are plotted only for comparison to the mean strength of the slender beam-columns.

Figure 5.18 (plotted for Column 6-50-4-66 having $\rho_{ss} f_y / f'_c$ = 0.33 and kl/r = 66) shows the ACI ultimate strength significantly underestimating the mean theoretical strength for e/h between 0.0 and 0.3. For e/h greater than 0.3, the ACI ultimate strength predicts strengths slightly higher than the mean theoretical strength. At the pure bending condition, the ACI ultimate strength prediction is nearly identical to the mean theoretical strength. The factored ACI strength curve plotted is very significantly less

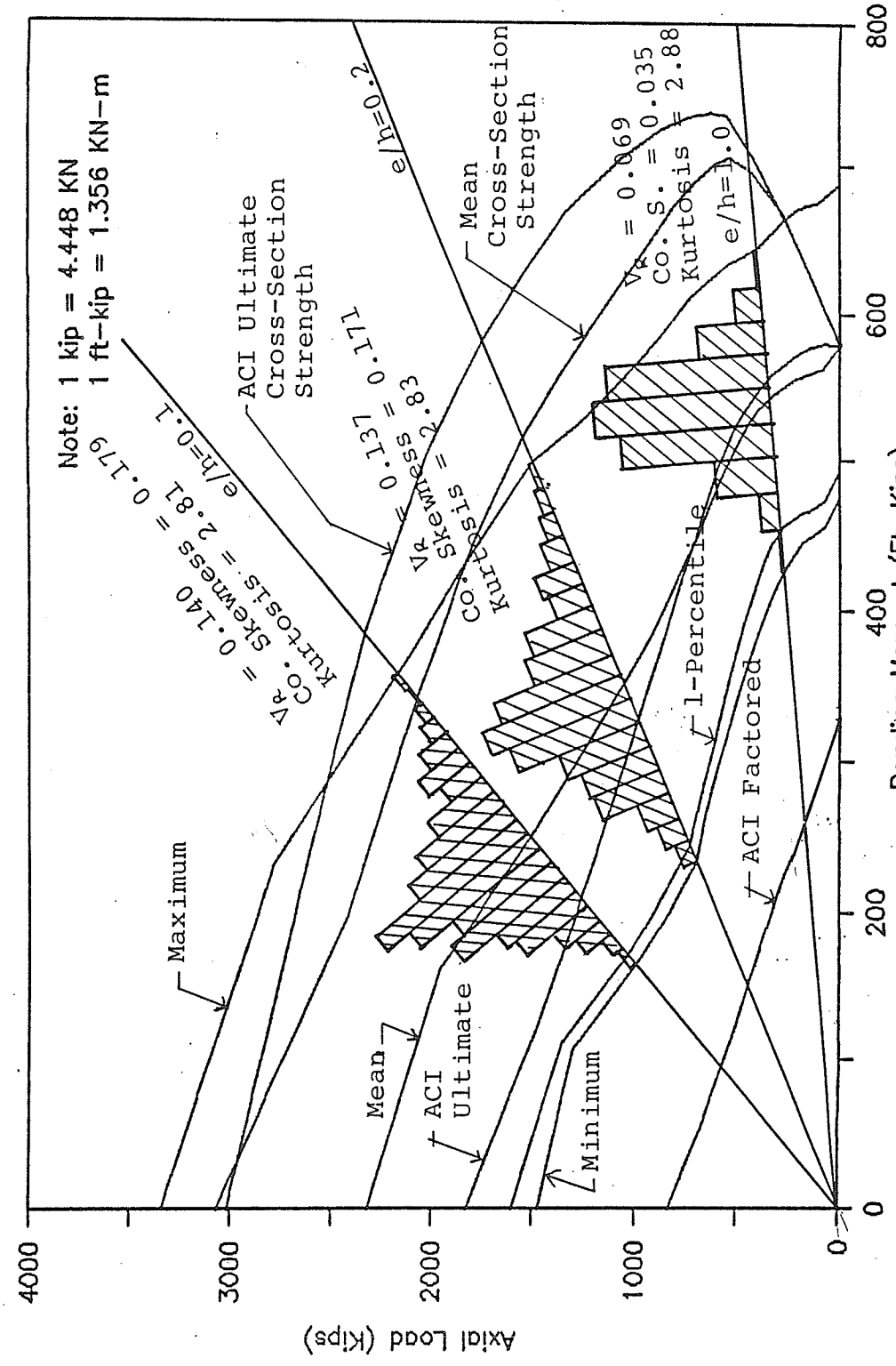

Figure 5.18 – Axial Load–Bending Moment Strength Interaction Curves of Randomly Generated Sample of 500 Slender Composite Columns [Column 6-50-4-66 (Table 5.2)]

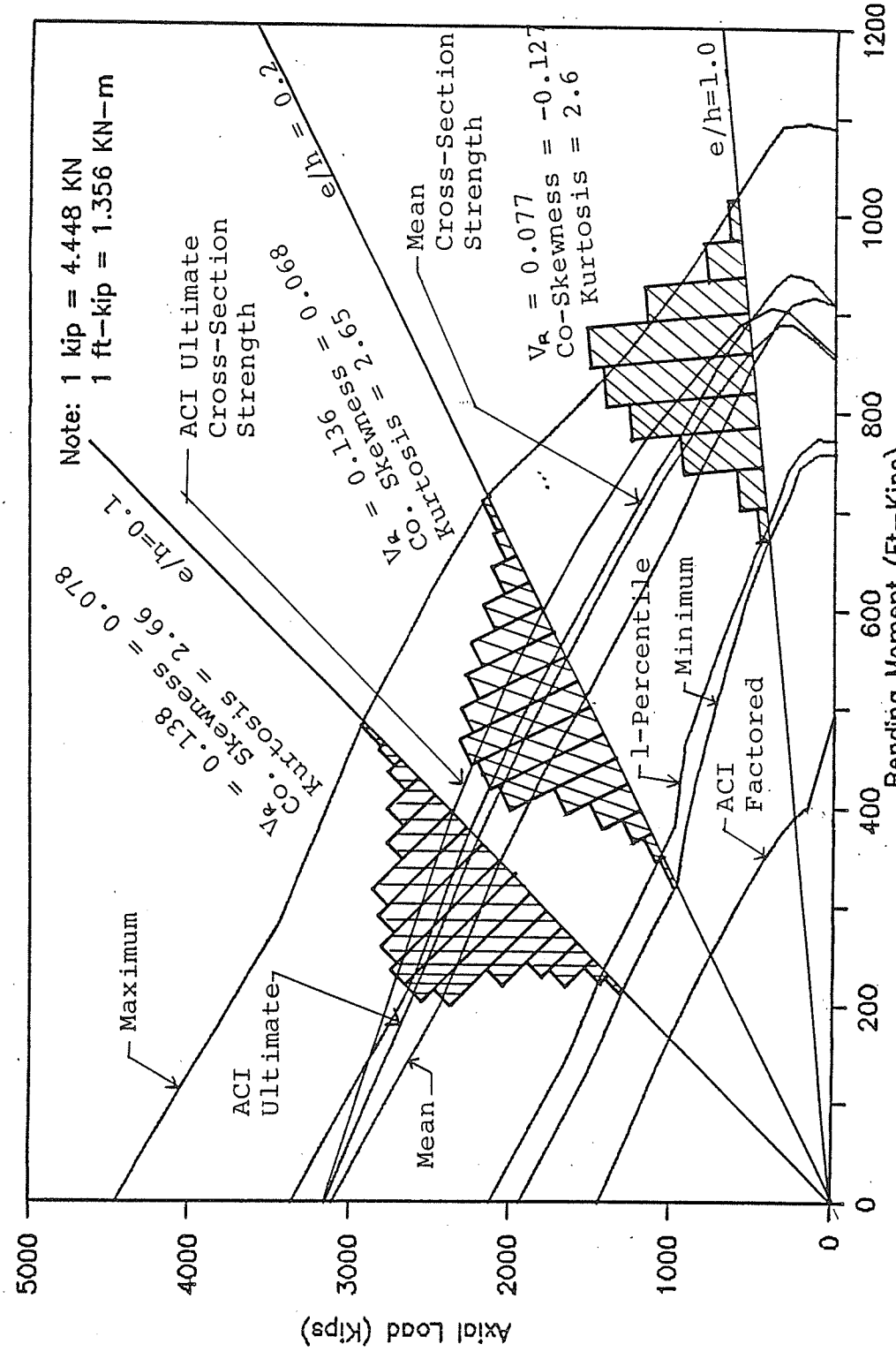

Figure 5.19 – Axial Load–Bending Moment Strength Interaction Curves of Randomly Generated Sample of 500 Slender Composite Columns [Column 4–50–8–33 (Table 5.2)]

than the 1-percentile strength for all values of e/h. However, the load combinations and variations may decrease the apparent conservativeness of the ACI factored strength.

In Figure 5.19, (plotted for Column 4-50-8-33 having $\rho_{ss} f_y / f'_c = 1.03$ and $kl/r = 33$), the ACI ultimate strength prediction somewhat overestimates the mean strength for e/h of 0.0 to 2.0. For e/h between 2.0 and infinity, the mean strength is somewhat underestimated by the ACI ultimate strength. The differences between the ACI ultimate strength and the mean theoretical strength are much less in Figure 5.19 than those displayed in Figure 5.18 and, perhaps, reflect the effect of lower slenderness ratio associated with the column data plotted in Figure 5.19. The factored ACI strength is less than the 1-percentile strength at all values of e/h as indicated in Figure 5.19.

Probability distribution histograms of the simulated theoretical strengths for e/h of 0.1, 0.2 and 1.0 are also plotted in Figures 5.18 and 5.19. The histograms are symmetric. This indicates that the positively skewed shape of the structural steel strength probability distribution does not influence the overall slender beam-column strength as much as it does for short columns. This can be seen by comparing Figures 5.4 and 5.19.

5.4.2 Effects Of Variables Used For Basic Study

The 16 slender columns in the basic study (Table 5.2) were chosen to investigate the effect of four variables on

the probability distribution properties of the ratio of theoretical to nominal strength (strength ratio). These variables are the slenderness ratio (kl/r), specified concrete strength (f'_c), ratio of structural steel area to gross area of cross-section (ρ_{ss}), and end eccentricity ratio (e/h). The strength ratios are plotted for e/h values in the range of 0.05 to ∞. The strength ratios at e/h of 0.0 (concentric loading) are not shown since the concentric capacity prediction of the theoretical strength model was based on the tangent modulus approach and the results were believed overly conservative.

5.4.2.1 Effect of slenderness ratio - The slender beam-columns shown in Table 5.2 were divided into 4 sets of 4 columns each to investigate the effect of slenderness ratio (kl/r) on the strength ratio. Each set had one column with slenderness ratio of 22.1, 33, 66 or 100. All other properties in each set of columns were identical. A kl/r of just greater than 22 is the minimum slenderness ratio requiring the inclusion of length effects by ACI 318-83 and by CAN3-A23.3-M84 for the types of columns studied. A kl/r of 100 is the maximum slenderness ratio allowed by the two design codes for evaluating the stability effects by the moment magnifier approach. Figures 5.20 and 5.21 plot the one-percentile, five-percentile and mean strength ratios for two of the column sets studied.

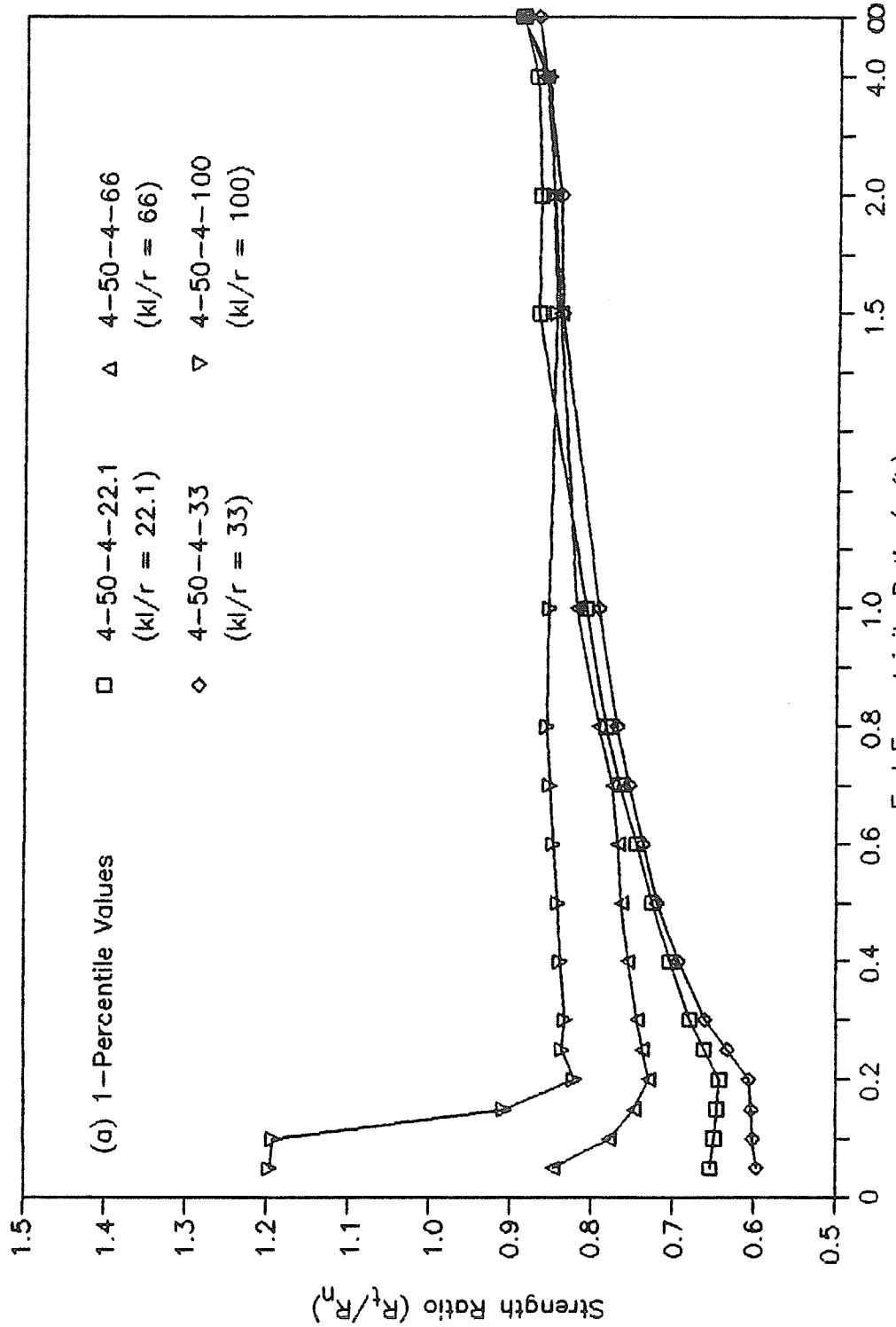

Figure 5.20 – Effect of Slenderness Ratio on the Ratio of Theoretical to Nominal Strength of Slender Composite Steel–Concrete Beam–Columns

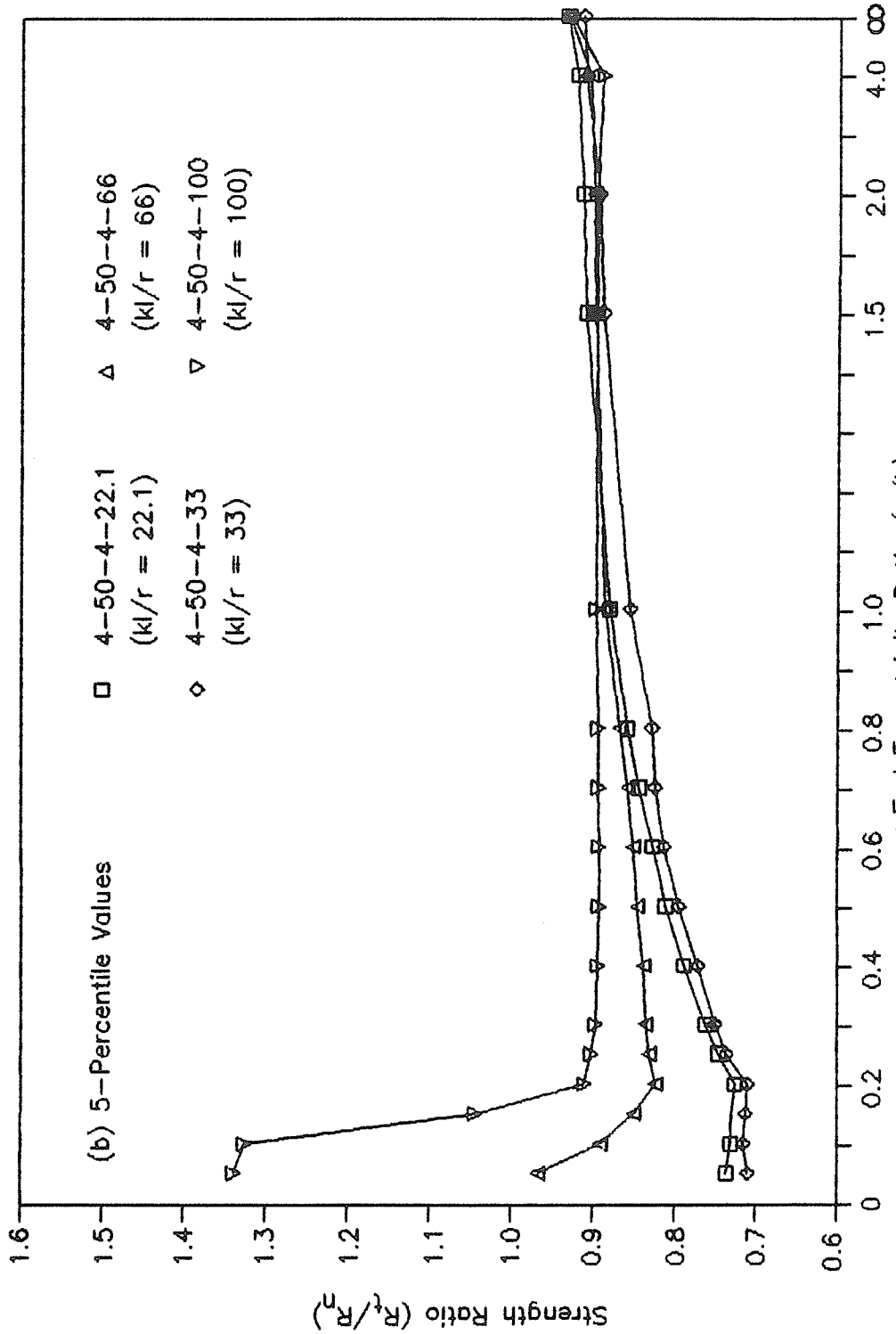

Figure 5.20 (cont.) – Effect of Slenderness Ratio on the Ratio of Theoretical to Nominal Strength of Slender Composite Steel–Concrete Beam–Columns

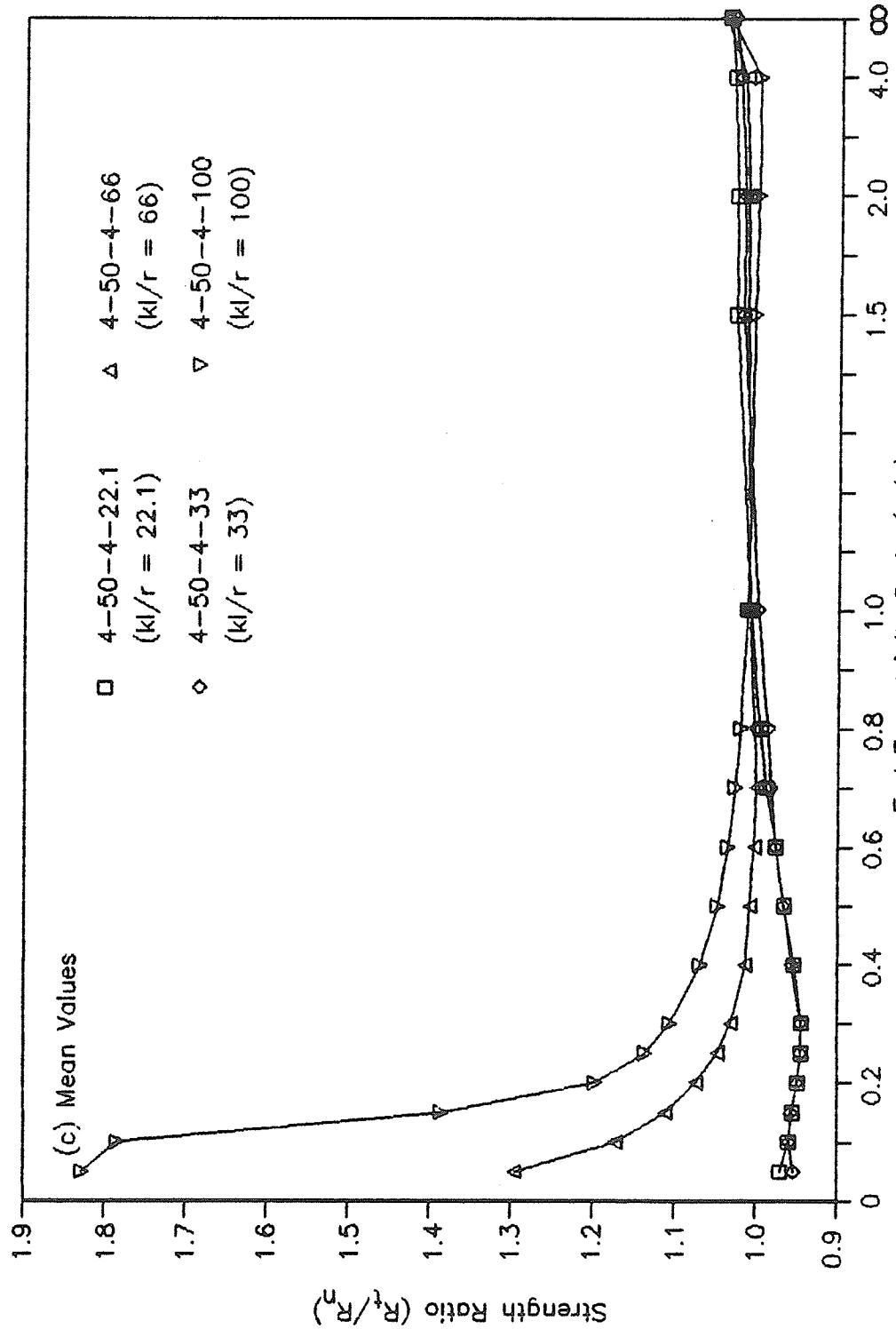

Figure 5.20 (cont.) – Effect of Slenderness Ratio on the Ratio of Theoretical to Nominal Strength of Slender Composite Steel–Concrete Beam–Columns

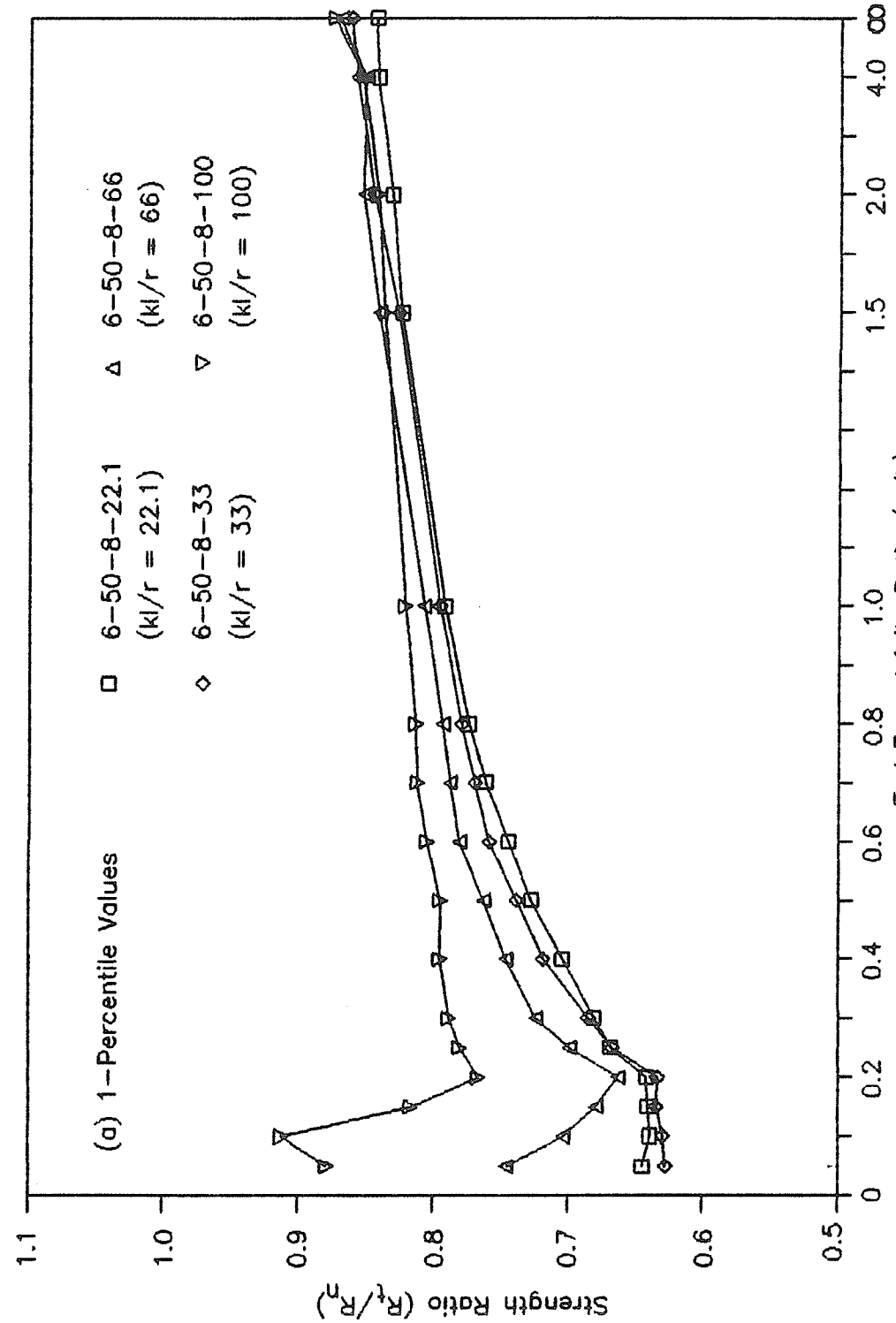

Figure 5.21 – Effect of Slenderness Ratio on the Ratio of Theoretical to Nominal Strength of Slender Composite Steel–Concrete Beam–Columns

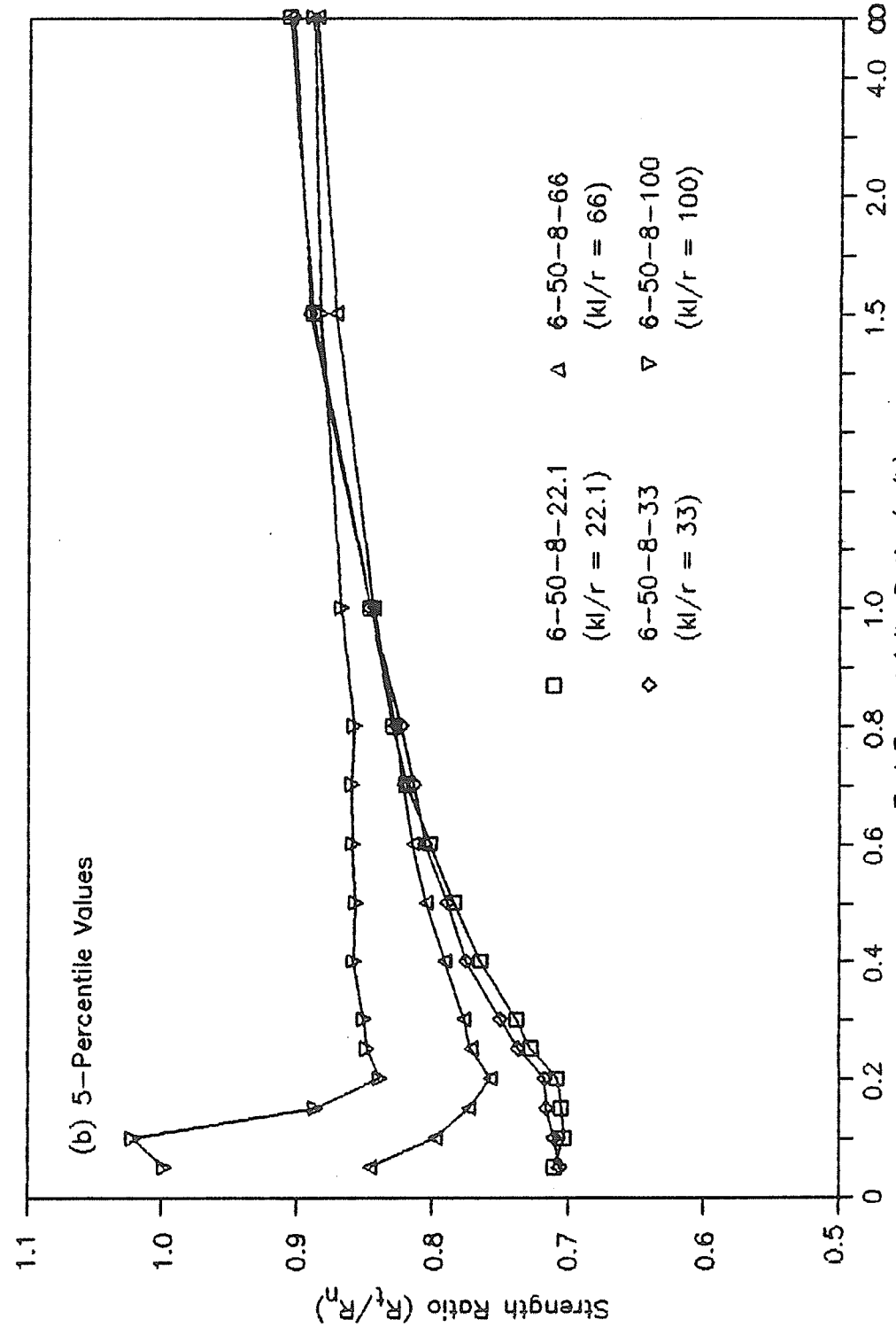

Figure 5.21 (cont.) – Effect of Slenderness Ratio on the Ratio of Theoretical to Nominal Strength of Slender Composite Steel–Concrete Beam–Columns

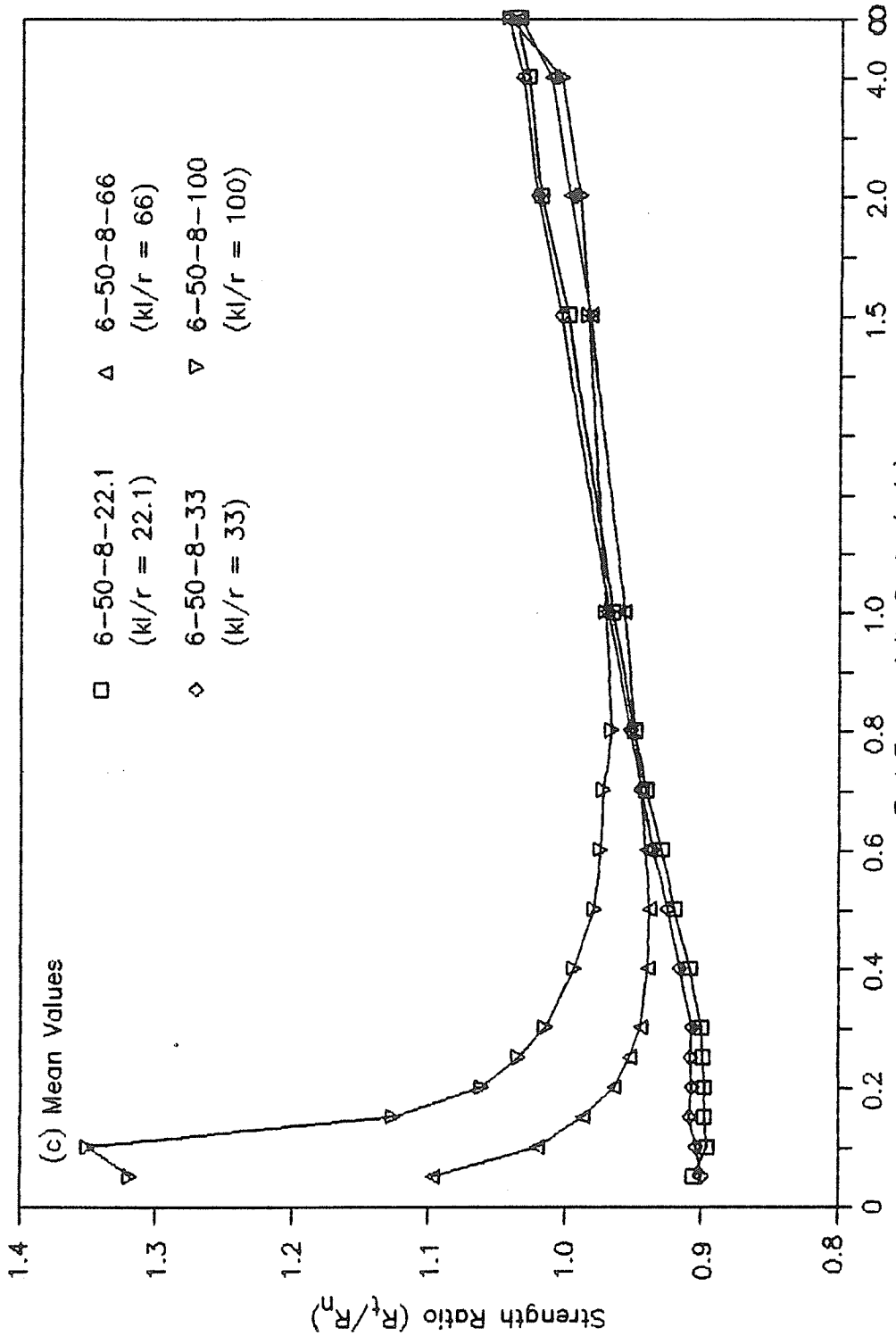

Figure 5.21 (cont.) – Effect of Slenderness Ratio on the Ratio of Theoretical to Nominal Strength of Slender Composite Steel–Concrete Beam–Columns

In most cases, one-percentile strength ratios for columns with kl/r of 33 were the lowest, followed by those with kl/r of 22.1 and 66. The highest one-percentile strength ratios were obtained for columns with kl/r = 100. In all cases, the differences in strength ratios of columns with different kl/r decreased as e/h increased from 0.05 to 1.2. For e/h values greater than 1.2, there were no significant differences in the strength ratios of beam-columns with different kl/r ratio regardless of e/h value. The effect of slenderness ratio described here was typical for all four sets of beam-columns and is evident from Figures 5.20(a) and 5.21(a).

Figure 5.20(a) shows that one-percentile strength ratios for the beam-column with kl/r of 33 are significantly lower than those for the beam-column with kl/r of 22.1 when e/h is less than 0.3. However, for higher values of e/h, the differences in one-percentile strength ratios for these two columns (kl/r = 22.1 and 33) are small [Figure 5.20(a)]. This behavior is different from the one observed from Figure 5.21(a) in which one-percentile strength ratios for columns with kl/r = 22.1 and 33 show small differences over the entire range of e/h studied. This difference in behavior of the two sets of beam-columns is, perhaps, due to different structural steel ratios used [ρ_{ss} = 0.040 for columns in Figure 5.20(a) and 0.082 for columns in Figure 5.21(a)].

The trends noted in the preceding paragraphs were found to be consistent with the 5-percentile and mean values of the strength ratios for all four sets of columns studied. This is indicated by Figures 5.20(b) and (c) and Figures 5.21(b) and (c).

From the foregoing discussions, it is concluded that the strength ratios for columns with kl/r = 22.1 to 33 are more critical than those for columns with kl/r = 66 to 100. In most cases, however, the lowest strength ratios were obtained for columns having kl/r = 33. Slenderness ratio is, therefore, an important variable for reliability analysis.

5.4.2.2 Effect of specified concrete strength - The slender columns listed in Table 5.2 provided 8 sets for investigating the effect of specified concrete strength on the strength ratio. Each set contained one column having f'_c = 4000 psi (27.6 MPa) and one column having f'_c = 6000 psi (41.4 MPa) with all other properties of both columns in the set being identical. Figures 5.22 and 5.23 plot the strength ratio data for two of the eight sets.

The strength ratios obtained for slender columns with the lowest slenderness ratios (kl/r = 22.1) were expected to be similar to those obtained for the short columns. In fact, the two sets of slender columns with kl/r = 22.1 used to study the effect of f'_c on strength ratios gave results nearly identical to those obtained for the short columns.

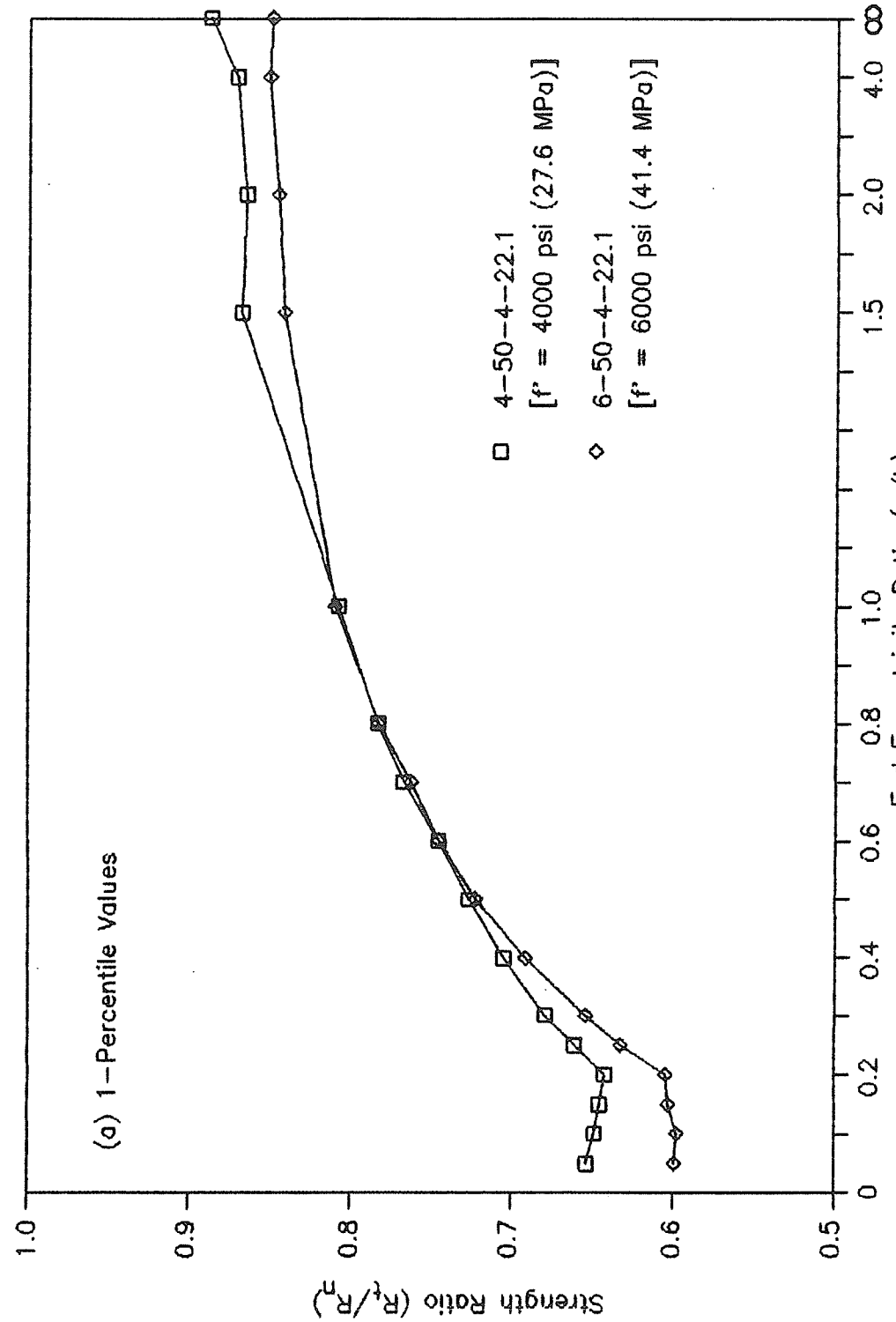

Figure 5.22 – Effect of Specified Concrete Strength on the Ratio of Theoretical to Nominal Strength of Slender Composite Steel–Concrete Beam–Columns

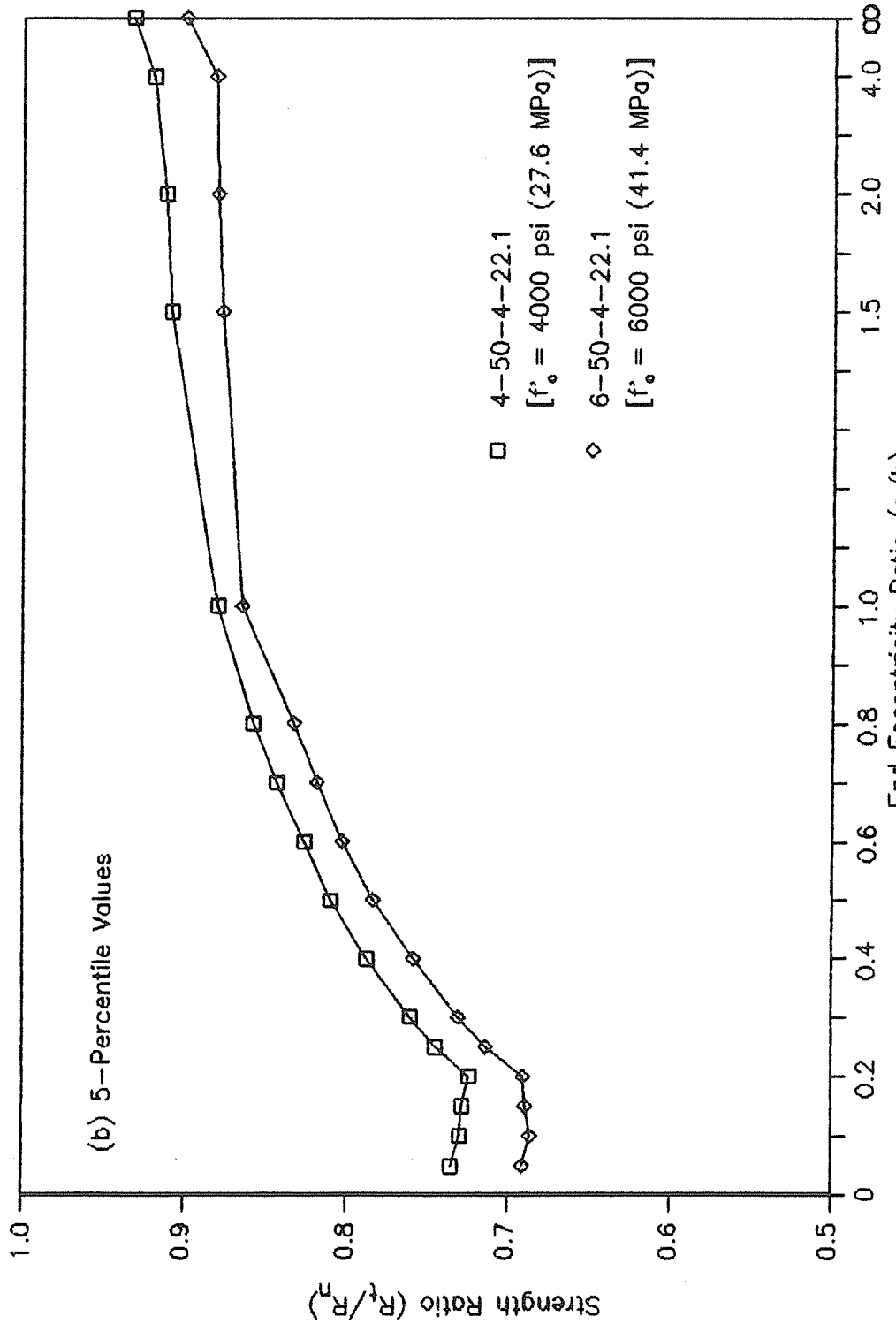

Figure 5.22 (cont.) – Effect of Specified Concrete Strength on the Ratio of Theoretical to Nominal Strength of Slender Composite Steel–Concrete Beam–Columns

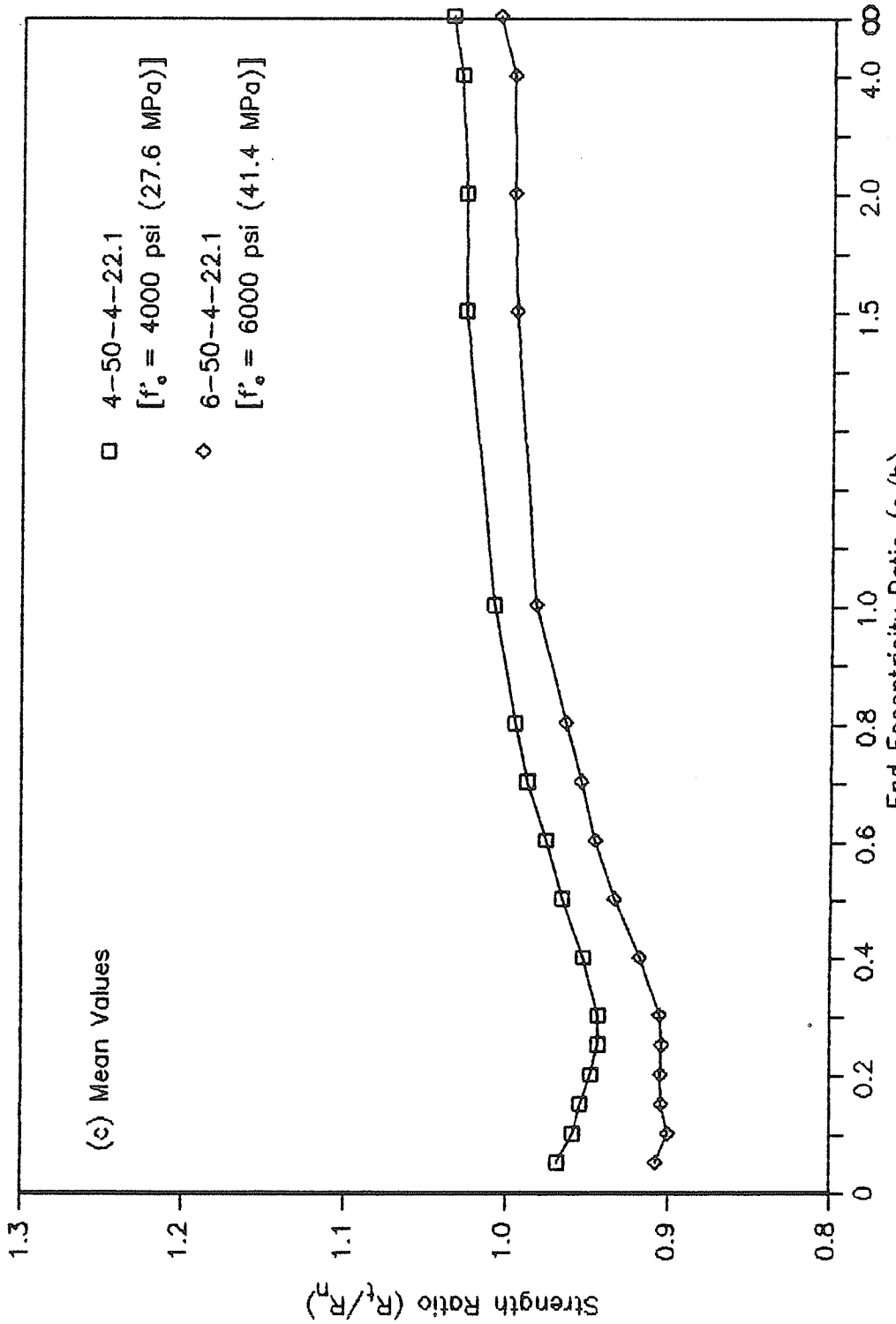

Figure 5.22 (cont.) – Effect of Specified Concrete Strength on the Ratio of Theoretical to Nominal Strength of Slender Composite Steel–Concrete Beam–Columns

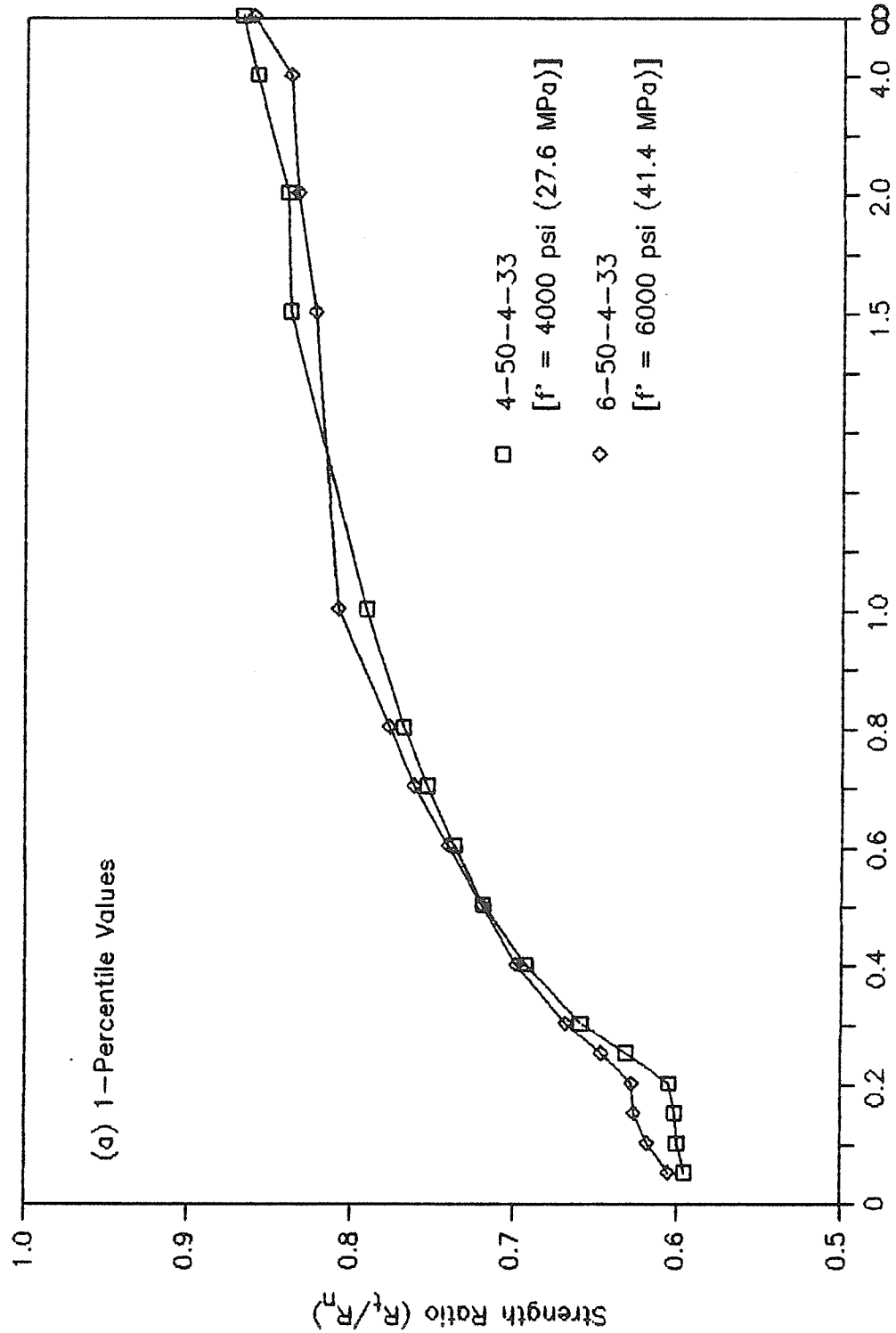

Figure 5.23 – Effect of Specified Concrete Strength on the Ratio of Theoretical to Nominal Strength of Slender Composite Steel–Concrete Beam–Columns

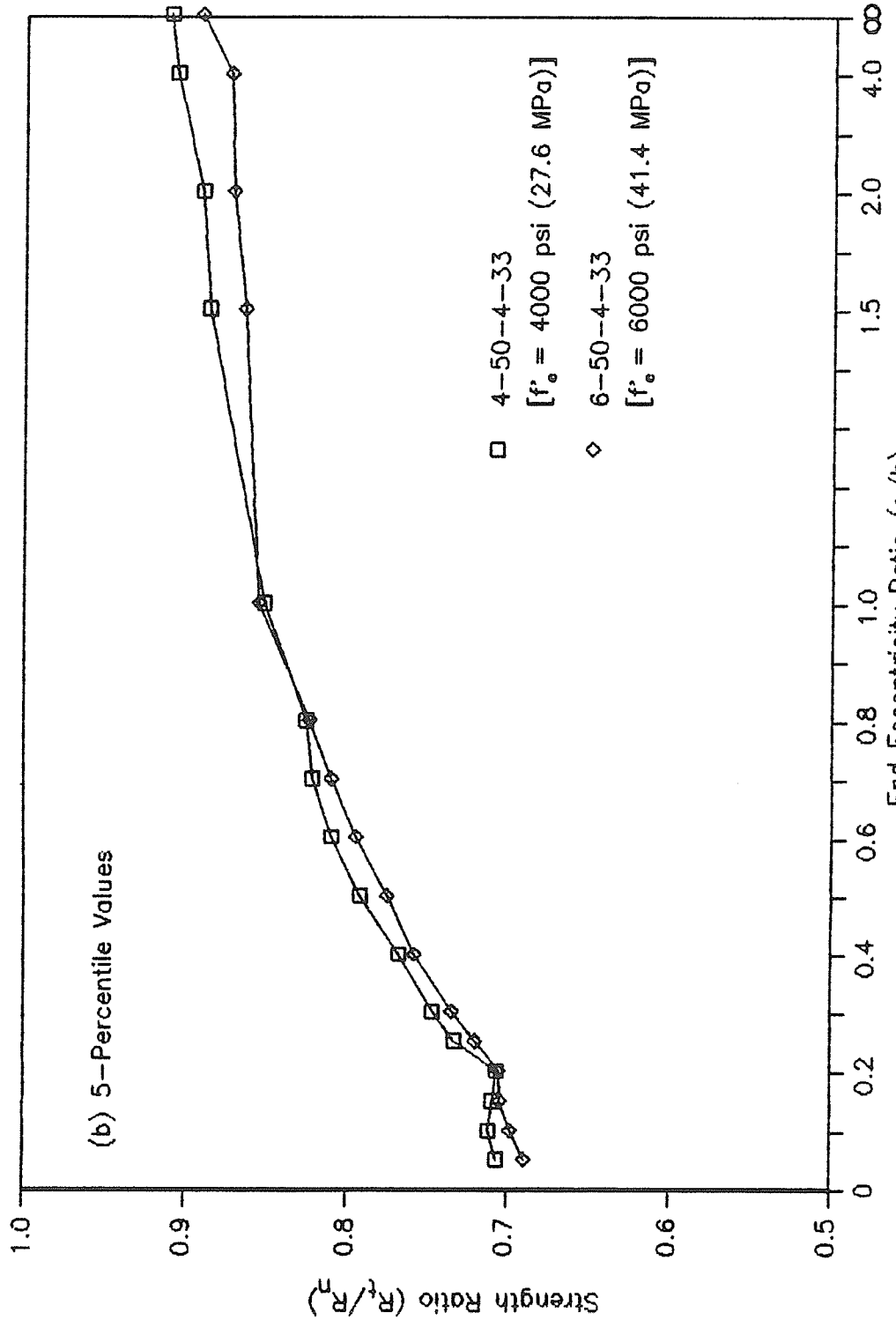

Figure 5.23 (cont.) – Effect of Specified Concrete Strength on the Ratio of Theoretical to Nominal Strength of Slender Composite Steel–Concrete Beam–Columns

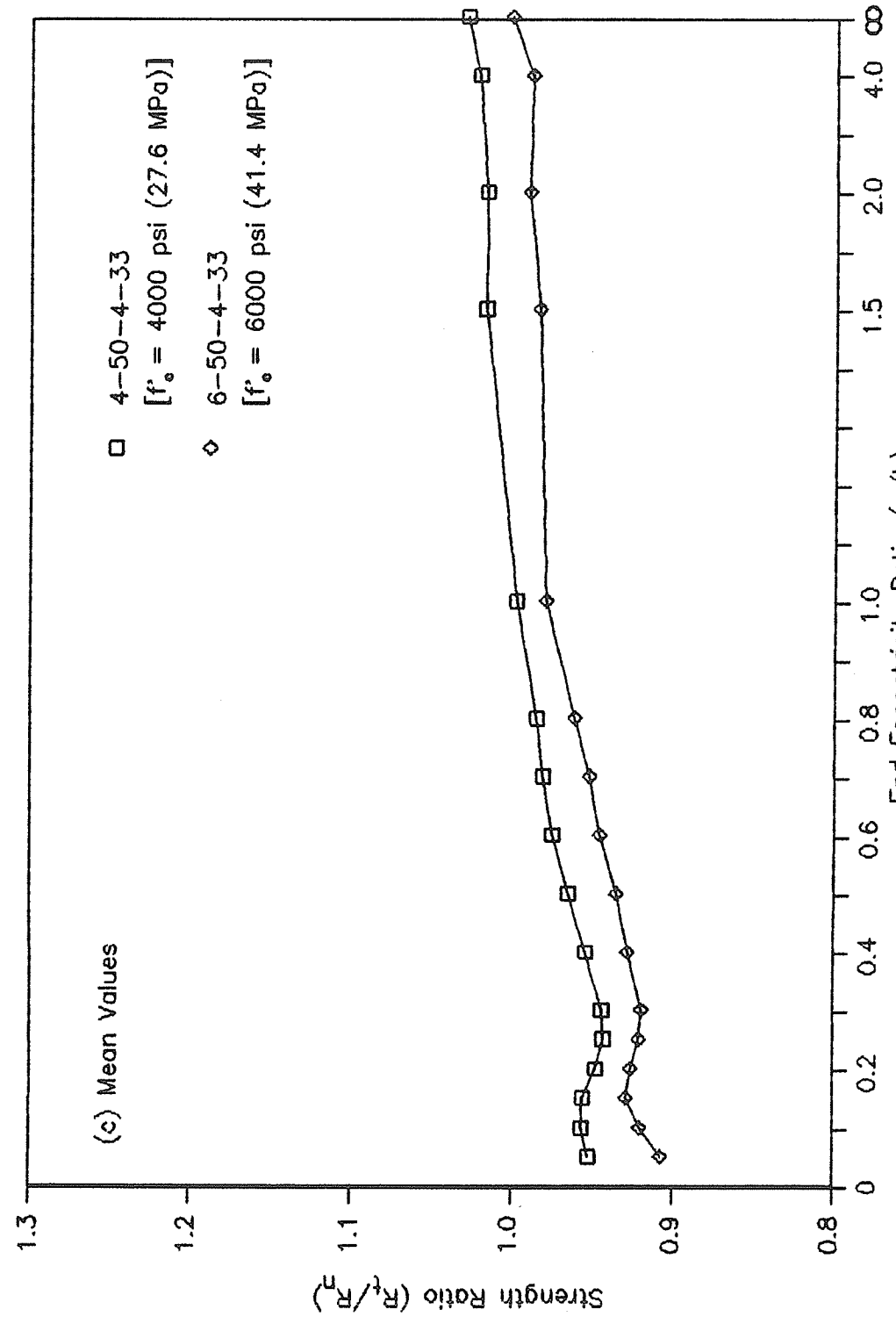

Figure 5.23 (cont.) – Effect of Specified Concrete Strength on the Ratio of Theoretical to Nominal Strength of Slender Composite Steel–Concrete Beam–Columns

This can be seen by comparing the strength ratio data in Figure 5.22 for one of the slender column sets to the plots in Figure 5.8 presented earlier for short columns.

Figure 5.22(a) plotted for slender columns having kl/r = 22.1 and ρ_{ss} = 0.040 shows that the 6000 psi (41.4 MPa) concrete gave lower one-percentile strength ratios than did the 4000 psi (27.6 MPa) concrete over almost the entire range of e/h. A similar behavior was observed for one-percentile strength ratios of slender columns having the same slenderness ratio but a higher structural steel ratio (ρ_{ss} = 0.082), except that the 4000 psi and 6000 psi (27.6 and 41.4 MPa) concretes produced identical one-percentile strength ratios for $e/h \leq 0.25$. At 5-percentile and mean value levels, the columns with higher strength concrete gave lower strength ratios for all e/h values, although the effect was more significant for columns with lower structural steel ratio as indicated by Figures 5.22(b) and (c).

As the slenderness ratio was increased to 33, the effect of specified concrete strength on the one-percentile and five-percentile strength ratios tended to disappear as indicated by Figures 5.23(a) and (b). However, the higher strength concrete produced lower mean strength ratios for columns with kl/r = 33 [Figure 5.23(c)].

For beam-columns having slenderness ratios of 66 and 100, the effect of the specified concrete strength on

strength ratios was noticeable only at e/h of less than 0.15. In this range of e/h, the lower concrete strength provided slightly lower strength ratios. This effect dissipated rapidly with increasing e/h due to the failure mode changing from compression to tension caused by increasing secondary bending moments acting on the beam-column.

From the data and discussions presented in this Section, it is concluded that for columns having slenderness ratios greater than or equal to 33, the specified concrete strength does not significantly affect the strength ratio. For slender columns with kl/r less than 33, the effect of specified concrete strength seems to be significant.

5.4.2.3 Effect of structural steel ratio - Eight comparisons were made to investigate the effect of ratio of structural steel area to gross area of concrete cross-section on the probability distribution properties of the strength ratios of the beam-columns listed in Table 5.2. Each comparison involved two beam-columns, one having $\rho_{ss} = 0.040$ and the other one having $\rho_{ss} = 0.082$ with all other properties being identical. Strength ratios from two typical comparisons are plotted in Figures 5.24 and 5.25. The data plotted involves columns with specified concrete strength of 4000 psi (27.6 MPa) and slenderness ratios of 33 (Figure 5.24) and 66 (Figure 5.25).

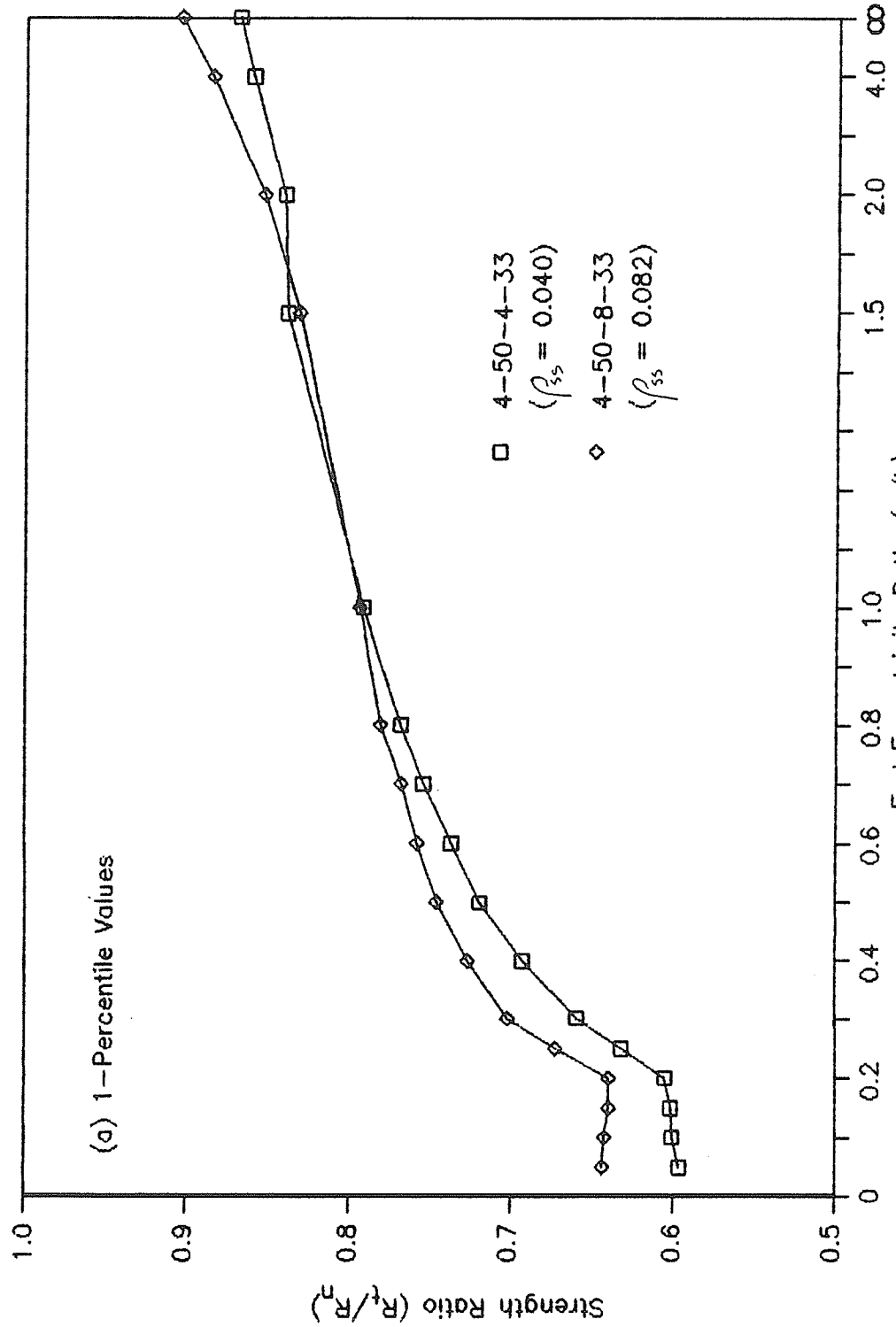

Figure 5.24 – Effect of Structural Steel Ratio on the Ratio of Theoretical to Nominal Strength of Slender Composite Steel–Concrete Beam–Columns

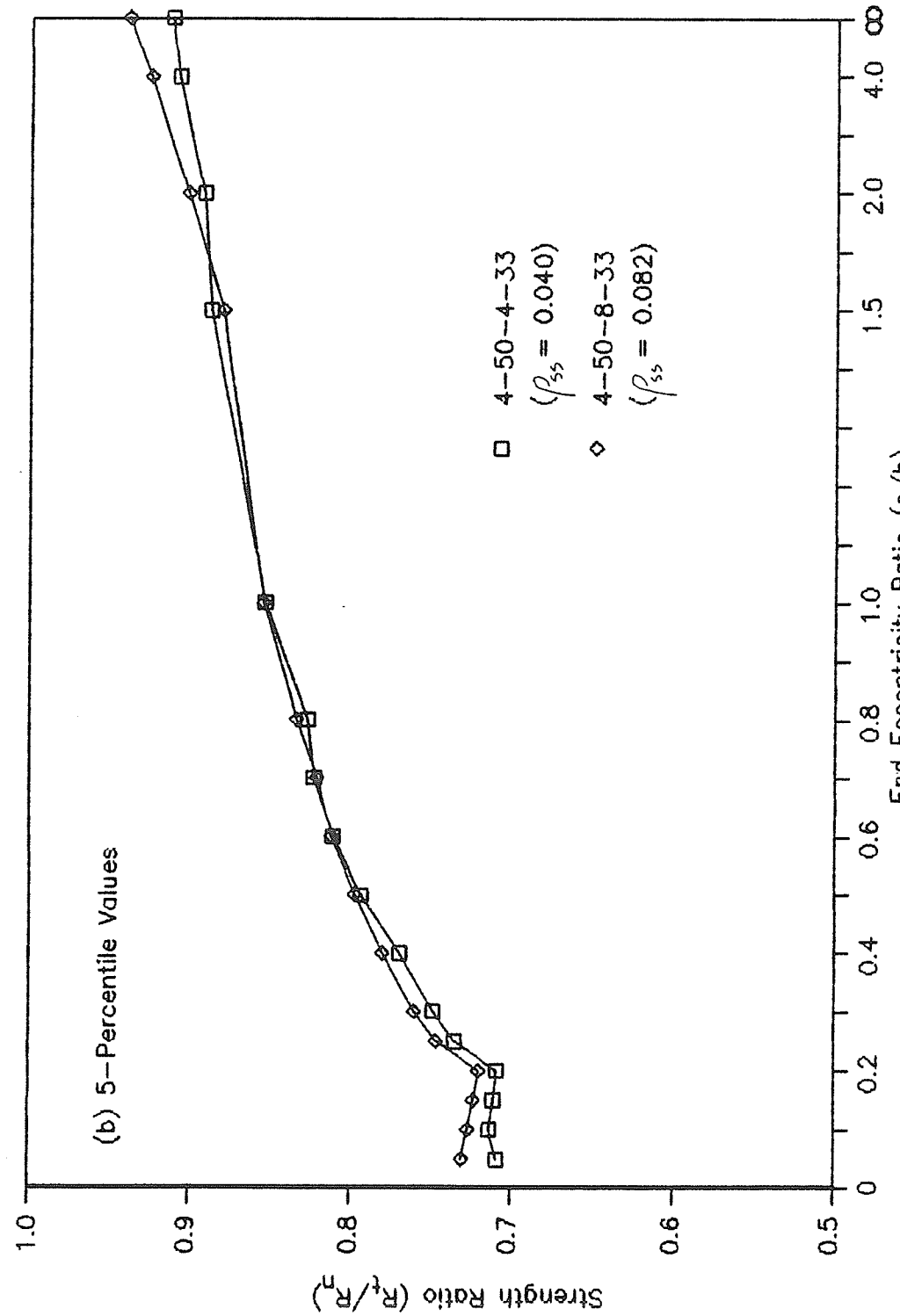

Figure 5.24 (cont.) – Effect of Structural Steel Ratio on the Ratio of Theoretical to Nominal Strength of Slender Composite Steel–Concrete Beam–Columns

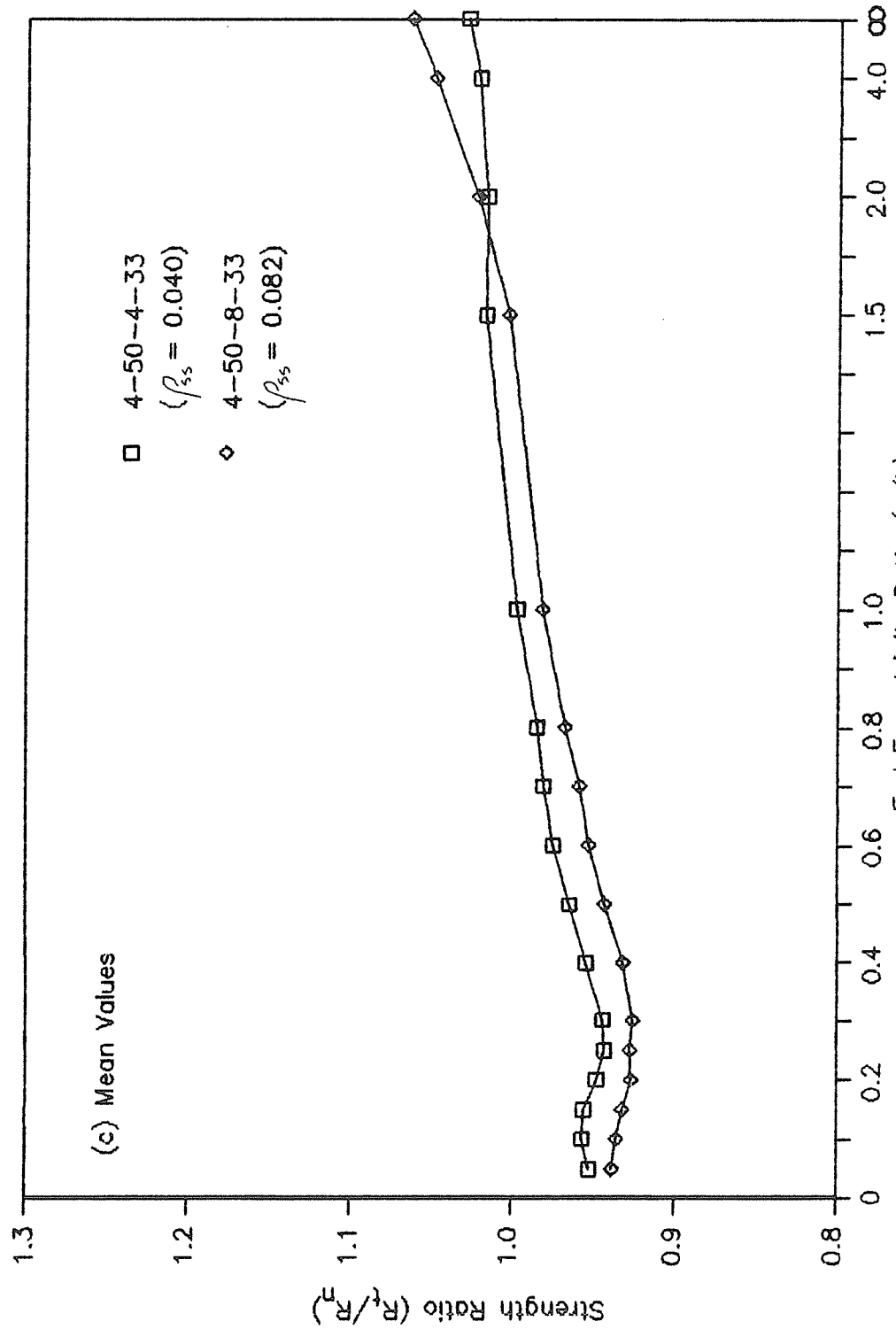

Figure 5.24 (cont.) – Effect of Structural Steel Ratio on the Ratio of Theoretical to Nominal Strength of Slender Composite Steel–Concrete Beam–Columns

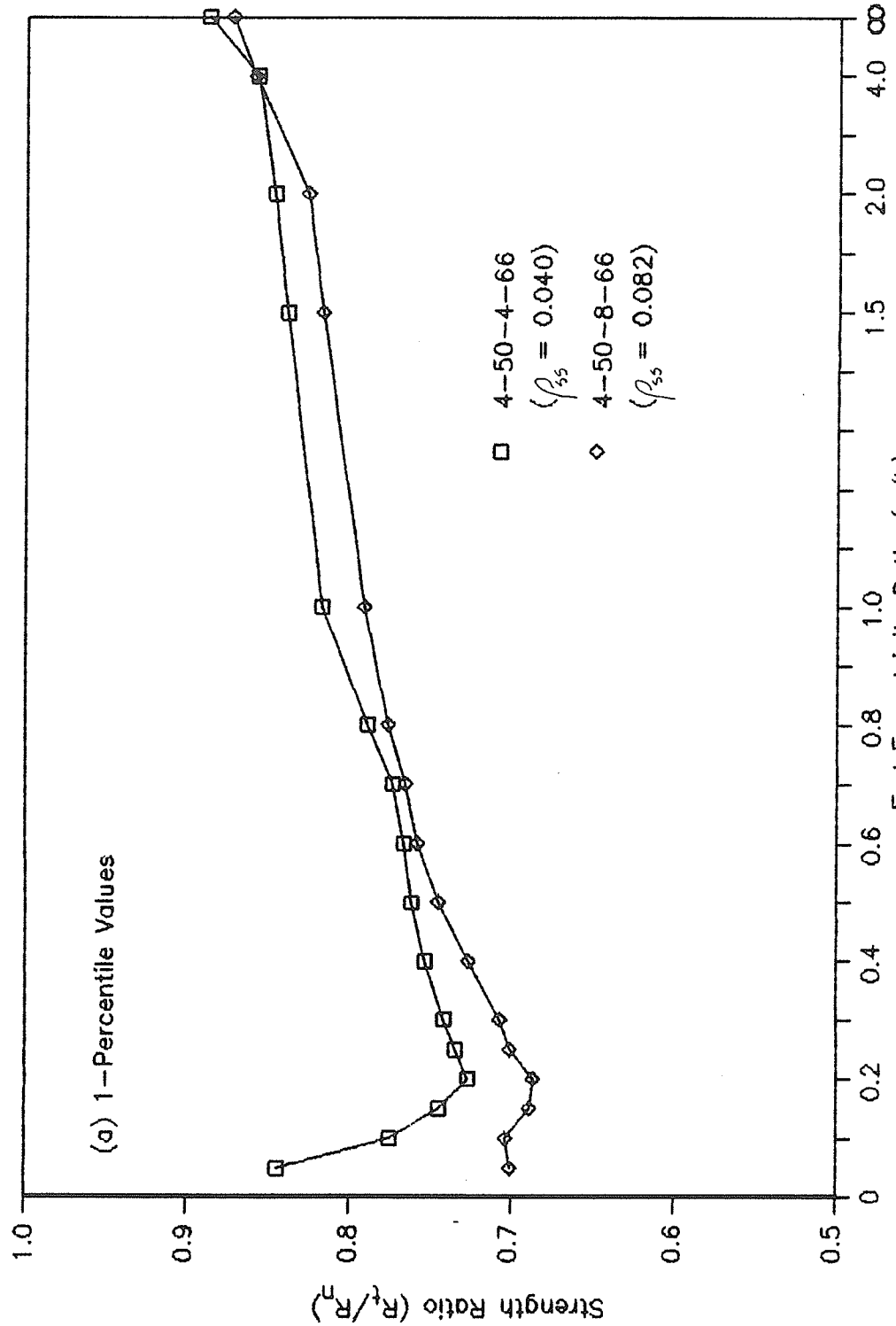

Figure 5.25 – Effect of Structural Steel Ratio on the Ratio of Theoretical to Nominal Strength of Slender Composite Steel–Concrete Beam–Columns

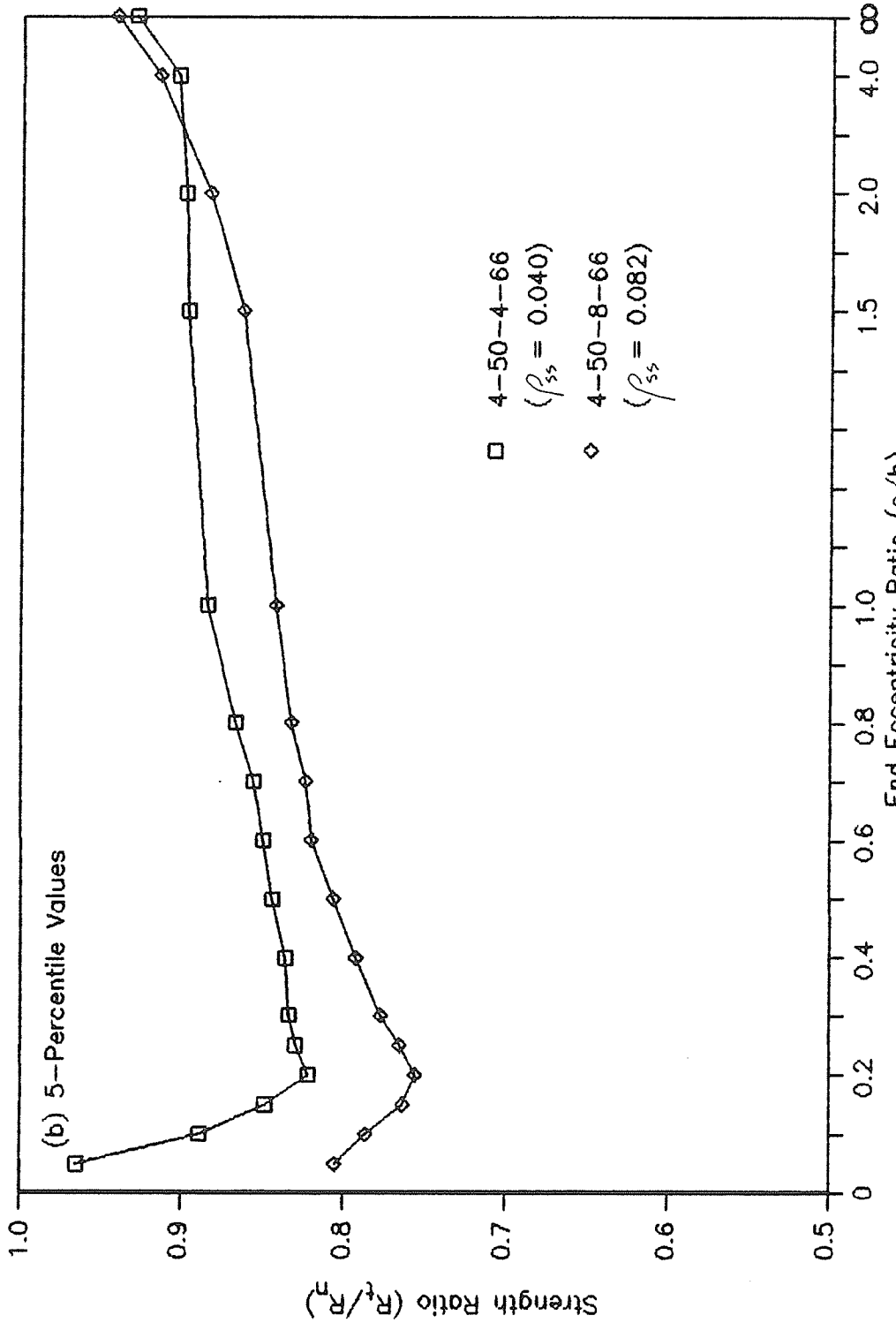

Figure 5.25 (cont.) – Effect of Structural Steel Ratio on the Ratio of Theoretical to Nominal Strength of Slender Composite Steel–Concrete Beam–Columns

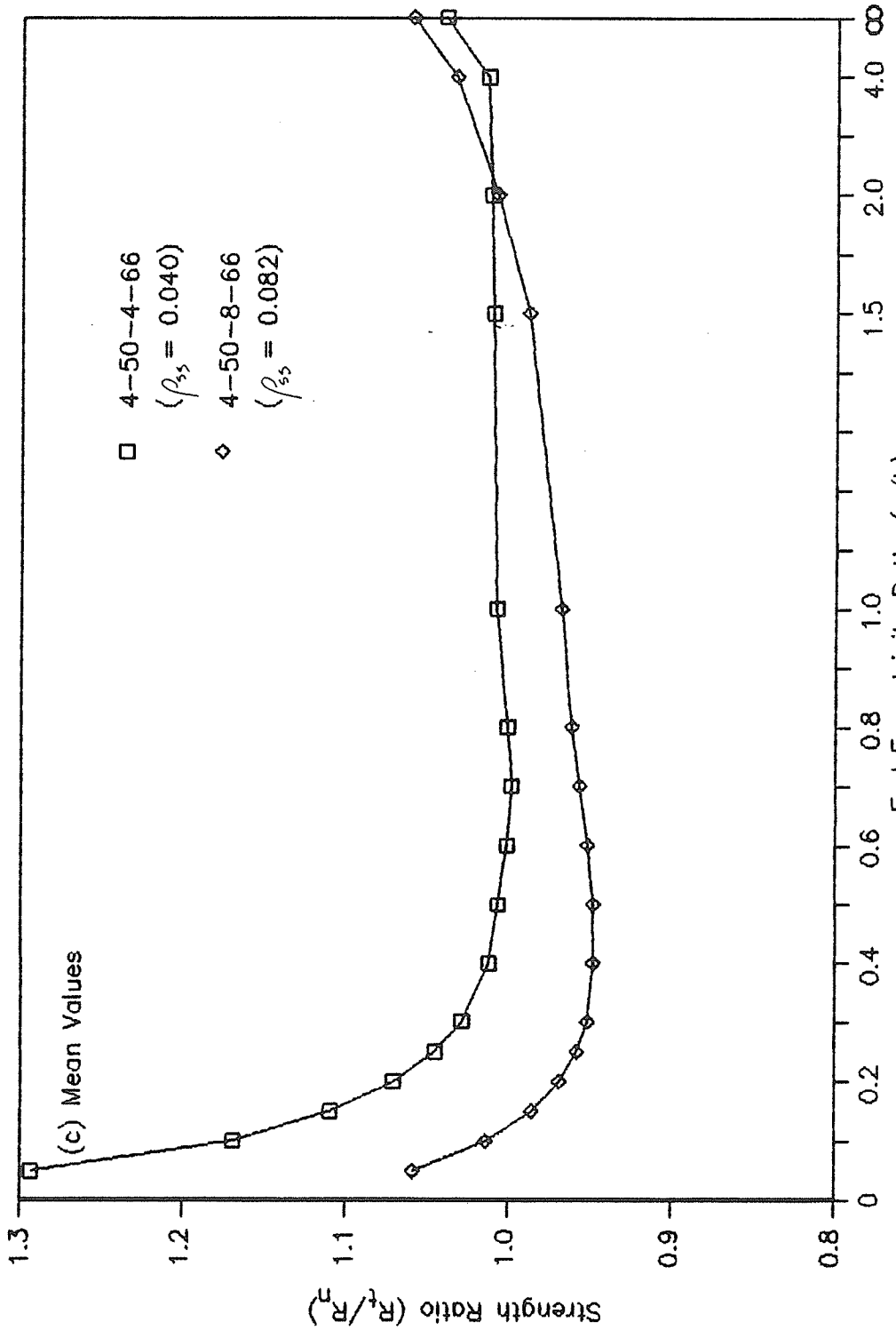

Figure 5.25 (cont.) – Effect of Structural Steel Ratio on the Ratio of Theoretical to Nominal Strength of Slender Composite Steel–Concrete Beam–Columns

The data for slender beam-columns with kl/r of 22.1 was similar to that presented earlier for short columns (Figures 5.10 and 5.11). These beam-columns with smaller structural steel ratio (ρ_{ss} = 0.040) produced lower one-percentile strength ratios than did the beam-columns with larger structural steel ratio (ρ_{ss} = 0.082). At 5-percentile and mean value levels, the columns with higher structural steel ratio provided slightly lower strength ratios but the differences in strength ratios were insignificant.

The trends noted above for columns having kl/r = 22.1 are similar to those for columns with kl/r = 33. Figure 5.24(a) shows that the beam-column with ρ_{ss} = 0.040 gives significantly lower one-percentile strength ratios than the beam-column having ρ_{ss} = 0.082 at $e/h \leq 0.8$. For e/h higher than 0.8, the differences in one-percentile strength ratios in Figure 5.24(a) seem to be negligible. The effect of ρ_{ss} is less significant for 5-percentile and mean strength ratios plotted in Figure 5.24(b) and (c), regardless of the end eccentricity ratio. For columns with kl/r = 33 and f'_c = 6000 psi (41.4 MPa), however, the effect of ρ_{ss} was negligible on all strength ratios (1-percentile, 5-percentile and mean values) at all e/h values studied.

When the slenderness ratio increased to 66, the columns with ρ_{ss} = 0.082 demonstrated significantly lower one-percentile, five-percentile and mean strength ratios than

those for columns with ρ_{ss} = 0.040; the differences in strength ratios being very significant for $e/h \leq 0.4$ as indicated by Figure 5.25. The effect of ρ_{ss} on strength ratios became even more significant when the slenderness ratio was increased to 100. This is probably because a very slender column must withstand high second-order bending moments and, therefore, depends on the structural steel to provide stiffness after the concrete has cracked.

In summary, the columns with low structural steel ratios (ρ_{ss} = 0.040) produced lower 1-percentile strength ratios when kl/r was 33 or less. This behavior is similar to that described earlier for short composite columns. Columns with slenderness ratios equal to and greater than 66, on the other hand, produced lower 1-percentile, 5-percentile, and mean strength ratios when the structural steel ratio was high (ρ_{ss} = 0.082). Hence, the structural steel ratio must be considered as a required parameter for reliability analysis.

5.4.2.4 Effect of end eccentricity ratio - To investigate the effect of e/h on the strength ratio, all columns from Table 5.2 were studied for e/h ratios ranging from 0.05 to infinity. An examination of Figures 5.20 to 5.25 shows that the strength ratios of slender columns vary with e/h. For further study, the data from the sixteen columns in Table 5.2 were grouped into three sets according to the slenderness ratio. Columns with kl/r of 22.1 and 33 were grouped

together because of the similar values of strength ratios obtained for these columns, as shown in Figure 5.20. The second set contained beam-columns with kl/r = 66, while the third set included column with kl/r = 100. For each set, the range of 1-percentile, 5-percentile, and mean strength ratios are plotted against e/h in Figures 5.26(a), (b), and (c), respectively.

Figure 5.26(a) shows that the widest range of one-percentile strength ratios occurs for e/h less than 0.2 with the highest strength ratios corresponding to kl/r of 100 and the lowest to kl/r of 22.1 and 33. The one-percentile strength ratios for columns with kl/r of 100 drop very significantly as e/h increases from 0.05 to 0.2. The beam-columns with slenderness ratios of 22.1 and 33 are least affected as e/h increases from 0.05 to 0.2 [Figure 5.26(a)]. Between e/h of 0.2 and 1.2, the ranges of one-percentile strength ratios decrease significantly for all three sets of columns with the differences among the three ranges also decreasing as e/h increases. For e/h values greater than 1.2, all three ranges overlap and remain nearly constant as indicated by Figure 5.26(a). It is worth noting that the one-percentile strength ratios significantly lower than 0.7 were obtained at $e/h \leq 0.3$ for columns in the set with kl/r = 22.1 and 33 and much higher than 0.7 for columns with kl/r = 100.

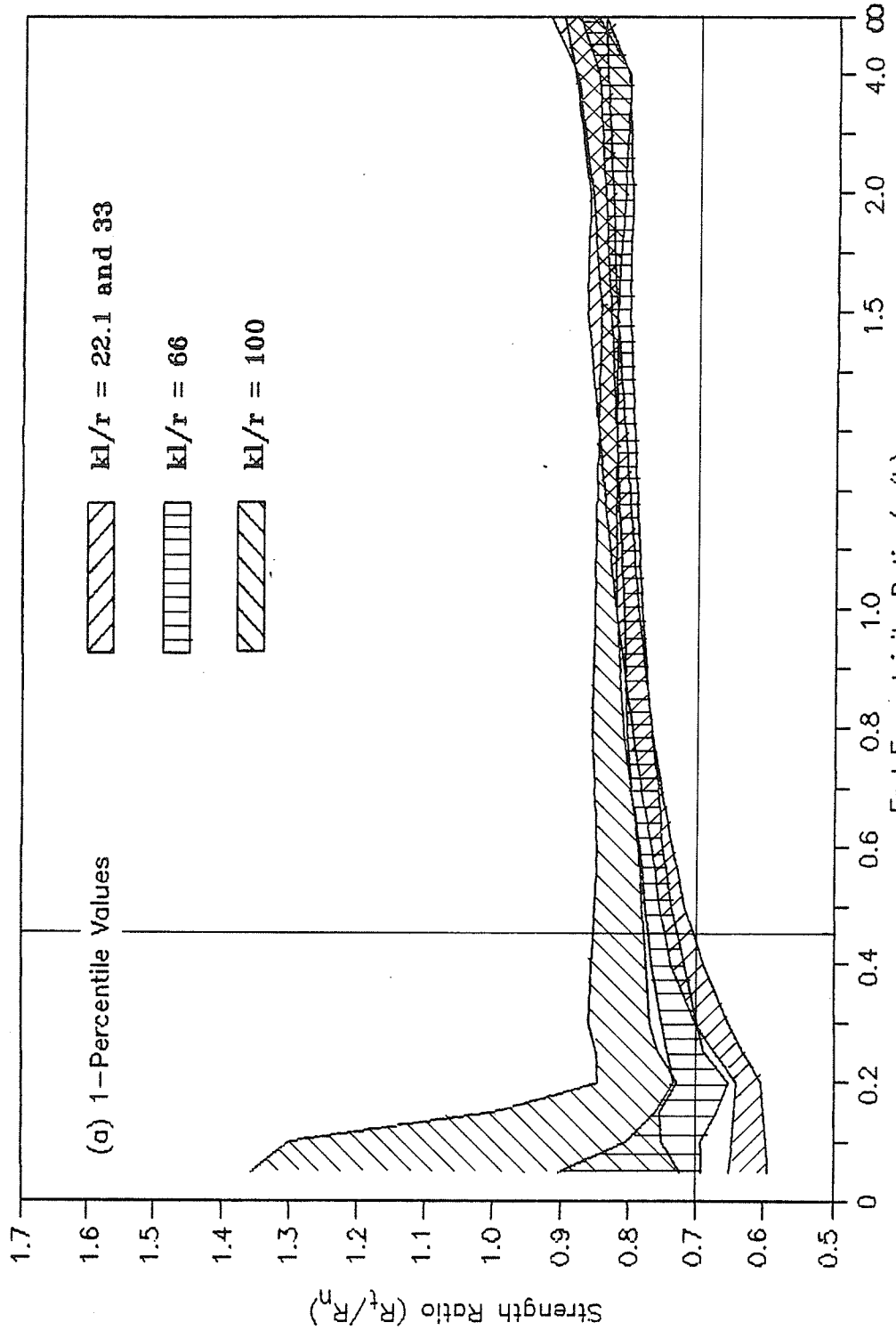

Figure 5.26 – Range of Ratio of Theoretical to Nominal Strength of Slender Composite Steel–Concrete Beam–Columns

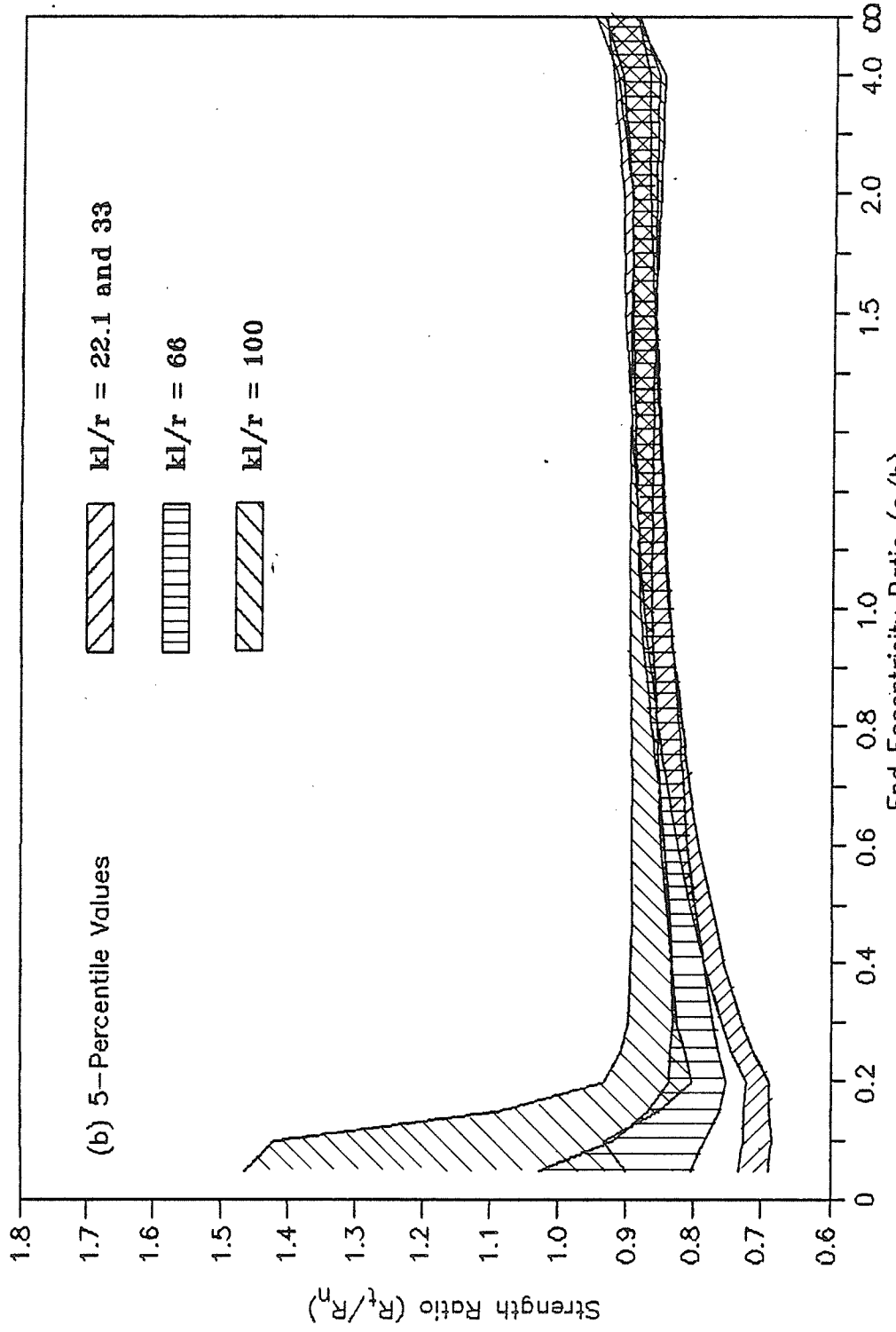

Figure 5.26 (cont.) – Range of Ratio of Theoretical to Nominal Strength of Slender Composite Steel–Concrete Beam–Columns

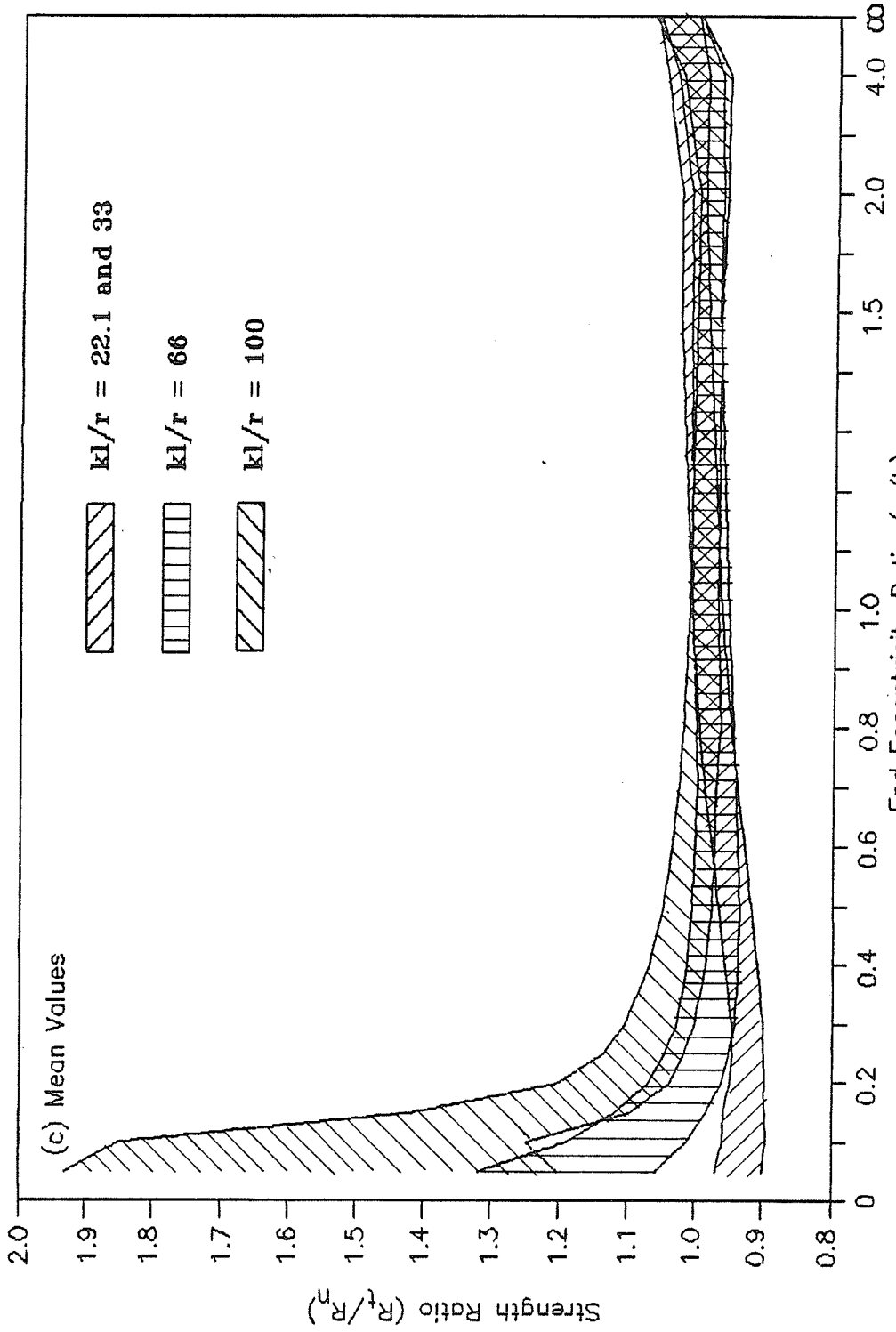

Figure 5.26 (cont.) – Range of Ratio of Theoretical to Nominal Strength of Slender Composite Steel–Concrete Beam–Columns

Figures 5.26(b) and (c) show that the above-noted trends for one-percentile strength ratios are also followed by the 5-percentile and mean values of the strength ratios. The only difference is that the five-percentile and mean strength ratios drop more sharply for columns with kl/r ratios of 100 and increase more slowly for columns in the set with kl/r of 22.1 and 33 as e/h increases from 0.05 to 0.2.

From the foregoing discussions, it is concluded that the end eccentricity ratio has the greatest effect on the strength ratio of very slender columns (kl/r = 100) at e/h values below 0.2. In this range of end eccentricity ratio, the least effect of e/h is experienced by columns with kl/r of 22.1 and 33. For end eccentricity ratios of 1.2 and higher, there is negligible effect of e/h on the strength ratios, regardless of the slenderness ratio used. Therefore, the future reliability analysis of slender columns should concentrate on data for e/h of 1.2 and less. The end eccentricity ratios below 0.45 are particularly critical because these e/h values produced some one-percentile strength ratios that fell below 0.7, as indicated by Figure 5.26(a). The effect of e/h on the strength ratio for end eccentricity ratios greater than 1.2 can be neglected.

Figure 5.27 shows the coefficient of variation of strength of composite beam-columns varying significantly

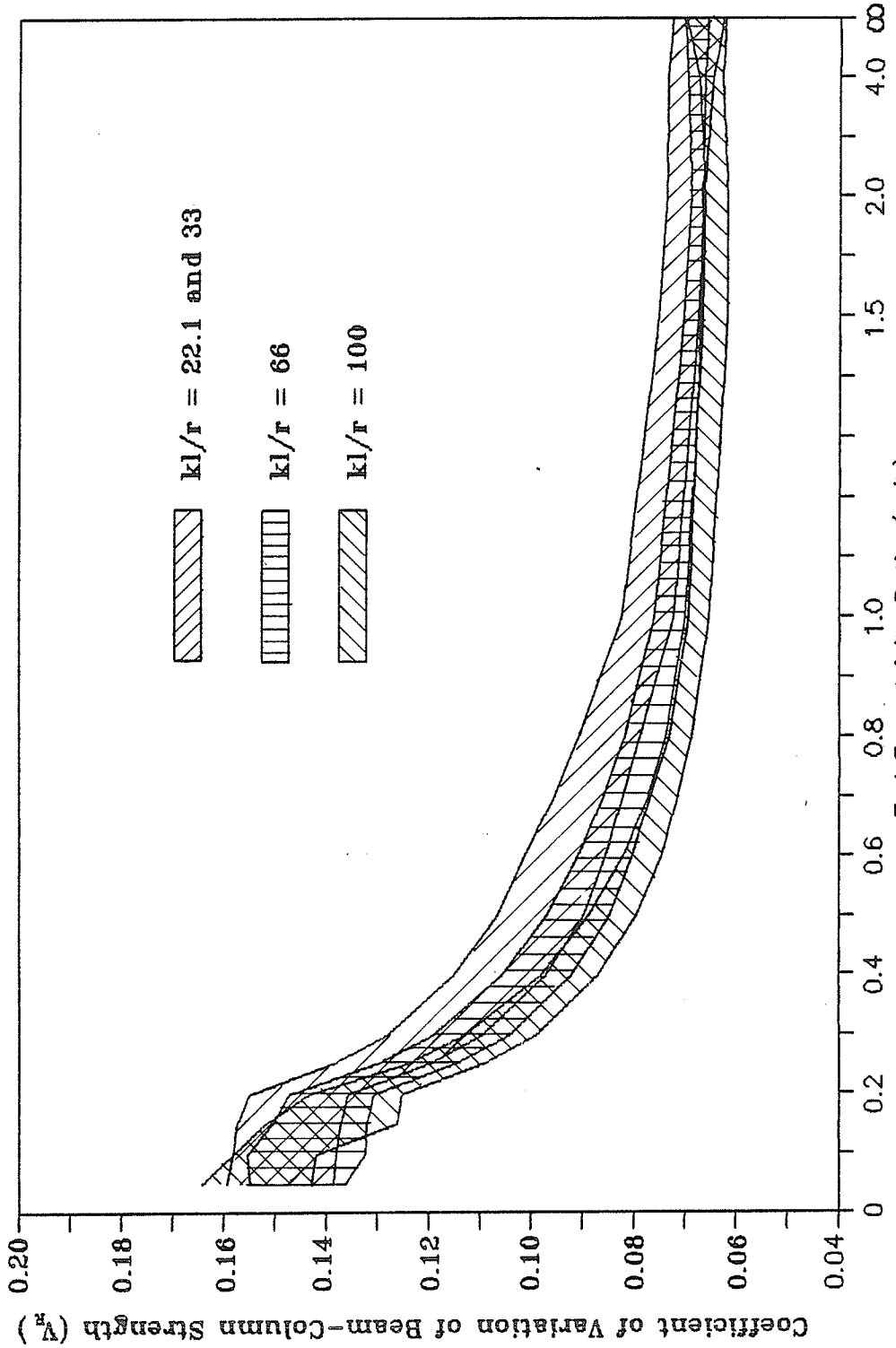

Figure 5.27 – Range of the Coefficient of Variation of the Ratio of Theoretical to Nominal Strength of Slender Composite Steel–Concrete Beam–Columns

with respect to end eccentricity ratio. Furthermore, columns with lower slenderness ratios correspond to higher coefficients of variation of strength and vice versa. This is especially apparent at e/h values greater than 0.2. For $e/h < 0.2$, the coefficients of variation of strength for all three sets of column seem to overlap. The strength coefficient of variation initially decreases rapidly and then at a reduced rate as e/h increases from 0.2 to ∞, as indicated by Figure 5.27.

The behavior of the strength coefficient of variation explained in the preceding paragraph can be at least partially attributed to the coefficient of variation of the theoretical strength model itself. As discussed in Chapter 2, the theoretical strength model error had a coefficient of variation that remained constant at its maximum value for $e/h \leq 0.2$. The model error coefficient of variation then decreased linearly with increasing e/h until it reached its minimum value at the pure bending condition. This partly explains the shape of the coefficient of variation curves in Figure 5.27. The decrease in strength coefficient of variation with increasing slenderness ratio of the column is likely caused by the increase in dependance on the structural steel to provide resistance against the increased probability of tension failure due to secondary moment effects. Since the coefficients of variation associated with the steel properties are less than those for concrete,

the columns deriving more of their streength capacity from the structural steel will be subjected to lower strength variations.

5.4.2.5 Sensitivity analysis - The portions of the overall variability of the column strength attributable to the variation in the mechanical properties of concrete, the mechanical and geometric properties of structural steel, and the theoretical strength model were determined for a typical slender beam-column. Column 4-50-4-66 (Table 5.2) was chosen for this analysis. To determine the beam-column strength variability due to each of the three sets of variables noted above, three separate computer runs of 500 simulations each were made. For each computer run, only the variables from one of the above-noted sets were allowed to vary while the remaining variables were kept constant at their mean value. The portions of the overall variability of the beam-column strength so determined were respectively designated as $V_{colconc}$, V_{colss}, and V_{model} for the three sets of variables noted above.

The squares of the coefficients of variation $V^2_{colconc}$, V^2_{colss}, and V^2_{model} computed for the strength of Column 4-50-4-66 at e/h values ranging from 0.05 to ∞ are plotted on Figure 5.28. These plots indicate that the overall variability of the strength of the above-noted column is mostly influenced by the variations in the theoretical strength

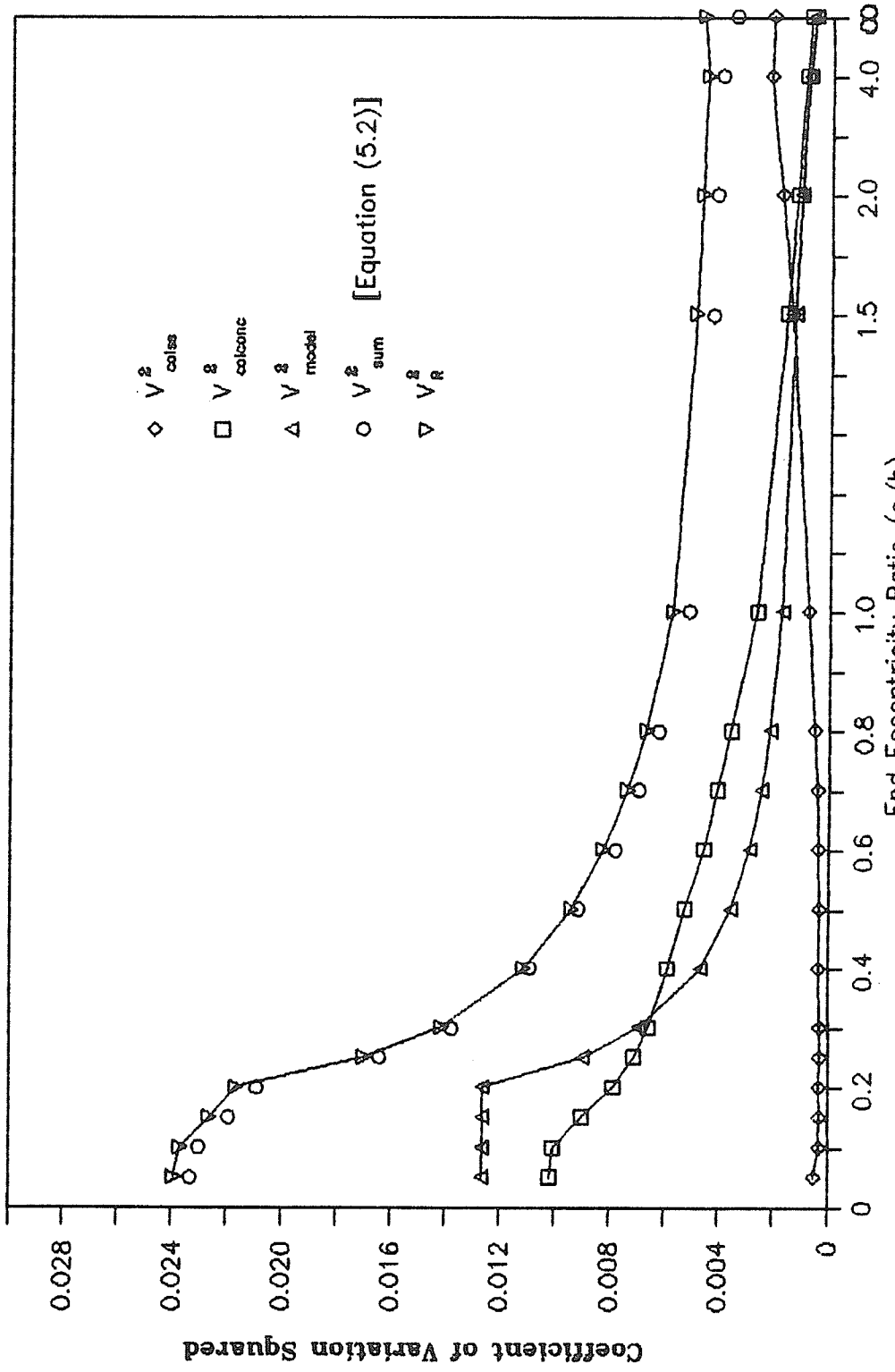

Figure 5.28 – Effect of Variabilities of Properties of Constituent Materials on Overall Strength Variability of Slender Beam–Column 4–50–4–66 (Table 5.2)

model and the concrete mechanical properties for $e/h \leq 1.0$. For $1.0 < e/h < \infty$, all three variations ($V_{colconc}$, V_{colss}, and V_{model}) seem to contribute to the overall strength variability of Column 4-50-4-66. At pure bending condition, the strength variability of Column 4-50-4-66 is identical to that of the cross-section and the variations in the structural steel properties mostly influence the overall variability of the column strength. Hence, the behavior of Column 4-50-4-66 at $e/h = \infty$ in Figure 5.28 is identical to that shown in Figure 5.14. Note the effects of the variability of the theoretical strength model and of the concrete properties decrease significantly as the end eccentricity ratio increases from e/h = 0.2. The effect of the variability of the structural steel properties increases somewhat as e/h increases from 1.0 to higher values.

The values of V_{sum}^2 plotted in Figure 5.28 represent the sum of the squares of the coefficients of variation of Column 4-50-4-66 strength obtained from individual variabilities of the three sets of variables as indicated in Equation (5.2). Also plotted in Figure 5.28 are the values of V_R^2 which is the square of the coefficient of variation of the beam-column strength obtained when variabilities from all sources were included simultaneously in computations. A comparison of values of V_{sum}^2 and V_R^2 plotted in Figure 5.28 indicates a good correlation of these values, especially in

the range of e/h = 0.2 to 0.6, with V^2_{sum} only slightly underestimating V^2_R on either side of this range of e/h. The underestimation of V^2_R by V^2_{sum} at $e/h < 0.2$ is likely due to variations in the cross-section dimensions. The underestimation by V^2_{sum} at $e/h > 0.6$ is likely due to variations in the properties of the reinforcing steel and the bar placements. Note the variations in the cross-section dimensions and reinforcing steel properties were not included for computing V^2_{sum}, as indicated by Equation (5.2).

The effects of variations in properties of reinforcing bars were insignificant in this study because ρ_{rs} was small compared to ρ_{ss} used for the composite columns studied. An earlier study (Mirza 1989) found that the cross-section dimensions had insignificant effect on composite column strength variability. Similarly, Mirza and MacGregor (1989) noted that the strength variability of slender reinforced concrete columns was sensitive to dimensional variations only at low e/h. From the discussions presented here and Figure 5.28, it is apparent that the relation proposed in Equation (5.2) is valid for the type of slender composite columns studied.

5.4.2.6 Summary of effects of variables used for basic study - The following summarizes the effects of variables used for the basic study of slender composite beam-columns:

(a) Slenderness ratios of 22.1 and 33 are more critical than 66 and 100 for the type of slender columns studied;

(b) the specified concrete strength is a significant variable for columns with slenderness ratios less than 33 but is insignificant for kl/r greater than or equal to 33;

(c) the ratio of structural steel area to gross area of cross-section is a major variable;

(d) the end eccentricity ratio has the greatest effect on very slender columns (kl/r = 100) and the least effect on less slender columns studied (kl/r = 22.1 and 33);

(e) the overall variability of the theoretical strength is primarily due to the variations in the mechanical properties of the concrete, the mechanical and geometric properties of the structural steel, and of the theoretical strength model.

5.4.3 Effect Of Variables Used For Supplemental Study

From the slender columns used for the supplemental study (Table 5.4), the effects of the specified yield strength of structural steel, the strain-hardening of structural steel section and reinforcing bars and the quality control of concrete on the beam-column strength ratios were studied. Plots of the one-percentile, five-percentile and mean strength ratios at various values of e/h were made for each variable studied.

5.4.3.1 Effect of specified yield strength of structural steel - To study the effect of the specified yield strength

of structural steel on the strength ratios, two slender columns from the basic study (Columns 4-50-4-33 and 6-50-4-33 in Table 5.2) were compared to four columns from the supplemental study (Columns 4-44-4-33, 4-36-4-33, 6-44-4-33, and 6-36-4-33 in Table 5.4). This provided two sets of three column each. Each set had a column with structural steel f_y = 50 ksi (345 MPa), a column with structural steel f_y = 44 ksi (303 MPa), and a column with structural steel f_y = 36 ksi (248 MPa). All other properties of the three columns in a set were identical. Figure 5.29(a), (b), and (c) respectively plot the one-percentile, five-percentile, and mean strength ratio data for one of the above-noted sets. The specified strength of concrete equal to 4000 psi (27.6 MPa) was used for the beam-columns shown in Figure 5.29.

At the 1-percentile level [Figure 5.29(a)], the lowest strength ratios were found for the column having 50 ksi (345 MPa) structural steel over almost the entire range of e/h. The one-percentile strength ratios for the column with 50 ksi (345 MPa) structural steel plotted significantly less than those for the column with 36 ksi and 44 ksi (248 MPa and 303 MPa) structural steel at $e/h \leq 0.5$. Between e/h of 1.2 and infinity, the data for the columns with 50 ksi and 36 ksi (345 MPa and 248 MPa) structural steel plot almost identically. The highest values of one-percentile strength ratios were obtained over almost the entire range of e/h

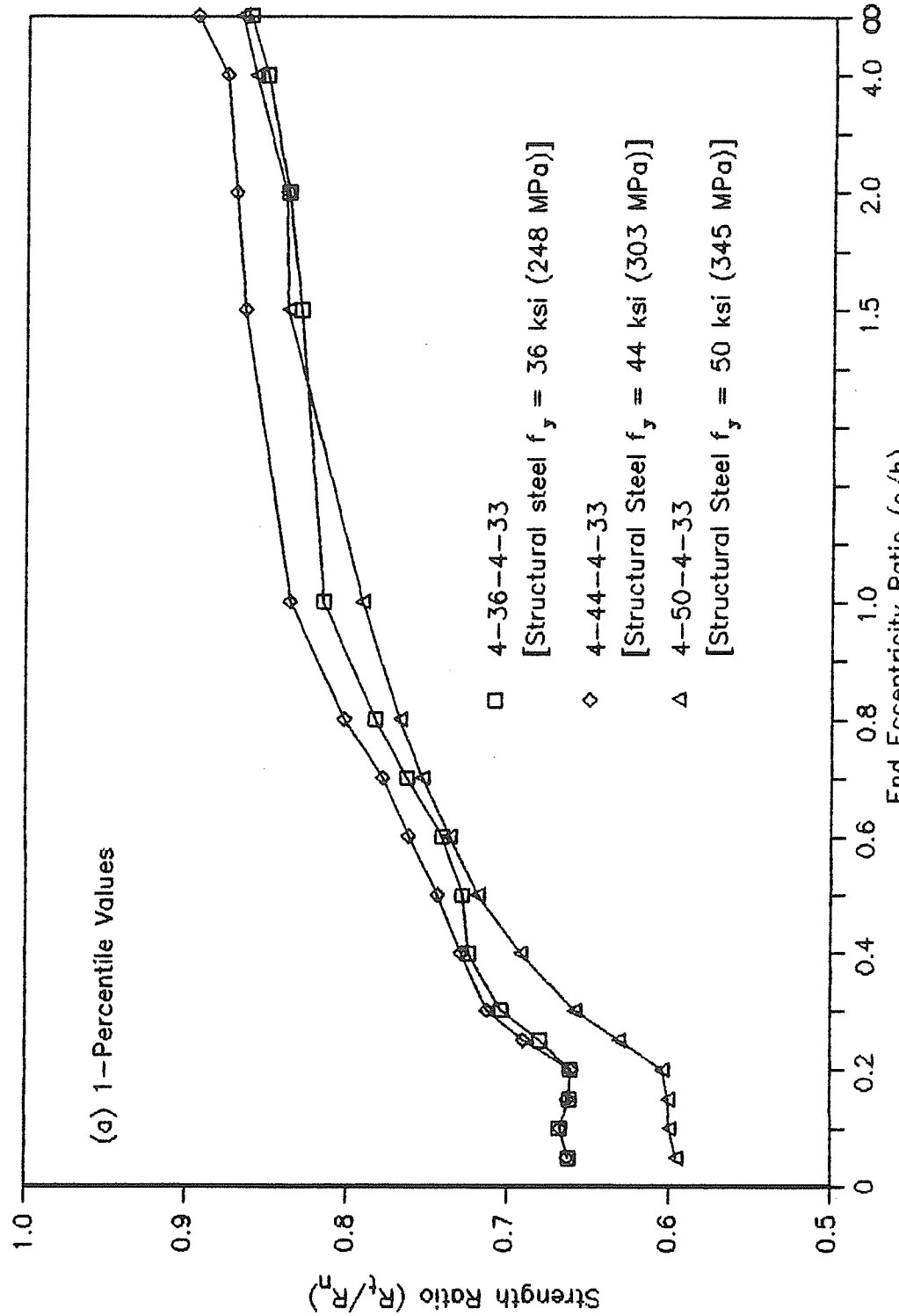

Figure 5.29 – Effect of Specified Structural Steel Yield Strength on the Ratio of Theoretical to Nominal Strength of Slender Composite Steel–Concrete Beam–Columns

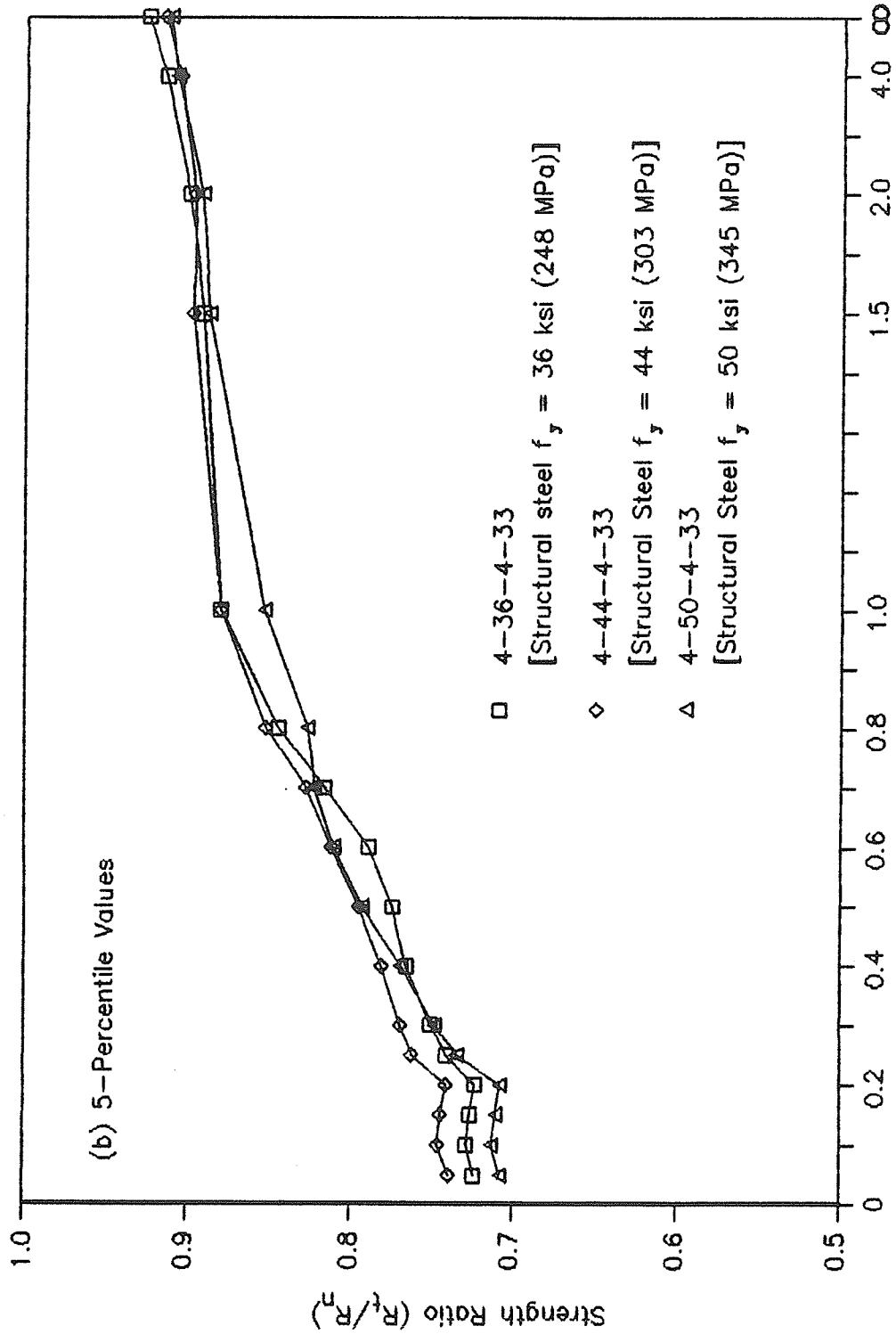

Figure 5.29 (cont.) – Effect of Specified Structural Steel Yield Strength on the Ratio of Theoretical to Nominal Strength of Slender Composite Steel-Concrete Beam-Columns

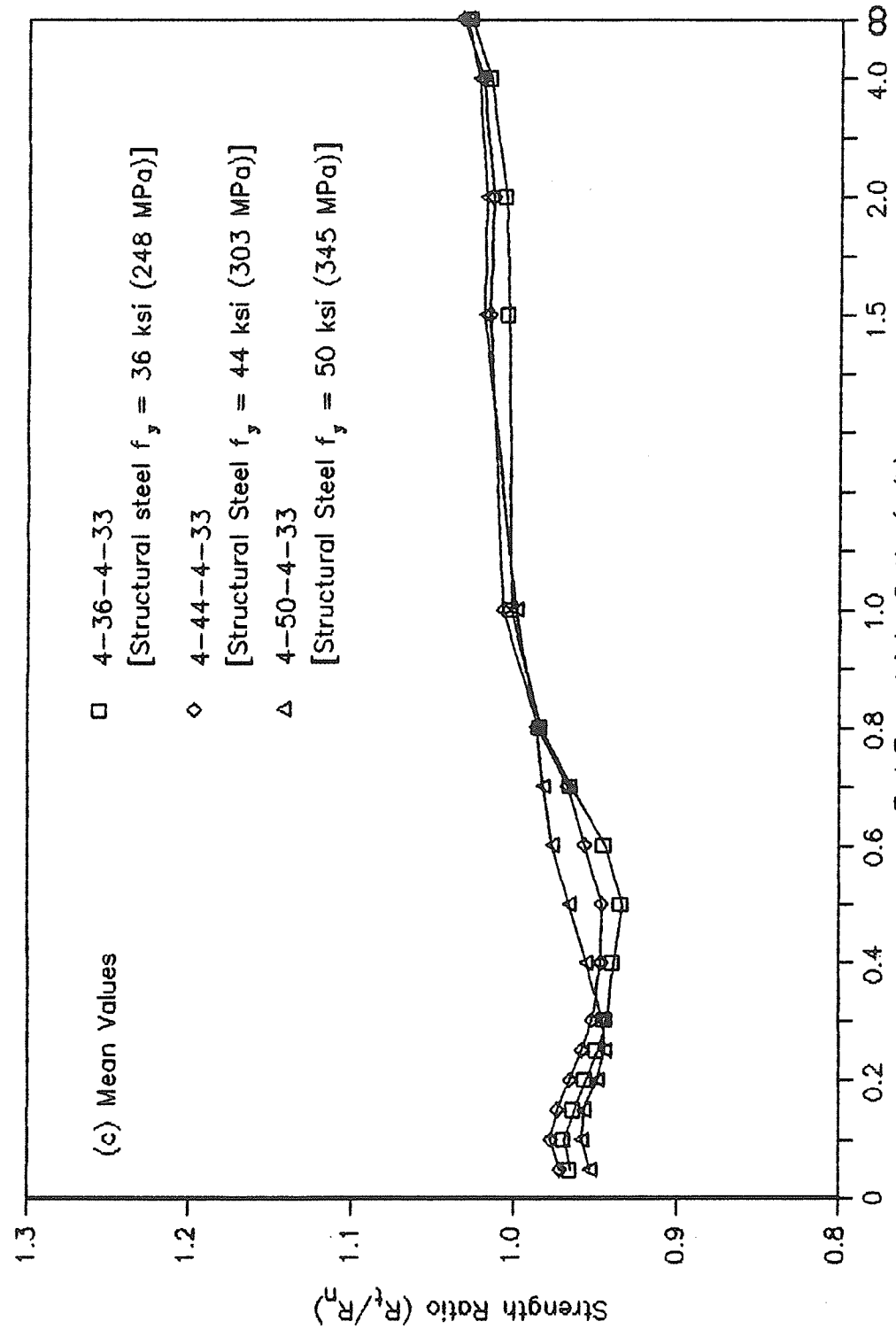

Figure 5.29 (cont.) – Effect of Specified Structural Steel Yield Strength on the Ratio of Theoretical to Nominal Strength of Slender Composite Steel–Concrete Beam–Columns

studied for the beam-column in which 44 ksi (303 MPa) structural steel was used, as indicated by Figure 5.29(a). A similar trend is observed from the 5-percentile strength ratios shown in Figure 5.29(b), but the differences among the 5-percentile strength ratios for columns with different grades of structural steel are significantly reduced.

The effect of structural steel grade on mean strength ratios seems to be negligible [Figure 5.29(c)]. Only between e/h of 0.4 and 0.8 does the mean strength ratio data show some spread. In this range of e/h, the lowest mean strength ratios were given by the column having 36 ksi (248 MPa) structural steel and the highest mean strength ratios by the column having 50 ksi (345 MPa) structural steel, as indicated by Figure 5.29(c).

Results from the other set of columns employing $f_c' =$ 6000 psi (41.4 MPa) and used to investigate the effect of structural steel grade (Columns 6-50-4-33, 6-44-4-33, and 6-36-4-33) indicated negligible effects of structural steel f_y on mean, five-percentile, and one-percentile strength ratios. This was valid over the entire range of e/h studied.

Since the 1-percentile strength ratios are more important for safety considerations and the lowest values for these strength ratios were obtained in Figure 5.29(a) for columns with structural steel f_y = 50 ksi (345 MPa), it is

recommended that 50 ksi (345 MPa) structural steel be used in future reliability analysis of slender composite columns. The 50 ksi (345 MPa) structural steel is the highest grade of steel presently allowed by the North American design codes for composite columns and will ensure relevancy as commonly used steel grades increase above the present values.

5.4.3.2 Effect of strain hardening of steel - To examine the effects of strain-hardening of the structural steel section and of the vertical reinforcing bars on the strength ratios of slender composite columns, the data from two columns of the basic study (Columns 4-50-4-66 and 6-50-4-66 in Table 5.2) were compared to the data from the corresponding columns of the supplemental study (Columns 4-50-4-66-STH and 6-50-4-66-STH in Table 5.4). Note the strain-hardening of both steels was included in theoretical strength computations of Columns 4-50-4-66-STH and 6-50-4-66-STH and it was neglected for columns 4-50-4-66 and 6-50-4-66. This provided two sets of columns, each set having one column in which strain-hardening was included and one column in which strain-hardening was not permitted. All other properties were identical for both columns in a set. The strength ratios for columns from one of these sets are shown in Figure 5.30.

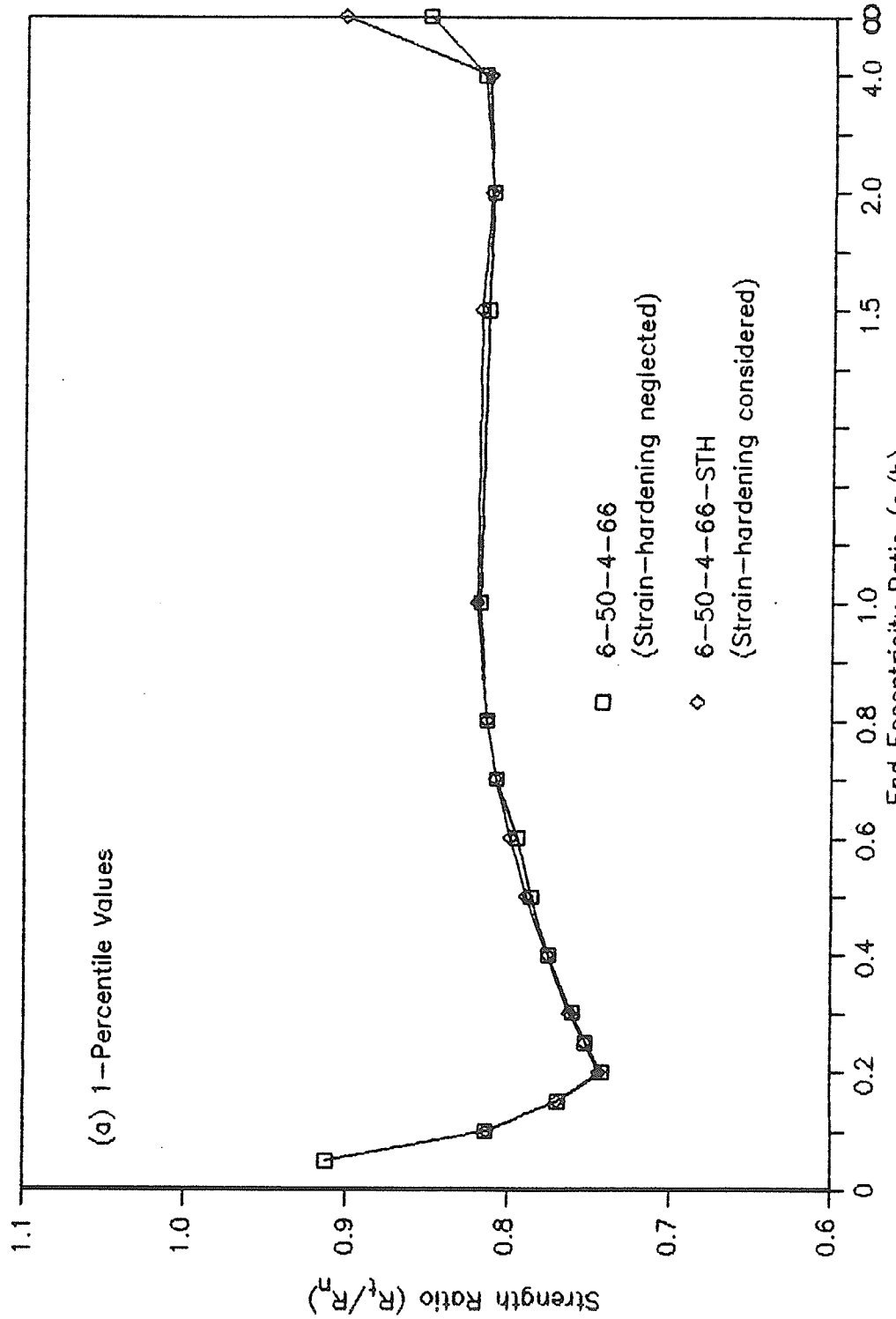

Figure 5.30 – Effect of Strain-Hardening of Steel on the Ratio of Theoretical to Nominal Strength of Slender Composite Steel-Concrete Beam-Columns

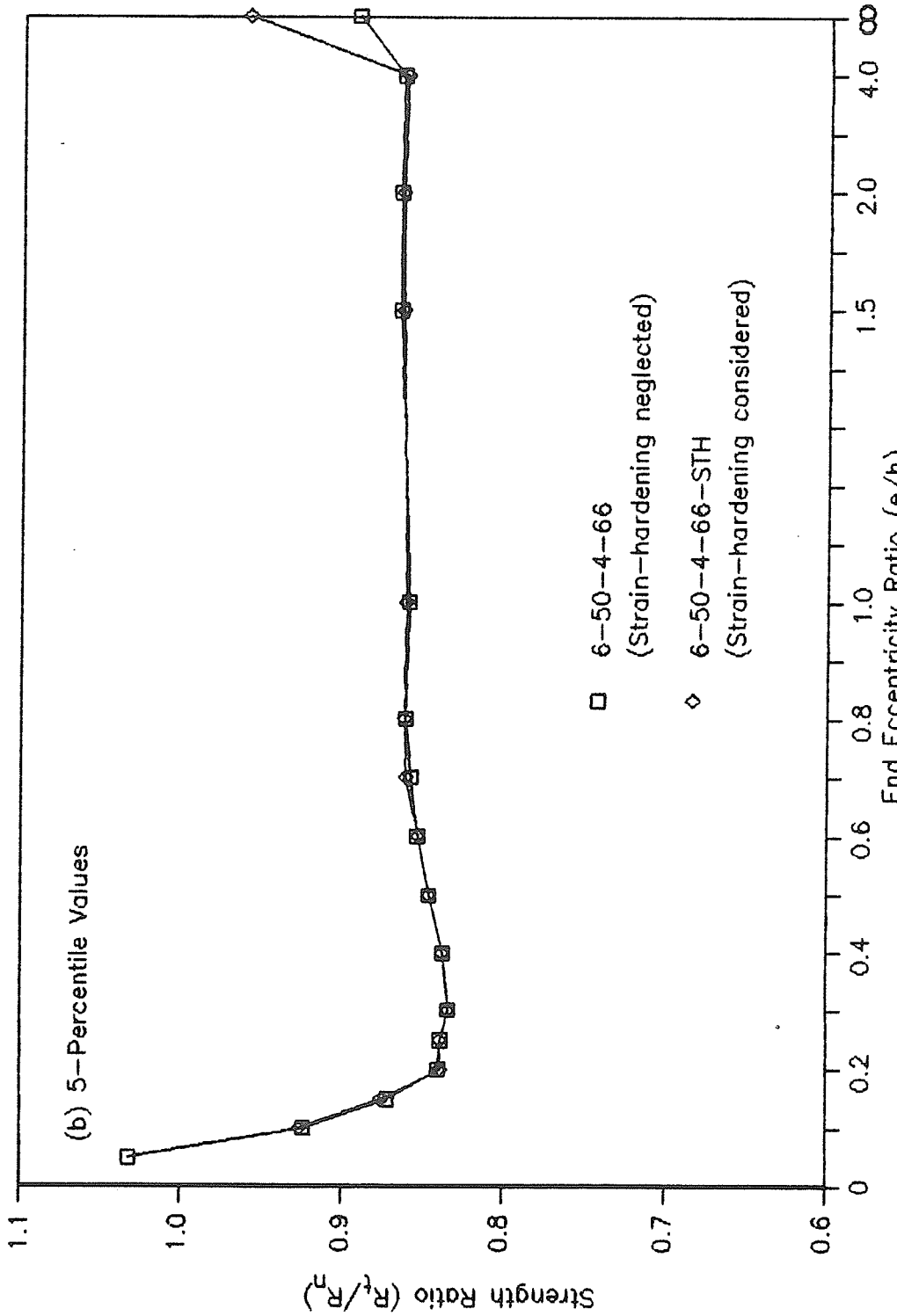

Figure 5.30 (cont.) – Effect of Strain-Hardening of Steel on the Ratio of Theoretical to Nominal Strength of Slender Composite Steel-Concrete Beam-Columns

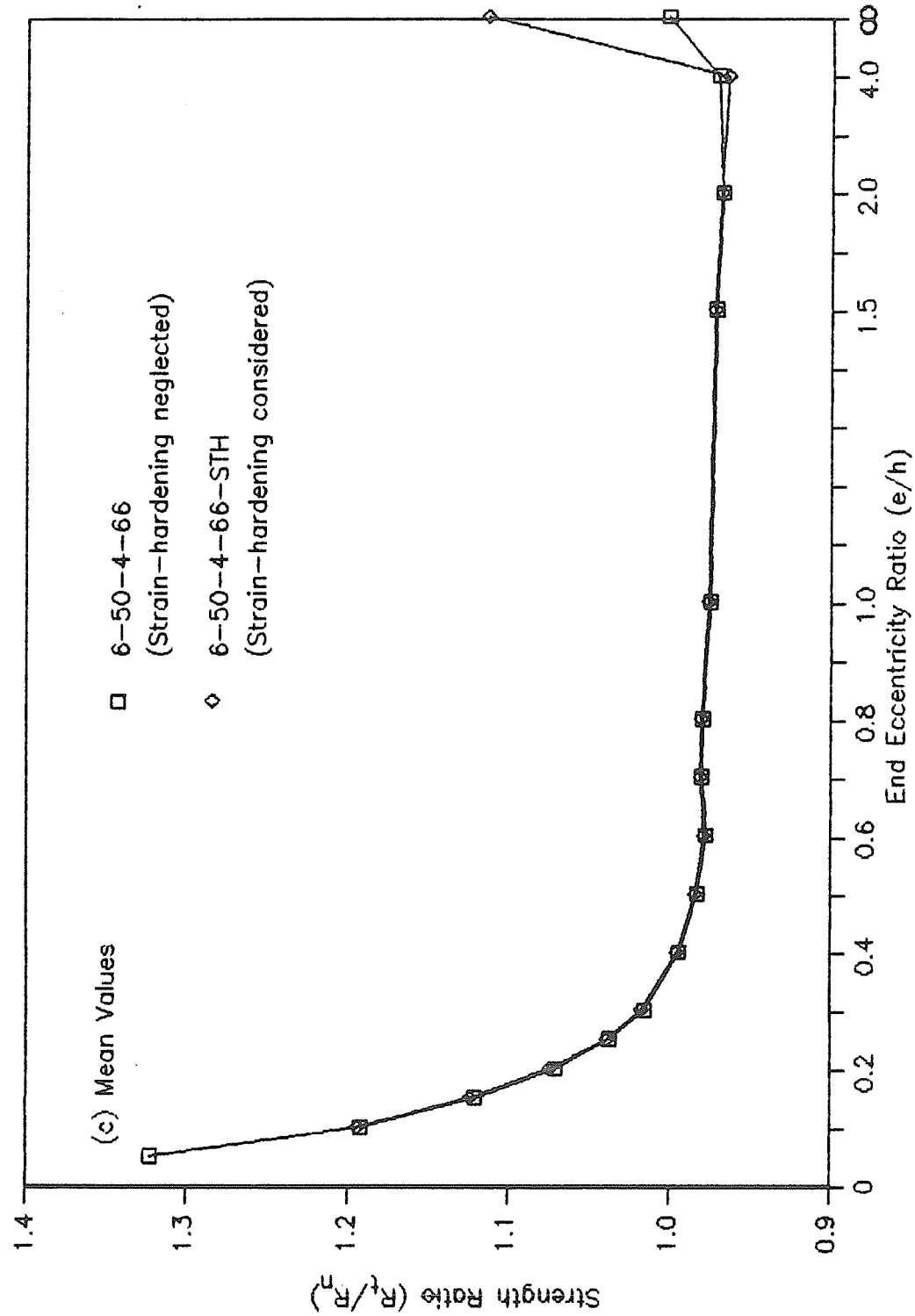

Figure 5.30 (cont.) – Effect of Strain-Hardening of Steel on the Ratio of Theoretical to Nominal Strength of Slender Composite Steel-Concrete Beam-Columns

Figure 5.30 shows that the effects of strain-hardening of steel on one-percentile, five-percentile, and mean strength ratios are insignificant over almost the entire range of e/h. Exceptions are the strength ratios close to pure bending region. The most significant effect of strain-hardening of steel was found on strength ratios at pure bending. Here, the strength ratios of a slender column are identical to those of the cross-section since there is no additional bending moment due to eccentric axial loads. Hence, the effect of strain-hardening on the cross-section strength in pure bending discussed in Section 5.3.3.2 is also valid for Figure 5.30. The conclusions derived from the second set of columns used to study the effect of strain-hardening of steel on slender composite columns were very similar to those stated for Figure 5.30.

Examination of moment - curvature data for columns at subject to axial loads less than 20 percent of their concentric axial load cross-section capacity showed that the secondary moments caused by deflection of the column were greater than any gain in strength due to strain-hardening of the steel components. Therefore, the highest bending moment capacities calculated for the columns where strain-hardening was allowed was identical to the bending moment capacity calculated for an identical column in which strain-hardening was not permitted.

Since significant effects of strain-hardening on strength ratios of slender columns occur only near and at pure bending condition, it is concluded that the strain-hardening of steel be neglected for reliability analysis of slender composite beam-columns.

5.4.3.3 Effect of quality of concrete - To study the effect of concrete quality control on the strength variations of slender composite beam-columns having f'_c = 6000 psi (41.4 MPa), the data for two columns from the basic study (Columns 6-50-4-33 and 6-50-8-33 with excellent concrete quality in Table 5.2) were compared to the data for the corresponding columns from the supplemental study (Columns 6-50-4-33-A and 6-50-8-33-A with average concrete quality in Table 5.4). This produced two sets of beam-columns, each set had one column with excellent quality concrete and one column with average quality concrete. All other properties were identical for both columns in a set. The strength ratios for beam-columns from one of these sets are given in Figure 5.31 and represent the typical behaviour.

At the 1-percentile level [Figure 5.31(a)], the beam-column having average quality concrete produced significantly lower strength ratios over the entire range of e/h. This can be attributed directly to the larger coefficient of variation associated with concrete of average quality. At the 5-percentile level, the effect of concrete quality on strength ratios reduces significantly as indicated by Figure

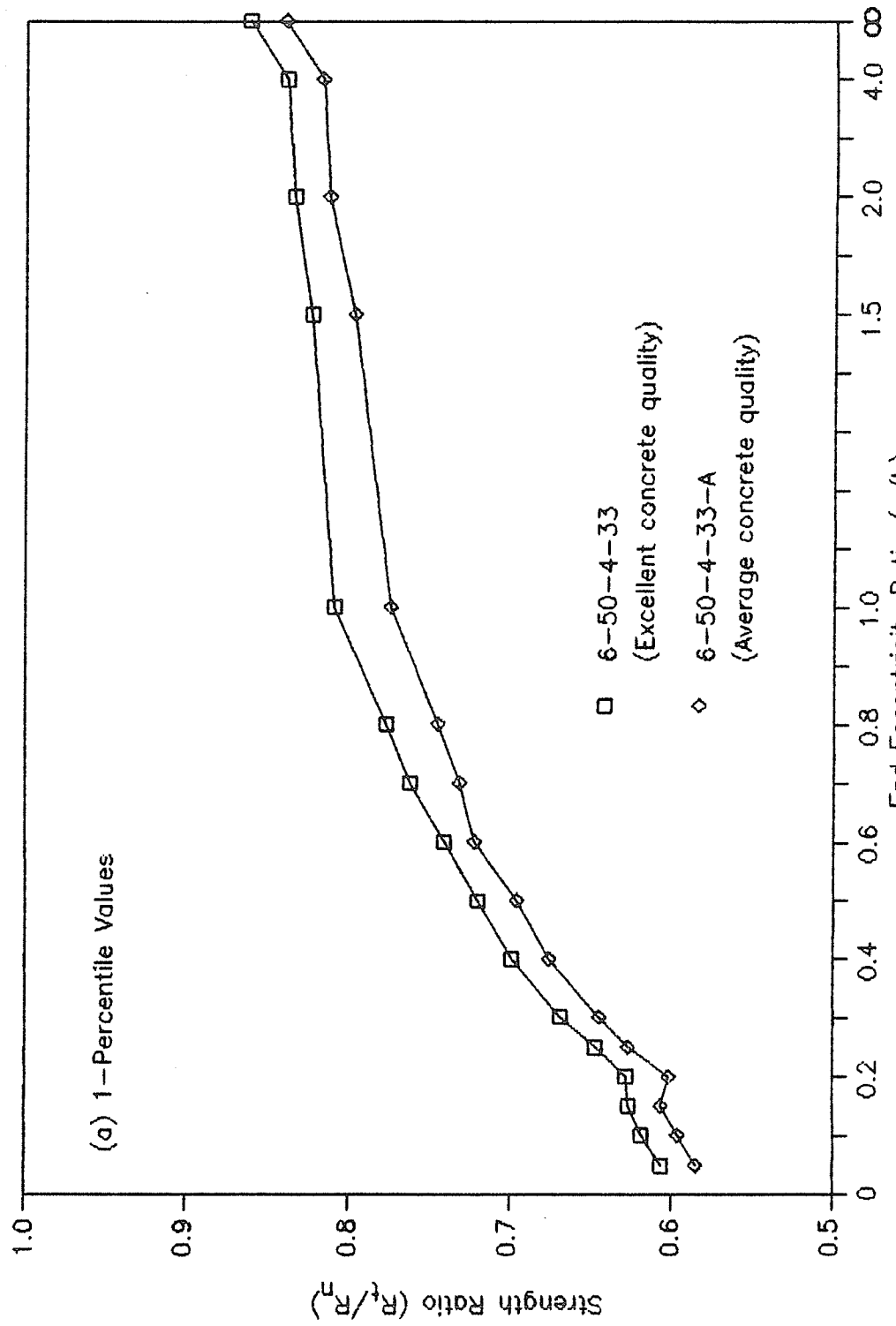

Figure 5.31 – Effect of Concrete Quality Control on the Ratio of Theoretical to Nominal Strength of Slender Composite Steel-Concrete Beam-Columns

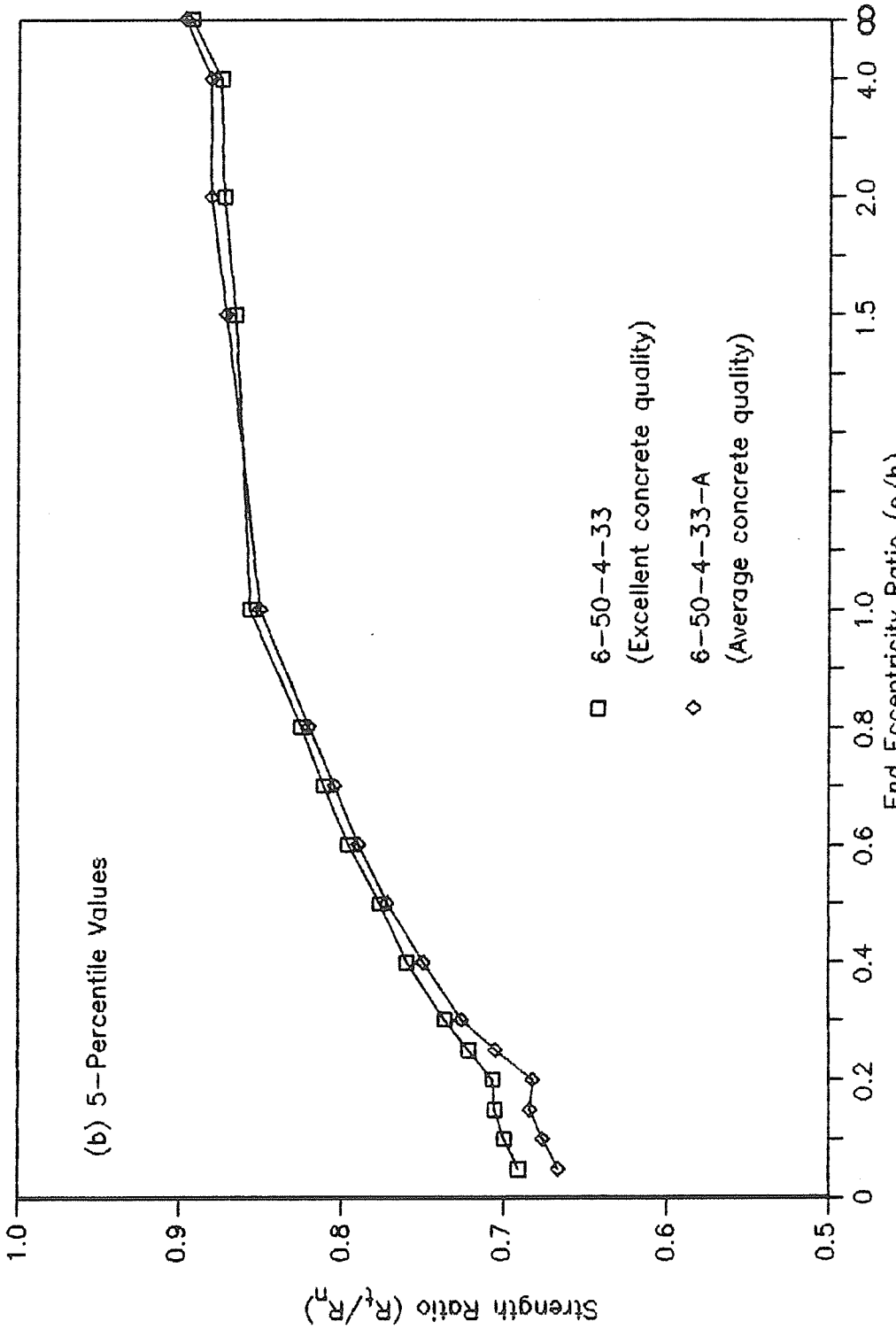

Figure 5.31 (cont.) – Effect of Concrete Quality Control on the Ratio of Theoretical to Nominal Strength of Slender Composite Steel–Concrete Beam–Columns

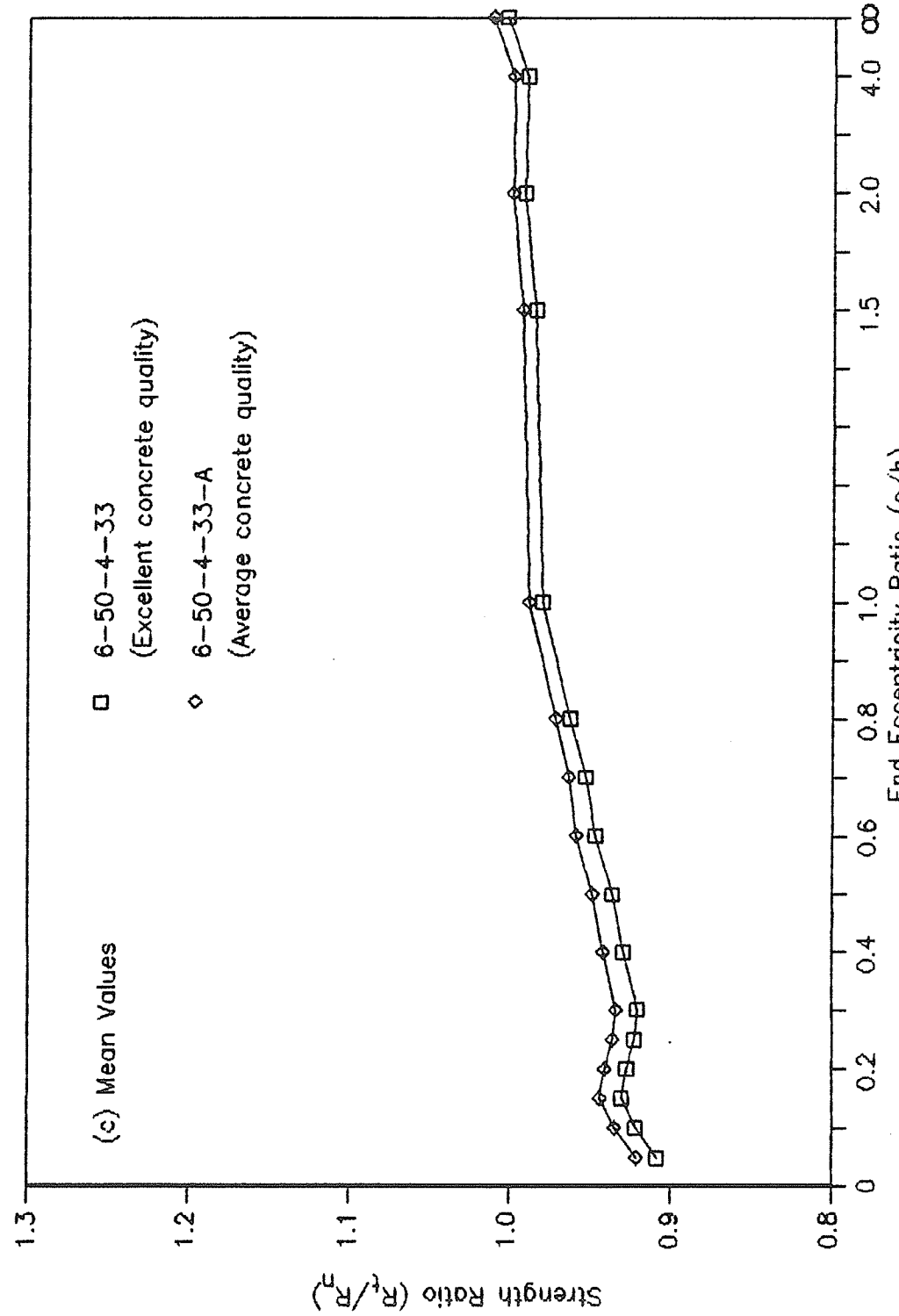

Figure 5.31 (cont.) – Effect of Concrete Quality Control on the Ratio of Theoretical to Nominal Strength of Slender Composite Steel–Concrete Beam–Columns

5.31(b). The mean strength ratios for columns with different concrete quality tend to be of the same magnitude [Figure 5.31(c)]. This behavior is expected and is very similar to the effect of concrete quality on strength variations of short composite columns.

Since the concrete quality has a significant effect on the lower tail of the strength probability distributions, it is important that the future reliability analysis considers the concrete quality as one of the variables.

5.4.3.4 Summary of effects of variables used for supplemental study - The following summarizes the effects of variables used for supplemental study of slender composite beam-columns:

(a) The beam-columns having structural steel of specified yield strength of 50 ksi (345 MPa) produced lower 1-percentile strength ratios than did the columns with lower grades of structural steel;

(b) the strain-hardening of steel only enhances the strength of the beam-column at and near the pure bending condition and, therefore, can be neglected for practical columns; and

(c) the quality control of concrete significantly affects the strength ratios at the 1-percentile level.

6 SUMMARY AND CONCLUSIONS

6.1 SUMMARY

The purpose of the study reported herein was to simulate the probability distributions of ultimate strength of composite columns in which steel shapes are encased in concrete and to define the major variables that affect the strength. The descriptions of the strength probability distributions developed in this study will be used in a reliability analysis currently underway at Lakehead University for developing limit states design criteria for composite columns in building structures.

The Monte Carlo technique was employed to simulate the statistical properties of the strength of composite beam-columns. Probability distributions of the geometric and mechanical properties of column components required for Monte Carlo simulation were either taken from the literature or were derived from available statistical data. An existing computer program to calculate the theoretical resistance of composite columns was extensively tested for numeric and logical accuracy and revised wherever required. The accuracy of the theoretical strength program was established by comparisons with existing test data of the ultimate strength of composite beam-columns. Repeated simulations of the strength of several column configurations

using the probability distributions of variables that affect the strength resulted in the definition of the strength probability distribution for each beam-column configuration.

An existing computer program to calculate the nominal capacity of composite beam-columns was tested extensively and modified wherever required. The nominal capacity was based on the specified geometric and mechanical properties of the column components and on the equations given in the North American building codes. The same column configurations that were used to define the theoretical strength probability distributions were also checked for their nominal capacities. By comparing the ratio of theoretical to nominal strength between various column configurations, the component variables having significant effects on the strength were defined.

6.2 CONCLUSIONS

The strength variability of composite columns is primarily due to the variability in concrete mechanical properties for compression failures and the variability of the steel section mechanical and geometric properties for tension failures.

6.2.1 Short Columns

The ratio of theoretical strength to nominal strength (strength ratio) of short composite columns ($kl/r \leq 22$) was influenced most significantly by the specified concrete

strength, the ratio of area of structural steel to gross area of the cross-section and the end eccentricity ratio. Beam-columns with slenderness ratios at the code limit of $kl/r = 22$ produced lower strength ratios than the corresponding cross-sections. The magnitude of the specified yield strength (f_y) of structural steel did not significantly affect the strength ratios for beam-columns with common grades of steel having $f_y \leq 50 ksi$ $(345 MPa)$. Strain-hardening of the reinforcing and structural steel in a composite column enhanced its strength only at and near the pure bending condition. Quality control of the concrete significantly influenced the lower tail of the strength probability distributions of the beam-columns studied.

6.2.2 Slender Columns

The ratio of theoretical to nominal strength of slender composite columns ($kl/r > 22$) was influenced most significantly by the slenderness ratio, the ratio of area of structural steel to gross area of the cross-section and the end eccentricity ratio. Both the slenderness ratio and the end eccentricity ratio have little effect on the strength ratios of columns with end eccentricity ratios greater than 1.2. The specified strength of concrete influenced the strength ratio only for columns with a slenderness ratio (kl/r) of less than or equal to 33. The lowest strength ratios were obtained for columns with slenderness ratios less than or

equal to 33 and the highest ratios were found for columns with a slenderness ratio of 100. Beam-columns with structural steel yield strength of 50 ksi (345 MPa) produced lower strength ratios than those produced by beam-columns having lower yield strength of structural steel. Strain-hardening enhances the strength only at and near the pure bending condition. The quality control of the concrete significantly affected the lower tail of the strength probability distribution of the column.

LIST OF REFERENCES

ACI Committee 214. 1965. Recommended practice for evaluation of compression test results of concrete. American Concrete Institute, Detroit, MI.

ACI 318-83. 1983. Building code requirements for reinforced concrete. American Concrete Institute, Detroit, MI.

Allen, D.E. 1970. Probabilistic study of reinforced concrete in bending. Technical Paper NRC 11139, National Research Council of Canada, Ottawa.

Allen, D.E. 1972. Statistical study of the mechanical properties of reinforcing bars. Building Research Note No. 85, Division of Building Research, National Research Council, Ottawa.

Alpsten, G.A. 1968. Thermal residual stresses in hot-rolled members. Fritz Engineering Laboratory Report No. 337.3, Lehigh University, Bethlehem, PA.

Alpsten, G.A. 1972. Variations in mechanical and cross-sectional properties of steel. Planning and Design of Tall Buildings, **Ib**(9): 755-805.

American Iron and Steel Institute Committee on Product Standards, 1972. Check tension tests - plates and wide flange beams. Proceedings, Specialty Conference on Safety and Reliability of Metal Structures, Pittsburgh, PA.

Basu, A.K. 1967. Computation of failure loads of composite columns. Procedures Institution of Civil Engineers (London), **36**(March): 557-578.

Basu, A.K., and Hill, W.F. 1968. A more exact computation of failure loads of composite columns. Procedures Institution of Civil Engineers (London), **40**(May): 37-60.

Beedle, L.S., and Tall, L. 1960. Basic column strength. Journal of the Structural Division ASCE, **86**(ST7): 139-173.

Bjorhovde, R. 1972. Deterministic and probabilistic approaches to the strength of steel columns. Ph.D. Dissertation, Lehigh University; Bethlehem PA.

Bolin, P. 1985. Parametric study of the strength variability of composite columns. B.Eng. thesis, School of Engineering, Lakehead University, Thunder Bay, Ontario.

Bolotin, V.V. 1969. Statistical methods in structural mechanics, translated by Samuel Aroni. Holden-Day Inc., San Francisco, California.

Bondale S. 1966a. Column theory with special reference to composite columns. The Consulting Engineer, July: 72-77.

Bondale S. 1966b. Column theory with special reference to composite columns. The Consulting Engineer, August: 43-48.

Bondale S. 1966c. Column theory with special reference to composite columns. The Consulting Engineer, September: 68-70.

Carreira, D.J. and Chu, K. 1986. Stress-strain relationship for reinforced concrete in tension. American Concrete Institute Journal, **83**(1): 21-28.

CSA. 1984. Design of concrete structures for buildings - a national standard of Canada. CAN3-A23.3-M84, Canada Standards Association, Ottawa, Ont.

Davis, S.G. 1976. Further investigations into the strength of concrete in structures. Technical Report, Cement and Concrete Association, London, England.

Doane, J.F. 1969. Inelastic instability of wide-flange steel beams. M.Sc. thesis, University of Texas at Austin, Austin, TX.

Galambos, T.V. 1963. Inelastic lateral buckling of beams. Journal of the Structural Division ASCE, **89**(ST5): p.217.

Galambos, T.V., and Ravindra, M.K. 1978. Properties of steel for use in LRFD. Journal of the Structural Division ASCE, **104**(ST9): 1459-1468.

Grant, L.H. 1976. Strength variability of concrete columns. M.Sc. thesis, University of Alberta, Edmonton, Alberta.

Grant, L.H., Mirza, S.A., and MacGregor, J.G. 1978. Monte Carlo study of strength of concrete columns. American Concrete Institute Journal, **75**(8):345-358.

Hognestad, E. 1951. A study of combined bending and axial load in reinforced concrete members. Bulletin **399**, Engineering Experiment Station, University of Illinois, Urbana ILL.

Hwang, L., and Rizkalla, S. 1983. Effective tensile stress-strain characteristics for reinforced concrete. Proceedings, Canadian Society for Civil Engineering Annual Conference, Ottawa, Ontario: 129-147.

Johnston, B.G. and Opila, F. 1941. Compression and tension tests of structural alloys. ASTM Proceedings, American Society for Testing and Materials, **41**:

Jones, P.G., and Richart, F.E. 1936. The effect of testting speed on strength and elastic properties of concrete. Proceedings, American Society for Testing and Materials **36**, Part II: 380-391.

Julian, O.G. 1957. Synopsis of first progress report on committee on safety factors. Journal of the Structural Division, ASCE, **83**(ST4), Proc. Paper 1316: 1-22.

Kennedy, D.L.J., and Gad Aly, M. 1980. Limit states design of steel structures - performance factors. Canadian Journal of Civil Engineering, **7**: 45-77

Kent, D.C., and Park, R. 1971. Flexural members with confined concrete. Journal of the Structural Division ASCE, **97**(ST7): 1968-1990.

Kikuchi, D.K., Mirza, S.A., and MacGregor, J.G. 1978. Strength Variability of Bonded Prestressed Concrete Beams. Structural Engineering Report no. 68, University of Alberta, Edmonton, Alberta.

Lachance, L. and Hays, C.O. 1980. Accuracy of Composite Section Nonlinear Solutions. Journal of the Structural Division ASCE **106**(ST11): 2203-2219.

Lay, M.G. 1965. Flange local buckling in wide-flange shapes. Journal of the Structural Division, ASCE, **91**(ST6), Proc. paper 4580: 49-66.

Llewellyn, S. 1986. Parametric study of the strength of composite columns. B.Eng. thesis, School of Engineering, Lakehead University, Thunder Bay, Ontario.

Lyse, I., and Keyser, C.C. 1934. Effect of size and shape of test specimen upon the observed physical properties of structural steel. ASTM Proceedings, American Society for Testing and Materials, **34**:

Mander, J.B. 1983. Seismic design of bridge piers. Ph.D. Thesis, Civil Engineering, University of Canterbury, Christchurch, New Zealand.

Mander, J.B., Priestley, M.J.N., and Park, R. 1988. Theoretical stress-strain model for confined concrete. Journal of Structural Engineering, ASCE, **108**(8): 1804-1826.

Massey, P.C. 1964. Effect of residual stresses on the lateral stability of steel I-beams. New Zealand Engineer **19**(9):

May, I.M., and Johnson, R.P. 1978. Tests on restrained composite columns. The Structural Engineer, **56B**(2): 21-27.

McNeely, D.J., and Lash, S.D. 1963. Tensile strength of concrete. American Concrete Institute Journal, **60**(6): 751-761.

Mirza, S.A., and MacGregor, J.G. 1979a. Variations in dimensions of reinforced concrete members. Journal of the Structural Division ASCE **105**(ST4): 751-766.

Mirza, S.A., and MacGregor, J.G. 1979b. Variability of mechanical properties of reinforcing bars. Journal of the Structural Division ASCE **105**(ST5): 921-937.

Mirza, S.A., Hatzinikolas, M., and MacGregor, J.G. 1979c. Statistical descriptions of strength of concrete. Journal of the Structural Division ASCE **105**(ST6): 1021-1037.

Mirza, S.A., and MacGregor, J.G. 1982. Probabilistic study of strength of reinforced concrete members. Canadian Journal of Civil Engineering, **9**(3): 431-448.

Mirza, S.A. 1985a. Resistance factors for concrete design using ACI 318-83. International Journal of Structures, **5**(1):1-22

MIrza, S.A. 1985b. Application of Monte Carlo simulation to structural engineering problems. Proceedings, Second International Conference on Computing in Civil Engineering, Hangzhou, China, June 5-9: 622-635.

Mirza, S.A., and MacGregor, J.G. 1989. Slenderness and strength reliability of reinforced concrete columns. American Concrete Institute Structural Journal, **86**(4): 428-438.

Mirza, S.A. 1989. Parametric study of composite column strength variability. Journal Constructional Steel Research, **14**: 121-137.

Mirza, S.A. 1990. Flexural stiffness of rectangular reinforced concrete columns. American Concrete Institute Structural Journal, **87**: (accepted for publication).

Moehle, J.P., and Cavanagh, T. 1985. Confinement effectiveness of crossties in RC. Journal of the Structural Division ASCE **111**(10): 2105-2120.

Morino, S., Matsui, C., and Watanabe, H. 1984. Strength of biaxially loaded SRC columns. Composite and Mixed Construction, American Society of Civil Engineers: 241-253.

Nethercot, D.A. 1974. Residual stresses and their influence upon the lateral buckling of rolled steel beams. The Structural Engineer, **54**(3): 89-96

Park, R., Priestley, M.J.N., and Gill, W.D. 1982. Ductility of square-confined concrete columns. Journal of the Structural Division ASCE **108**(ST4): 929-950.

Park, R., and Paulay, T. 1975. Reinforced concrete structures. John Wiley and Sons.

Procter, A.N. 1967. Full size tests facilitate derivation of reliable design methods. The Consulting Engineer, **31**(8): 54-60.

Quast, U. 1970. Geeignete vereinfachungen fur die losung des traglastproblems der ausmittig gedruckten prismatischen stahlbetonstutze mit rechtekc-querschnitt. Dr.-Ing. Dissertation, Fakultat fur Bauwesen at Technischen Universitat Carlo-Wilhelmina, Braunschweig, FRG.

Rao, N.R.N., Lohrman, M., and Tall, L. 1964. Effect of strain rate on the yield stress of structural steel. Report No. 249.23, Fritz Engineering Laboratory, Lehigh University, Bethlehem, PA.

Scott, B.D., Park, R., and Priestley, M.J.N. 1982. Stress-strain behavior of concrete confined by overlapping hoops at low and high strain rates. American Concrete Institute Journal **79**(1): 13-27.

Sheikh, S.A., and Uzumeri, S.M. 1980. Strength and ductility of tied concrete columns. Journal of the Structural Division ASCE **106**(ST5): 1079-1101.

Sheikh, S.A. and Uzumeri, S.M. 1982. Analytical model for concrete confinement in tied columns. Journal of the Structural Division ASCE **108**(ST12): 2703-2721.

Sheikh, S.A., and Yeh, C.C. 1986. Flexural behavior of confined concrete columns. American Concrete Institute Journal, **83**(3): 389-404.

Suzuki, T., Takiguchi, K., Ichinose, T., and Okamoto, T. 1983. Effects of hoop reinforcement in steel and reinforced concrete composite sections. Third South Pacific Regional Conference on Earthquake Engineering. Wellington, New Zealand.

Tall, L. and Alpsten, G.A. 1969. On the scatter in yield strength and residual stresses in steel members. Final Report, Symposium on Concepts of Safety of Structures and Methods of Design, International Association for Bridge and Structural Engineering, London, England.

Trahair, N.S., and Kitipornchai, S. 1972. Buckling of inelastic I-beams under uniform moment. Journal of the Structural Division ASCE, **98**(ST11): 2551-2566.

Virdi, K.S., and Dowling, P.J. 1973. The ultimate strength of composite columns in biaxial bending. Procedures Institution of Civil Engineers (London), **56**(May): 251-272.

Virdi, K.S., and Dowling, P.J. 1982. Composite columns in biaxial loading. Axially Compressed Structures, Stability and Strength, edited by R. Narayanan. Applied Science Publishers, London: 129-147.

Wakabayashi, M. 1976. A proposal for design formulas of composite columns and beam-columns. Second International Colloquium on Stability Of Structures, Tokyo: 65-87.

Wright, P.J.F. 1952. The effect of the method of test cubes on mean strength and standard deviation. Magazine of Concrete Research, **4**(11): 67-76.

Young, B.W. 1971. Residual stresses in hot-rolled sections. Report CUED/C-Struct/TR.8. Dept. of Engineering, University of Cambridge.

Zhen-hai, G. and Xiu-qin, Z. 1987. Investigation of complete stress-deformation curves for concrete in tension. American Concrete Institute Materials Journal **84**(4): 278-285.

LIST OF SYMBOLS

b	flange width of structural steel section.
c	depth of neutral axis measured from compression face (Figure 3.1)
d	depth of structural steel section.
e	eccentricity of axial load at column ends
e/h	eccentricity ratio
e_m	deflection of slender column at mid-height
e_t	total eccentricity of axial load at mid-height of slender column
f_{yr}	specified yield strength of reinforcing bars
f_c	stress in concrete
f'_c	specified strength of concrete
$\overline{f}_{cstrR}$	mean 28-day in-structure compressive strength of concrete loaded at a rate of R.
$\overline{f}_{cstr35}$	mean 28-day in-structure compressive strength of concrete loaded at a rate of 35 psi (0.241 MPa) per second.
f_r	modulus of rupture of concrete
$\overline{f}_r$	mean value of modulus of rupture of concrete in structure.
f_y	specified yield strength of structural steel.
f_{cr}	critical column buckling stress.
f_{ys}	static yield strength of structural steel.
f_{yd}	dynamic yield strength of structural steel.
f_{yu}	upper yield strength of steel.
f_{yl}	lower yield strength of steel.
f_{us}	static ultimate strength of structural steel.
h	overall depth of composite section.
kl/r	slenderness ratio of column.
k	effective column length factor (equal to 1.0 in this study).

l	column length.
r	radius of gyration.
t	flange thickness of structural steel section.
w	web thickness of structural steel section.
A_f	area of one flange of structural shape (bt).
A_w	area of web of structual shape $(w(d-2t))$.
A_g	gross area of cross-section.
A_s	area of structural steel section.
C_m	factor to relate actual bending moment diagram to an equivalent uniform bending moment diagram (taken equal to 1.0 in this study).
DNA	perpendicular distance from plastic centroid of column to neutral axis (see Figure 2.6).
E_c	initial tangent modulus of elasticity of concrete.
$\overline{E}_{cR}$	mean value of initial tangent modulus of elasticity of concrete test cylinders loaded at rate R.
$\overline{E}_{cistrR}$	mean value of initial tangent modulus of elasticity of in-situ concrete loaded at rate R.
$\overline{E}_{c35}$	mean value of initial tangent modulus of elasticity of concrete test cylinders loaded at a rate of 35 psi/sec (0.241 MPa/sec).
E_s	modulus of elasticity of structural steel.
E_t	tangent modulus of elasticity of element.
E_{rstrn}	initial tangent modulus of strain-hardening curve of reinforcing bars.
E_{sstrn}	initial tangent modulus of strain-hardening curve of structural steel.
E_r	modulus of elasticity of reinforcing steel.
I	moment of inertia.
I_g	gross moment of inertia of cross-section.
I_s	moment of inertia of structural steel section.
M	bending moment.
M_m	bending moment at mid-height of slender column.
P	axial load.

P_c nominal slender column buckling load capacity.

P_n nominal column cross-section axial load capacity.

PDF probability density function.

R_t theoretical resistance of structural member.

R_n nominal resistance of structural member.

$V_{t/c}$ coefficient of variation of ratio of tested to calculated member strength.

$V_{in-batch}$ coefficient of variation of laboratory control specimens due to in-batch variations of material strength and dimensions.

V_{test} coefficient of variation of test procedures.

V_{model} coefficient of variation of theoretical strength model.

V_{cstrR} coefficient of variation of in-situ compressive strength of concrete.

V_{creal} coefficient of variation of the relation between cylinder strength and specified design strength of concrete.

V_R coefficient of variation in the relation between concrete loaded at 35 psi/sec (0.241 MPa) and concrete loaded at a rate of R.

V_{ccyl} coefficient of variation of strength of concrete test cylinders.

V_{cstr35} coefficient of variation of in-situ compressive strength of concrete loaded at a rate of 35 psi/sec (0.241 MPa/sec).

V_{cistrR} coefficient of variation of the initial tangent modulus of in-situ normal weight concrete.

β safety index as defined in Chapter 1 and Figure 1.1.

β_1 ratio of depth of rectangular compression block to depth of neutral axis (Figure 3.1).

β_d absolute value of the ratio of maximum factored dead load moment to the maximum factored total load moment (taken equal to 0.0 in this study).

δ_b moment magnification factor to reflect the effects of member curvature between ends of compression members.

ϵ_c strain in concrete.

ϵ_o strain in unconfined concrete at peak compressive stress.

ϵ_{uc} ultimate strain of concrete in compression.

ϵ_{sstrn} strain at start of strain-hardening curve of structural steel.

ϵ_{us} ultimate strain of structural steel.

ϵ_{ys} yield strain of structural steel.

ϵ_{rstrn} strain at start of strain-hardening curve of reinforcing bars.

ϵ_{ru} ultimate strain of reinforcing bars.

ϵ_{ry} yield strain of reinforcing bars.

ϕ curvature (inclination of strain gradient) or design code understrength factor.

ϕ_m curvature at mid-height of slender column.

ϕ_e curvature at column ends.

ρ_{rs} ratio of area of vertical reinforcing bars to gross cross-section area.

ρ_{ss} ratio of area of structural steel to gross cross-section area.

σ_{rw} residual stress at centroid of structural steel section.

σ_{rft} residual stress at flange tip of structural steel section.

σ_{rfw} residual stress at juncture of flange and web of structural steel section.